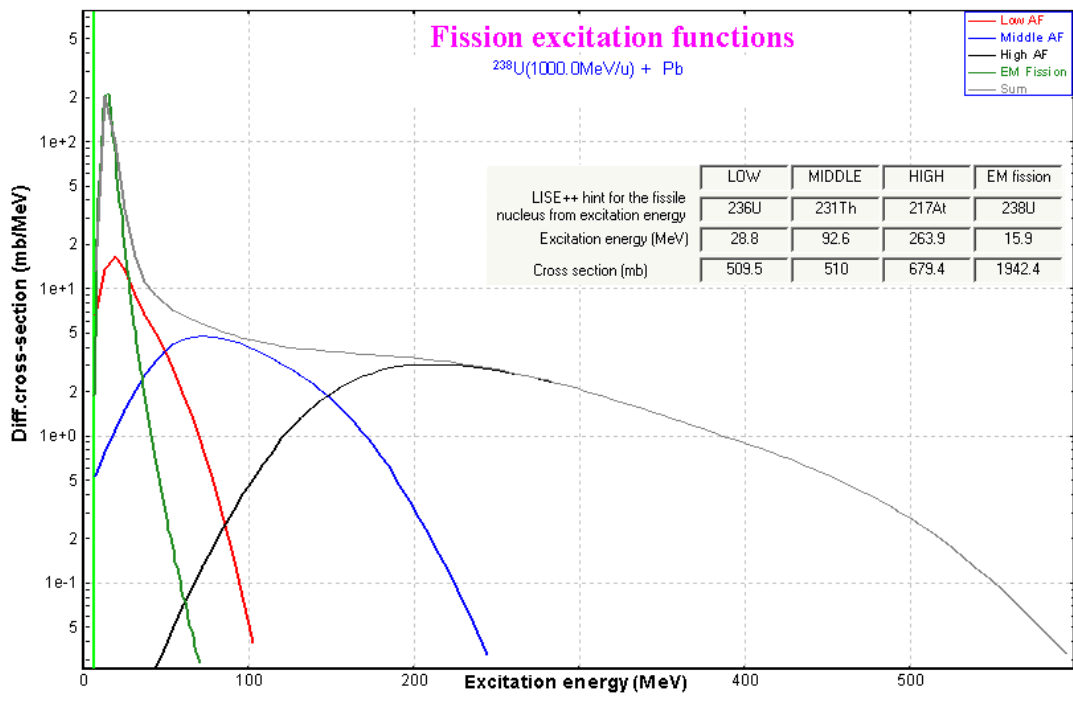


# LISE++

version 7.5

## Abrasion - Fission



# Contents:

<b>1. INTRODUCTION</b> .....	<b>5</b>
<b>2. DE-EXCITATION PROCESS</b> .....	<b>6</b>
2.1. THE BREAK-UP CHANNEL IN THE EVAPORATION CASCADE .....	7
2.1.1. <i>The limiting temperature as a function of mass number</i> .....	7
2.2. DISSIPATION EFFECTS IN FISSION .....	9
2.3. EVAPORATION CALCULATOR MODIFICATIONS .....	11
<b>3. FISSION BARRIERS</b> .....	<b>13</b>
3.1. THE FISSION BARRIER DIALOG .....	13
3.2. ETFSI AND EXPERIMENTAL FISSION BARRIERS .....	14
3.3. CALCULATION MODELS (#0,1,2) .....	14
3.3.1. <i>Shell corrections</i> .....	14
3.3.2. <i>Odd-Even corrections</i> .....	14
3.4. FISSION BARRIER PLOT .....	16
3.5. INFLUENCE OF CORRECTIONS FOR FISSION BARRIERS ON ABRASION-FISSION CROSS-SECTIONS .....	17
<b>4. SECONDARY REACTIONS IN TARGET</b> .....	<b>18</b>
4.1. REEXAMINATION OF SECONDARY REACTIONS CALCULATION PROCEDURE .....	18
4.1.1. <i>Dependence on the distribution dimension (<math>NP_{evap}</math>)</i> .....	18
4.1.2. <i>The "Secondary reactions" dialog modification</i> .....	19
4.1.2.1. Secondary reactions analysis plots .....	19
4.1.3. <i>Determination of the region of nuclei for secondary reactions calculations</i> .....	20
4.1.4. <i>Revision of optimal target thickness calculations for SR mode</i> .....	21
4.2. CALCULATION OF SECONDARY REACTION CONTRIBUTIONS TO FRAGMENTS WITH ZERO PRIMARY PRODUCTION CROSS-SECTION .....	23
4.2.1. <i>Secondary Reactions plots: SR coefficients &amp; reduced cross-sections</i> .....	24
4.3. SR CALCULATION SPEED .....	25
4.3.1. <i>Acceleration filters for secondary reactions calculations</i> .....	26
4.3.1.1. Corner rectangle filter .....	26
4.3.1.2. Diagonal filter .....	28
4.3.1.3. Application of acceleration filters .....	29
<b>5. ABRASION-FISSION</b> .....	<b>31</b>
5.1. THREE EXCITATION ENERGY REGIONS AF MODEL .....	31
5.1.1. <i>Abrasion-Fission dialog</i> .....	31
5.1.2. <i>Fission excitation function</i> .....	32
5.1.3. <i>Calculation of final fission fragment production</i> .....	34
5.1.3.1. Width of charge distribution .....	34
5.1.3.2. Modification of evaporation cascade subroutines .....	34
5.1.4. <i>Additional settings</i> .....	36
5.2. KINEMATICS .....	37
5.2.1. <i>Production of <math>^{100}\text{Zr}</math></i> .....	37
5.2.2. <i>Angular acceptance</i> .....	38
5.2.3. <i>Thick target</i> .....	39
5.3. ABRASION-FISSION PLOTS .....	40
5.3.1. <i>New plot options</i> .....	41
5.3.1.1. Final (after de-excitation) and initial cross-section plots .....	41
5.3.1.2. Excitation energy plot .....	42
5.4. ABRASION-FISSION SETTINGS DISCUSSIONS .....	42
5.4.1. <i>Excitation energy of fission fragment (TXE)</i> .....	42
5.4.2. <i>Excitation energy region (EER) boundaries</i> .....	45
5.4.3. <i>Excitation energy per abraded nucleon for Abrasion-Ablation</i> .....	48
5.4.4. <i>Dissipation effects in fission</i> .....	50
5.4.5. <i>Break-up de-excitation channel</i> .....	50
5.4.6. <i>Fission barrier</i> .....	51
5.4.7. <i>Cross-section suppression coefficient</i> .....	52
5.4.8. <i>Restore previous AF settings</i> .....	52
5.5. SECONDARY REACTIONS FOR ABRASION-FISSION .....	53
5.6. SETTING UP LISE TO CALCULATE YIELD OF AF PRODUCTS THROUGH THE SPECTROMETER .....	55
5.6.1. <i>Experiment settings</i> .....	55
5.6.1.1. Spectrometer choice .....	55
5.6.1.2. Primary beam, target, selected fragment .....	55
5.6.2. <i>Abrasion-Fission settings</i> .....	56
5.6.3. <i>Spectrometer tuning for the fragment of interest</i> .....	56
5.6.4. <i>Yield calculation</i> .....	57
5.6.5. <i>Optimum target</i> .....	57

5.6.6. Secondary reactions .....	58
5.6.7. Cleaning .....	59
5.6.8. Charge states .....	60
5.6.9. Go to more exotic case of <sup>83</sup> Zn .....	61
5.6.10. Examples .....	61
5.7. LISE'S OPTIONS MODIFICATIONS CONNECTED WITH THE AF MECHANISM .....	62
5.7.1. New transmission parameter "Sum of reactions" .....	62
5.7.2. User cross-section file .....	65
5.7.3. Transmission result file .....	65
5.8. INC FISSION .....	66
5.8.1. Recommended EER parameters for light targets in the LISE++ Abrasion-Fission model .....	70
5.8.1.1. Hydrogen target .....	70
5.8.1.2. Deuterium target .....	72
5.8.1.3. Targets with Z ≥ 2 .....	72
5.9. COMPARISON WITH EXPERIMENTAL DATA .....	73
5.9.1. Total fission cross-sections of <sup>238</sup> U at relativistic energies .....	73
5.9.2. <sup>208</sup> Pb(1AGeV) + p,d .....	74
5.9.3. <sup>238</sup> U(1AGeV) + Pb .....	79
5.9.4. <sup>238</sup> U(750AMeV) + Be .....	81
5.9.5. <sup>238</sup> U(1AGeV) + p .....	82
<b>6. NEW UTILITIES .....</b>	<b>85</b>
6.1. USER CROSS-SECTION ANALYSIS USING ABRASION-ABLATION MODEL .....	85
6.1.1. AA parameters corresponding to EPAX .....	87
6.2. OPTIMUM CHARGE STATE COMBINATION .....	90
6.3. CHARGE STATE COMBINATION CALCULATION FOR THE OPTIMAL TARGET THICKNESS UTILITY .....	91
6.3.1. Target optimization options .....	92
6.3.2. Optimal target searching methods .....	93
6.4. RATE & TRANSMISSION CALCULATION BATCH MODE .....	93
6.5. TARGET AND WEDGE OPTIMIZATION .....	95
6.5.1. Secondary Reactions contribution option .....	98
6.5.2. "Keep value" parameter .....	99
6.5.3. Target and wedge optimization for charge states .....	100
6.5.3.1. No charge states .....	100
6.5.3.2. Spectrometer tuned to only one charge state combination .....	101
6.5.3.3. Optimization of the charge state combination .....	102
6.5.3.4. Results .....	102
6.5.4. Wedge-shape and curved profile degraders properties .....	104
6.5.5. Setting discussions .....	107
6.5.5.1. Acceptance .....	107
6.5.5.2. Wedge selection slits .....	109
6.5.5.3. Isobars A=32 .....	109
<b>7. MASSES. AME2003 .....</b>	<b>111</b>
7.1. NEW MASS EXCESS FILES IN THE LISE PACKAGE .....	112
7.2. "UNKNOWN" - NEW TYPE OF ISOTOPE DESIGNATION FOR THE TABLE OF NUCLIDES .....	112
7.2.1. Particle bound, quasi bound and unbound nuclei .....	112
7.2.2. How to load information from the user mass excess file in the navigation scheme .....	114
7.2.3. Modifications in the database plot .....	114
<b>8. LISE++ BLOCK STRUCTURE DEVELOPMENT .....</b>	<b>115</b>
8.1. NEW MATERIAL BLOCK: FARADAYCUP .....	115
8.2. APPEND BLOCKS IN THE CURRENT OPEN CONFIGURATION FROM OTHER LISE FILES .....	115
<b>9. DIFFERENT .....</b>	<b>116</b>
9.1. USER CROSS-SECTION FILE .....	116
9.1.1. User cross-section file: reaction property .....	116
9.1.2. User file of reduced cross-sections .....	117
9.1.3. CS files in LISE++ package .....	117
9.2. CURVED PROFILE DEGRADER MODIFICATIONS .....	118
9.3. LOGOTYPES AND REFERENCES .....	120
9.4. 2D-PLOTS: CONTOURS & PROJECTIONS .....	121
9.4.1. Contour dialog .....	121
9.4.1.1. Window and contour projections on an axis for 2D Cross-section plot .....	121
9.5. FISSION CHANNEL FOR THE FUSION-EVAPORATION EXCITATION FUNCTION PLOT .....	122
9.6. ABRASION-ABLATION: FAST MODE FOR HEAVY PROJECTILES .....	123
9.7. THE "ABOUT" DIALOG MODIFICATIONS .....	123
9.8. PACE4: USER'S LIMITS FOR ANGULAR AND ENERGY DISTRIBUTIONS OF RESIDUES .....	123
9.9. GAS DENSITY DIALOG .....	124

9.10. BLOCK LABELS FOR THE TRANSPORT ENVELOPE .....	124
9.11. DRIFT BLOCK.....	124
9.12. COMPOUND TARGETS FOR AA CALCULATIONS, FUSION-RESIDUES AND FISSION REACTIONS .....	125
9.13. CHOICE OF HORIZONTAL AXIS FOR 2D-PLOTS .....	125
9.14. VERSION NUMBERS.....	125
9.15. LISE USER STATISTICS .....	125
<b>10. USER REQUESTS AND BUGS REPORT.....</b>	<b>127</b>
10.1. CORRECTIONS .....	127
10.2. USER REQUESTS.....	128
<b>11. NEXT STEPS DEVELOPMENT .....</b>	<b>129</b>
11.1. FIRST PRIORITY.....	129
<i>Long-term</i> .....	129
<i>Short-term</i> .....	129
11.2. SECOND PRIORITY TASK.....	129
11.3. THIRD PRIORITY TASK.....	129
<b>ACKNOWLEDGEMENTS.....</b>	<b>130</b>
<b>REFERENCES:.....</b>	<b>130</b>



## 1. Introduction

Fission observed after the collision of Uranium projectiles with target nuclei is due to both electro-magnetic and to nuclear processes. At large impact parameters, the long-range Coulomb force dominates (Coulomb fission). The projectile is excited mostly to the region of giant resonance by exchange of virtual photons; the system then decays by neutron emission or by fission (see Fig.1).

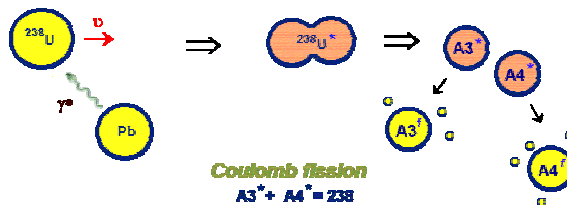


Fig.1. Coulomb fission scheme.

### Abrasion-Fission : fission of a heavy projectile after abrasion by a target heavier than Be

At smaller impact parameters, peripheral nuclear collisions take place, and the fissile projectile is left abraded and excited. After de-excitation by nucleon emission, it can undergo fission with a finite probability [Hes96] as well as of break-up. Three de-excitation channels should be taken into account after abrasion: fission (Fig.2), break-up (Fig.3), and evaporation of light particles (Fig.4).

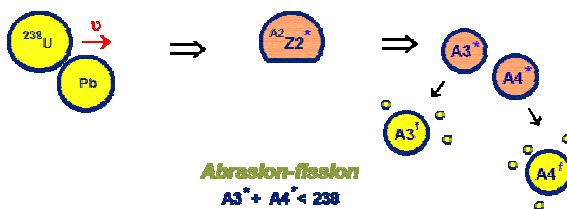


Fig.2. Abrasion-fission scheme.



Fig.3. Abrasion-Break-up scheme.

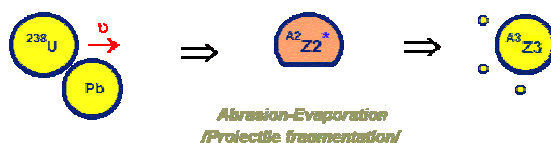


Fig.4. Abrasion-Evaporation scheme.

In the case of fission of an incident projectile in result of collisions with a light target nucleus (see Fig.5) we will be using the term “INC<sup>\*</sup> fission” in this documentation.

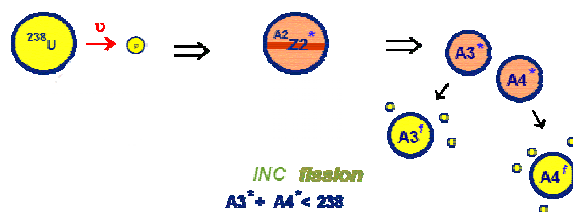


Fig.5. INC fission scheme.

### INC fission : fission of a heavy projectile on light targets (p,d,<sup>3</sup>He,α).

A new model based on the fast analytical calculation of ABRASION-FISSION fragment transmission through a fragment separator has been developed in the framework of the code LISE++.

Before discussing Abrasion-Fission it is necessary to explain a number of changes and new developments in the program that were included to provide all of the important components to analyze the Abrasion-Fission fragment production, such as dissipation effects in fission, break-up de-excitation channels, secondary reactions in the target, and a reexamination of fission barriers.

\* Intra-Nuclear Cascade

## 2. De-excitation process

The decay of highly excited nuclei takes place via various processes, which have great practical importance [Sch02] such as fission, spallation, fragmentation and others. The compound-nucleus mechanism dominating at low excitation energies changes into simultaneous decay into many fragments with increasing energy. In order to describe qualitatively the de-excitation process of highly excited nuclei there are three principal approaches pursued in the new version of the code. They are available through the “Evaporation options” dialog (in the case of fusion or fission reactions set in the code, see Fig.6) or from the “Prefragment search and Evaporation option” dialog (in the case of projectile fragmentation) (see Fig.7):

- Dissipative effects in fission (frames “A”),
- Break-up channel (frames “B”),
- Fission barrier reexamination (frame “C”).

These new features were implemented to achieve better agreement between LISE calculations and data from GSI experimental and theoretical approaches. In this chapter we will explain the nature of these new effects. The influence of these parameters on the models in the final Abrasion-Fission fragment production will be presented in chapter 5. Abrasion-Fission.

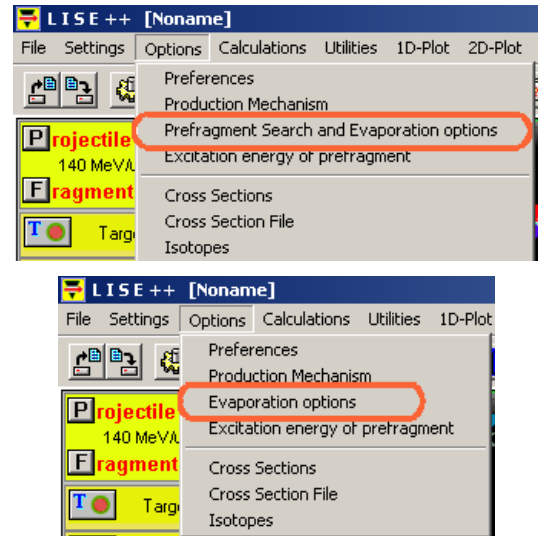


Fig.6. The “Options” menu

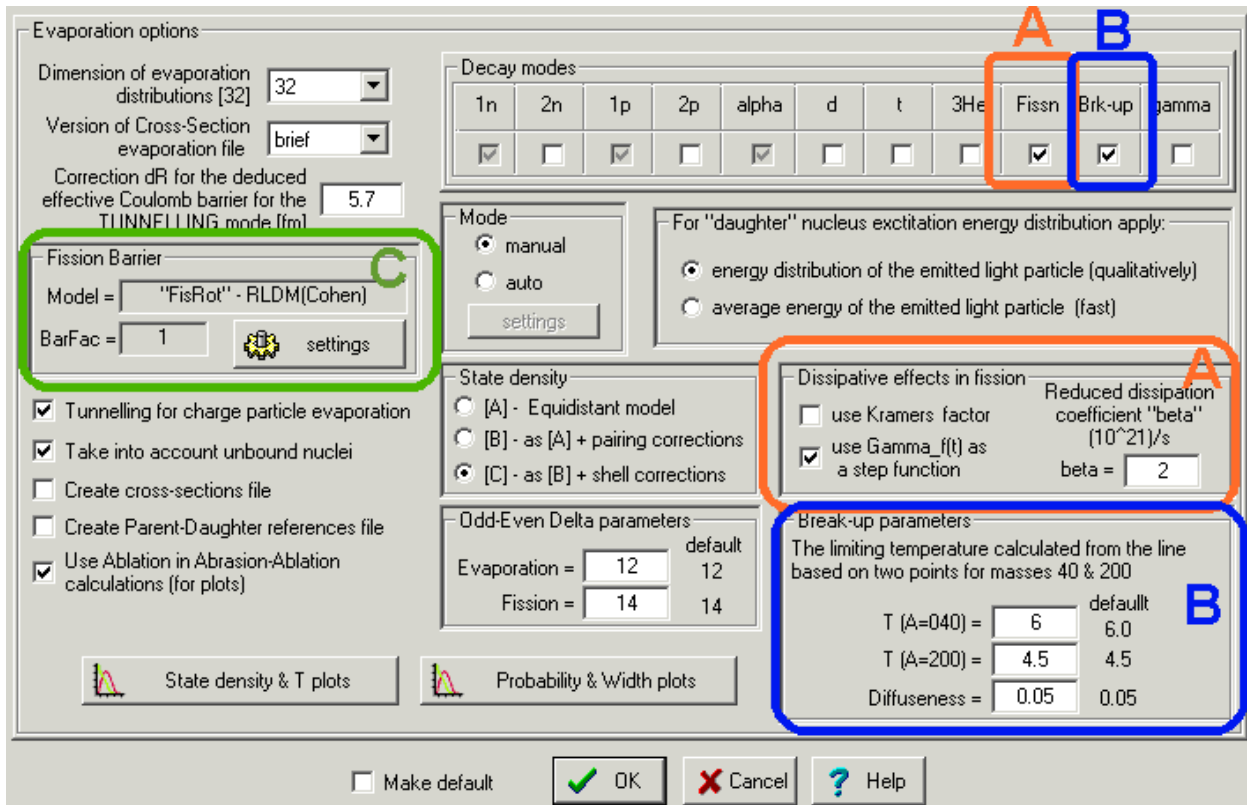


Fig.7. The “Evaporation option” dialog.

## 2.1. The break-up channel in the evaporation cascade

It is suggested that the “**break-up channel**” is a simultaneous decay of a highly excited nucleus into many fragments. **Abrasion-breakup** is break-up of the projectile residue after abrasion by a target when the nuclear temperature of the fragment exceeds the limiting temperature.

*The code doesn’t calculate mass and element distributions of fragments after break-up\**! The principal aim of this version is calculation of Abrasion-Fission products. This is the reason why break-up events are excluded from the following calculations. Future plans are to make an analysis of the products from Abrasion-Breakup with sequential decay as was done for Abrasion-Evaporation and Abrasion-Fission channels in the current version of LISE++.

### 2.1.1. The limiting temperature as a function of mass number

The limiting temperature is calculated as a function of the mass between  $A=40$  and  $A=200$  (see Fig.7, frame “B”). The default values are taken from the paper [De96] (see Fig.8). If you prefer the limiting temperature to be constant for all masses as in [Sch02] just set the same value for both masses in the dialog. To avoid a jump in the widths calculation of de-excitation channels, the break-up channel shape is represented by a Fermi distribution  $\rho(T) = 1 - 1/(1 + \exp[(T - T_{lim})/d])$ , where  $d$  is the diffuseness (default value is equal to 0.05), which can be modified in the “Evaporation options” dialog (see Fig.7, frame “B”).

By clicking the “Probability & Widths plots” button in the “Evaporation options” dialog it is possible to match the probabilities of different de-excitation channels as a function of excitation energy (see Fig.9).

**Note:** Comparison between Abrasion-Ablation calculations with the break-up option and experimental values of fragment production cross-sections in fragmentation of intermediate beams ( $Z=16-28$ ) indicates that the limiting temperature should be larger for fragments with masses less than 40 was predicted in [De96]. Consequently we propose increasing the limiting temperature for this case for low masses or turning off the break-up channel, since its contribution should be insignificant.

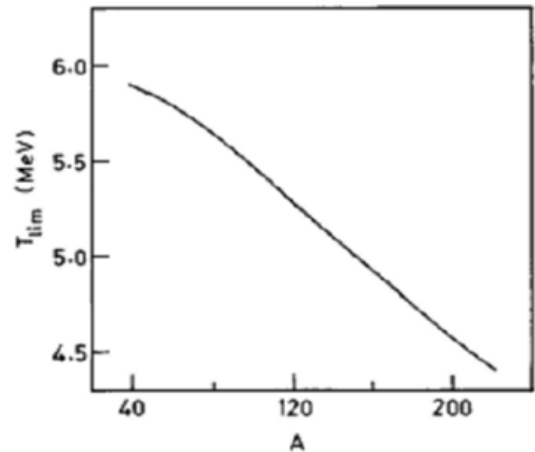


Fig.8. The limiting temperature  $T_{lim}$  as a function of mass number on the  $\beta$ -stability line [De96].

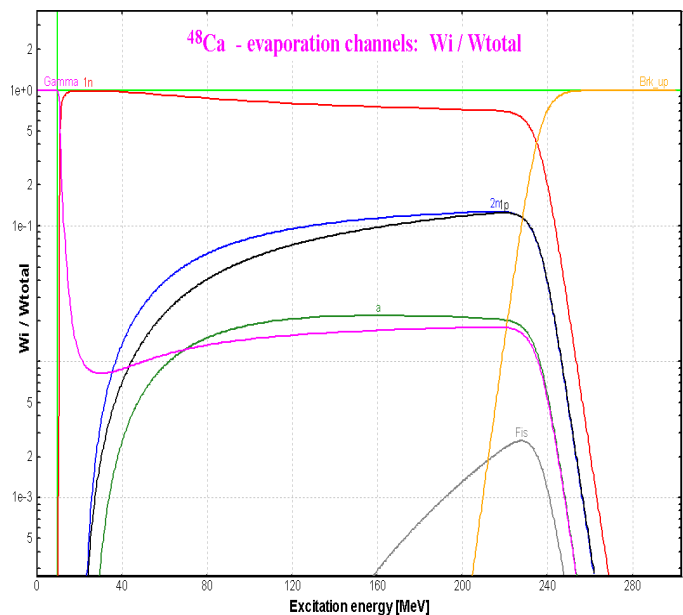
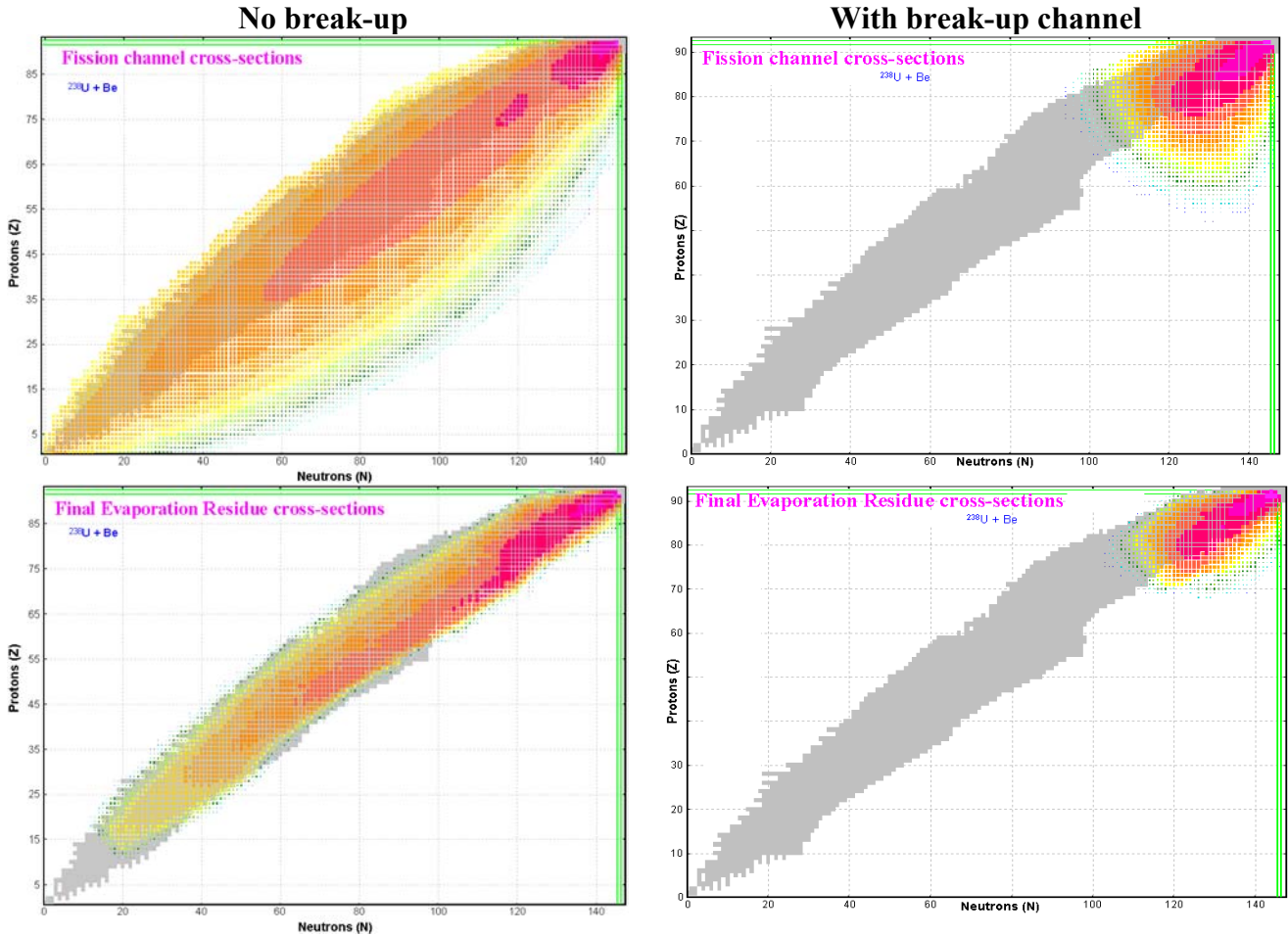


Fig.9.  $^{48}\text{Ca}$  de-excitation channel probabilities as a function of the excitation energy. The break-up is taken into account and begins to dominate at energies above 240 MeV.

\*as it was done in [Sch02]. In order to simulate the production of residues in the fragmentation of  $^{238}\text{U}$  projectiles with LISE++ you have to turn off the break-up channel and use the “triangle” excitation function. See chapter 4.6 “Excitation energy of Prefragment” of the documentation for version 6.4 ([http://groups.nsl.msu.edu/lise/6\\_4/lise++\\_6\\_4.pdf](http://groups.nsl.msu.edu/lise/6_4/lise++_6_4.pdf)).

### 2.1.1.1. The crucial role of the break-up channel in heavy projectile fragmentation

The crucial role of break-up channel contributions in the fragment production in reactions with heavy projectiles at relativistic energies is demonstrated well in Fig.10 and Fig.11.



**Fig.10.** Fission channel cross-sections resulting from  $^{238}\text{U}(1\text{AGeV})$  abrasion by a Be target (top panel). The bottom pictures show the final evaporation residue cross-sections in the same reaction. Calculations shown on the left plots were done without the Break-up channel, whereas for the plots on the right side the break-up channel was taken into account.

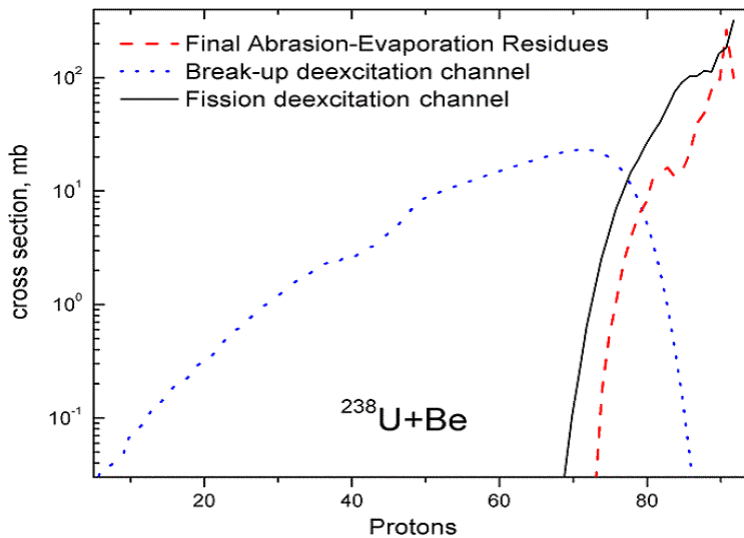


**Fig.11.** Nuclear charge yields for different de-excitation channels after  $^{238}\text{U}(1\text{AGeV})$  abrasion on a Be-target.

**Notes:** Several cross-sections shown in Fig.10 are outside the LISE nuclide table due to fact that unbound nuclei are taken into account for the fission de-excitation channel. In the case of evaporation residues, only particle-bound nuclei can be produced. The code calculates separation energies from LISE LDM2 using AME2003 data, but the LISE nuclide table is based on old measurements and can be modified manually by the user.

## 2.2. Dissipation effects in fission

Dissipation is a fundamental process in nuclei that determines the time an excited nucleus needs to populate the available space and to reach equilibrium [Jur02]. The concept of dissipation was already introduced by Kramers [Kra40] more than sixty years ago, but the success of the transition-state model of Bohr and Wheeler [Boh39] prevented his idea from being established [Jur02,Jur03]. However, it was shown by different groups in the 80's that measured pre-scission neutron multiplicities were much larger than the predictions of the transition-state model. This discrepancy was interpreted as an indication that **the de-excitation process of a highly excited heavy nucleus is a dynamical process.**

Recently at GSI an analysis of dissipative effects in nuclear fission observed in the fragmentation of  $^{238}\text{U}$  projectiles was performed by A.Ingatyuk et al [Ign95], and new signatures of dissipation in fission induced by relativistic heavy-ion collisions were obtained by B.Jurado et al. [Jur02,Jur03]. Using results of these studies, the dissipation effects in fission were implemented in the LISE++ code.

In the quasi-stationary approximation Kramers obtained the following equation for the fission width:

$$\Gamma_f^K = K \cdot \Gamma_f^{BW} \quad /1/$$

where  $\Gamma_f^{BW}$  is the fission-decay width given by the transition-state model, and  $K$  is the factor:

$$K = \sqrt{1 + \gamma^2} - \gamma \quad /2/$$

with

$$\gamma = \beta/2\omega_0 \quad /3/$$

where  $\beta$  is the reduced dissipation coefficient, and  $\omega_0$  is the frequency of the harmonic-oscillator potential that osculates the fission barrier at the saddle point. LISE fixed this potential equal to  $\hbar\omega_0 = 1 \text{ MeV}$  for the fission width calculations.

The fission process requires a finite time. The dependence of this transient time  $\tau$  on the dissipation coefficient for the underdamped and the overdamped regions is the following:

$$\tau_{under} = \frac{1}{\beta} \ln \frac{10B_f}{T}, \quad \text{for } \beta > 2\omega \quad /4/$$

$$\tau_{over} = \frac{\beta}{2\omega^2} \ln \frac{10B_f}{T}, \quad \text{for } \beta < 2\omega \quad /5/$$

The transient times defined in following Equations /4,5/ are shown in Fig.12<sup>♦</sup> together with numerical solutions of the Fokker-Planck equation [Bha86].

Taking into account the transient time, the ratio of the widths for fission and neutron emission can be written as

$$\frac{\Gamma_f(\beta)}{\Gamma_n + \Gamma_p + \Gamma_\alpha} = K(\beta) \cdot \frac{\Gamma_f^{BW}}{\Gamma_n + \Gamma_p + \Gamma_\alpha} \cdot \exp\left(-\frac{\tau(\beta)}{\tau_{v\pi}}\right) \quad /6/$$

where  $\tau_{v\pi} = \hbar/(\Gamma_n + \Gamma_p + \Gamma_\alpha)$  is the mean life-time against neutron, proton and alpha-particle emission.

---

<sup>♦</sup> it was taken from [Ign95].

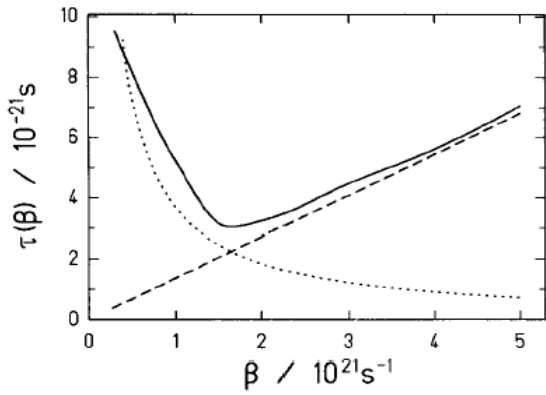


**Fig.12.** Calculated transient times  $\tau(\beta)$  for the overdamped and underdamped regimes (Eqs./4,5/ with  $B_f = 4$  MeV,  $T = 1$  MeV,  $\omega = 1.31 \cdot 10^{21} \text{ s}^{-1}$ ) [Bha86]. The dashed line corresponds to overdamped motion: the transient time increases with increasing viscosity. The dotted curve shows the case of underdamped motion, which leads to an increase in the transient time when the viscosity becomes very small and the energy is slowly dissipated into collective motion. The solid curve is calculated from a numerical solution of the Fokker-Planck equation.

The transient time is defined as  $\tau(\beta) = \max(\tau_{\text{under}}, \tau_{\text{over}})$  in LISE. The factor  $K$  is set to 1 in Equation /6/ to calculate the fission-width if “Use Kramers factor” is turned off in the “Evaporation options” dialog (see Fig.7, frame “A”). The user can modify the reduced dissipation coefficient  $\beta$  and turn on/off the dissipation effects for fission based on Equation /6/.

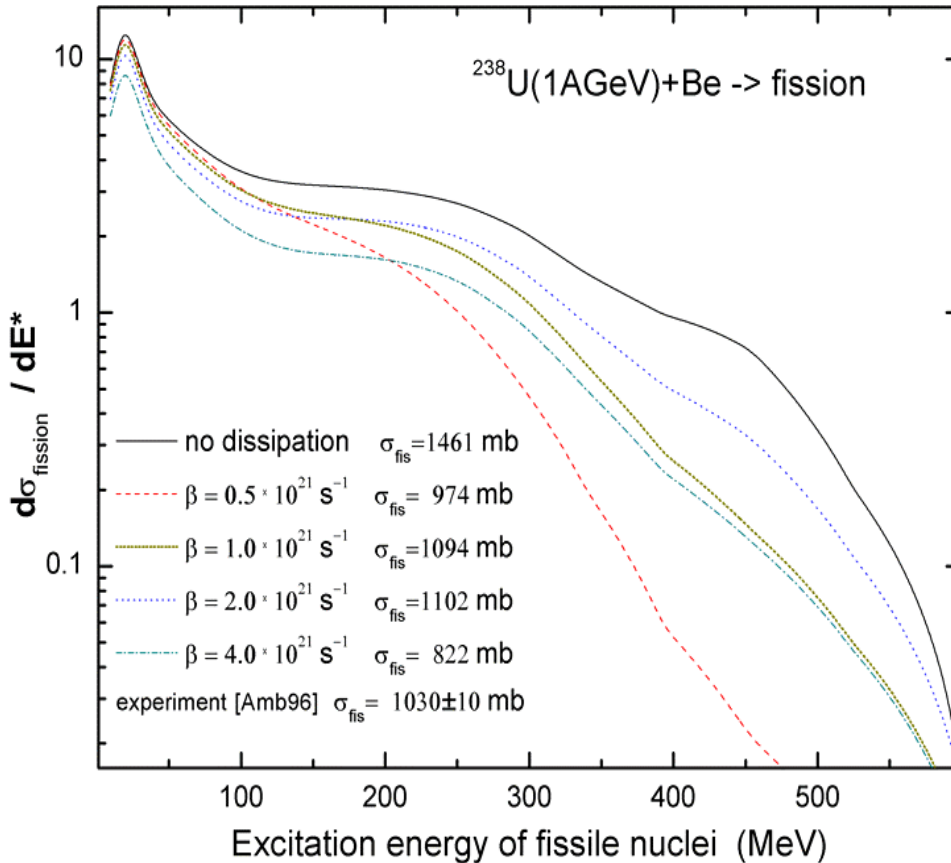


**Fig.13.** Fission summary excitation functions with different reduced dissipation coefficients and without dissipation effects for fissile nuclei produced in the reaction  $^{238}\text{U}(1\text{AGeV})+\text{Be}$ .

The following parameters for the Abrasion-Ablation model were used to produce these calculations:

Excitation energy:  
 Method #2  
 $Ex = 13.3 \text{ dA}$   
 $\sigma = 9.6 (\text{dA})^{0.5}$

Channels:  
 $p, n, 2n, \alpha, \text{fission, break-up}$

Break-up:  
 $T(40)=6.0, T(200)=4.5$

$NP = 16; SE: \text{DB0}+\text{Cal2};$

Kramers factor: YES

BarFac=1; Mode: auto

Fission summary excitation functions without dissipation effects and with different reduced dissipation coefficients for fissile nuclei produced in the reaction  $^{238}\text{U}(1\text{AGeV})+\text{Be}$  are shown in Fig.13 to demonstrate how total nuclear fission cross-section and the shape of the fission excitation functions can depend on the dissipation effects. A more detailed analysis of the dissipation effects in the fission summary excitation function and comparisons with experimental data will be presented in chapter “5.4.4. Dissipation effects in fission”.



### 2.3. Evaporation calculator modifications

Some modifications were made in the Evaporation calculator related to the introduction of a new decay channel (see Fig.14, frame “A”). The initial<sup>♦</sup> abrasion cross-section, the summed cross-sections of residues production, the cross-sections for fission and break-up de-excitation channels are given in frame “B” in Fig.14. The initial cross-section consists of residue (Abrasion-evaporation) cross-sections, fission and break-up channels.

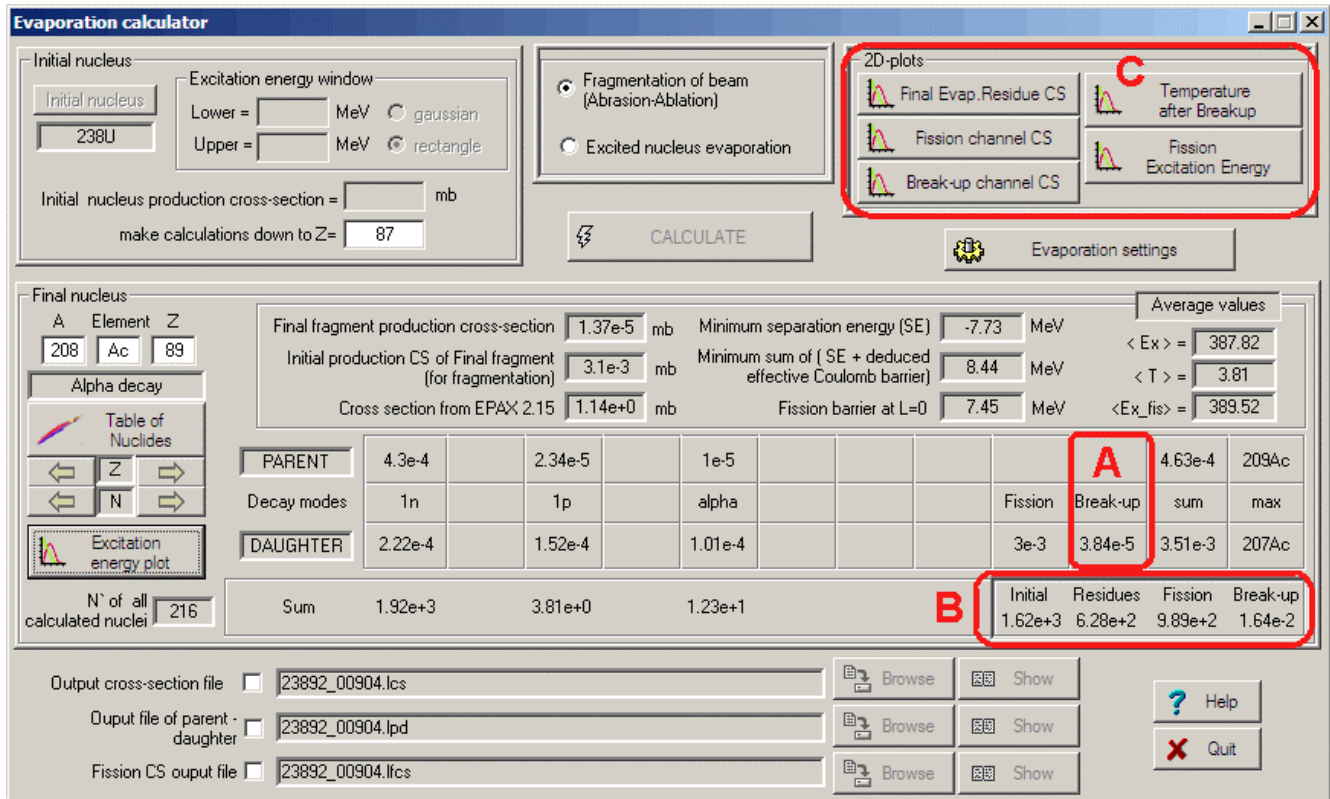


Fig.14. The Evaporation calculator. New modifications are marked by red rectangles.

The Evaporation calculator allows one to visualize the dynamics of the de-excitation of the nucleus, and the history of excitation. The input parent excitation channels for the <sup>208</sup>Ac nucleus in <sup>238</sup>U(1AGeV)+Be are shown in Fig.15, the corresponding de-excitation channels in Fig.16. From Fig.15 it is possible to conclude that the more intense component of the excitation function corresponds to the initial abrasion (blue curve), but the main channel producing the final fragment <sup>208</sup>Ac in the ground state (Abrasion-Evaporation) is the 1n-channel (low energy part of the excitation function between zero and the minimum separation energy marked by the green vertical line). The sum dominating de-excitation channel is fission, but it is easy to see from Fig.16 that the break-up channel begins to prevail at energies above 520 MeV. Parameters of these calculations are given in the break-up channel 2D-plot in Fig.17. Fission channel and final evaporation residue cross-section 2D-plots with and without break-up channel were already shown in Fig.10.

<sup>♦</sup> The sum of cross-sections from the initial nucleus down to an element Z (see Fig.14), down to which calculations were done.

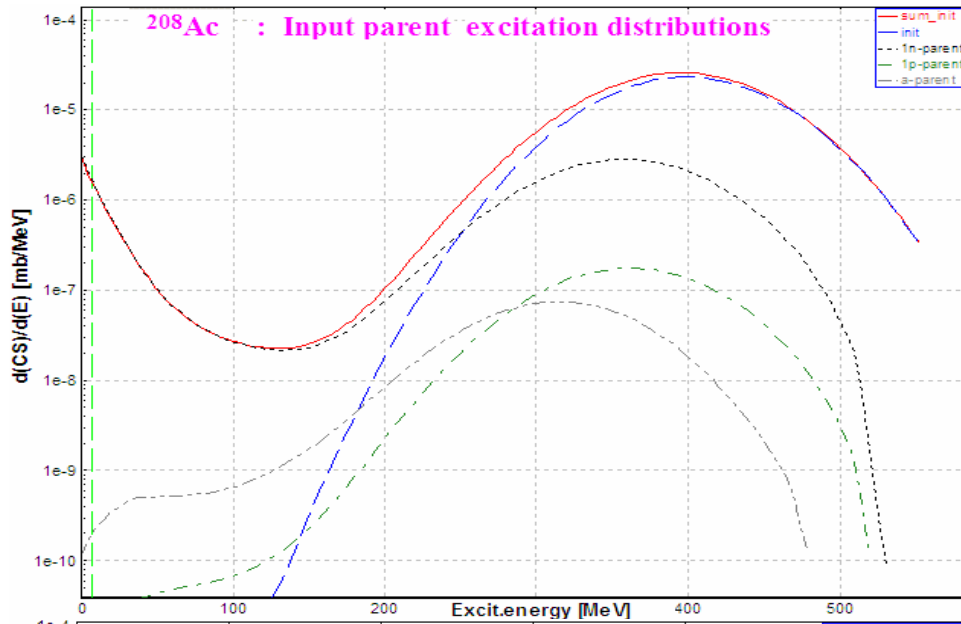


Fig.15. Input parent and initial abrasion contributions to the excitation function of  $^{208}\text{Ac}$  in the reaction  $^{238}\text{U}(1\text{AGeV})+\text{Be}$ .

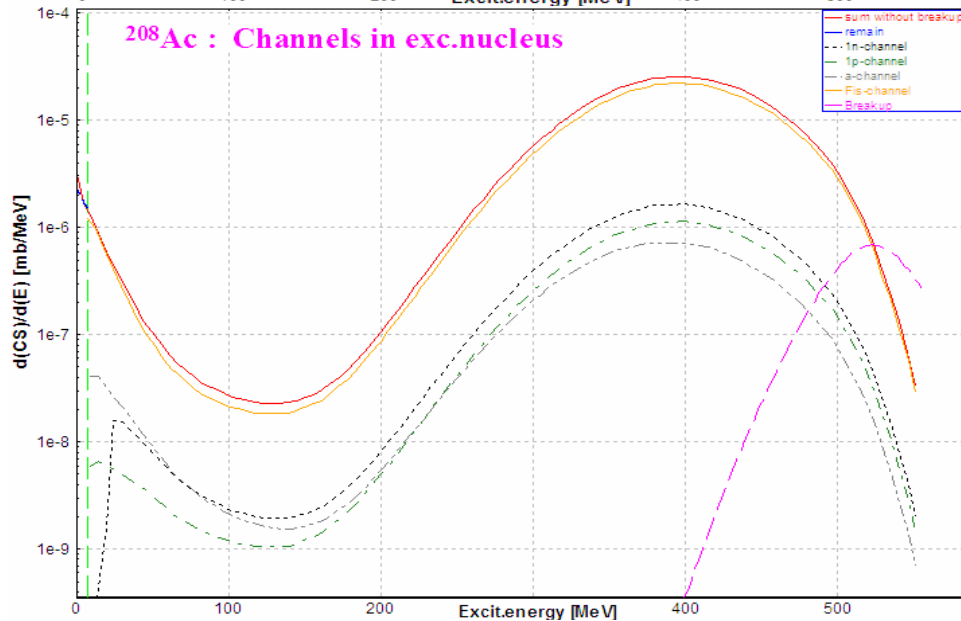


Fig.16. De-excitation channels of  $^{208}\text{Ac}$  in the reaction  $^{238}\text{U}(1\text{AGeV})+\text{Be}$ .

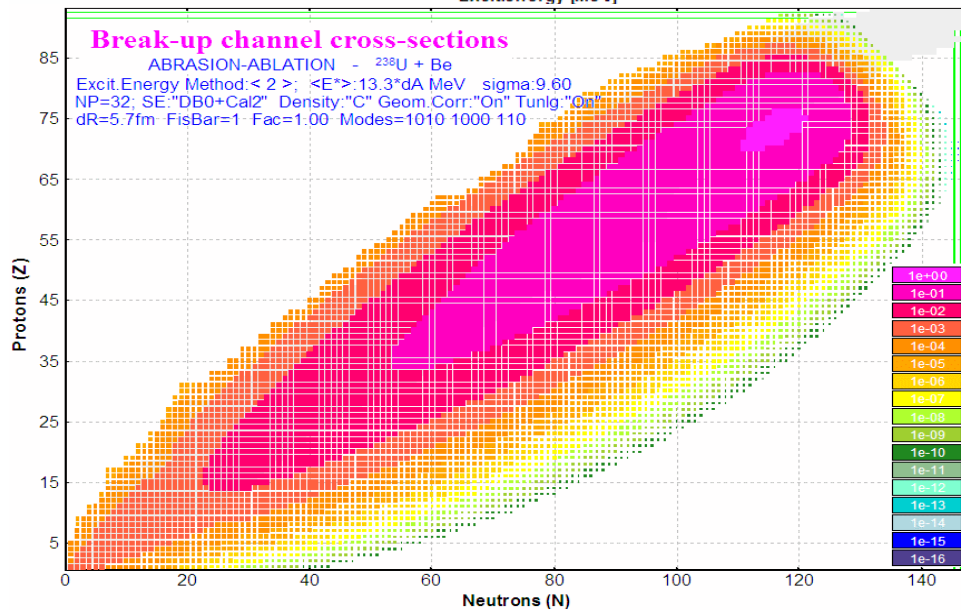


Fig.17. 2D-plot of break-up de-excitation channel cross-sections for  $^{238}\text{U}(1\text{AGeV})$  abrasion on a Be-target.



### 3. Fission barriers

The LISE code needs fission barriers for:

- Calculation of fission de-excitation channels for the estimation of the total cross-sections of Coulomb and Abrasion fission as well as abrasion-evaporation residues. For the next version, plans are to develop the model to calculate fusion-fission production cross-sections in the low excitation energy region where the fission barrier plays a crucial role<sup>♦</sup>.
- Calculation of decay widths in the post-scission nucleon emission procedure.

The Cohen-Plasil-Swiatecki rotating liquid drop fission barrier [Coh74] without shell and odd-even corrections was used in the previous version of LISE. A large fission yield was found close to the proton shell  $Z=82$  during the development of the Abrasion-Fission model in the LISE code. This high yield contradicted experimental data. It was explained by the small height of the fission barrier, which is expected to grow near shell closures. In this context it was a necessity to introduce shell corrections and odd-even effects. Other fission barrier models and the possibility to use experimental values for the fission barrier were implemented in the code.

#### 3.1. The Fission barrier dialog

The “Fission barrier” dialog (see Fig.18) can be reached by clicking on the “Settings” button of the “Fission barrier” frame in the “Evaporation option” dialog (see Fig.7, frame “C”).

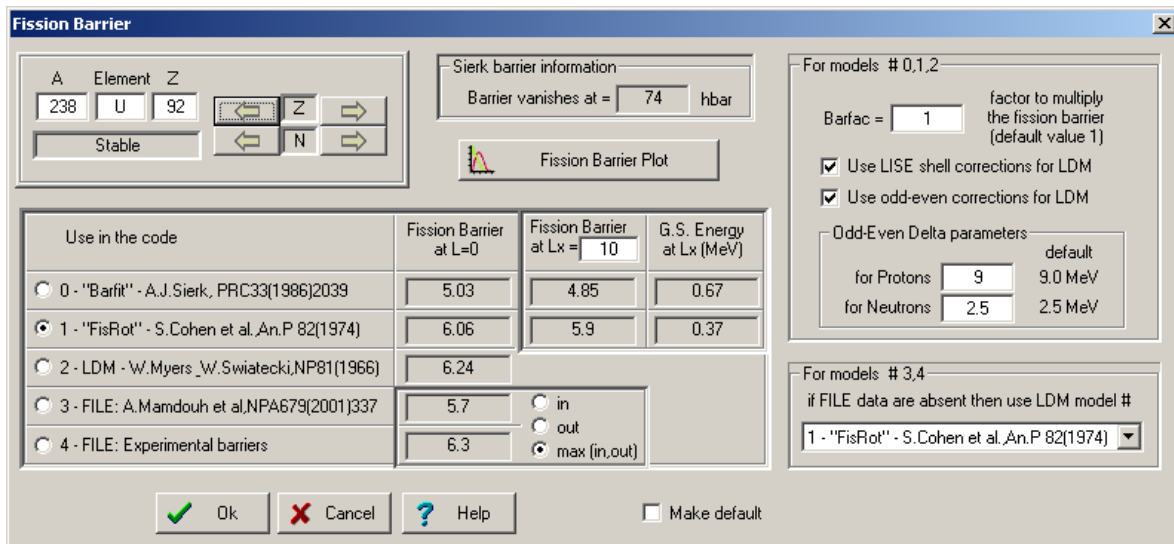


Fig.18. The “Fission barrier” dialog.

The user can choose from five options available in the code: three models (Sierk [Sie86], Cohen [Coh74], Myers[Mye66]) to calculate a fission barrier or extract it from files (Mamdout [Mam01] and experimental data [Smi93]). If the selected option is “take data from the file” (model #3,4) and interested data are absent in the corresponding data-file then the code uses one of three calculation models which is set in the dialog (right bottom frame in the Fission barrier dialog).

<sup>♦</sup> As well as to take into account an angular momentum of the compound nucleus for fission barrier calculation and subsequent fission fragment production cross-section calculations.

### 3.2. ETFSI and experimental fission barriers

The file “**fis-barrier-etfsi.dat**” in the directory “bin” contains calculated fission barriers by the ETFSI<sup>♥</sup> method [Mam01]. The file “**fis-barrier-user.dat**” contains information about experimental fission barrier values extracted from the site <http://www.ndc.tokai.jaeri.go.jp/~fukahori/RIPL-2/>.

#### **File format:**

The separation between values can be by tab, comma, or space.

If one of the barriers (“Bin” or “Bout”) is absent then substitute any letter (We used “X”) “#”-char in the beginning of line denotes comments.

The line contains four values:        Z ,    A ,    Bin ,    Bout

for example:                        90 ,    230 ,    6.1 ,    6.8

Using one of three buttons “In”, “Out”, “Max(in,out)” the user can define which kind of fission barrier will be used in the code for models #3 and #4.

### 3.3. Calculation models (#0,1,2)

The fission barrier used in the code is equal to the sum of the calculated value in the selected model at  $L=0$  plus shell and odd-even corrections:

$$B_{f\_final} = B_{f\_init}(at L=0) \cdot b + \Delta_{shell} + \Delta_{odd-even} , \quad /7/$$

where  $b$  (Barfac) is the factor to multiply the fission barrier. The default value is  $b=1$ . This factor can be changed by user in the Fission barrier dialog (right bottom frame in Fig.18).

#### 3.3.1. Shell corrections

For shell corrections the code takes the difference between LISE LDM#2 with shell corrections and LISE LDM#2 without shell corrections using the new compilation of Atomic Mass Evaluation 2003 (Chapter 7. Masses. AME2003). For details about shell corrections see chapter “5. Improved mass formula with shell crossing corrections” in the LISE v.6 documentation [http://groups.nslc.msu.edu/lise/6\\_1/lise++\\_6.pdf](http://groups.nslc.msu.edu/lise/6_1/lise++_6.pdf).

Fig.19 and Fig.20 show the fission barriers of Polonium isotopes ( $Z=84$ ) without and with shell corrections.

#### 3.3.2. Odd-Even corrections

Odd-even corrections are calculated in the following way:

$$\Delta_{odd-even} = ((N\%2) \cdot V_N + (Z\%2) \cdot V_Z) / \text{sqrt}(N+Z) , \quad /8/$$

where  $N$  is the number of neutrons in the nucleus,  $Z$  is the number of protons,  $V_N$  is the value for neutrons (from LISE fit<sup>▲</sup> is equal to 2.5 MeV),  $V_Z$  is the value for protons (from LISE fit is equal to 9.0 MeV).

Fig.21 and Fig.22 show fission barriers of Uranium isotopes ( $Z=92$ ) without and with odd-even corrections. The grey curve corresponds to experimental data.

---

<sup>♥</sup> Predictions of the fission barriers and saddle point deformations obtained within the Extended Thomas-Fermi plus Strutinsky Integral (ETFSI) method for 2301 nuclei with  $78 \leq Z \leq 120$  [Mam98, Mam01, Smi93]

<sup>▲</sup> Calculated fission barriers (Sierk and Choen) with shell corrections and ALL ( $Z=80-96$ ) experimental data (file “fis-barrier-user.dat”) were fitted to get factors for odd-even corrections.

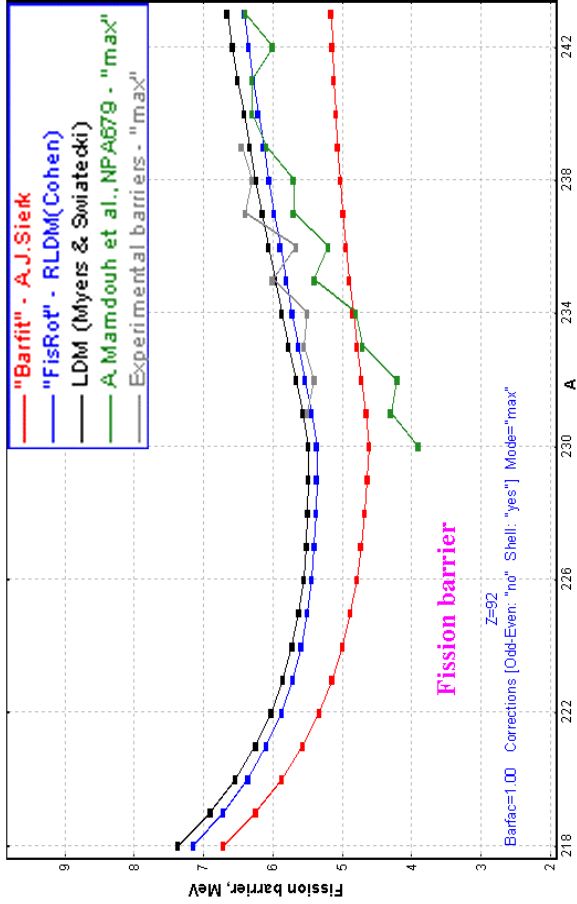


Fig.21. Fission barriers of Uranium isotopes calculated with shell and without odd-even corrections.

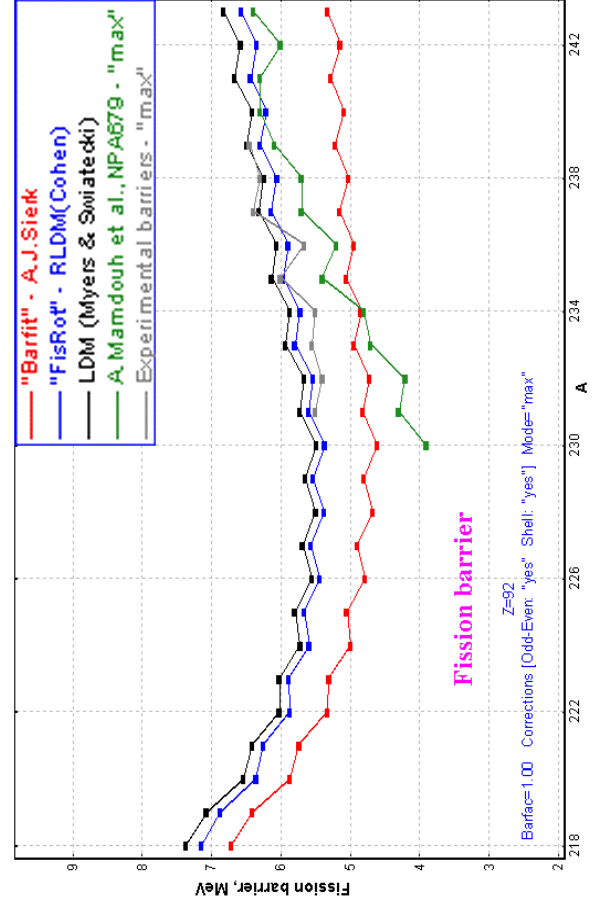


Fig.22. Fission barriers of Uranium isotopes calculated with shell and odd-even corrections.

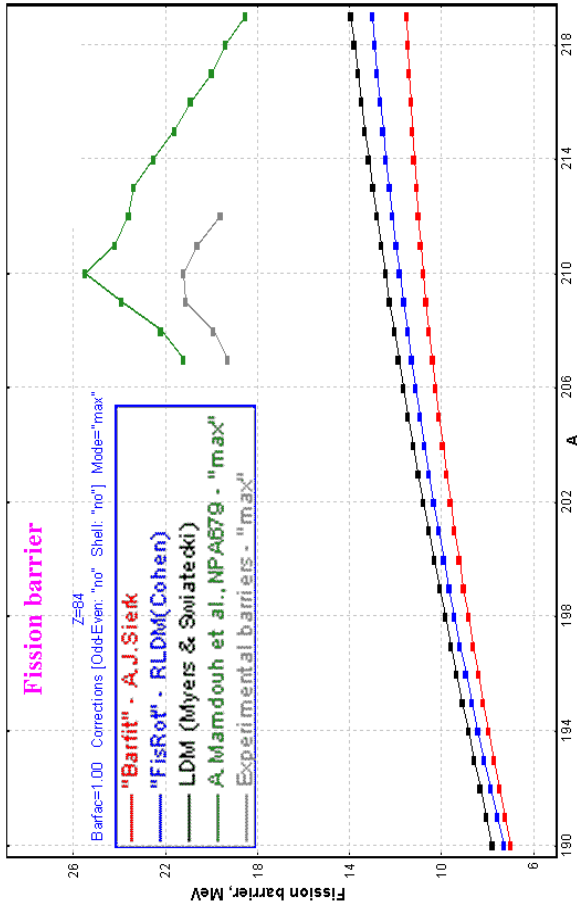


Fig.19. Fission barriers of Polonium isotopes calculated without shell and odd-even corrections.

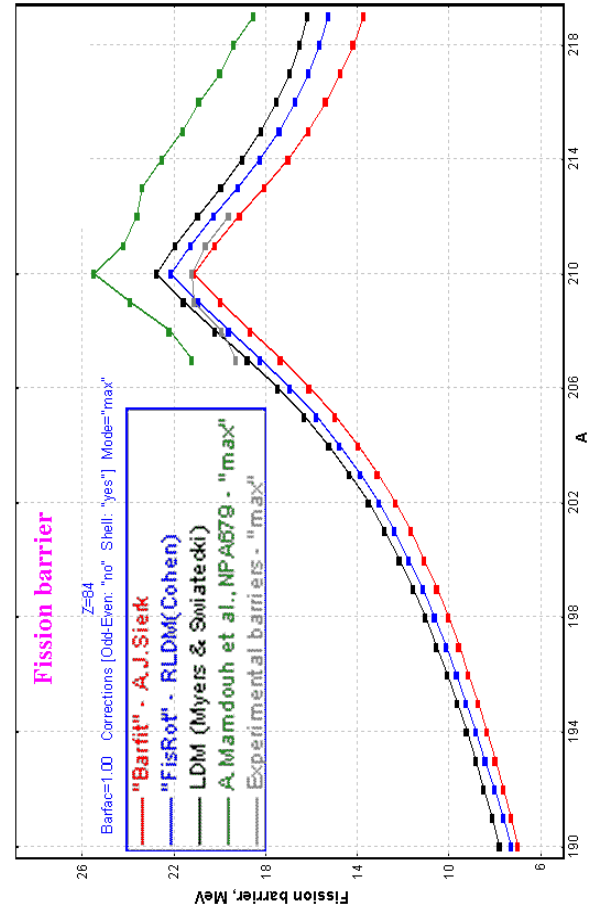


Fig.20. Fission barriers of Polonium isotopes calculated with shell and without odd-even corrections.

### 3.4. Fission barrier plot

Some LISE fission barrier plots have already been shown in the previous chapter. Use the “Fission barrier plot” button from the “Fission barrier” dialog (see Fig.18) to build the “Fission barrier plot” dialog (see Fig.23).

There are several opportunities to plot fission barrier values:

- One and two dimensional plots
- Differences between models
- ALL models together in one plot (see Fig.23).

But it works only if

- one-dimensional plot mode is selected
- plot one data set is selected (**not** difference between data sets)
- $X_{min} = X_{max}$

If one of these requirements is not met then the “All methods” string disappears in the drop-down list box.

An example of a 2D fission barrier plot is given in Fig.24 and an example of a plot of the difference between methods in Fig.25.

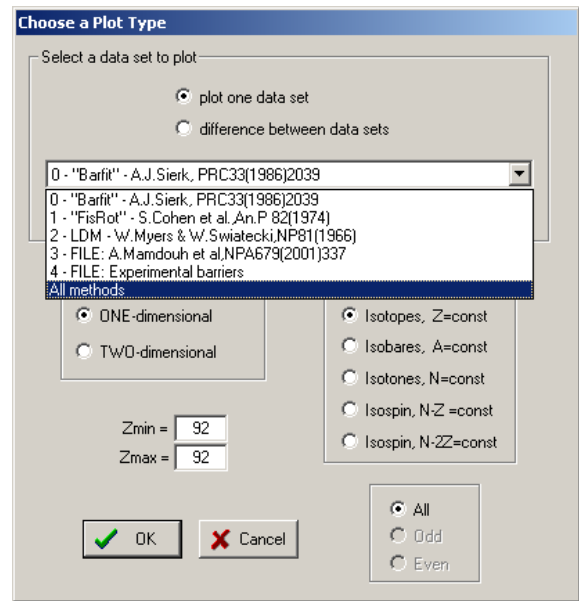


Fig.23. The “Fission barrier plot” dialog.

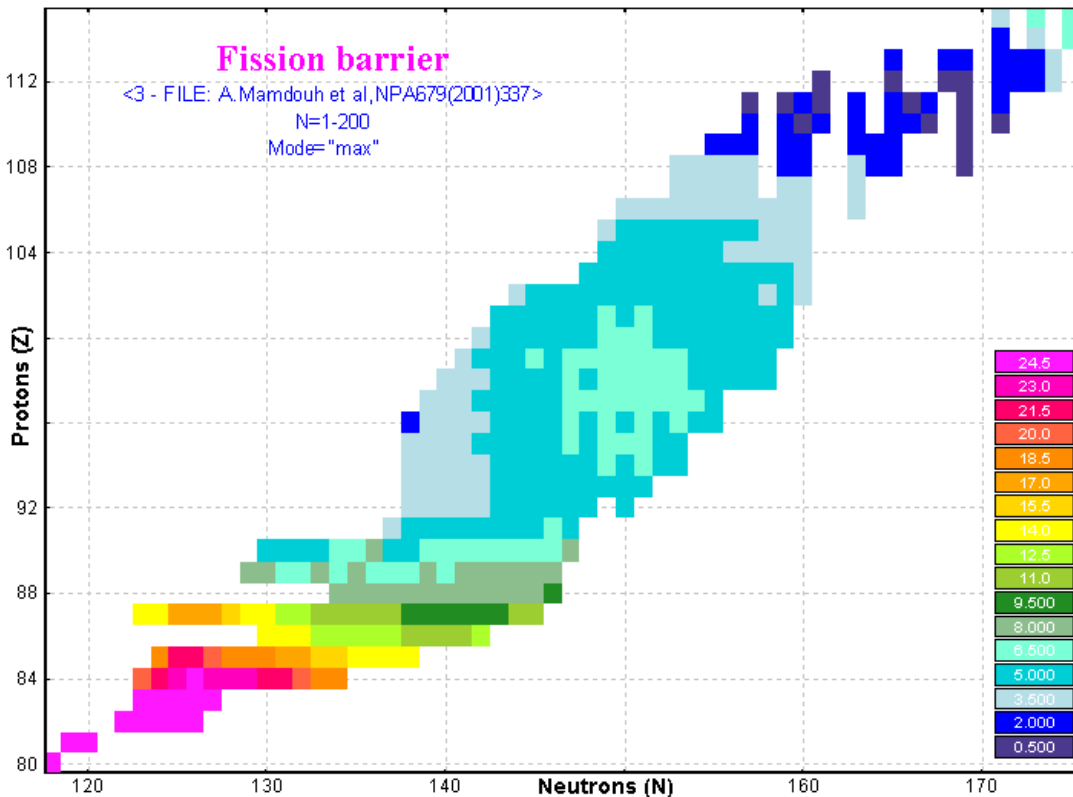
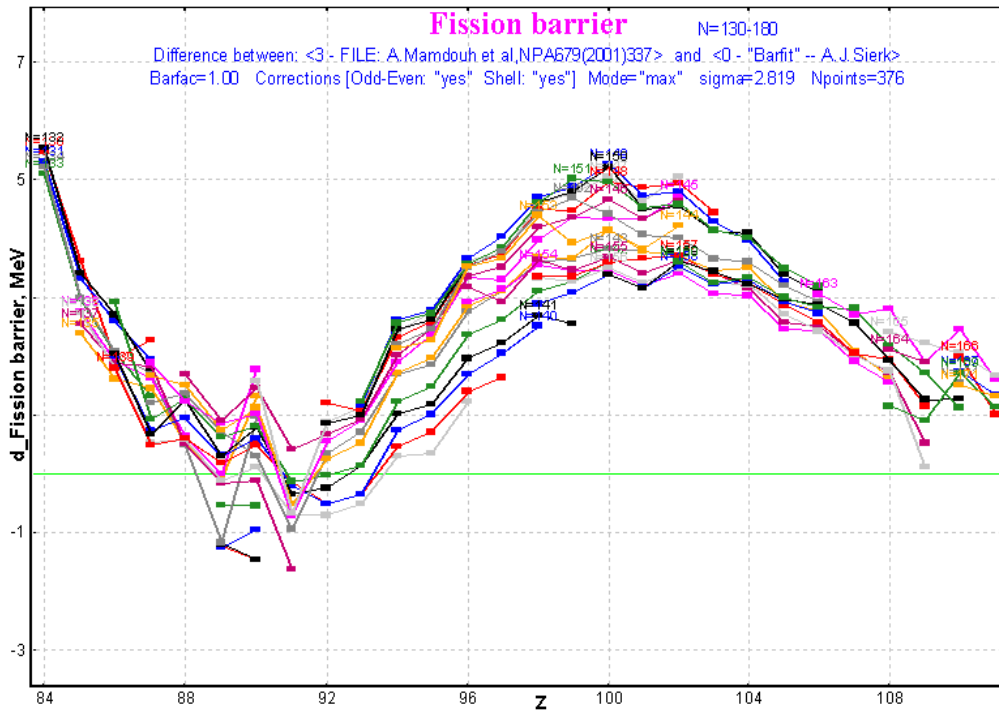


Fig.24. Example of the 2D fission barrier plot for the fission barrier model #3 (A.Mamdouh et al.)



**Fig.25.** Example of the fission barrier plot of the difference between models #3 (A.Mamdouh et al.) and #0 (A.Sierk).

### 3.5. Influence of corrections for fission barriers on abrasion-fission cross-sections

Fission summary excitation functions with and without shell corrections for fission barriers of fissile nuclei produced in the reaction  $^{238}\text{U}(1\text{A GeV})+\text{Be}$  are shown in Fig.26. The insert on the figure shows channel cross-sections. It can be seen that shell corrections for fission barriers increase residue production by 40% and decrease the fission channel probability. Abrasion-ablation model parameters used were the same as shown in Fig.13 except Kramers' factor was turned off and the reduced dissipation coefficient  $\beta$  was set to  $1.5 \cdot 10^{21} \text{ s}^{-1}$ .

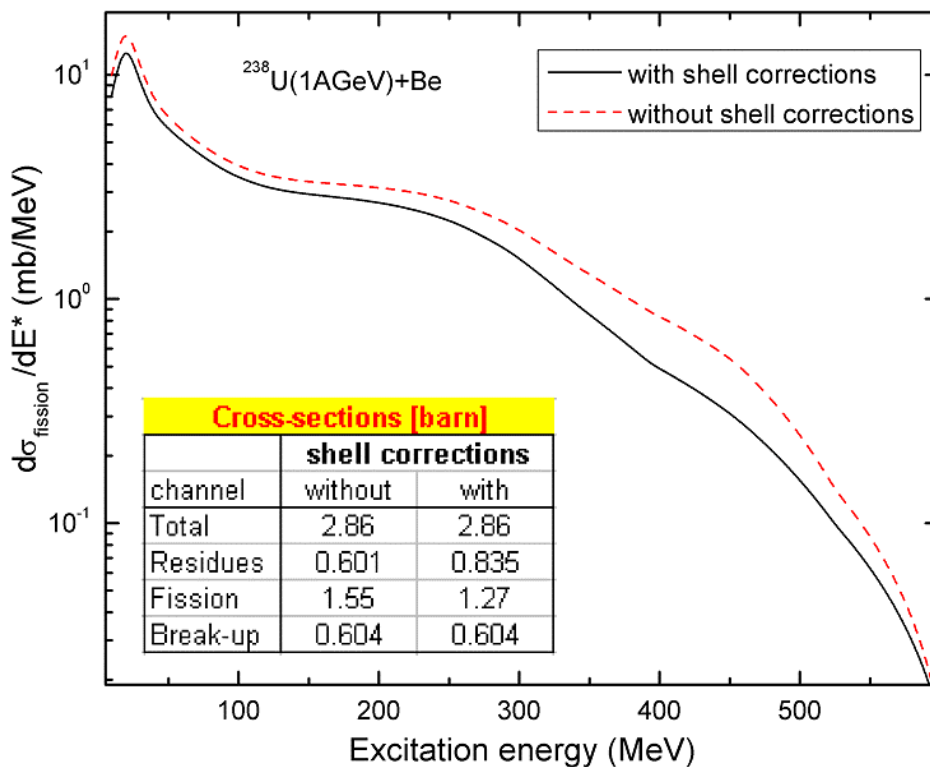


**Fig.26.** Fission summary excitation functions with/without shell corrections for fission barriers of fissile nuclei produced in the reaction  $^{238}\text{U}(1\text{A GeV})+\text{Be}$ .

## 4. Secondary reactions in target

### 4.1. Reexamination of secondary reactions calculation procedure

The secondary reactions (SR) calculation procedure has undergone some cardinal changes due to the following causes:

□ **The dependence on the dimension value** ( $NP_{evap}$ ) of SR distributions. The previous algorithm of calculations was valid, when the target ( $T$  - thickness) was divided into  $NP_{evap}$  slices, the condition  $T \cdot \sigma / NP_{evap} \rightarrow 0$  is true. In other words there should not be a difference at the end of the target between calculations if different values of  $NP_{evap}$  are used.

□ **A zero primary fragment cross-section.** The code multiplied a coefficient by the primary fragment cross-section output to include a SR contribution:  $Y_{final} = Coef_{secondary} \cdot Y_{primary}$ .

This is correct for EPAX where a non-zero production cross-section exists for each nucleus if its neutron and proton numbers do not exceed the neutron and proton numbers of the primary beam correspondingly. But in the case of Abrasion-Ablation or fission induced reactions there are a lot of nuclei produced just due to secondary reactions with a zero primary production cross-section.

□ **The new reaction mechanism: Abrasion-fission.** In this case the first-step reaction is assumed to always correspond to the reaction mechanism set in the code, but for the second and the following steps the projectile fragmentation mechanism is assumed, and just the EPAX parameterization is used to calculate secondary cross-sections to make it faster.

□ **The calculation speed is a very important factor in the case of heavy projectiles like  $^{238}\text{U}$ .**

#### 4.1.1. Dependence on the distribution dimension ( $NP_{evap}$ )

To expedite the evaluation of the analytical formulas for two-step reactions, and in order to include all multi-step processes, the program LISE++ uses numerical integration. At each target slice  $dx$  the yield of each fragment  $i$  produced by secondary reactions (i.e. other than the direct-one-step-fragmentation) is calculated using the formula:

$$dN_i = \sum_j^{\text{rhombus}} \sigma_{j \rightarrow i} N_j dx - \sigma_i N_i dx, \quad /9/$$

with initial conditions  $N_i = 0$  and  $N_P = 1$ , where  $P$  stands for the projectile and  $i$  for the fragments. The summation in Eq./9/ is limited to a rhombus domain which includes the projectile and the fragment, in order to exclude contributions from negligible secondary reactions. The contribution from secondary reactions is then added to the total yield of each fragment before the next iteration. The number of iterations can be varied and as already was said in the case of thick slices ( $dx = T / NP_{evap}$ ) this method is not correct.

The new procedure to calculate SR contributions constitutes an iteration method with a complicated analytical solution based on equations (5-11) of the LISE paper [Baz02].

After this reexamination of secondary reactions, it is recommended not to use large dimensions of SR distributions in the case of calculation of SR coefficients for all fragments (mode #1 in the “Secondary



reactions in target“ dialog in Fig.28). The default value is 16 and the user can make sure himself there is not a huge difference in SR coefficients with the use of  $NP_{evap} = 16$  or  $NP_{evap} = 128$ . In the mode #1 the code uses SR calculations just at the end of the target, but a large value of  $NP_{evap}$  is required for the optimal thickness target procedure where the code needs to get the SR coefficient at any point in the target. In this case the code automatically increases the  $NP_{evap}$  value up to 128 just temporarily.

#### 4.1.2. The "Secondary reactions" dialog modification

In the new version all operations with secondary reactions were moved from the "Preferences" dialog to the "Secondary reactions in target" dialog (see Fig.28), which is available from the "Options" menu (see Fig.27). If you want to set SR calculations then use the checkbox in the upper part of the dialog.

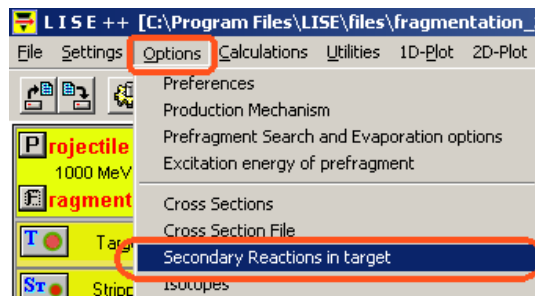


Fig.27. The "Options" menu.

Where are secondary reactions used in LISE?

#0 - Optimum target thickness calculations. The SR coefficient is needed just for the fragment of interest, but the coefficient should be calculated at different thickness values.

#1. Produce secondary reaction coefficients for all fragments transmitted through a spectrometer to calculate final rates of fragments. It is necessary to use SR coefficients only at the end of the target.

#2. Secondary reactions contribution analysis in the "Secondary Reactions" dialog. Use the corresponding button (see Fig.28).

Note: Don't forget to click the "Apply" button to accept changes for any calculations in this dialog. If the user clicks the "Ok" button, then he leaves the dialog and all changes done by him will be automatically accepted.

#### 4.1.2.1. Secondary reactions analysis plots

There are very convenient tools to analyze the dependence of the output of secondary reactions on target thickness (Fig.29), to get information on what intermediate fragments give the largest contribution of secondary reactions to the final output of the nucleus of interest (Fig.30), and to see if the filter was effectively chosen.

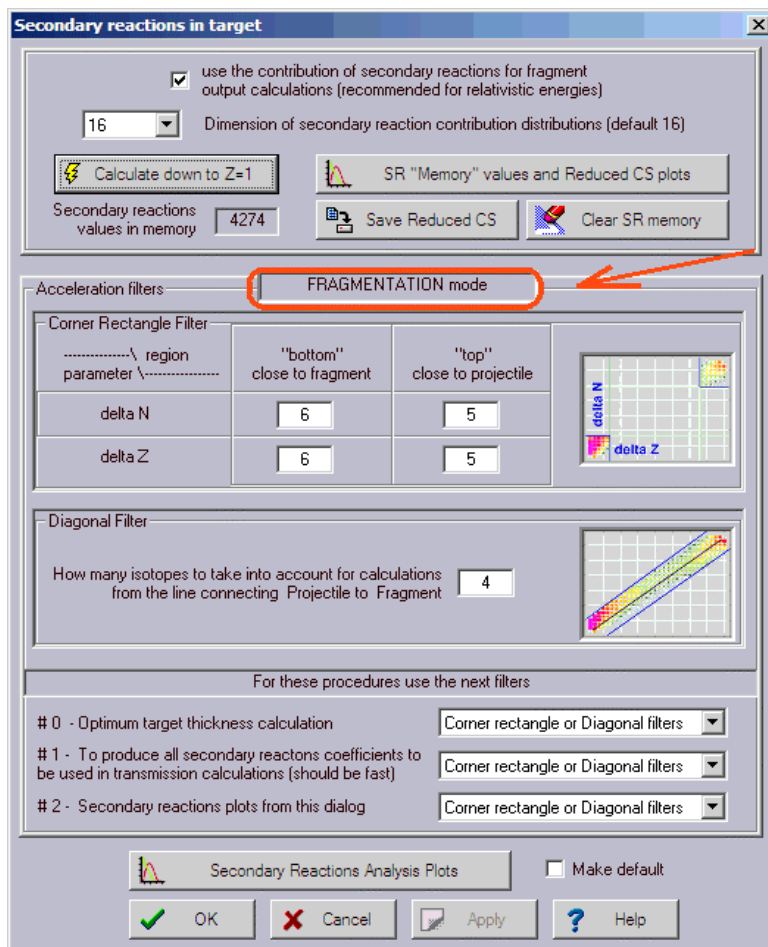
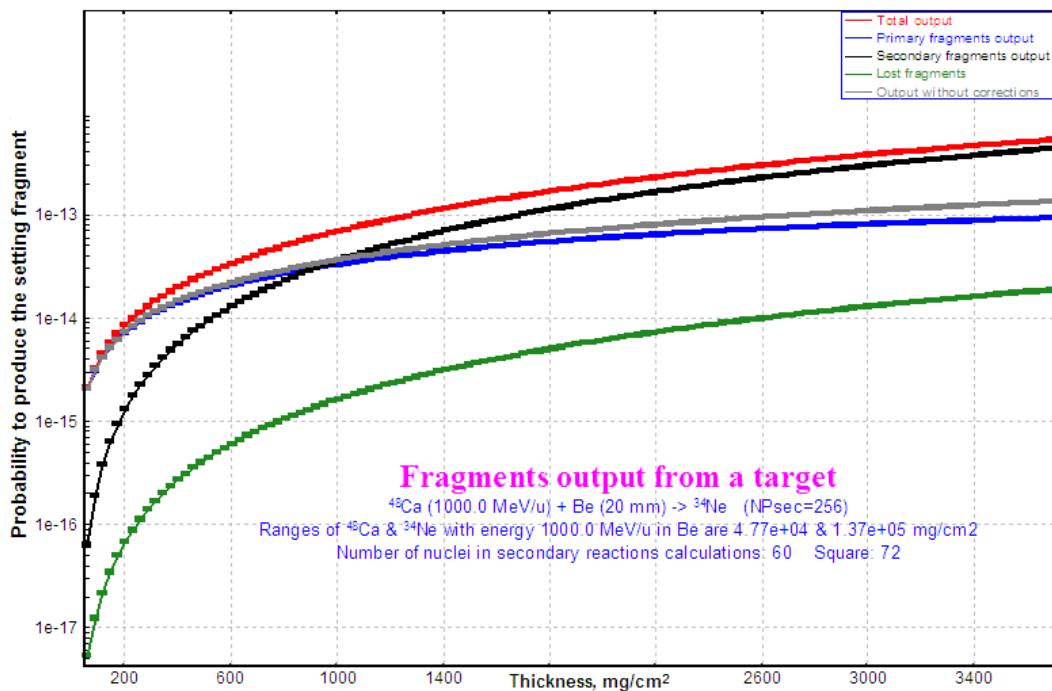


Fig.28. The "Secondary reactions in target" dialog.



**Fig.29.** Probability (per one particle of the primary beam) from Be-target thickness value to produce the  $^{34}\text{Ne}$  nucleus in the fragmentation of  $^{48}\text{Ca}$  beam, taking into account secondary reactions in the target. See Table 1 for definitions of curves.

**Table 1.** Definitions of curves in Fig.29.

Value	Definition
Total output	Sum of primary output ( $^{48}\text{Ca} \rightarrow ^{34}\text{Ne}$ ) and secondary contributions ( $^{48}\text{Ca} \rightarrow ** \rightarrow ^{34}\text{Ne}$ ) taking into account the loss of fragments of interest and primary beam particles due to reactions with atoms of the target.
Primary fragment output	primary output ( $^{48}\text{Ca} \rightarrow ^{34}\text{Ne}$ ) taking into account losses of fragment of interest and primary beam particles due to reactions with atoms of the target.
Secondary output	secondary contributions ( $^{48}\text{Ca} \rightarrow ** \rightarrow ^{34}\text{Ne}$ ) taking into account the loss of fragment of interest and primary beam particles due to reactions with atoms of the target.
Lost fragments	Loss of $^{34}\text{Ne}$ fragments in a target slice (produced in primary reactions as well as in secondary reactions) due to reactions with target atoms.
Output without corrections	No secondary reactions, no reactions of produced $^{34}\text{Ne}$ fragments with the target. This is valid for very thin targets.

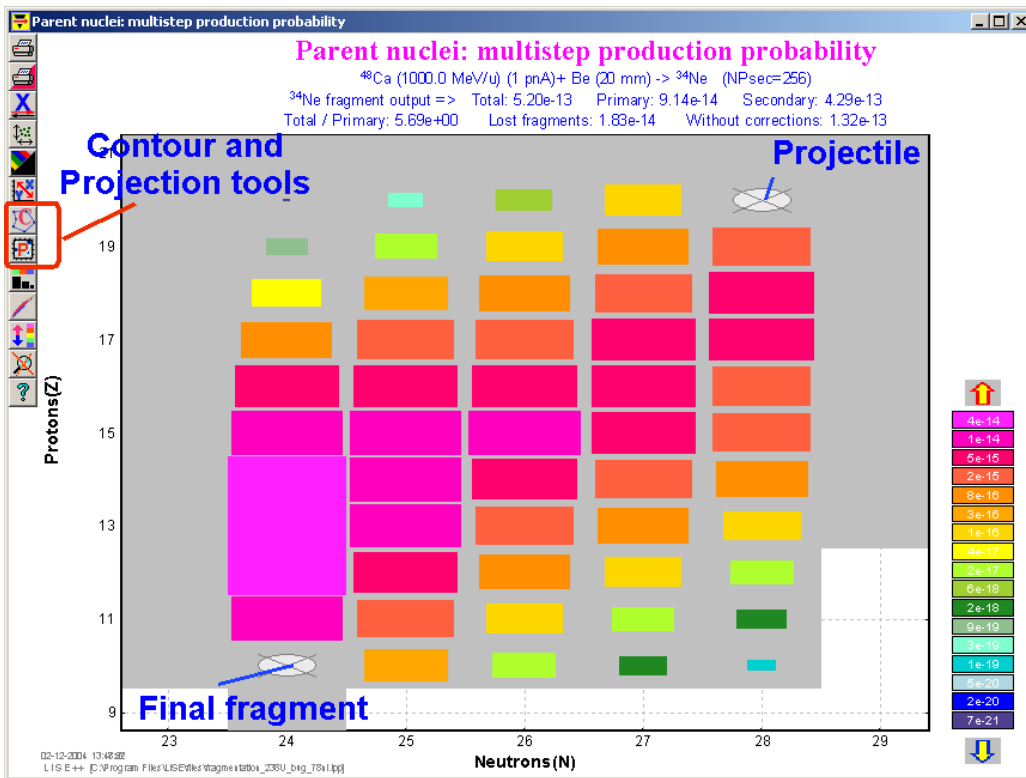
Fig.29 shows the probability to produce the fragment of interest ( $^{34}\text{Ne}$ ) per one particle of the primary  $^{48}\text{Ca}$  beam. It can be seen that at the Be-target thickness equal to  $1\text{g}/\text{cm}^2$ , the secondary reactions contribution begins to dominate over the primary fragment output.

Fig.30 shows the probability to produce the final fragment through intermediate nuclei. It is possible to see from the figure that isotones  $N=24$  ( $^{36}\text{Mg}$ ,  $^{37}\text{Al}$ ,  $^{38}\text{Si}$ ) are the most probable intermediate nuclei to produce  $^{34}\text{Ne}$  in secondary reactions.

#### 4.1.3. Determination of the region of nuclei for secondary reactions calculations

It is possible to load the procedure to calculate secondary reaction coefficients in two ways: from the SR dialog (the “Calculate down to  $Z=1$ ” button in Fig.28) and by clicking on the isotope of interest ( $Z_i, N_i$ ) with the right mouse button. In the previous version in the second case, the code calculated SR coefficients just for nuclei in a rectangle ( $Z_i, N_i, Z_p, N_p$ ) determined by the projectile ( $Z_p, N_p$ ) and the





**Fig.30.** Two-dimensional plot of the probability to produce the  $^{34}\text{Ne}$  nucleus through intermediate nuclei from fragmentation of the  $^{48}\text{Ca}$  beam on a Be-target (20mm).

fragment clicked. But if the user clicked the next left isotope or the next lower isotone the code began to recalculate SR coefficients again, for the new rectangle ( $Z_i, N_i-1, Z_p, N_p$ ) for example.

In the new version if the user clicks on the isotope in the table of nuclides, with mode secondary reactions turned on, then the code asks the user to choose a range for nuclei (see Fig.31). There are three possibilities to define the user's region for calculations. After 5 seconds if the user did not choose something in this dialog then the dialog will be closed, selecting the mode "All nuclei".

The user can press the "Escape" key to break secondary reactions calculations.

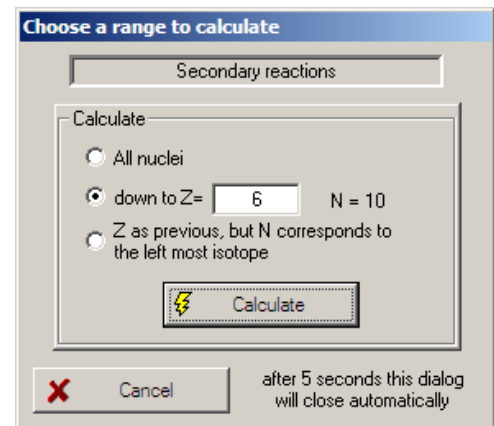


**Fig.31.** The "Choose a range for calculations" dialog in the "secondary reactions in target" mode.

#### 4.1.4. Revision of optimal target thickness calculations for SR mode

There are two principal changes done in the new version:

- ❑ Plot of the secondary reaction coefficient versus target thickness;
- ❑ Consideration of the situation when a fragment primary production cross-section is equal to zero.

The code plots the distribution (pink curve in Fig.32) of the SR coefficient from the target thickness in the "Transmission for optimal target plot" if SR mode is turned on. If a fragment primary production cross-section is equal to zero then the SR coefficient is always equal to 1.

Fig.33 and Fig.34 show LISE++ calculation examples of optimal thickness target plots for cases with non-zero and with zero primary production cross-sections respectively.

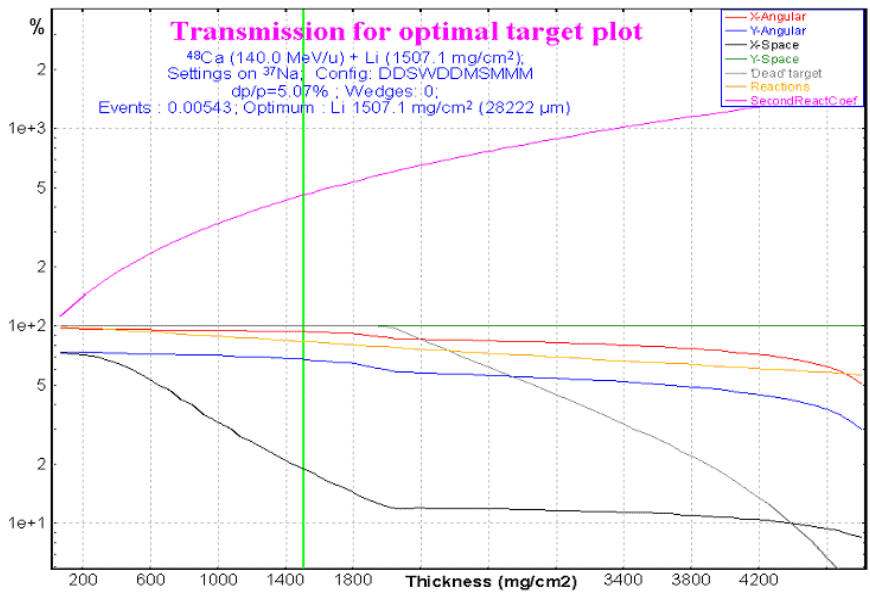


**Fig.32.** Transmission coefficients versus target thickness for production of the  $^{37}\text{Na}$  nucleus in the reaction  $^{48}\text{Ca}(140\text{AMeV}) + \text{Be}$  with the A1900 fragment separator. The secondary reaction coefficient (pink color) is always more or equal to 1.

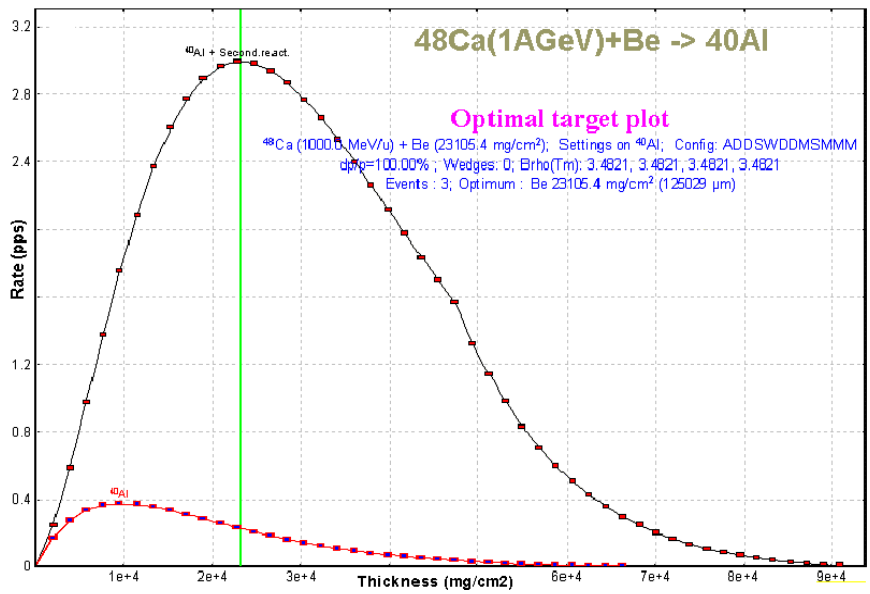


**Fig.33.** Rates of  $^{40}\text{Al}$  fragments produced in fragmentation of the  $^{238}\text{U}(1\text{AGeV})$  for different Be-target thickness with SR contribution (black curve) and without SR contribution (red curve).

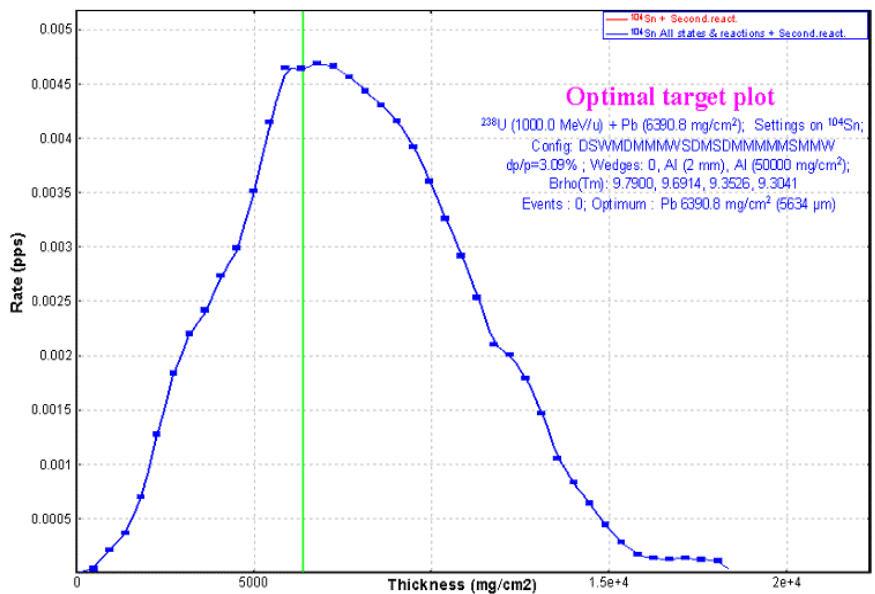


**Fig.34.** Rates of  $^{104}\text{Sn}$  fragments produced in induced fission of the  $^{238}\text{U}(1\text{AGeV})$  beam for different Pb-target thicknesses with SR contribution. The primary cross-section to produce  $^{104}\text{Sn}$  is equal to zero.

## 4.2. Calculation of secondary reaction contributions to fragments with zero primary production cross-section

As was already mentioned before, the code in the previous version used a coefficient multiplied with the primary fragment cross-section output to include a SR contribution:  $Y_{final} = Coef_{secondary} \cdot Y_{primary}$ . This means it was not possible to calculate the SR contribution to a nucleus' rate if the primary production cross-section was equal to 0.

In order to use the SR contribution for nuclei with zero primary production cross-sections the following assumptions have been implemented in the code:

- If the primary production cross-section is equal to zero in the user cross-section file or in the calculations when the SR mode is turned on, then the code sets the primary production cross-section ( $\sigma_{primary}$ ) equal to  $1e-99$  mb.
- The code calculates the SR coefficient ( $\tau_{SR}$ ) relative to the new primary production cross-section ( $\sigma_{primary}^*$ ).
- The code calculates the reduced production cross-section of the fragment, which will be used for the next step in the calculations of the fragment rate.

$$\sigma_{reduced} = \sigma_{primary}^* \cdot \tau_{SR} \quad /10/$$

*Note:* A reduced cross-section is a function of the target thickness!

- Then LISE++ sets  $\tau_{SR}$  equal to 1. In this case, if you click on the isotope in the table of nuclides, you will get the statistics window with the message “Zero cross-section has been changed due to secondary reactions” (see left plot in Fig.35) and with the **reduced** cross-section value. In the case of fragments with non-zero primary cross-section the code shows the **primary** production cross-section value and the **un-modified** SR coefficient (see right plot in Fig.35).

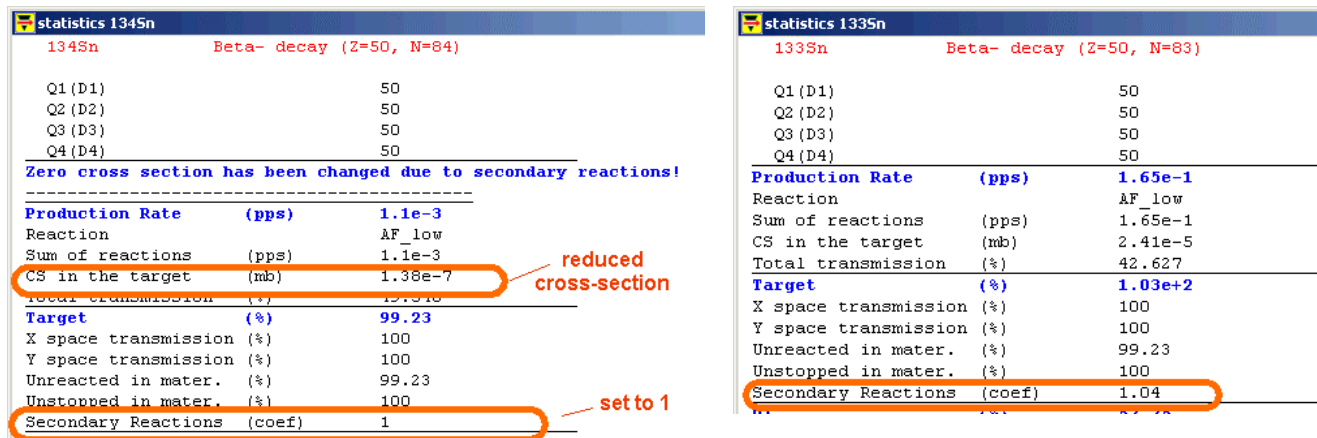


**Fig.35.** Statistics windows for transmission of  $^{134}\text{Sn}$  and  $^{133}\text{Sn}$  fragments produced in induced fission of  $^{238}\text{U}$  (1 AGeV) beam using a Be target (0.2 mm thickness).

Fig.36 shows the production rates of fragments produced in the abrasion-evaporation of a  $^{238}\text{U}$  (1 AGeV) beam just after the Be-target (10 mm). The left (right) plot shows production rates without(with) SR con-

tributions. The calculations were done with the primary production cross-sections calculated by LISE’s Abrasion-Ablation model taking into account fission and break-up de-excitation channels.

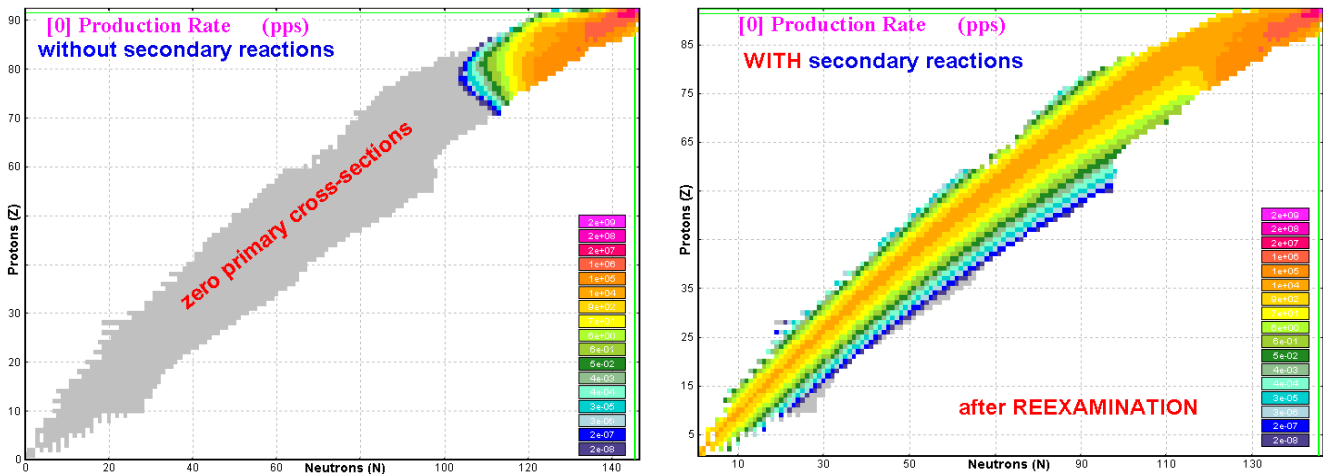


**Fig.36.** Production rates of fragments just after the 10 mm Be-target produced in Abrasion → Residues reaction with a  $^{238}\text{U}(1\text{AGeV})$  beam without (left) and with (right) SR contribution.

#### 4.2.1. Secondary Reactions plots: SR coefficients & reduced cross-sections

It is possible to visualize the results of the SR coefficients calculations using the “SR memory plot” button in the “Secondary reactions in target” dialog (see Fig.28).

Fig.37 shows the SR coefficients for fragments with non-zero primary cross-sections produced in the fragmentation of a  $^{86}\text{Kr}(400\text{AMeV})$  beam on a Lithium target (10 mm). Primary cross-sections were calculated with the EPAX parameterization. From this plot it is visible for which nuclei it is possible to gain in final fragment output due to the contribution of secondary reactions.

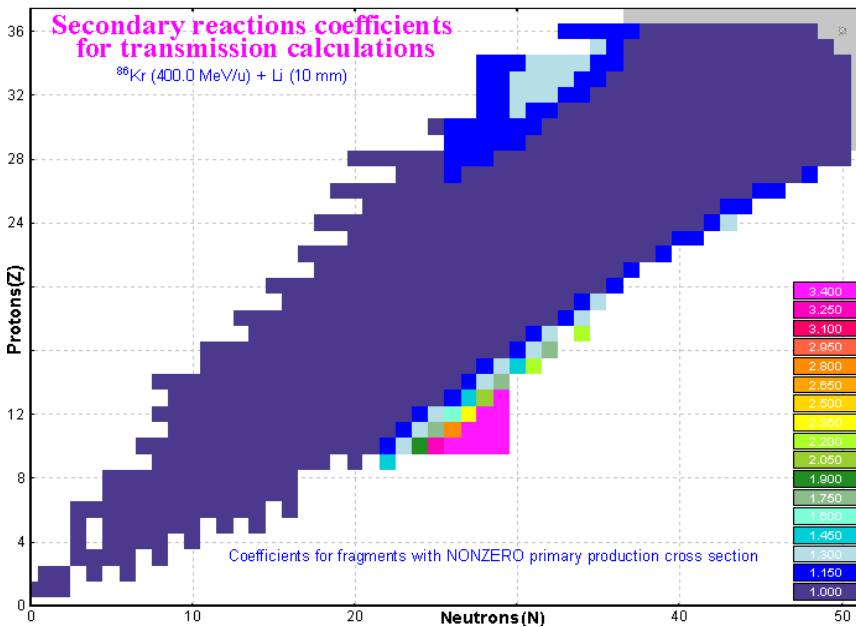
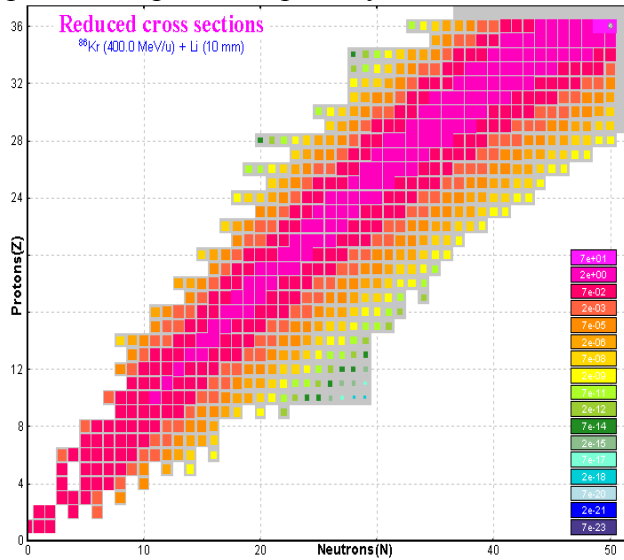


**Fig.37.** Secondary reactions coefficients for fragments produced in fragmentation (EPAX 2.15) of a  $^{86}\text{Kr}(400\text{AMeV})$  beam on a Lithium target (10 mm).

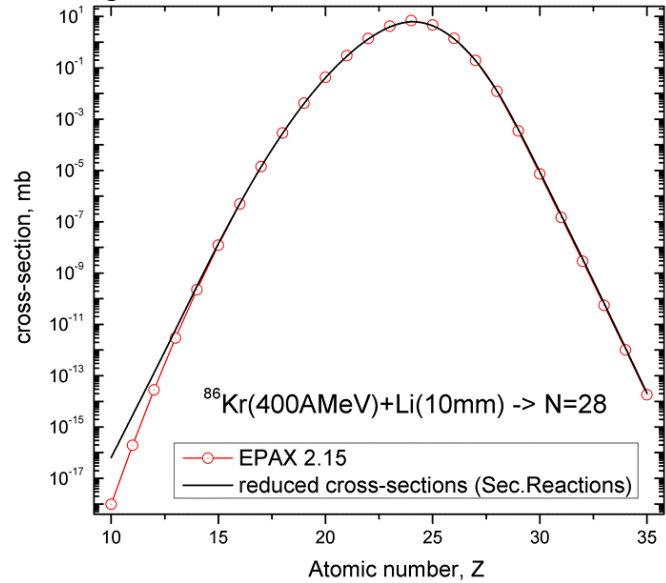
Reduced cross-sections can be saved (see Fig.28) in the user cross-section file with extension “cs2” and then the user can load them as “user” cross-sections through the “cross-section file dialog”.

Fig.38 shows the reduced cross-sections for fragments produced in the fragmentation (EPAX 2.15) of a  $^{86}\text{Kr}(400\text{AMeV})$  beam on a Lithium target (10 mm). Reduced cross-sections are calculated using Eq./10/ and provide very important information in the case of zero-primary cross-sections. Using this plot and the new tool of projection onto an axis for two-dimensional plots (see 9.4.1.1. Window and

contour projections on an axis for 2D Cross-section plot) the user can extract data to a projection 1D-plot to compare with primary cross-sections as shown in Fig.39 for isotones with  $N=28$ .



**Fig.38.** Reduced cross-sections for fragments produced in the fragmentation (EPAX 2.15) of a  $^{86}\text{Kr}(400\text{AMeV})$  beam on a Lithium target (10 mm).



**Fig.39.** Reduced cross-sections (black curve) and EPAX calculations (red curve) for isotones with  $N=28$  produced in the fragmentation of a  $^{86}\text{Kr}(400\text{AMeV})$  beam on a Lithium target.

The SR calculation procedure in the case of Abrasion – Fission has several peculiarities which will be described later on in chapter 5.5. Secondary reactions for Abrasion-Fission.

### 4.3. SR calculation speed

SR calculation speed becomes a very important characteristic with increasing projectile mass. In the case of light projectiles ( $^{40}\text{Ar}$ ,  $^{48}\text{Ca}$ ), the elapsed time to calculate all SR coefficients is about several seconds, whereas for projectile fragmentation of a  $^{238}\text{U}$  beam ( $N_{\text{Pevap}}=16$ ) it increases to 224 seconds! To calculate all SR coefficients, the code takes from the table of nuclides the most left ( $N_{\text{min}}$ ), right ( $N_{\text{max}}$ ), top ( $Z_{\text{max}}$ ) and bottom ( $Z_{\text{min}}$ ) nuclei to create an initial rectangle of calculations. This means the rectangle is defined by the projectile and proton ( $0, 1, N_{\text{beam}}, Z_{\text{beam}}$ ) and the number of isotopes participating in SR calculations is equal to  $(N_{\text{beam}}+1) \cdot Z_{\text{beam}}$ . The code calculates final SR coefficients only for existing nuclei in the table of nuclides. As a result there are 2536 nuclei used to calculate SR coefficients for the projectile fragmentation of  $^{238}\text{U}$  beam and 194 nuclei for the  $^{40}\text{Ar}$  beam respectively.

One of the possibilities was already mentioned above in chapter 4.1.3., “Determination of the region of nuclei for secondary reactions calculations”, to avoid SR calculations for elements with low atomic number ( $Z$ ), if not needed by the user.

After reexamination of the SR calculations procedure (see chapter 4.1.1. Dependence on the distribution dimension ( $N_{\text{Pevap}}$ )) it is recommended to the use smallest value of the SR distribution dimension, which is 16. The quality of the calculations does not undergo crucial changes when increasing the calculation speed. Table 2 demonstrates that an increase of the SR distribution dimension by a factor of 16 corresponds to an increase of the elapsed time by a factor of 17 and a decrease of in calculation quality of about 6 percent.

**Table 2.** Results of the  $^{78}\text{Ni}$  SR coefficient calculations produced in the fragmentation of a  $^{238}\text{U}(1\text{AGeV})$  beam on a Beryllium target ( $11\text{ g/cm}^2$ ) as a function of the SR distribution dimension. Calculations were done without acceleration filters using mode #2 (Secondary reactions contribution analysis). EPAX parameterization was used to calculate the primary production cross-sections.

Dimension, NPevap	Time elapsed, sec	$^{78}\text{Ni}$ SR coefficient	Total probability to produce $^{78}\text{Ni}$ per one particle of the beam
16	82	59.6	4.58e-17
32	170	61.5	5.10e-17
64	354	62.4	5.27e-17
128	715	62.8	5.46e-17
256	1380	63.0	5.52e-17

#### 4.3.1. Acceleration filters for secondary reactions calculations

To significantly decrease SR calculation time in the case of heavy projectiles, the “acceleration filters” have been developed and incorporated into the code. The main idea of the acceleration filters is to decrease the number of intermediate parent nuclei. The filters exclude intermediate nuclei with small SR contribution to the final nucleus. There are two kinds of filters “corner rectangle” and “diagonal” based on methods to truncate regions.

**Note:** It is recommended for a new combination of beam & target to run the SR calculations procedure without filters to clarify from the “Parent nuclei: multi-step production probability” plot what kind of filters and parameters are needed.

##### 4.3.1.1. Corner rectangle filter

Results of the multi-step production probability of  $^{78}\text{Ni}$  fragment SR calculations produced in a fragmentation of a  $^{238}\text{U}(1\text{AGeV})$  beam on a Beryllium target ( $11\text{ g/cm}^2$ ) are shown in Fig.40. The EPAX parameterization has been used to calculate the primary production cross-sections.

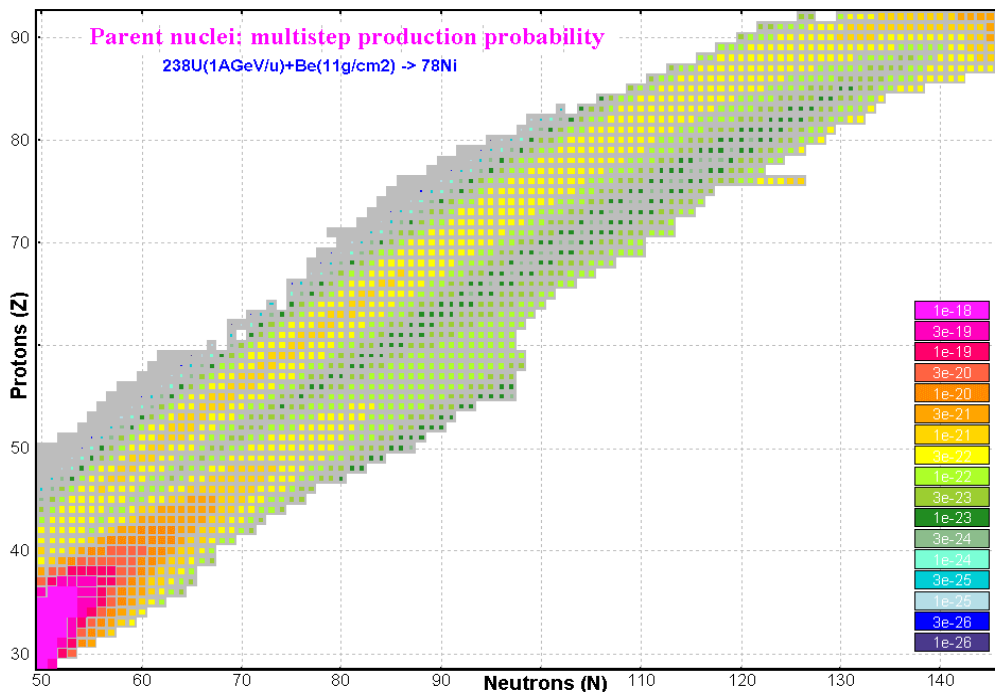


**Fig.40.** The “Parent nuclei: multi-step production probability” plot for  $^{78}\text{Ni}$  fragments from the fragmentation of  $^{238}\text{U}(1\text{AGeV})$  on a Be target (thickness  $11\text{g/cm}^2$ ). No filters were applied for calculation of this plot.



Projections of the 2D-plot in Fig.40 on the horizontal and the vertical axis are shown in Fig.41. Blue rectangles on both plots of Fig.41 indicate regions with insignificant production contribution to  $^{78}\text{Ni}$  final output. More intense parent nuclei are located close to the final fragment and projectile. In order to increase the SR calculations speed it is necessary to cut the regions with insignificant production contribution or in other words just to select regions close to the final fragment and the projectile. To exclude nuclei with small contributions, the rectangle filter has been incorporated into the code for SR calculations.

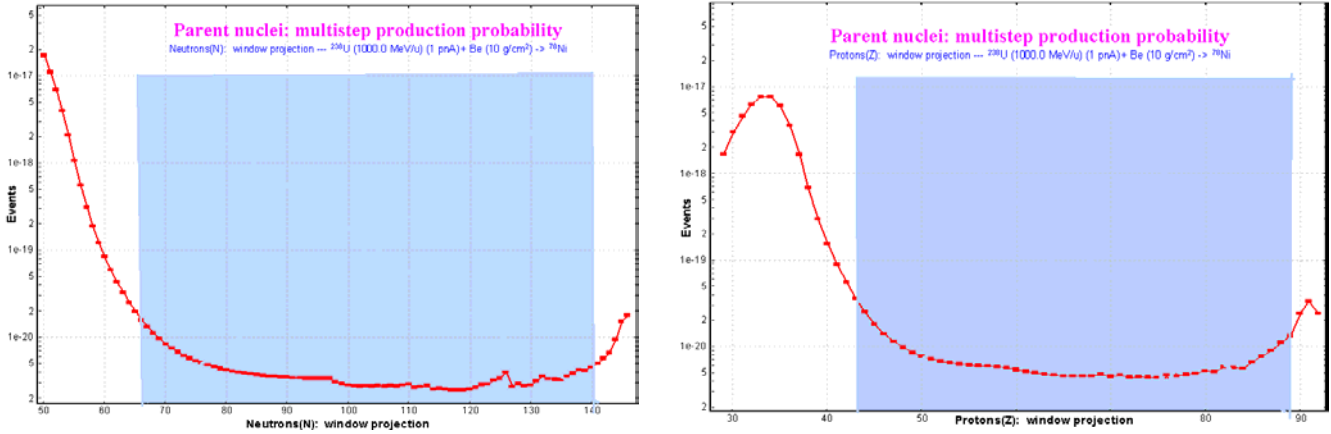


**Fig.41.** Projections of the 2D-plot in Fig.40 on horizontal (corresponds to neutrons) and vertical (corresponds to proton) axis.

The rectangle filter can be applied for all three modes using secondary reactions (see the “Secondary reactions in target” dialog in Fig.28). The rectangle filter has four parameters (two  $\delta N$  and two  $\delta Z$ ), which determine the sizes of two rectangles (top and bottom) to cut the necessary regions. How the filter works and what the parameters mean is easy to understand from Fig.42, which shows the same plot as Fig.40 but with the rectangle filter applied.

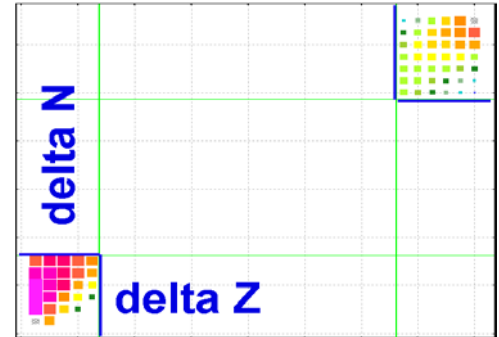


**Fig.42.** The same plot as Fig.40 but the rectangle filter has been applied.

Table 3 shows the elapsed time and SR coefficient values depending on the parameters of the rectangle filter to estimate the SR contribution for  $^{78}\text{Ni}$  fragments produced in the fragmentation of a  $^{238}\text{U}$  (1AGeV) beam on a Beryllium target ( $11\text{ g/cm}^2$ ).

**Table 3.** Results of the  $^{78}\text{Ni}$  SR coefficient calculations produced in fragmentation of a  $^{238}\text{U}$  (1AGeV) beam on a Beryllium target ( $11\text{ g/cm}^2$ ) depending on the parameters for the rectangle filter. Calculations were done for SR distribution dimension 16 (except the last row where  $NP_{\text{evap}}=128$ ) using mode #2 (Secondary reactions contribution analysis). The EPAX parameterization was used to calculate the primary production cross-sections.

Rectangle filter				Time elapsed (sec)	$^{78}\text{Ni}$ SR coefficient	Total probability to produce $^{78}\text{Ni}$ per one beam particle
bottom		top				
$\delta N$	$\delta Z$	$\delta N$	$\delta Z$			
No filter	No filter	No filter	No filter	84	59.6	4.58e-17
35	35	20	20	21.5	53.9	4.14e-17
25	25	10	10	6.5	50.9	3.91e-17
20	15	8	8	1.32	49.2	3.79e-17
15	12	4	4	< 0.3	47.7	3.67e-17
15	12	4	4	4.69 (NP=128)	48.3	4.19e-17

### 4.3.1.2. Diagonal filter

Results of multi-step production probabilities of  $^{26}\text{Ne}$  fragment SR calculations produced in the fragmentation of a  $^{48}\text{Ca}$  (1AGeV) beam on a Beryllium target (20 mm) are shown in Fig.43. The EPAX parameterization has been used to calculate the primary production cross-sections.

Projections of the 2D-plot in Fig.43 on horizontal and vertical axes are presented in Fig.44. It is possible to see that in this case the difference between the maximum values and values in the center ( $N=22$  and  $Z=16$ ) is less than one order of magnitude, whereas in the case of  $^{78}\text{Ni}$  fragment SR calculations produced in the fragmentation of a  $^{238}\text{U}$  (1AGeV) beam on a Beryllium target (11 g/cm<sup>2</sup>) shown in Fig.40 this difference is more than 4 orders of magnitude. More intense parent nuclei are located close to the line connecting the final fragment and the projectile. In order to increase the SR calculation speed in this case it is necessary to select a region close to this line. This line looks like the diagonal of a rectangle; this is the reason why the new filter has been named “diagonal”.

#### Parent nuclei: multistep production probability

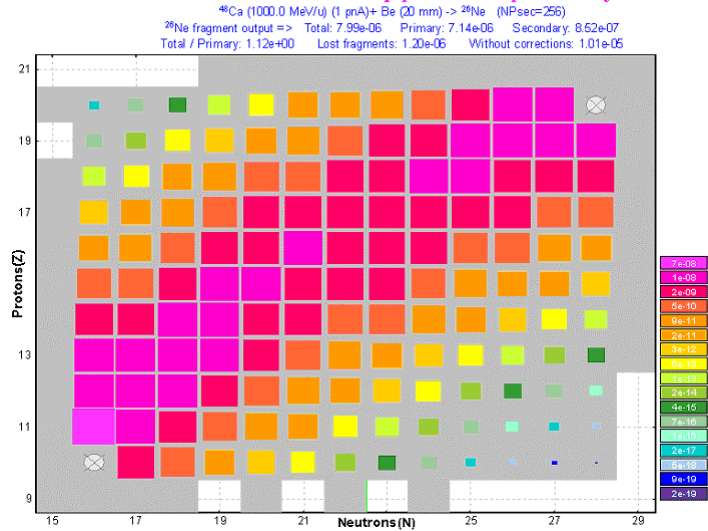


**Fig.43.** The “Parent nuclei: multi-step production probability” plot for  $^{26}\text{Ne}$  fragment in the fragmentation of a  $^{48}\text{Ca}$ (1AGeV) on Be target (thickness 10 mm). No filters were applied for this plot.

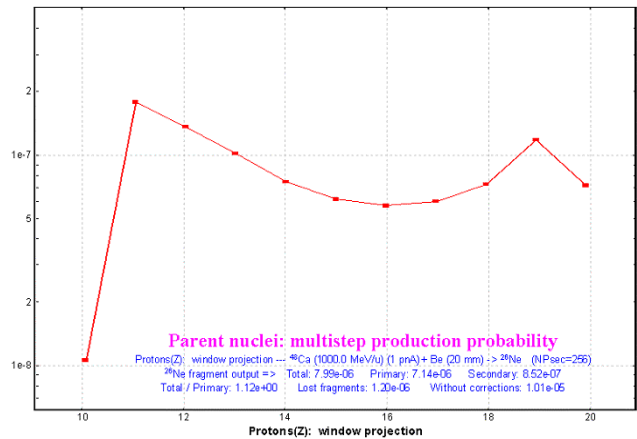
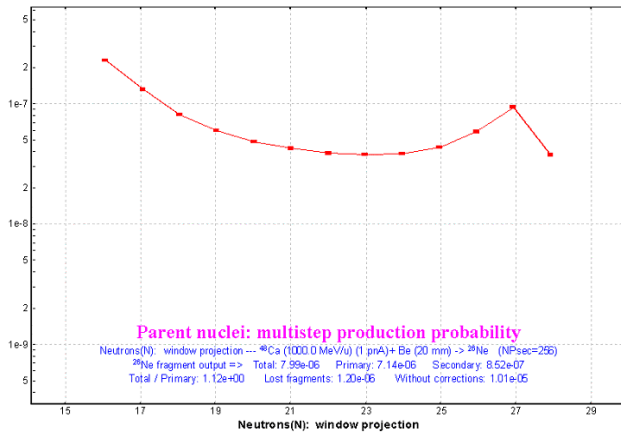


**Fig.44.** Projections of the 2D-plot in Fig.43 on horizontal (corresponds to neutrons) and vertical (corresponds to proton) axes.

The diagonal filter has just one parameter which is the “stripe width” of the cut. How the filter works and the parameter meaning is easy to understand from Fig.45, which shows the same plot as Fig.43 but with the diagonal filter applied.

Table 4 shows the elapsed time and SR coefficient values depending on the parameter of the diagonal filter to estimate the SR contribution for  $^{26}\text{Ne}$  fragments produced in the fragmentation of a  $^{48}\text{Ca}$  (1AGeV) beam on a Beryllium target (108 mm).

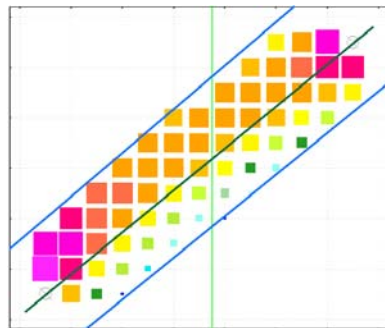


**Fig.45.** The same plot as Fig.43 but the **diagonal** filter has been applied. The “stripe width” parameter is equal to 3.



**Table 4.** Results of the  $^{26}\text{Ne}$  SR coefficient calculations for fragmentation of a  $^{48}\text{Ca}$  (1AGeV) beam on a Beryllium target ( $20\text{ g/cm}^2$  or  $108\text{ mm}$ ) depending on the parameter of the diagonal filter. Calculations were done for SR distribution dimension equal to 512 using mode #2 (Secondary reactions contribution analysis). The EPAX parameterization was used to calculate the primary production cross-sections.

Diagonal filter: Stripe width	Time elapsed, sec	$^{26}\text{Ne}$ SR coefficient	Total probability to produce $^{26}\text{Ne}$ per particle of the beam
No filter	16.6	1.80	$1.51\text{e-}5$
8	15.7	1.80	$1.51\text{e-}5$
6	13.4	1.80	$1.51\text{e-}5$
5	10.9	1.80	$1.51\text{e-}5$
4	7.9	1.79	$1.50\text{e-}5$
3	5.2	1.72	$1.44\text{e-}5$
2	2.3	1.53	$1.29\text{e-}5$
1	< 0.5	1.21	$1.02\text{e-}5$

### 4.3.1.3. Application of acceleration filters

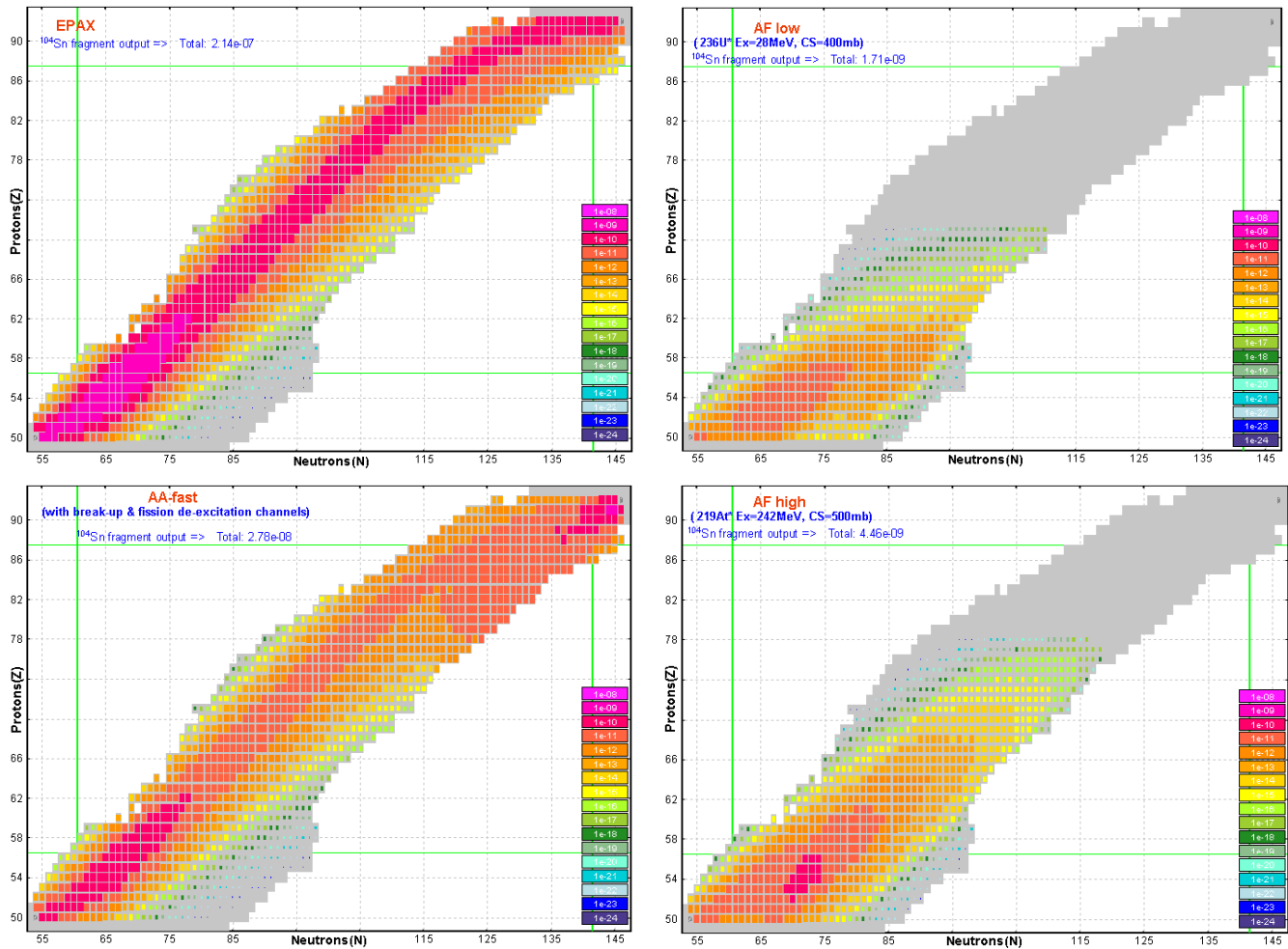


**Fig.46.** Multi-step production probabilities to produce  $^{104}\text{Sn}$  from the primary reaction  $^{238}\text{U}(1\text{AGeV}) + \text{Be}(11\text{g/cm}^2)$  using different reaction mechanisms. Left top: fragmentation (EPAX), Left bottom: fragmentation (Abrasion-Ablation, fast mode), Right top: Abrasion-Fission "low" ( $E_x=28\text{ MeV}$ ), Right bottom: Abrasion-Fission "high" ( $E_x=242\text{ MeV}$ ).

The selection of the filter type is determined by **the mode of SR calculation** (see Fig.28) and **the type of reaction mechanism** (see Fig.46). Based on this picture we can conclude:

- For fission reactions we do not need diagonal and top rectangle filter, but the bottom rectangle filter should have a large size;
- For fragmentation reaction we need the diagonal filter as well as both rectangle filters.

The code has two sets of filters: fragmentation and fission, and automatically uses the fragmentation set if the reaction mechanism is set to fragmentation. The fission filter set is used for all other reactions. If you want to edit the fission filter set you have to be sure that you are not working under fragmentation conditions. The current filter mode is shown in the middle of the “Secondary reactions” dialog (see Fig.28). Initially both these sets use acceleration filters and their default values are shown in Table 5.

**Table 5.** Initial values of filters sets.

Filter			Filters set	
			Fragmentation	Fission
Corner rectangle	bottom	dN	6	25
		dZ	6	20
	top	dN	5	0
		dZ	5	0
Diagonal	Parameter		4	-
Procedure mode			Combined (Corner+ Rectangle)	Rectangle
#0 - optimal target thickness				
#1 – to produce all secondary reactions coefficients to be used in transmission calculations				
#2 - secondary reaction plots from this dialog				

Fig.47and Fig.48 demonstrate the use of different filter sets in the reaction  $^{238}\text{U}$  (1AGeV) + Be (1g/cm<sup>2</sup>) to produce  $^{202}\text{Pt}$  assuming the fragmentation mechanism, and the  $^{132}\text{Sn}$  isotope using AF reaction mechanism.

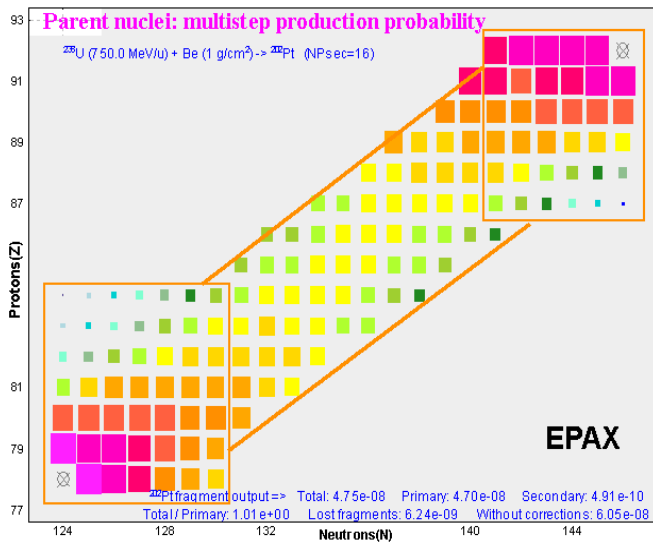


**Fig.47.** Multi-step production probabilities to produce a  $^{202}\text{Pt}$  fragment from the primary reaction  $^{238}\text{U}$  (1AGeV)+ Be (1g/cm<sup>2</sup>) [fragmentation] using the **fragmentation filters set** (see Table 5).

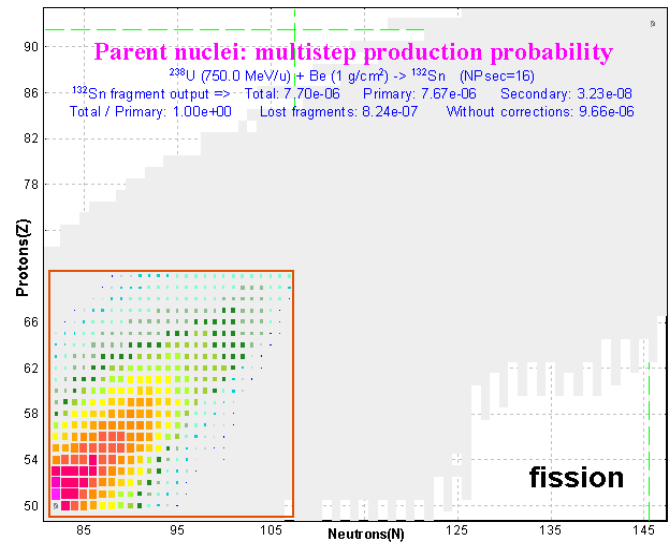


**Fig.48.** Multi-step production probabilities to produce  $^{132}\text{Sn}$  from the primary reaction  $^{238}\text{U}$  (1AGeV)+ Be (1g/cm<sup>2</sup>) [Abrasion-Fission] using the **fission filters set** (see Table 5).

## 5. Abrasion-Fission

The basic complexity in the case of Abrasion-Fission is the fact that there are more than 1000 fissile nuclei (see right top plot in Fig.10.) after abrasion of a fast heavy projectile by a target compared to only one fissile nucleus in the case of Coulomb fission. To overcome this problem, a model with three-excitation energy regions has been recently developed in the framework of LISE for calculations of Abrasion-Fission fragment production.

### 5.1. Three excitation energy regions AF model

The model suggests just three fissile nuclei for different excitation energy regions, which are calculated by using LISE++ Abrasion-Ablation model. The excitation region is determined by three parameters: excitation energy, cross-section, and fissile nucleus. A two-excitation energy region model has been proposed by M. Bernas et al. [Ber03]. For nuclear fission from  $^{238}\text{U}+p$  at 1AGeV they concluded that experimental results are compatible with two mean primary fissioning nuclei: for the asymmetric mode  $^{234}\text{U}$  and for the symmetric mode  $^{221}\text{Th}$ , with 6 post-scission neutrons added. We began also by developing a two-excitation-energy-region model for analytical fast calculation of AF products, but a drop in isotope cross-sections took place (see Fig.49). To eliminate this discrepancy the third (Middle) excitation energy region has been incorporated into the model. It certainly has complicated the program and takes more time for calculation.

#### 5.1.1. Abrasion-Fission dialog

The Abrasion-Fission dialog (see Fig.50) allows the modification of three EER model settings (see “5.6.2. Abrasion-Fission settings” for how to load this dialog alternatively). LISE initializes three excitation regions, regardless of target material and primary beam energy, in the following way for the  $^{238}\text{U}$  primary beam:

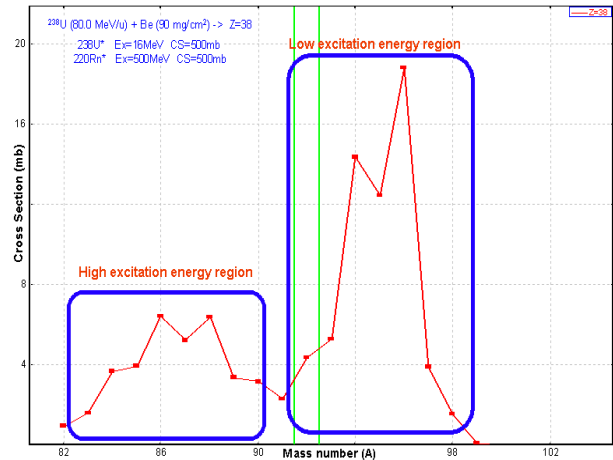


**Fig.49.** Mass distribution of Strontium fission fragments for  $^{238}\text{U}(80\text{AMeV})+\text{Be}$  calculated by the two-excitation energy region model.

Excitation region	Fissile nucleus	Ex.energy, MeV	Cross section, mb
Low	$^{237}\text{U}$	25	300
Middle	$^{232}\text{Th}$	100	1000
High	$^{226}\text{Ra}$	250	800

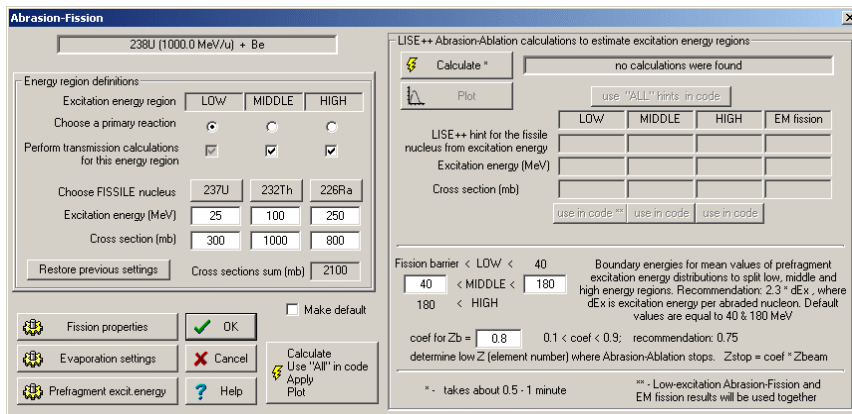


**Fig.50.** The “Abrasion-Fission” dialog. An initial state of the dialog is shown: no calculations were found.

You can define parameters of EERs manually or use hints from LISE Abrasion-Ablation calculations.

### 5.1.2. Fission excitation function

By clicking the “Calculate” button in the Abrasion-Fission dialog, you start Abrasion-Ablation calculations for nuclei from the projectile down to “coef\_for\_Zb” $\times$  Zb, where Zb is the atomic number of the projectile, and coef\_for\_Zb is the value defined in the dialog (default 0.75). There is no necessity to calculate cross-sections for more light elements because break-up channel dominates.

The code temporarily sets the following parameters to calculate the fission de-excitation function:

NPevap:	16	Tunneling:	Yes
Mode (Auto/Manual):	Manual	State density:	[C] (pairing + shell corrections)
Daughter excitation energy distribution calculate:		qualitatively	
Take into account unbound nuclei:		Yes	
De-excitation channels:		n, 2n, p, $\alpha$ , fission, break-up	

After AA calculations, the code restores the previous parameters. Statistics parameters (mean value, standard deviation, and area) of the de-excitation fission function (see Fig.16) of each isotope are saved in the operating memory. Based on the boundaries of excitation regions and the mean values of de-excitation fission functions, the code sorts nuclei by regions. The next step is summing de-excitation fission functions by region and calculating the most probable fissile nucleus, assuming for simplicity that de-excitation fission functions have a Gaussian distribution.

It is necessary to remember about Coulomb fission! In the case of a heavy target and relativistic energy of primary beam, its contribution is very significant. Electro-magnetic fission and Low excitation energy AF will result if you click the “use in code” button for Low EER. LISE AA calculation results are shown in the AF dialog (Fig.51) and can be plotted.

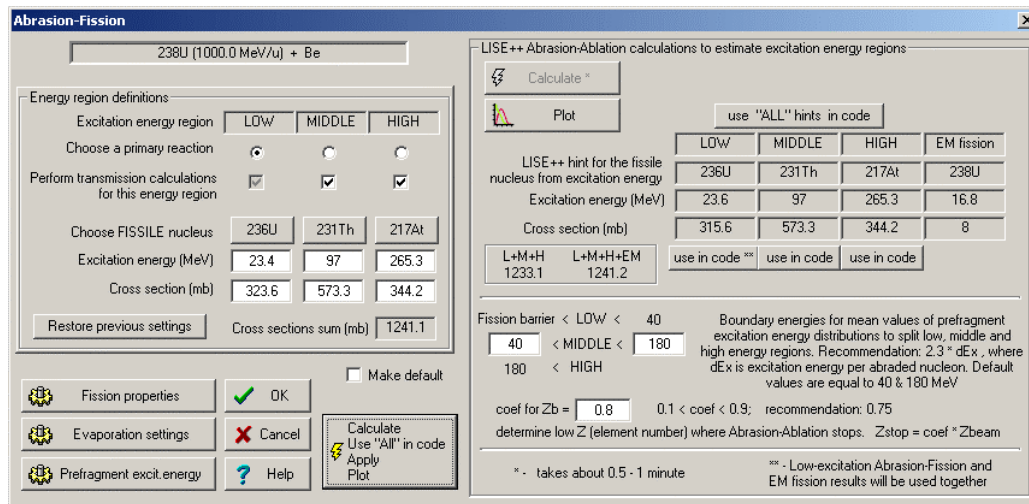
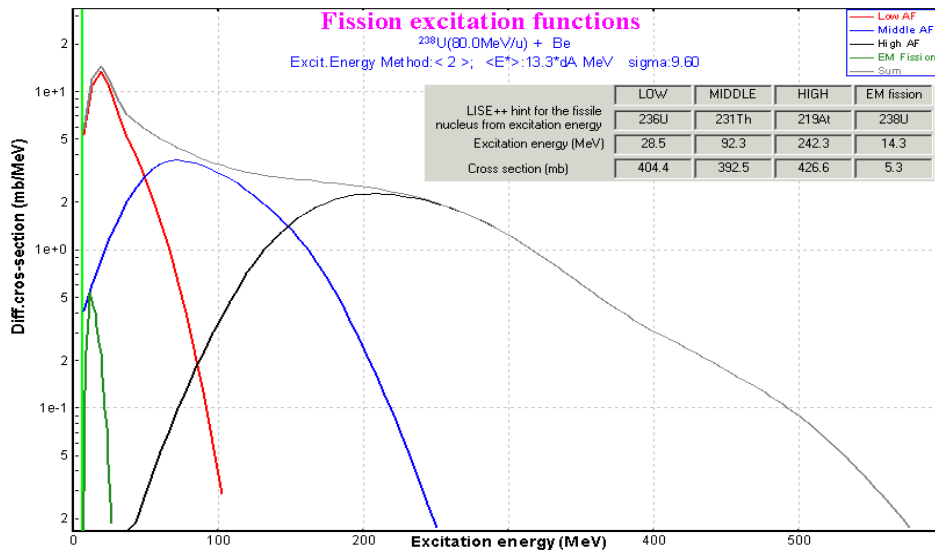
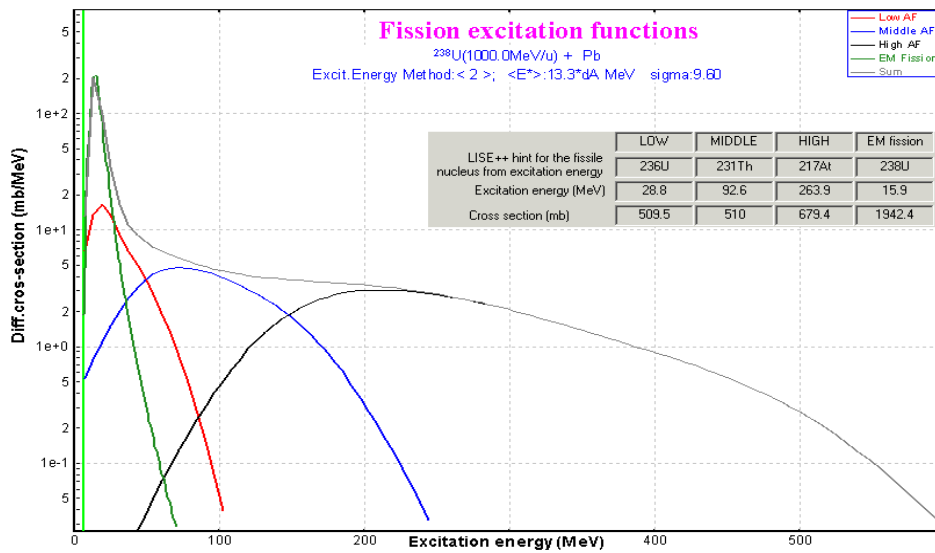


Fig.51. The “Abrasion-Fission” dialog after AF settings calculations.

Fig.52 and Fig.53 show calculated fission excitation functions in the reaction  $^{238}\text{U}(80\text{AMeV})+\text{Be}$  and  $^{238}\text{U}(1\text{AGeV})+\text{Pb}$  respectively. It is possible to see from the inserts in these figures that EM fission dominates in the case of the lead target at relativistic energies. Fig.54 shows a 2D-plot of fission de-excitation channels after the abrasion of  $^{238}\text{U}(1\text{AGeV})$  by a lead target. Locations of the most probable fissile nuclei in the excitation energy regions are shown in the figure.



**Fig.52.** Calculated excitation distribution of fissile nuclei produced in the reaction  $^{238}\text{U}(80\text{A MeV})+\text{Be}$ . Parameters of excitation energy regions are shown in the insert.



**Fig.53.** Calculated excitation distribution of fissile nuclei produced in the reaction  $^{238}\text{U}(1\text{A GeV})+\text{Pb}$ . Parameters of excitation energy regions are shown in the insert.

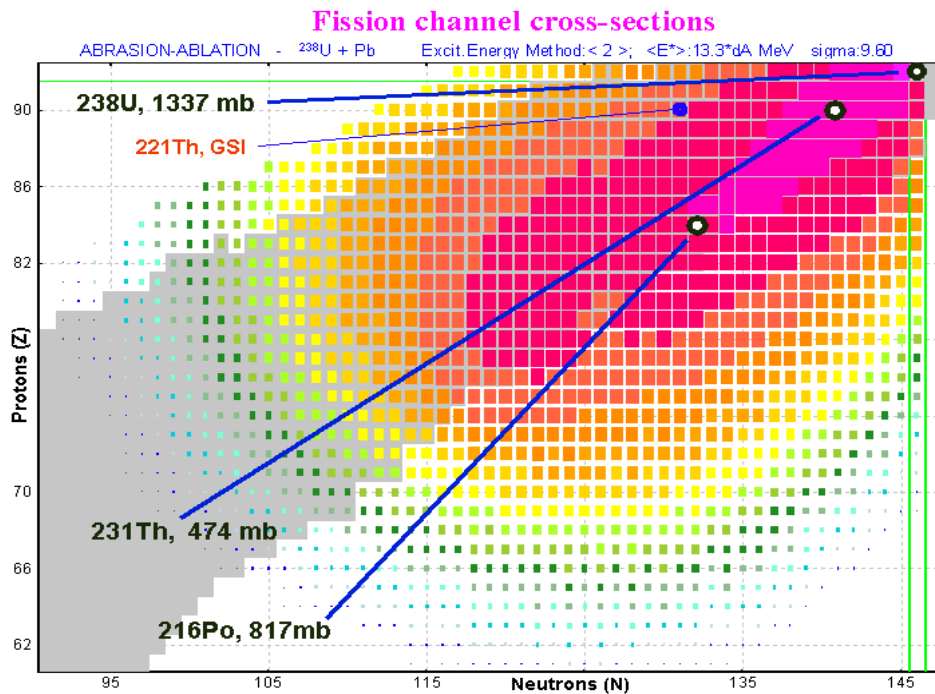


**Fig.54.** Calculated fission de-excitation channels after the abrasion of  $^{238}\text{U}(1\text{A GeV})$  by a lead target. The most probable fissile nuclei in the excitation energy regions are shown in the figure.

$^{221}\text{Th}$  is the primary fissile nucleus for asymmetric fission from ( $^{238}\text{U}+p$ ) at 1A GeV [Ber03].

### 5.1.3. Calculation of final fission fragment production

To calculate AF fission production for each excitation energy region the code uses the approach developed in the previous version for Coulomb fission [LISE71]:

- Calculation of the initial fission cross-section matrix ( $CS_{init}$ ) of production cross-sections for excited fragments uses the semi-empirical model [Ben98], but the charge distribution was modified in the new version (see chapter 5.1.3.1. Width of charge distribution).
- Post-scission nucleon emission. Based on the “LisFus” method [Tar03], the code calculates final cross-section matrices using the  $CS_{init}$  matrix, but in the new version the cascade procedure has been optimized for faster calculations (see 5.1.3.2. Modification of evaporation cascade subroutines).

Each of three excitation energy regions is considered as a separate reaction mechanism. But for cross-section, TKE, and nucleon emission plots, the calculation results of final production cross-section for each EER can be used together (see Fig.55).

Calculation of fission final cross-section production takes about *one and a half minutes* with the fission cross-section suppression value set equal to  $1e-9$  mb.

#### 5.1.3.1. Width of charge distribution

The width in proton number for fixed neutron number  $\sigma_{Z/N}$  in the semi-empirical model is calculated by using the following formula [Ben98 -Eq.24]:

$$\sigma_{Z/N}^2 = \frac{1}{2} \frac{\sqrt{E_{mac}(E_0^*, N)}}{\sqrt{\tilde{a}} C_{Z/N}} + k^2 \sigma_0^2, \quad /11/$$

where the term  $\sigma_0^2 = 0.4^*$ . The curvature  $C_{Z/N}$  defined in [Ben98] may be close to zero for some combinations of  $Z$  and  $N$  if using binding energy values from the AME2003 database. In this case LDM calculations without shell and pairing corrections are used for curvature calculations. The coefficient  $k$  initially being equal to 1 [Ben98] was set in the code to be equal to the ratio  $A_{CN} / N_{CN}$  following after relations [Sch00]:  $Z \sigma(N)_{[Z=const]} = N \sigma(Z)_{[N=const]} = A \sigma(Z)_{[A=const]}$ .

#### 5.1.3.2. Modification of evaporation cascade subroutines

The code temporarily sets the following parameters to calculate emission of light particles by excited fission fragments:

NPevap:	4	Tunneling:	Yes
Mode (Auto/Manual):	Manual	State density:	[C] (pairing + shell corrections)
De-excitation channels	n, p, $\alpha$	Acceleration Filter:	Yes

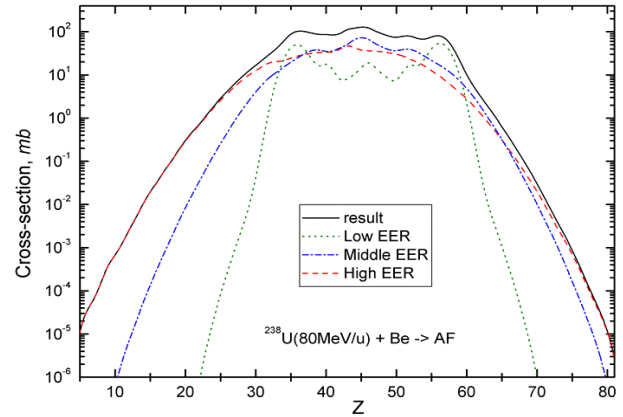


**Fig.55.** Calculated charge distributions of fission residues from the reaction  $^{238}\text{U}(1\text{AGeV})+\text{Be}$ . Parameters of excitation energy regions are shown in the insert of Fig.52.

\* in the paper [Ben98] it was mistakenly indicated  $\sigma_0 = 0.4$  instead  $\sigma_0^2 = 0.4$ . This value was extracted from isobaric charge distributions (i.e  $\sigma(Z)_{[A=const]}$ ) [Lan80].



Daughter excitation energy distribution calculate:	Qualitatively
Take into account unbound nuclei:	Yes

It was necessary to optimize the process of calculation in the case of Abrasion-Fission, because excitation energy is equal to several hundred MeV for the High EER, which takes significantly more time than in the case of Coulomb-Fission where the excitation energy is about 15-20 MeV. For this purpose an acceleration filter was developed to be used only for calculations of light particle emission by excited fission fragments. You can see from Table 6 that calculations without this filter take more than one hour!

**Table 6.** Statistical characteristics of the sum (three EER) neutron distribution of fission residues from the reaction  $^{238}\text{U}(80\text{A MeV})+\text{Be}$  depending on the dimension of evaporation distribution and use of the acceleration filter.

NP <sub>evap</sub>	filter	$\langle N \rangle$	$\sigma_N$	Elapsed time
4	yes	64.97	12.77	80 sec
8	yes	65.07	12.75	140 sec
16	yes	64.35	12.80	15 min
4	no	64.66	12.79	11 min
8	no	64.90	12.67	35 min
16	no	64.43	12.84	> 1 hour

How does the acceleration filter work? The new parameter  $\sigma_{\text{lim}}$  has been added in the evaporation subroutine. At the beginning of the cascade this parameter is set equal to  $0.01 \sigma_{\text{init}}$  (initial production cross-section value from the CSinit matrix). The following constraints are checked:

- If  $\sigma_{\text{lim}} > 1e6 \sigma_{\text{Residual}}^i$  (final fragment cross-section of residual nucleus), then this final fragment is not included in the final matrices, and  $\sigma_{\text{Killed}} = \sigma_{\text{Killed}} + \sigma_{\text{Residual}}^i$  ;
- If  $\sigma_{\text{lim}} > 10 \sigma_{\text{i-decay}}^k$  ( $k$  decay channel of  $i$  excited intermediate nucleus), then the code cancels calculation in the  $k$  decay direction, and  $\sigma_{\text{Killed}} = \sigma_{\text{Killed}} + \sigma_{\text{i-decay}}^k$  ;
- If  $\sigma_{\text{i-sum}}$  (total production cross-section of  $i$  excited intermediate nucleus)  $> 50 \sigma_{\text{i-decay}}^k$ , then the code cancels calculation in the  $k$  decay direction, and  $\sigma_{\text{Killed}} = \sigma_{\text{Killed}} + \sigma_{\text{i-decay}}^k$  .

To show how and what the filter cuts, take from the CSinit matrix for example the  $^{100}\text{Zr}$  nucleus ( $E^* = 114$  MeV,  $\sigma = 4.8$  mb) produced in High EER fission (fissile nucleus  $^{220}\text{Rn}^*$ ,  $E^* = 232$  MeV,  $\sigma_{\text{fission}} = 476$  mb). Fig.56 shows  $^{100}\text{Zr}$  evaporation residues calculated with and without the filter.

This filter acts first of all against emission of alpha-particles and protons by low-excited nuclei in the neutron-rich region. In the process of calculating light particle emission from excited fission fragments, it is possible to see in the left bottom corner of the code a state line with the current status of the calculation: . The “NumN” parameter denotes the number of isotopes in the CSinit matrix for the currently calculating element, and the “Killed” parameter gives the average ratio  $\sigma_{\text{Killed}} / \sigma_{\text{init}}$  for this element. The filter cuts about 0-2 % for the Low EER, 1-5 % for Middle, and 5-16% for the High EER respectively.

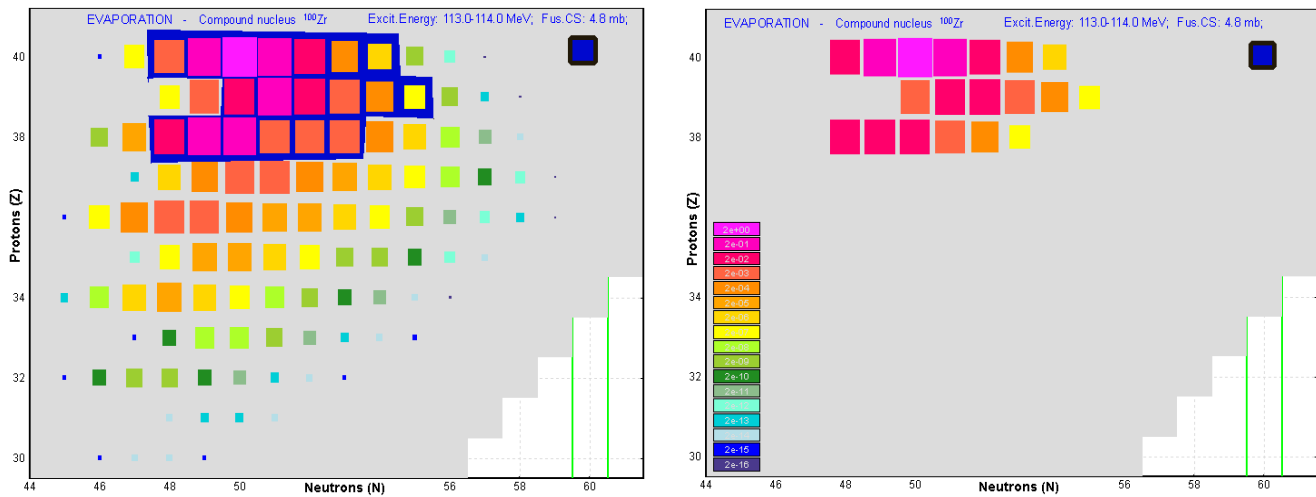


**Fig.56.**  $^{100}\text{Zr}$  ( $E^* = 113 \text{ MeV}$ ,  $\sigma = 4.8 \text{ mb}$ ) evaporation residues calculated by the Evaporation calculator without/with the acceleration filter are shown in the left/right plot.

### 5.1.4. Additional settings

Tools to modify fission characteristics (Shell structures, TXE, angular distribution etc.) were moved from the Coulomb fission dialog to the separate dialog “Fission properties” (see Fig.57), which is accessible from the Abrasion-Fission and Coulomb Fission dialogs (see Fig.50).

It is possible from the Abrasion-Fission dialog to modify the settings of mechanisms involved in the production of the final fragment distribution:

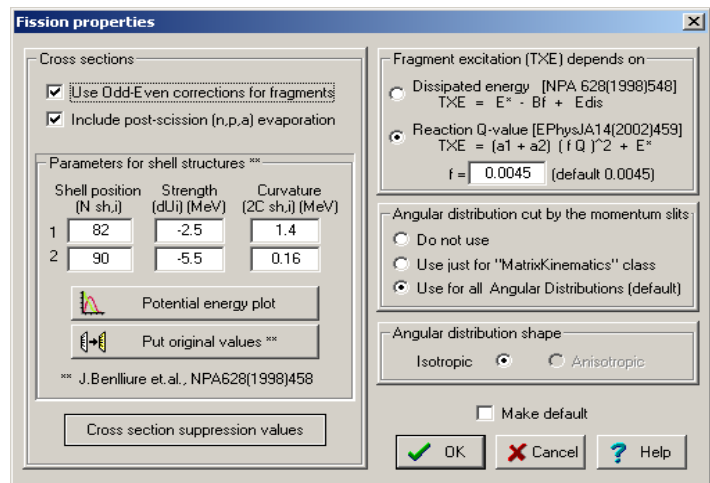


**Fig.57.** The “Fission properties” dialog.

**Table 7.**

Dialog	Properties	Daughter dialog
Fission properties dialog	Shell structures, TXE (excitation energy of fragment), angular distributions	Cross-section suppression values
Prefragment energy	Excitation energy for Abrasion-Ablation model to define fissile nuclei for EERs	
Evaporation settings	Dissipative effects in fission, break-up parameters to produce the fission excitation function	Fission barrier
Fission barrier dialog	Calculation of fission de-excitation channels	
Cross-section suppression values	To exclude low-probability events and to reduce the time of fragment cross-section calculation	



## 5.2. Kinematics

In order to calculate kinematics of Abrasion-Fission fragments, the code uses algorithms developed for the Coulomb version [LISE71]. Both *MCmethod* and *DistrMethod* can be used for these aims. We remind the reader that *DistrMethod* is the fast analytical method applied to calculate the fragment transmission through all optical blocks of the spectrometer. *MCmethod* has been developed for a qualitative analysis of fission fragment kinematics and is utilized in the Kinematics calculator.

We shall show some examples of AF fragment kinematics calculation by both methods for different excitation energy regions, and also depending on angular acceptance and target thickness.

### 5.2.1. Production of $^{100}\text{Zr}$

Let's again take the reaction  $^{238}\text{U}(80\text{AMeV})+\text{Be}$  with EERs defined in the insert of Fig.52. Initial emittances are  $\theta_x = \theta_y = 3.3\text{mrad}$  and  $\delta P=0.07\%$ . Set the target thickness equal to  $1\text{mg}/\text{cm}^2$ , and set the desired fragment to  $^{100}\text{Zr}$ , because this fragment may be produced by each EER:

**Table 8.** Calculated production of  $^{100}\text{Zr}$  fission residues produced in the reaction  $^{238}\text{U}(80\text{AMeV})+\text{Be}$ .

EER	Fissile nucleus	$E^*$ MeV	Most probable excited fission fragment to produce $^{100}\text{Zr}$	Excitation energy ( $E^*$ ) of most probable excited fragment	$^{100}\text{Zr}$ production cross-section, mb
Low	$^{236}\text{U}$	28	$^{102}\text{Zr}$	27.7	10.7
Middle	$^{231}\text{Th}$	92	$^{104}\text{Zr}$	55.3	3.07
High	$^{219}\text{At}$	242	$^{106}\text{Zr}$	124.4	1.34

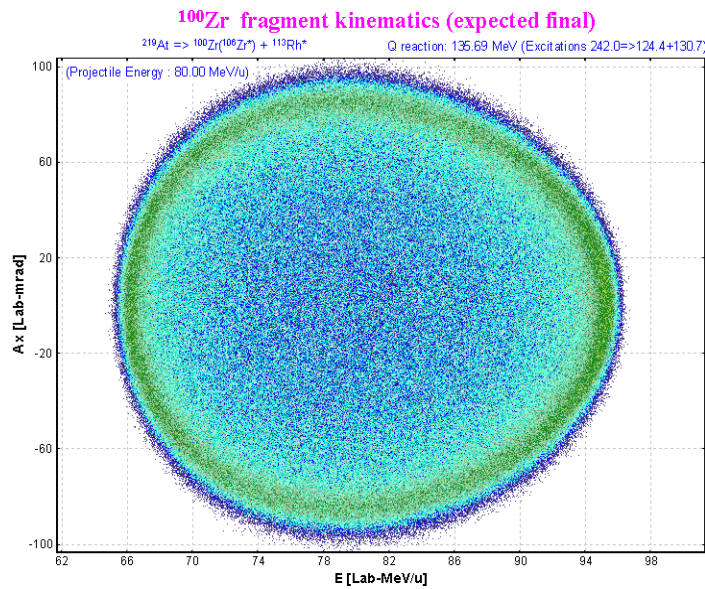


**Fig.58.** MCmethod (Monte Carlo) 2D-plot  $A_x$ (horizontal component of the angle in the laboratory frame) versus Energy per nucleon of  $^{100}\text{Zr}$  final fragments produced in fission of the  $^{219}\text{At}(E^*=242\text{MeV})$  nucleus.

**Fig.59.** Angular distributions of  $^{100}\text{Zr}$  fragments after the target calculated by the *DistrMethod* (analytical solution) for the reaction  $^{238}\text{U}(80\text{AMeV})+\text{Be}(1\text{mg}/\text{cm}^2)$ .

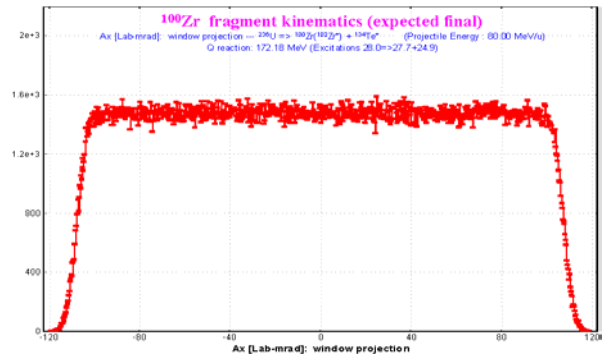


**Fig.60.** The projection of the 2D-plot in Fig.58 onto the  $A_x$  vertical axis.

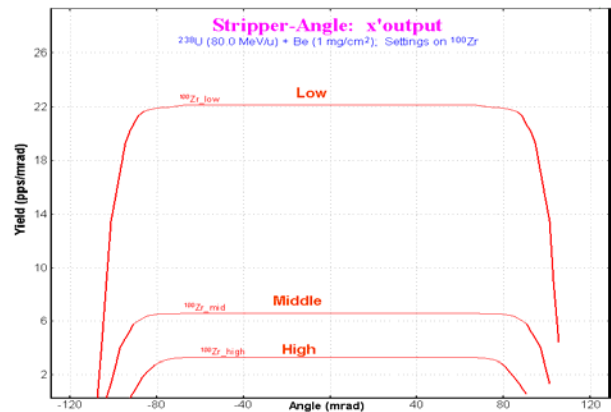
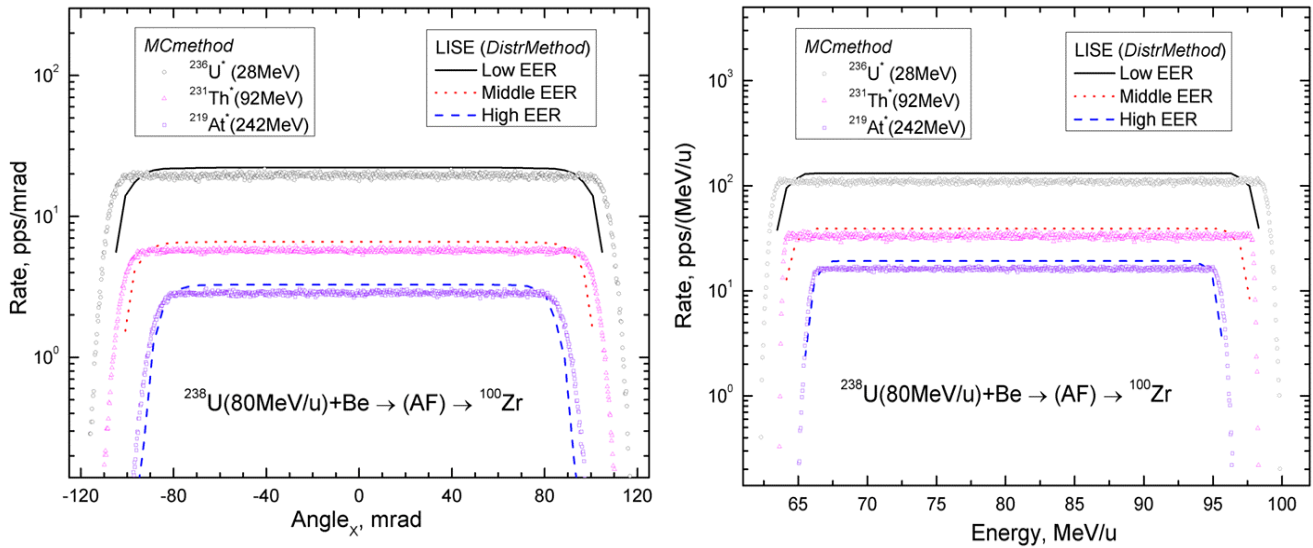


Fig.58 shows a kinematic Monte Carlo calculation of  $^{100}\text{Zr}$  final fragments produced in fission of the  $^{219}\text{At}(E^*=242\text{MeV})$  nucleus that corresponds to the High EER settings calculated for the AF reaction  $^{238}\text{U}(80\text{ MeV/u}) + \text{Be}(1\text{ mg/cm}^2)$ .

Fig.59 shows angular distributions of  $^{100}\text{Zr}$  fragments after the target, calculated for all of three EERs by the *DistrMethod* (analytical solution) for the reaction  $^{238}\text{U}(80\text{AMeV})+\text{Be}(1\text{mg/cm}^2)$ . This plot is the regular LISE plot developed to show transmission distributions through spectrometer blocks.

Fig.60 shows the projection of the 2D-plot (Fig.58) onto its vertical axis. Projections onto energy and angular axes of the 2D-plot of  $^{100}\text{Zr}$  fragment kinematics for different excited fragments done in this way are used to compare *DistrMethod* and *MCmethod* (see Fig.61). *MCmethod*'s angular and energy distributions produced by 2D-plot projections onto axes were normalized for Fig.61.



**Fig.61.** Matching of angular(left) and energy(right) distributions calculated by *DistrMethod* and *MCmethod* for the  $^{100}\text{Zr}$  final fragment produced by different excited fission fragments (or EERs).

### 5.2.2. Angular acceptance

Set the angular acceptances of the first optical block after the target to  $\pm 60\text{ mrad}$  in both directions and repeat the same calculation procedure as in the previous chapter.

Fig.62 shows a kinematics Monte Carlo calculation of  $^{100}\text{Zr}$  final fragments produced in fission of the  $^{231}\text{Th}(E^*=92\text{MeV})$  nucleus that corresponds to the Middle EER settings calculated for the reaction  $^{238}\text{U}(80\text{ MeV/u}) + \text{Be}(1\text{ mg/cm}^2)$ .

Table 9 shows, calculated by *MCmethod* and *DistrMethod*, angular transmissions of  $^{100}\text{Zr}$  fragments produced by different EERs in the reaction  $^{238}\text{U}(80\text{AMeV})+\text{Be}$ .

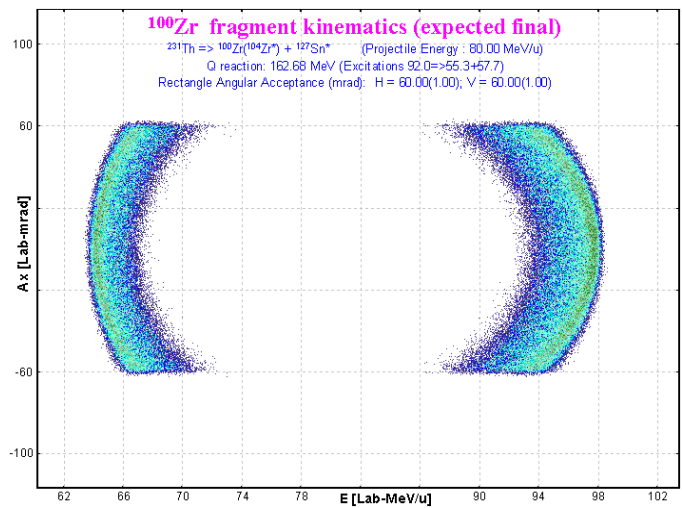


**Fig.62.** *MCmethod* (Monte Carlo) 2D-plot  $A_x$ (horizontal component of the angle in the laboratory frame) versus Energy per nucleon of  $^{100}\text{Zr}$  final fragments produced in fission of the  $^{231}\text{Th}(E^* = 92\text{ MeV})$ . Angular acceptances of the first optical block after the target are equal to  $\pm 60\text{ mrad}$  in both directions.

**Table 9.** Calculated by *MCmethod* and *DistrMethod*, transmission of  $^{100}\text{Zr}$  fragments produced by different EERs in the reaction  $^{238}\text{U}(80\text{A MeV})+\text{Be}$ . Angular acceptances of the first optical block after the target are equal to  $\pm 60$  mrad in both directions.

EER	Fissile nucleus	$E^*$ MeV	<i>MCmethod</i> Monte Carlo transmission, %	<i>DistrMethod</i> LISE transmission, %
Low	$^{236}\text{U}$	28	22.9	23.0
Middle	$^{231}\text{Th}$	92	26.0	25.2
High	$^{219}\text{At}$	242	36.5	33.6

### 5.2.3. Thick target

Let's set the target thickness to  $150\text{ mg/cm}^2$  instead of the previous value of  $1\text{ mg/cm}^2$  and repeat the same calculation procedure as in the previous chapter.

Fig.64 shows Monte Carlo kinematics of  $^{100}\text{Zr}$  final fragments, Table 10 shows transmission statistics, and Fig.65 shows comparable *MCmethod* and *DistrMethod* energy distributions of  $^{100}\text{Zr}$  fragments produced by different EERs in the reaction  $^{238}\text{U}(80\text{A MeV})+\text{Be}(150\text{ mg/cm}^2)$ . It is possible to see in Fig.65 a large discrepancy between angular distributions calculated by the *MCmethod* and *DistrMethod* models, because in the case of the *DistrMethod* the code assumes that the reaction takes place in the middle of the target.

**Table 10.** Calculated by *MCmethod* and *DistrMethod*, transmissions of  $^{100}\text{Zr}$  fragments produced by different EERs in the reaction  $^{238}\text{U}(80\text{A MeV})+\text{Be}$  ( $150\text{ mg/cm}^2$ ). Angular acceptances of the first optical block after the target are equal to  $\pm 60$  mrad in both directions.

EER	Fissile nucleus	$E^*$ MeV	<i>MCmethod</i> MC transmission, %	<i>DistrMethod</i> LISE transmission, %
Low	$^{236}\text{U}$	28	17.9	14.9
Middle	$^{231}\text{Th}$	92	20.3	16.4
High	$^{219}\text{At}$	242	27.6	21.2

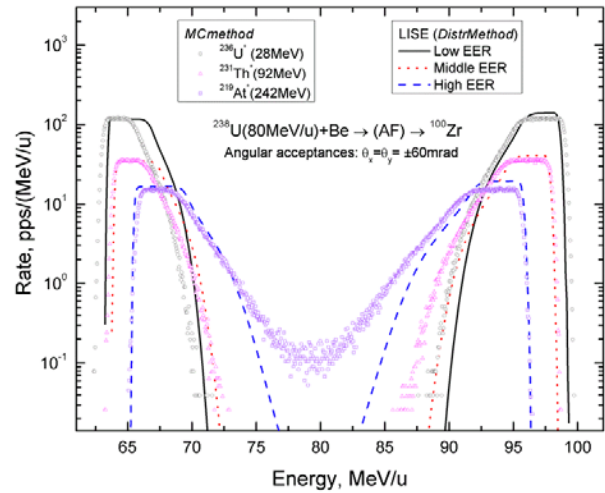


**Fig.63.** Comparison of energy distributions calculated by *DistrMethod* and *MCmethod* for the  $^{100}\text{Zr}$  final fragments produced by different excited fission fragments (or EERs).

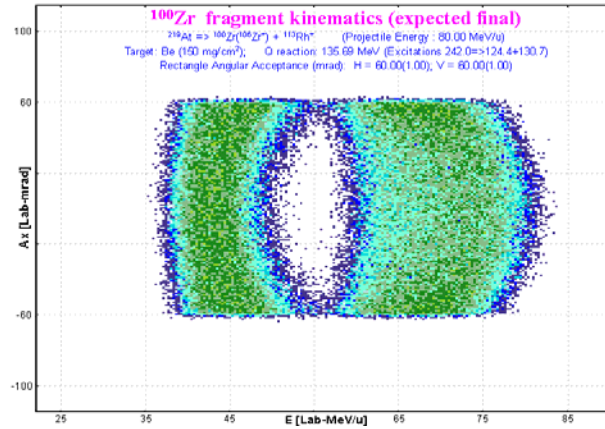


**Fig.64.** Kinematics of  $^{100}\text{Zr}$  final fragments produced in fission of  $^{219}\text{At}$  ( $E^* = 242$  MeV). Angular acceptances of the first optical block after the target are equal to  $\pm 60$  mrad in both directions. Thickness of the Be-target is equal to  $150\text{ mg/cm}^2$ .

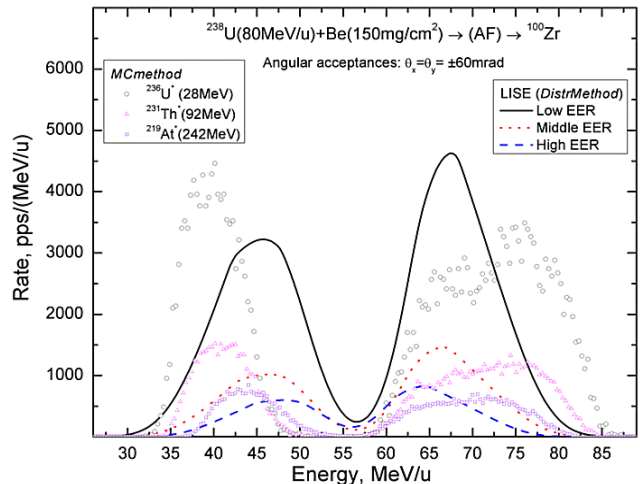


**Fig.65.** Matching of energy distributions in the case of a thick target.

### 5.3. Abrasion-Fission plots

Cross-section and TKE plot dialogs for the "Coulomb fission" reaction have been modified for the Abrasion-Fission mode and they are available in the menu "1D-plots". The complexity of the AF case lies in that AF is a result of three excitation energy regions, where each of them is an independent reaction mode for the program. It would be desirable to see them both separately and together. In connection with this, the cross-section and TKE dialogs were revamped (see Fig.66 and Fig.67). See examples of 2D cross-section plots in Fig.68.

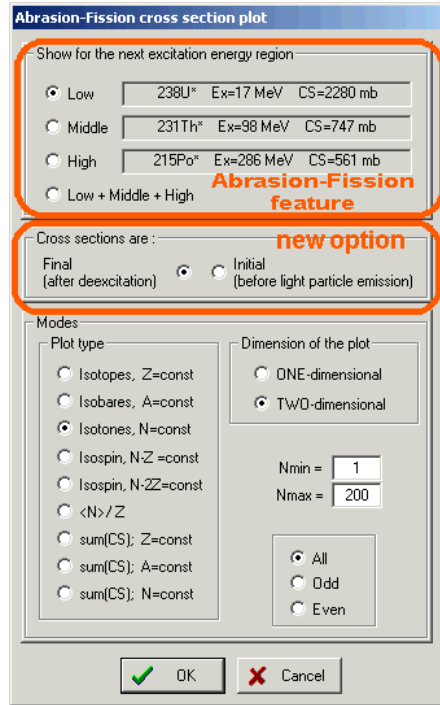


Fig.66. The "Abrasion-Fission cross-section plot" dialog.

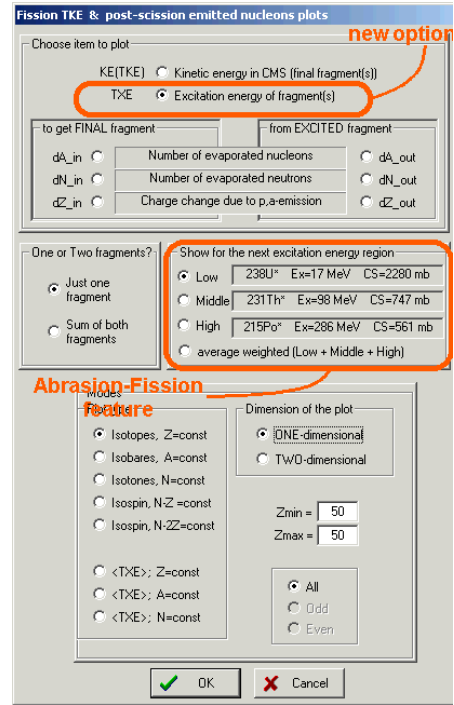


Fig.67. The "Fission TKE & post-scission emitted nucleons plot" dialog.

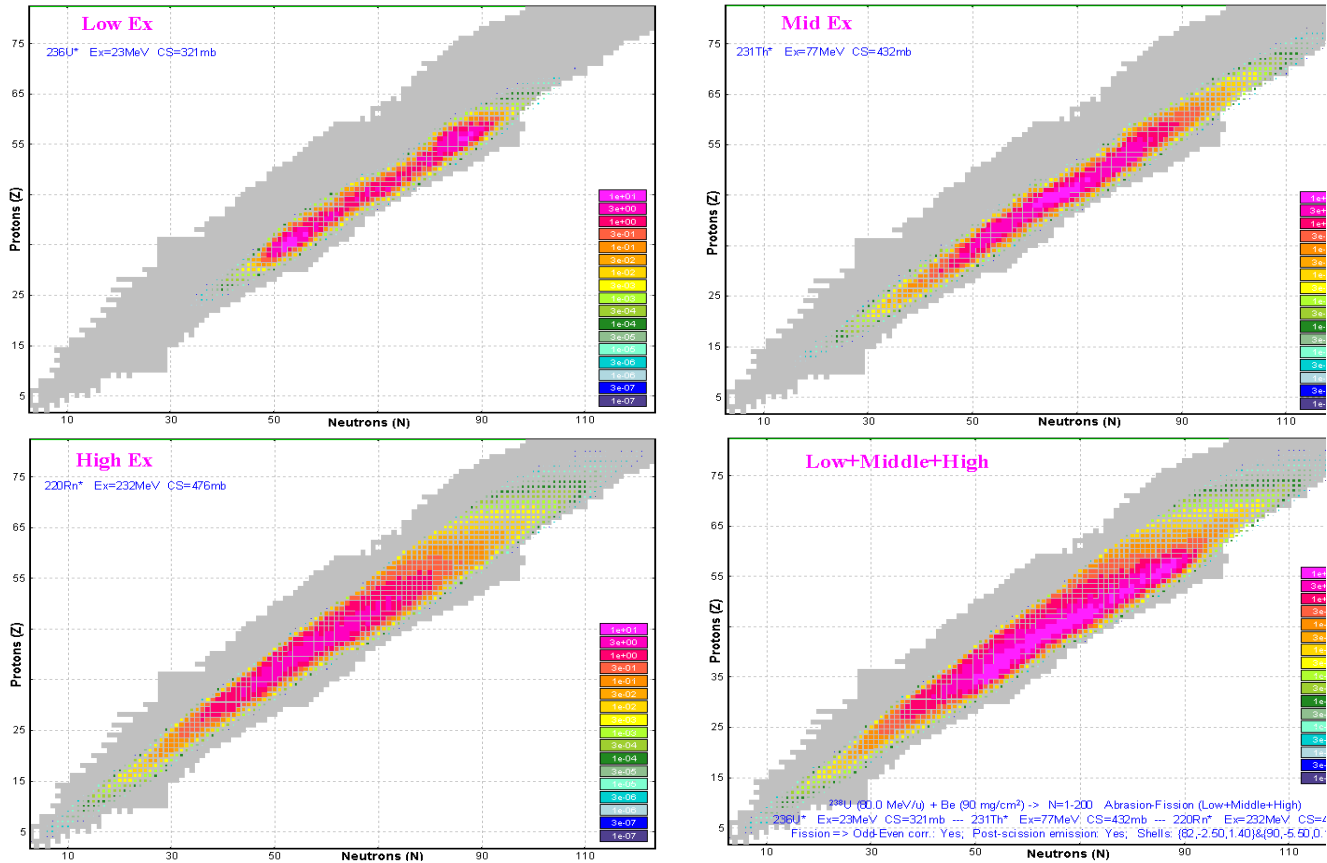


Fig.68. 2D fission fragment production cross-section plot for Low, Middle, High EERs and their sum (right bottom) for the reaction  $^{238}\text{U} (1\text{AGeV}) + \text{Be} (90 \text{ mg/cm}^2)$ . Projections on the vertical axis (Z) are shown in Fig.55.



### 5.3.1. New plot options

New options to plot fission fragment distributions have been developed in the new version (see Fig.66 and Fig.67). These new options are also available in the Coulomb fission mode.

#### 5.3.1.1. Final (after de-excitation) and initial cross-section plots

In the new version the user can plot not only fission fragment cross-section distributions, when the fragments are already in a ground state, but also distributions immediately after fission before emission of light particles to release excitation energy. The  $^{238}\text{U}(750\text{AMeV})+\text{Be}$  reaction was used to illustrate this new possibility. The LISE parameters and a link with corresponding LISE++ file are given in chapter “5.9.4.  $^{238}\text{U}(750\text{AMeV}) + \text{Be}$ ”. Fig.69 shows the initial distribution of zirconium isotopes before and after emission of light particles. The experimental data [Ber97] are shown for comparison.

Fig.70 shows the mean quantity of nucleons emitted by exited Zirconium isotopes ( $dA_{out}$ ), and also the quantity of nucleons emitted before reaching a final fragment ( $dA_{in}$ ).

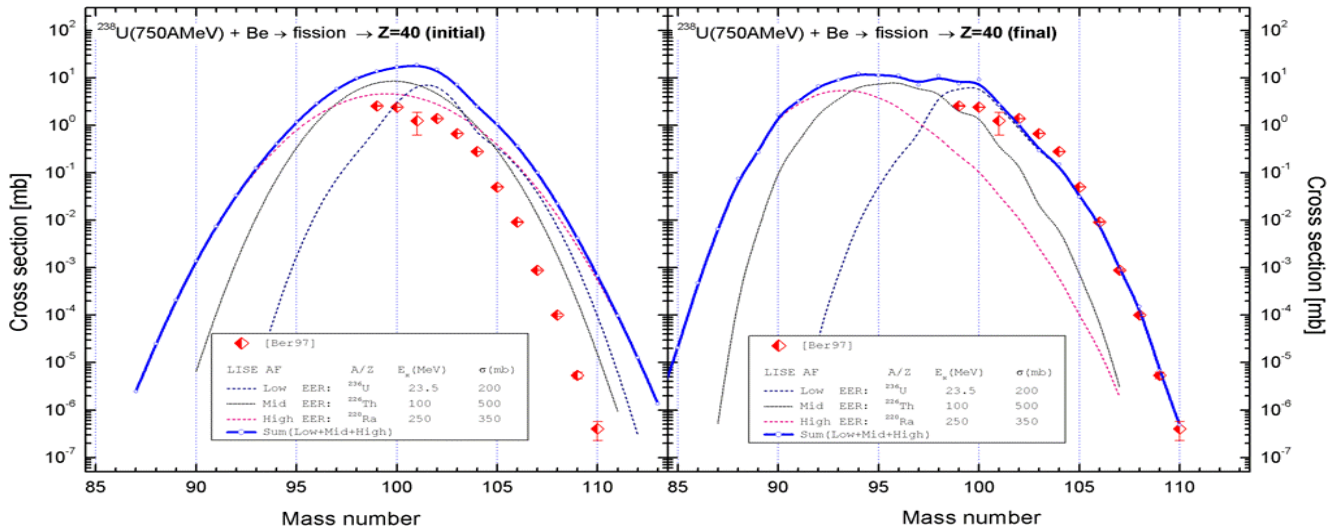


**Fig.69.** Initial (left plot) and final (right plot) Zirconium fission fragment distributions for different EERs in reaction  $^{238}\text{U}(750\text{AMeV})+\text{Be}$  reaction.

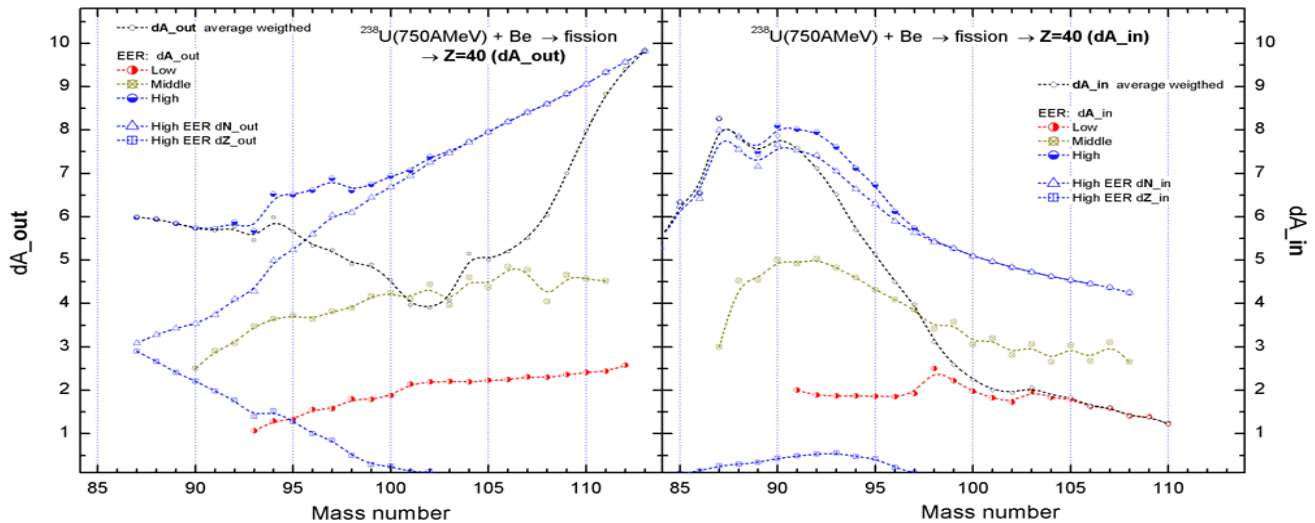


**Fig.70.** Left plot: Mean quantity of nucleons emitted by exited Zirconium fission fragments ( $dA_{out}$ ) produced in  $^{238}\text{U}(750\text{AMeV})+\text{Be}$  reaction. Right plot: Quantity of evaporated nucleons emitted before reaching a final fragment ( $dA_{in}$ ).

### 5.3.1.2. Excitation energy plot

The excitation energy plot is available through the dialog “Fission TKE & post-scission emitted nucleons plot” (Fig.67). The excitation energy plot of Zirconium isotopes produced in fission of  $^{238}\text{U}(750\text{AMeV})$  on a Be target is shown in Fig.71. The LISE parameters and a link with the corresponding LISE++ file are given in chapter “5.9.4.  $^{238}\text{U}(750\text{AMeV}) + \text{Be}$ ”.

Fig.72 shows average isobar excitation energy plots of fission fragment for different EERs in the  $^{238}\text{U}(750\text{AMeV})+\text{Be}$  reaction.

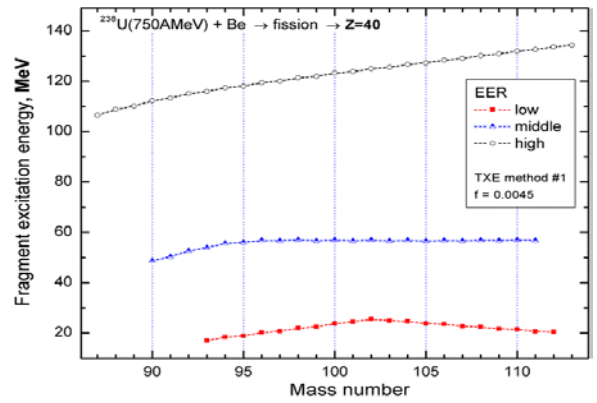


**Fig.71.** Excitation energy of Zirconium isotopes produced in fission of  $^{238}\text{U}(750\text{AMeV})$  on a Be target.

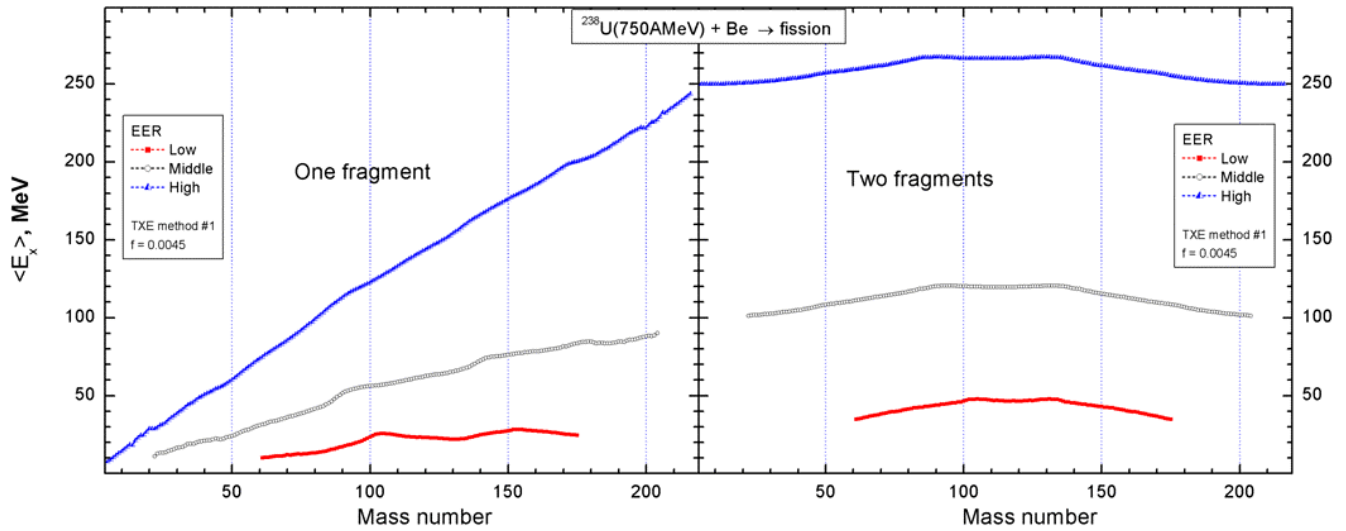


**Fig.72.** Average isobar excitation energy of one (left plot) and two (right plot) fission fragment(s) for different EERs in the  $^{238}\text{U}(750\text{AMeV})+\text{Be}$  reaction.

## 5.4. Abrasion-Fission settings discussions

In this chapter we would like to show by example where and how Abrasion-Fission settings influence the final calculation results. Abrasion-Fission settings and where to access them are given in Table 7.

### 5.4.1. Excitation energy of fission fragment (TXE)

Two models of fragment excitation energy (TXE) are included in LISE (see the “Fission properties” dialog in Fig.57). In the calculations for the TXE model based on Reaction Q-value (TXE #1), we will use two values, 0.0035 and 0.0045, for the  $f$  parameter. Calculated mass-distributions of fission fragments from  $^{238}\text{U}(750\text{MeV/u})+\text{Be}$  for different EERs are shown in Fig.73.

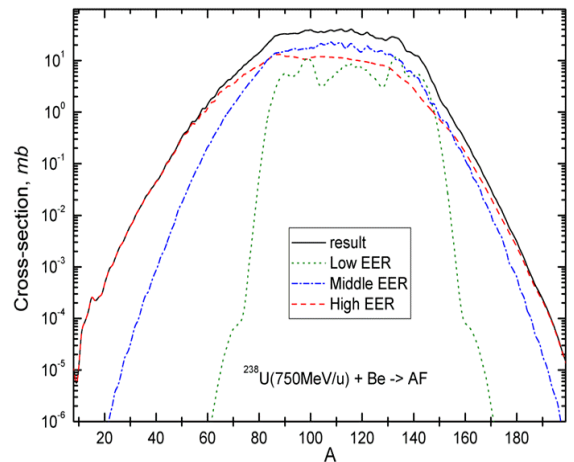


**Fig.73.** Calculated mass distribution of fission fragments in  $^{238}\text{U}(750\text{MeV/u})+\text{Be}$  (TXE #1,  $f=0.0045$ ).

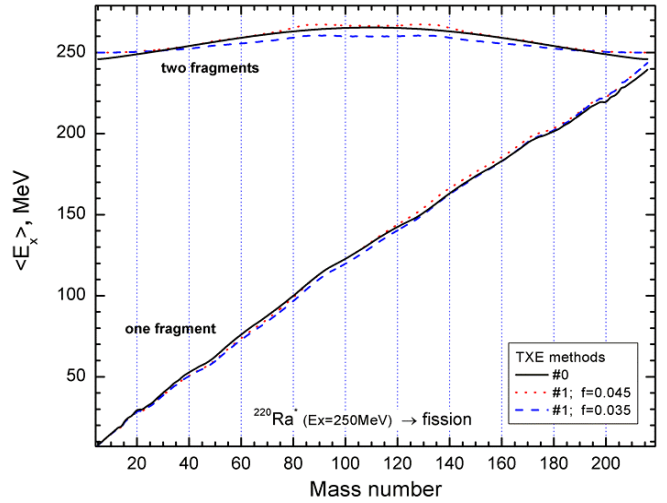
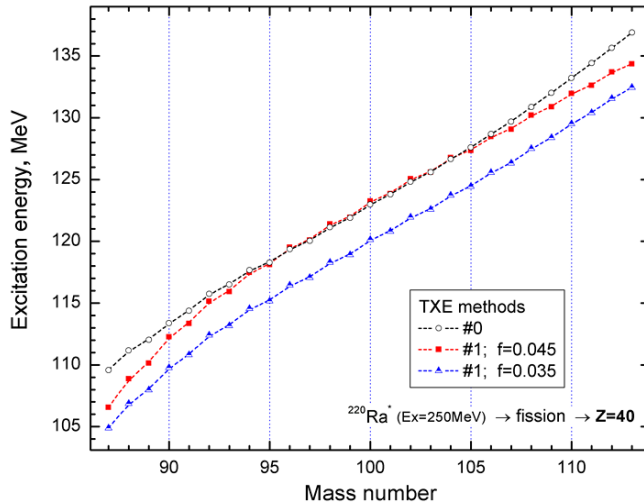
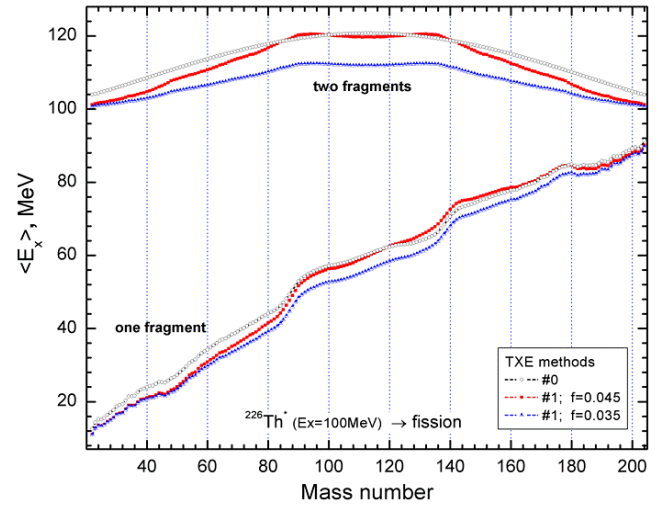
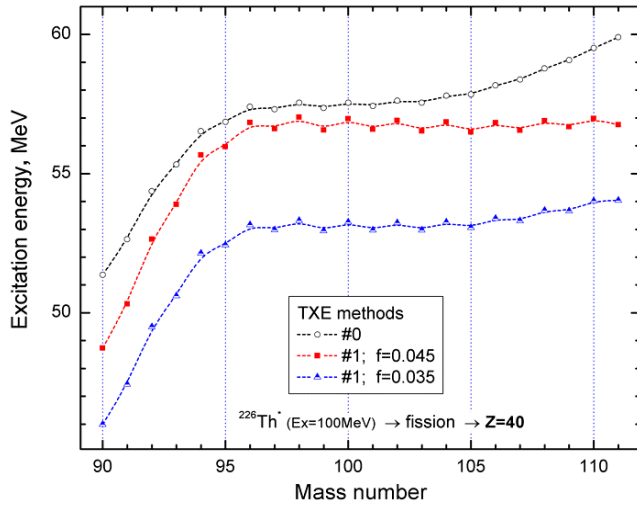
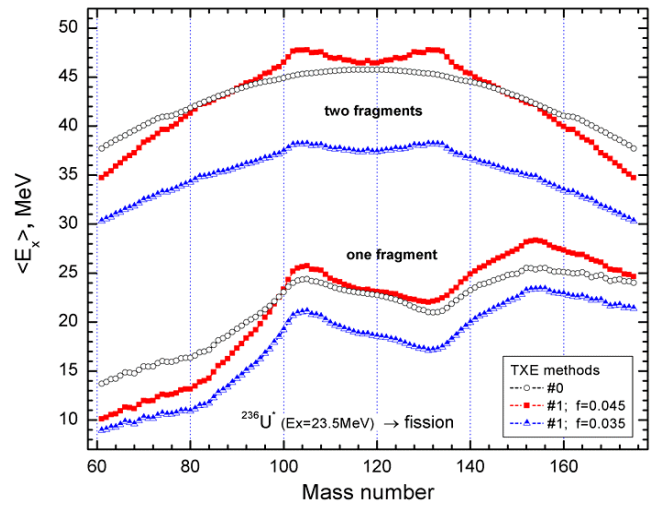
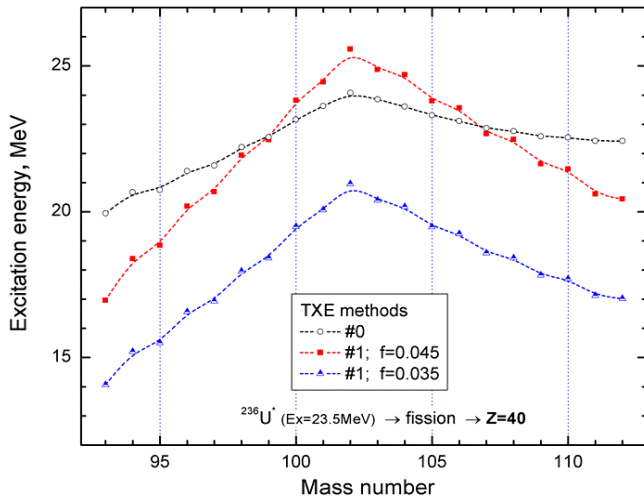


**Fig. 74.** Excitation energy of Zirconium fragments depending on an excitation energy method. Fragments are produced in fission of excited nuclei  $^{236}\text{U}$  ( $E_x=23.5\text{MeV}$ ) in top plot,  $^{226}\text{Th}$  ( $E_x=100\text{MeV}$ ) in middle plot, and  $^{220}\text{Ra}$  ( $E_x=250\text{MeV}$ ) in bottom plot. These excited nuclei correspond to EERs for the calculation of fission fragment production in the reaction  $^{238}\text{U}$  ( $750\text{MeV/u}$ )+Be.

**Fig. 75.** Average weighted excitation energy of fragments depending on an excitation energy method. Fragments are produced in fission of excited nuclei  $^{236}\text{U}$  ( $E_x=23.5\text{MeV}$ ) in top plot,  $^{226}\text{Th}$  ( $E_x=100\text{MeV}$ ) in middle plot, and  $^{220}\text{Ra}$  ( $E_x=250\text{MeV}$ ) in bottom plot. These excited nuclei correspond to EERs for the calculation of fission fragment production in the reaction  $^{238}\text{U}$  ( $750\text{MeV/u}$ )+Be.



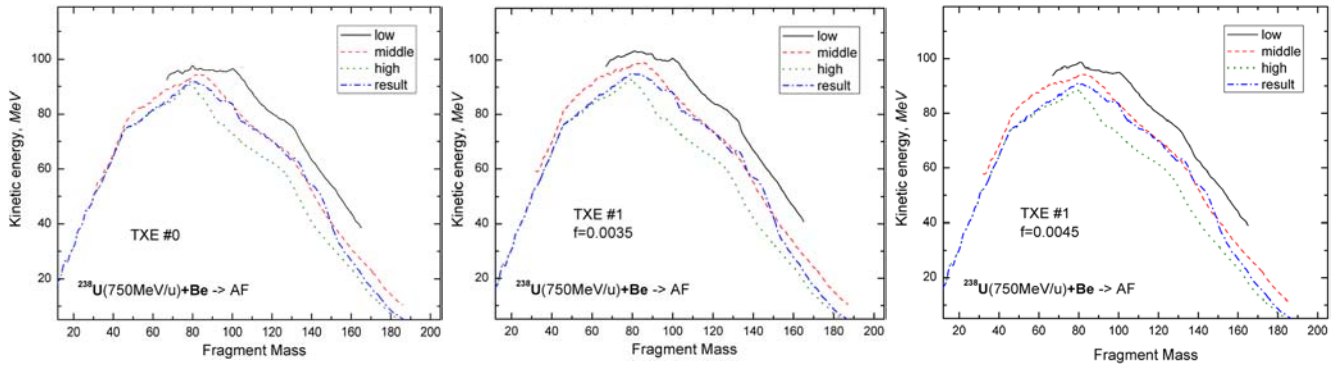


**Fig. 76.** Average kinetic energy of a fission fragment in the reaction  $^{238}\text{U}(750\text{MeV}/u)+\text{Be}$ . Left (TXE #0), middle (TXE #1,  $f=0.0035$ ), and right (TXE #1,  $f=0.0045$ ) plots show calculations for different EERs.

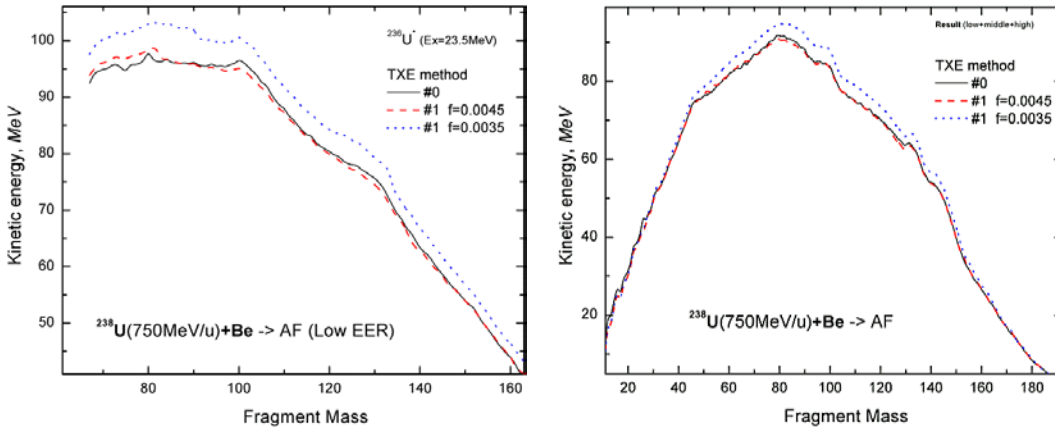


**Fig. 77.** Average kinetic energy of a fission fragment in the reaction  $^{238}\text{U}+\text{Be}$ . The left plot corresponds to the low EER [ $^{236}\text{U}^*(E_x=23.5\text{MeV})$ ], the right plot is the average weighted result of three EERs.

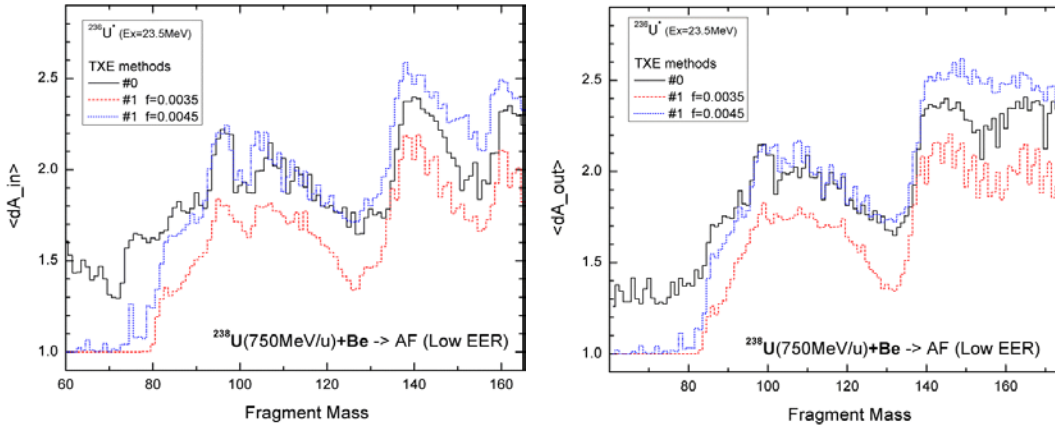


**Fig. 78.** Calculated average number of evaporated nucleons for / from a final / excited fragment produced by fission of the excited nucleus  $^{236}\text{U}$  ( $E_x=23.5\text{MeV}$ ).

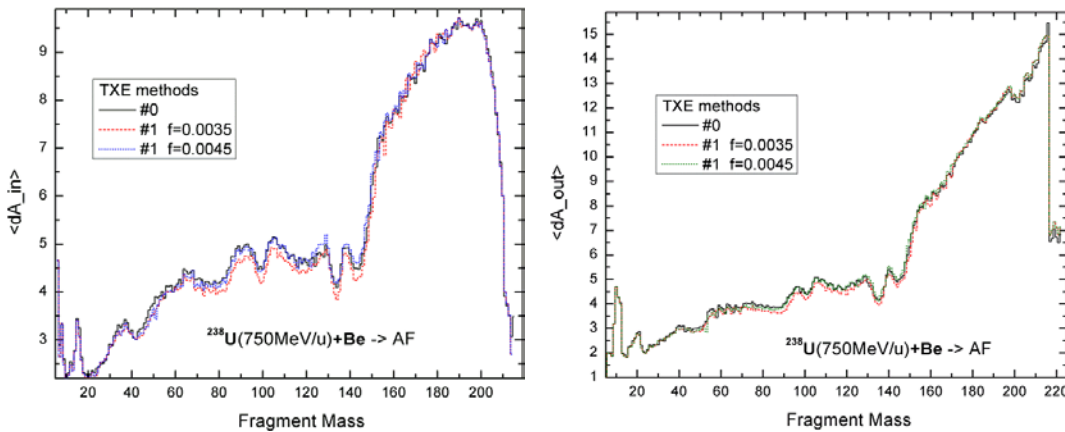


**Fig. 79.** Calculated average number of evaporated nucleons for / from a final / excited fission fragment produced in the reaction  $^{238}\text{U}+\text{Be}$ .

Fig.74 shows excitation energy of Zirconium fragments and Fig.75 shows average weighted excitation energy of all fission fragments depending on the excitation energy method. Calculations were done for three different excited nuclei which correspond to EERs for the calculation of fission fragment production in reaction  $^{238}\text{U}$  (750MeV/u)+Be.

Fig.76 and Fig.77 show the average kinetic energy of a fission fragment in the reaction  $^{238}\text{U}$  (750MeV/u)+Be depending on the excitation energy method.

Fig.78 and Fig.79 show the calculated average number of evaporated nucleons for / from a final /excited fragment produced by fission of the excited nucleus  $^{236}\text{U}$  ( $E_x=23.5\text{MeV}$ ) and in the reaction  $^{238}\text{U}$ +Be.

It is possible to conclude from figures given above, that excitation energy values calculated by TXE method #1 ( $f=0.0045$ ) and method #0 are very close to each other if compared with method #1 ( $f=0.0035$ ). We recommend the use of method #1 ( $f=0.0045$ ).

### 5.4.2. Excitation energy region (EER) boundaries

To see how boundary settings influence final fission fragment production, we chose four sets of boundaries to calculate EER characteristics (see Table 11). It is possible to visualize fissile nuclei for each boundary setting in Fig.80.

**Fig.80.** Fission de-excitation channel cross-sections calculated by the LISE Abrasion-Ablation model for the reaction  $^{238}\text{U}$ +Be. AA settings are shown in the figure. Circles correspond to the fissile nuclei of EERs given in Table 11

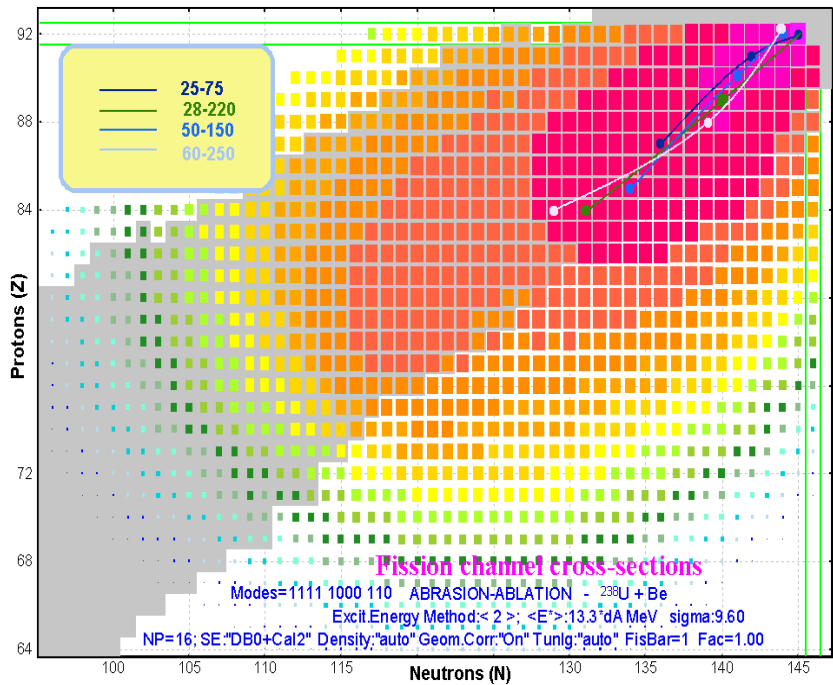


**Table 11.**

Boundaries		Low			Middle			High		
Left	Right	A, Z, N	$E^*$	$\sigma$	A, Z, N	$E^*$	$\sigma$	A, Z, N	$E^*$	$\sigma$
25	75	$^{237}_{92}\text{U}_{145}$	20.4	241.7	$^{234}_{91}\text{Pa}_{143}$	49.7	299.3	$^{223}_{87}\text{Fr}_{136}$	191.2	688.0
28	220	$^{237}_{92}\text{U}_{145}$	20.4	241.7	$^{229}_{89}\text{Ac}_{140}$	104.0	748.2	$^{215}_{84}\text{Po}_{131}$	288.4	239.0
50	150	$^{236}_{92}\text{U}_{144}$	28.3	409.7	$^{231}_{90}\text{Th}_{141}$	92.3	392.5	$^{219}_{85}\text{At}_{134}$	242.3	426.6
60	250	$^{236}_{92}\text{U}_{144}$	31.7	461.1	$^{227}_{88}\text{Ra}_{139}$	142.4	608.2	$^{213}_{84}\text{Po}_{129}$	314.8	159.6

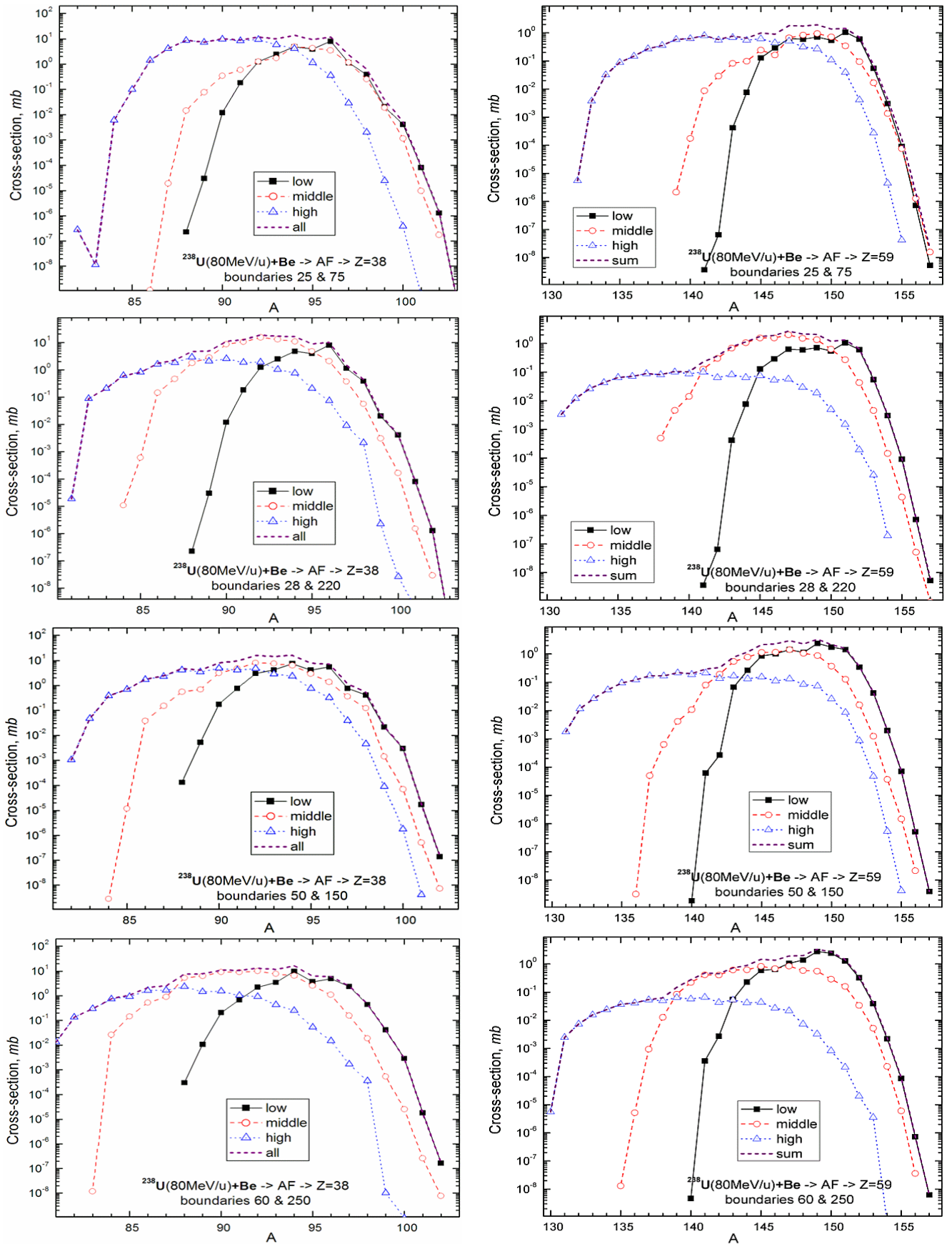


**Fig.81.** Partial and total mass distributions of Strontium (left plots) and Praseodymium (right plots) fission fragments in the reaction  $^{238}\text{U}(80\text{MeV/u})+\text{Be}$  calculated for different sets of EER boundaries. See legends in plots.

Fig.81 shows partial and total mass distributions of Strontium and Praseodymium fission fragments in the reaction  $^{238}\text{U}(80\text{MeV/u})+\text{Be}$  calculated for different sets of EER boundaries. Fig.82 shows total mass distributions of Strontium and Praseodymium fission fragments in the reaction  $^{238}\text{U}(80\text{MeV/u})+\text{Be}$  calculated for different sets of EER boundaries given in Table 11.

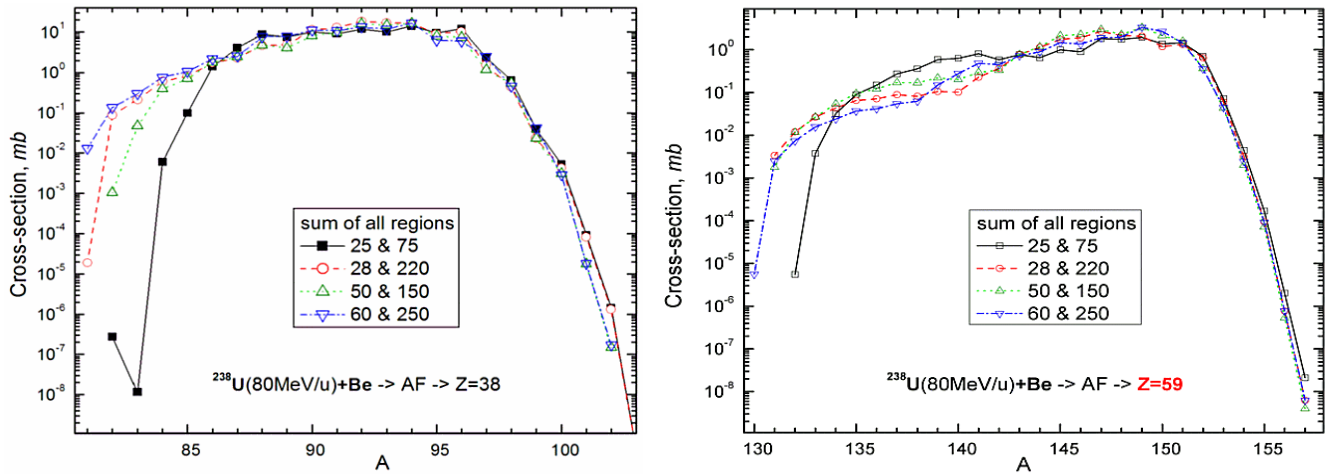


**Fig.82.** Total (sum of all regions) mass distributions of Strontium (left plot) and Praseodymium (right plot) fission fragments in the reaction  $^{238}\text{U}(80\text{MeV/u})+\text{Be}$  calculated for different sets of EER boundaries.

Based on Fig.81 and Fig.82 it is possible to make these three principal conclusions:

1. High left boundary (50 MeV in the third set and 60 MeV in the fourth set) leads to underestimation of super neutron-rich isotopes.
2. Low right boundary (75 MeV in the first set and even 150 MeV in the third set for Strontium isotopes) leads to LARGE underestimation of proton-rich isotopes (see left plot in Fig.82).
3. Large distance between boundaries (28 & 220 MeV in the second set and 60 & 250 MeV in the fourth) leads to a hole between High and Middle isotope cross-section distributions (see right plot in Fig.82).

Based on these conclusions we recommend the following boundaries<sup>♥</sup>: Left 30-40 MeV, Right 180-200 MeV. Fig.83 demonstrates the significant difference in N/Z ratio and element integrated distributions between boundary sets for elements with  $Z < 25$  and  $Z > 60$ .

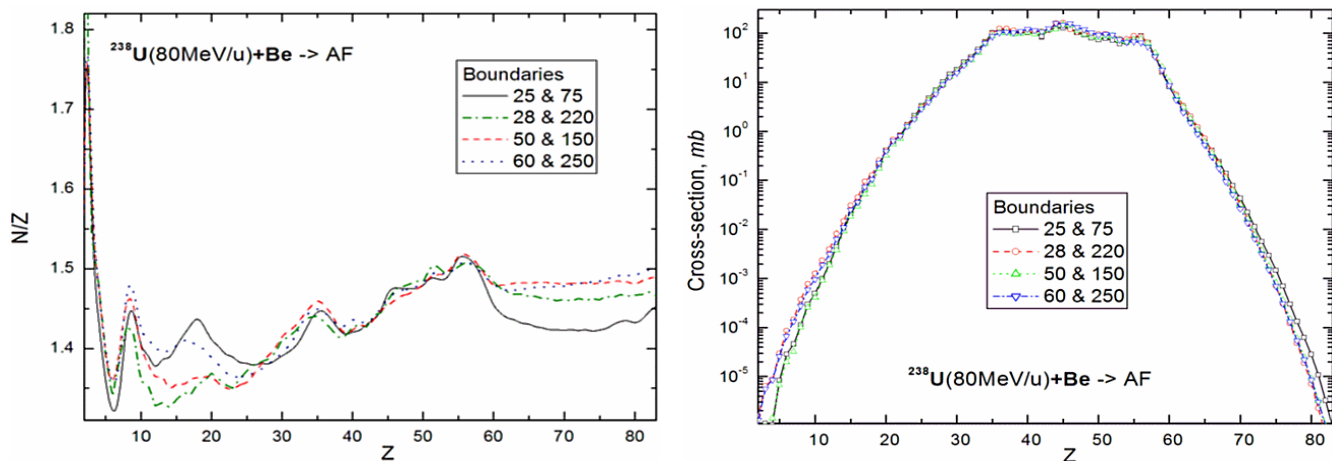


**Fig.83.** N/Z ratio (left plot) and element integrated (right plot) distributions of fission fragments from ( $^{238}\text{U}+\text{Be}$ ).

<sup>♥</sup> Boundary positions depend on excitation energy per abraded nucleon, which is used by the Abrasion-Ablation model to define EER characteristics. In above examples the excitation energy was equal to 13.3 MeV/dA.

### 5.4.3. Excitation energy per abraded nucleon for Abrasion-Ablation

To calculate the fission de-excitation function after abrasion of a heavy projectile by a target in previous examples, the excitation energy value 13.3 MeV per abraded nucleon was used. This value is set by default in the code. What decay channel will follow after an abrasion is determined first of all by the value of excitation energy (see Fig.9). The analysis of excitation energy is the subject of very complicated theoretical and experimental research, and is not a subject of this chapter, where we only want to show the influence of the excitation energy value on fission fragment production. Excitation energy depends on the target material and projectile energy<sup>\*</sup>, as well as the reaction mechanism involved in fragment production, for example abrasion or INC (chapter 5.8. INC fission). We speak about the abrasion of a projectile and suggest simplistically that the excitation energy is proportional to the number of abraded nucleons without any dependence on the target material or projectile energy.

**Table 12.** EER characteristics as a function of excitation energy per abraded nucleon

per abr.nucleon		$\Sigma\sigma$ mb	boundaries		Low			Middle			High		
$E^*$	$\sigma$		Left	Right	A, Z, N	$E^*$	$\sigma$	A, Z, N	$E^*$	$\sigma$	A, Z, N	$E^*$	$\sigma$
<b>9</b>	5	965	30	150	$^{236}_{92}\text{U}_{144}$	17.7	280.9	$^{228}_{89}\text{Ac}_{139}$	78.0	489.3	$^{210}_{83}\text{Bi}_{127}$	244.8	189.6
<b>13.3</b>	9.6	1228	30	180	$^{236}_{92}\text{U}_{144}$	23.5	312.8	$^{231}_{90}\text{Th}_{141}$	96.7	576.1	$^{217}_{85}\text{At}_{132}$	263.5	334.6
<b>27</b>	19	1361	45	200	$^{237}_{92}\text{U}_{145}$	38.7	292.4	$^{234}_{91}\text{Pa}_{143}$	114.5	573.2	$^{225}_{87}\text{Fr}_{138}$	320.8	489.9
<b>40</b>	28	1251	50	200	$^{236}_{92}\text{U}_{144}$	49.4	183.5	$^{234}_{91}\text{Pa}_{143}$	108.8	608.4	$^{228}_{89}\text{Ac}_{139}$	301.9	448.6

Table 12 shows EER characteristics calculated with different excitation energy values per abraded nucleon ( $E_{dA}^*$ ), which will be used for the following analysis of the influence of the excitation energy on fission fragment production. It is necessary to notice that with increasing  $E_{dA}^*$ , fissile nuclei become heavier. For example for Middle EER the masses of fissile nuclei are equal to 228, 231, 234, 234 for  $E_{dA}^*$  values of 9, 13.3, 27, 40 respectively, and for the High EER the masses are equal to 210, 217, 225, 228. It is explained that more abraded projectiles in the case of higher excitation energy proceed by the break-up channel. The following decay parameters were used for calculations:

Channels:  $p, n, 2n, \alpha, \text{fission}, \text{break-up}$   
 Break-up:  $T(40)=6.0, T(200)=4.5$   
 Dissipation: "Kramers' factor"=NO and beta=1  
 BarFac=1 & mode: auto.

Fig.84 shows the fission de-excitation cross-section as a function of  $E_{dA}^*$ . A reduced experimental cross-section value of  $1.16 \pm 0.10$  barn [Rub96] corresponds to an excitation energy equal to 13 MeV/dA. We talk a little bit more about total cross-sections in chapter "5.9. Comparison with experiment".

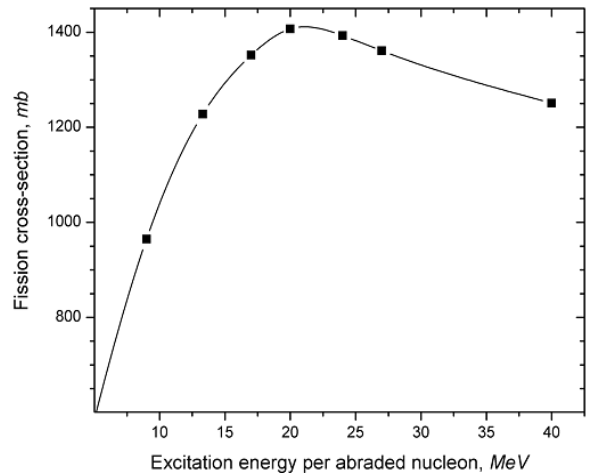


**Fig.84.** Fission de-excitation channel cross-section for  $^{238}\text{U} (80\text{MeV}/u)+\text{Be}$  as a function of excitation energy per abraded nucleon.

<sup>\*</sup> it is planned to make this analysis within the LISE development framework soon.



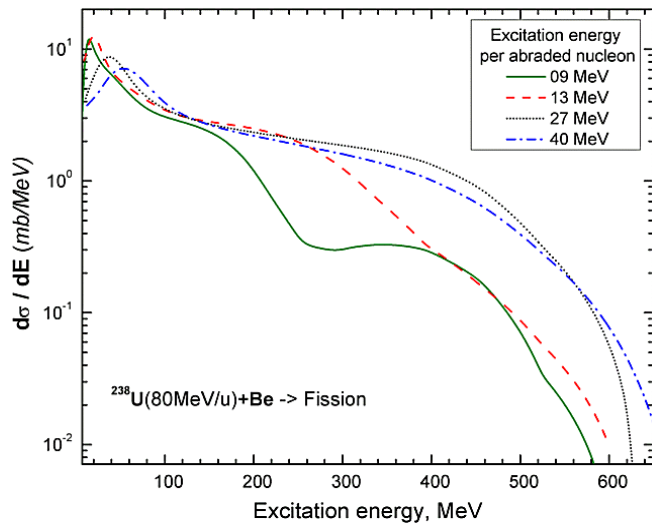


**Fig.85.** Fission de-excitation function for the reaction  $^{238}\text{U}+\text{Be}$  as a function of the excitation energy per abraded nucleon.

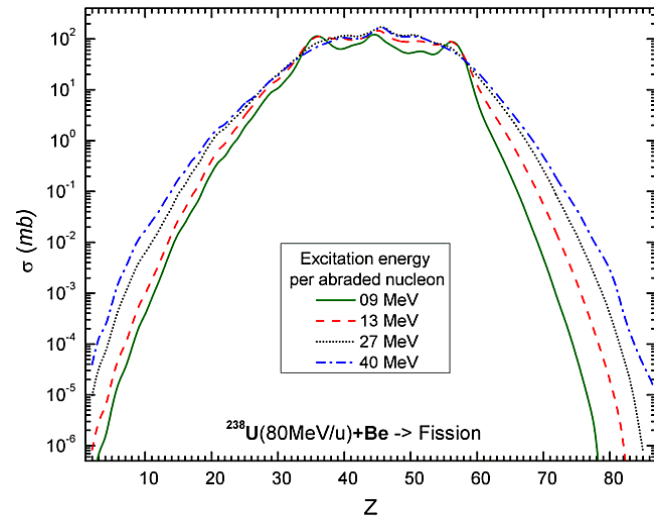


**Fig.86.** Elemental fission cross-sections for the reaction  $^{238}\text{U}(80\text{MeV}) + \text{Be}$  as a function of  $E_{dA}^*$ .

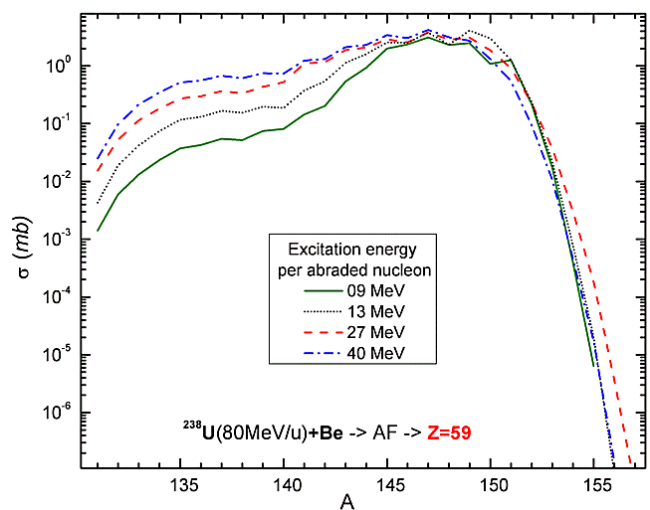
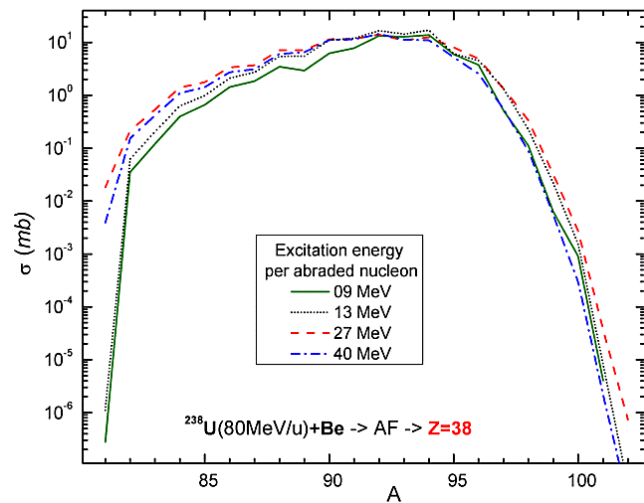


**Fig.87.** Total (sum of all regions) mass distributions of Strontium (left plot) and Praseodymium (right plot) fission fragments in the reaction  $^{238}\text{U}(80\text{MeV/u})+\text{Be}$  calculated for different values of excitation energy per abraded nucleon.

Fig.85-87 demonstrate the influence of the excitation energy value in abrasion on fission de-excitation functions, elemental fission cross-sections, and mass distributions of Strontium and Praseodymium fission fragments in the reaction  $^{238}\text{U}(80\text{MeV/u})+\text{Be}$ .

Fig.88 shows partial and total mass distributions of Praseodymium fission fragments in the reaction  $^{238}\text{U}(80\text{MeV/u})+\text{Be}$  calculated for  $E_{dA}^* = 27 \text{ MeV/dA}$ .

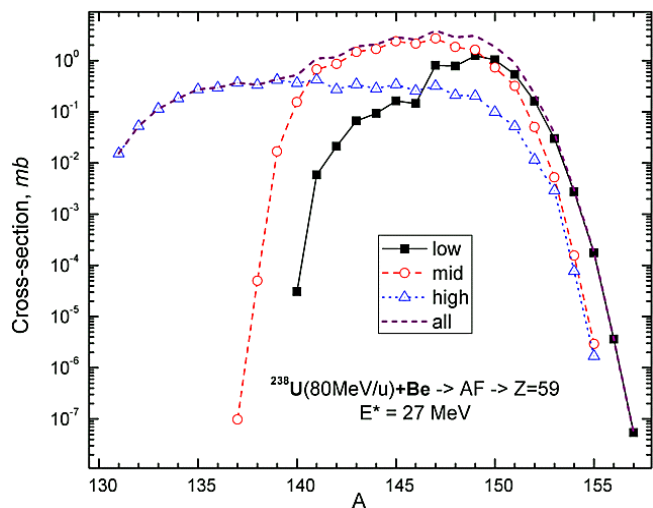


**Fig.88.** Calculated mass distributions of Praseodymium fission fragments in the reaction  $^{238}\text{U}(80\text{MeV/u})+\text{Be}$ .

#### 5.4.4. Dissipation effects in fission

The influence of dissipation effects on the fission de-excitation functions has already been considered in chapter “2.2. Dissipation effects in fission”, where Fig.13 demonstrates how the total nuclear fission cross-section and the shape of the fission excitation functions can depend on the dissipation effects.

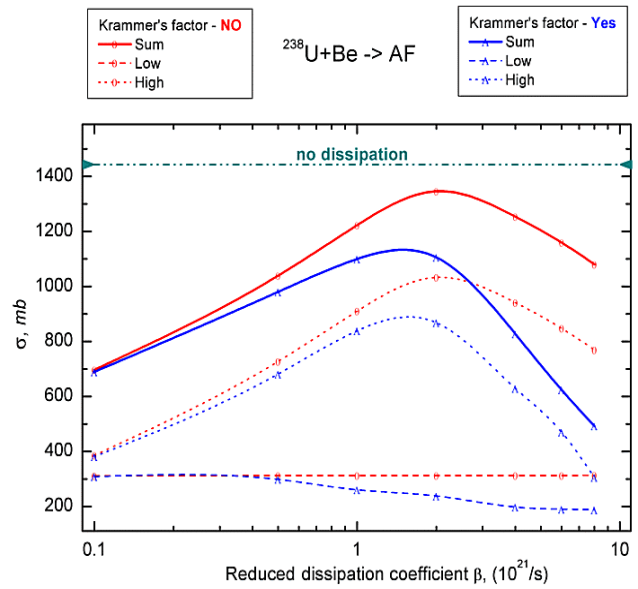
Here we would like to notice a correlation between the reduced dissipation parameter, Kramers’ factor, and the total fission cross-section. Recall that parameters for dissipation effects are in the “Evaporation options” dialog (see Fig.7, frame “A”).

Fig.89 and Fig.90 show fission cross-section and excitation energy of the High EER fissile nucleus in the reaction  $^{238}\text{U}(80\text{MeV/u})+\text{Be}$  as a function of reduced dissipation coefficient. These calculations were done for the 2-EER model. The boundary between Low and High regions was set to 30 MeV. In the case of excitation energy per abraded nucleon equal to 13.3 MeV/dA it is recommended to use a reduced dissipation coefficient equal to  $1 \cdot 10^{21}/\text{s}$  and turn off Kramers’ factor to exclude dissipation effects at low-excitation energies.

#### 5.4.5. Break-up de-excitation channel

The crucial role of the break-up channel has been already demonstrated in chapter 2.1.1.1. The dependence of break-up parameters (limiting temperature, diffuseness) on de-excitation channel cross-sections it is possible to see in Fig.91, based on calculation results given in Table 13. These calculations were done for the 3-EER model with boundaries 40 and 180 MeV. The excitation energy per abraded nucleon was set to 13.3 MeV/dA. It is possible to conclude for the limiting temperature “working” region (4-7 MeV) that:

- If we take dissipation effects into account, then the fission cross-sections do not depend on the limiting temperature. There is competition between break-up channels and light particle evaporation.
- If we do not take dissipation effects into account then light particle evaporation cross-sections do not depend on the limiting temperature. There is competition between break-up and fission de-excitation channels.



**Fig.89.** Fission cross-section in the reaction  $^{238}\text{U}(80\text{MeV/u})+\text{Be}$  as a function of reduced dissipation coefficient. Calculations were done for the 2-EER model. The boundary between Low and High regions was set to 30 MeV.

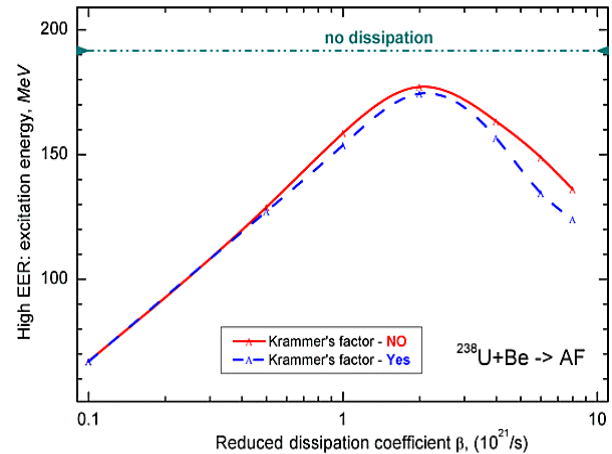


**Fig.90.** Excitation energy of the High EER fissile nucleus in the reaction  $^{238}\text{U}(80\text{MeV/u})+\text{Be}$  as a function of reduced dissipation coefficient. Calculations were done for the 2-EER model. The boundary between Low and High regions was set to 30 MeV.



**Table 13.** Channel cross-sections as a function of the limiting temperature.

Break-up parameters			Dissipation <i>Use Step function</i>	High ERR Excit. energy	AF cross-sections, [mb]		Evaporation calculator cross-section [barn]		
T A=40	T A=200	Diffuse- ness			High EER	Sum of EERs	Residues	Fission	Break-up
4.5	6	0.05	Yes	263.5	334.6	1223.5	0.904	1.18	0.604
4.5	6	<b>0.5</b>	Yes	256.4	275.6	1150.7	0.784	1.14	0.694
4.5	6	0.05	No	305.7	487.5	1464.2	0.721	1.44	0.603
3	3	0.05	Yes	200.1	127.3	1014.8	0.7	1.01	1.01
4	4	0.05	Yes	249	307.7	1196.6	0.838	1.16	0.702
5	5	0.05	Yes	282.4	362.4	1251.2	0.967	1.20	0.519
6	6	0.05	Yes	294.7	385.0	1273.9	1.09	1.22	0.372
7	7	0.05	Yes	294.9	387.1	1276.0	1.2	1.22	0.258
3	3	0.05	No	203.1	163.5	1079.9	0.658	1.09	1.01
4	4	0.05	No	263.8	473.1	1381.1	0.707	1.36	0.7
5	5	0.05	No	326	646.5	1554.5	0.728	1.53	0.517
6	6	0.05	No	359.5	798.4	1706.4	0.731	1.67	0.37
7	7	0.05	No	360.7	914.9	1822.9	0.733	1.79	0.257

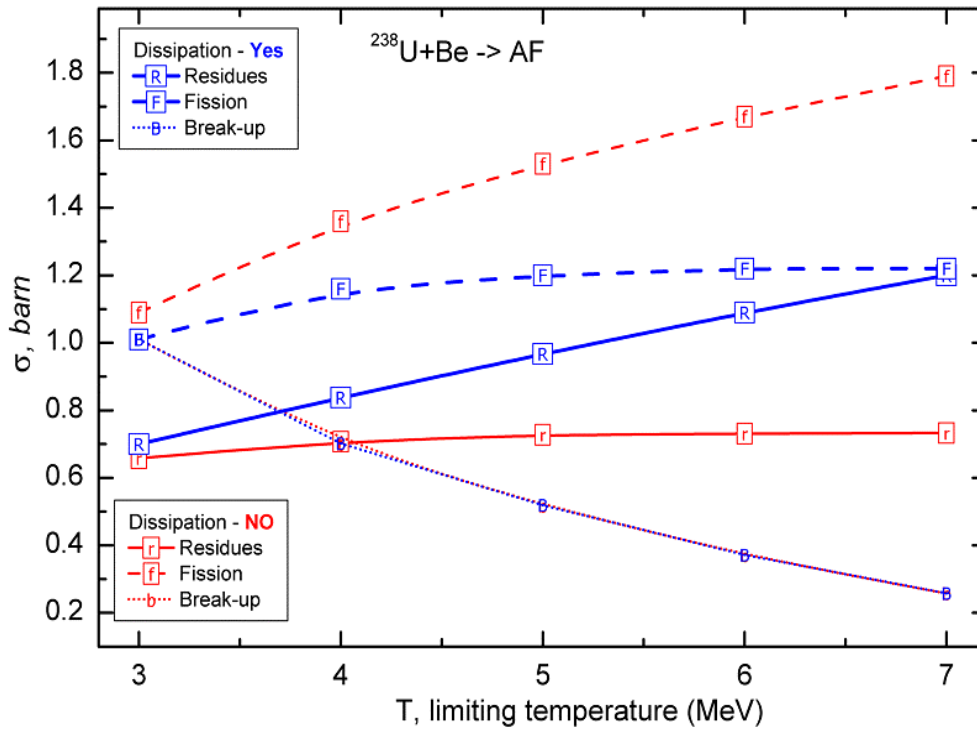


**Fig.91.** Fission cross-section in the reaction  $^{238}\text{U}(80\text{MeV}/u)+\text{Be}$  as a function of reduced dissipation coefficient. Calculations were done for the 2-EER model. The boundary between Low and High regions was set to 30 MeV.

#### 5.4.6. Fission barrier

Correlation between the fission barrier and the fission de-excitation function has already been considered in chapter “3.5. Influence of corrections for fission barriers on abrasion-fission cross-sections”.

Increasing fission barrier height leads to a decrease of fission cross-sections and increasing light particle evaporation production.

### 5.4.7. Cross-section suppression coefficient

The cross-section suppression coefficient is applied to the initial fission cross-section matrix (*CSinit*) of production cross-sections for excited fragments before the calculation of light particle emission. This coefficient is set by default to 1e-10mb. Using this coefficient decreases calculation time for cross-sections and frees the operating memory. With the coefficient equal to 1e-10 mb the code uses 90 seconds whereas for values 1e-15, 1e-20, and 1e-30 mb respectively, it uses 121, 142, and 206 seconds. It is necessary to note two moments:

- Decreasing the suppression coefficient does not lead similarly to low cross-sections for proton-rich fragments, because in the first place the acceleration filter (see “5.1.3.2. Modification of evaporation cascade subroutines”) works against low cross-section production after reaching the maximum of the final fragment distribution (see Fig.56).
- Secondary reactions contribution is very important in the case of Abrasion-Fission, and we recommend always using the SR option. As you will see in the next chapter, there is no difference between reduced cross-sections calculated with different cross-section limit values if the target is not very thin.

Fig.92 shows Tin fission fragment cross-sections for production in the reaction  $^{238}\text{U}+\text{Be}$  calculated for different cross-section suppression values.

### 5.4.8. Restore previous AF settings

If the user is working in the Abrasion-Fission reaction mode and changes the parameters of the target or the primary beam, then the program automatically

- ❑ initiates the AF EER settings,
- ❑ sends a message to the user (see Fig.93),
- ❑ shows AF settings by red colors in the Set-up window (see Fig.99).

If the user wants to go back to previous AF settings, it is necessary to open the “AF settings” dialog (for more details about it look at “5.6.2. Abrasion-Fission settings”) and click the “Restore previous settings” button to load the dialog of the same name, which shows the previous settings and prompts the user either to accept them or to refuse.

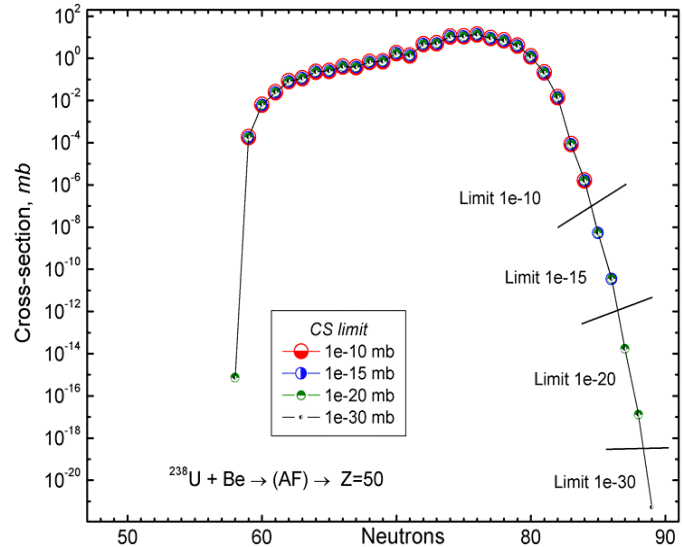


Fig.92. Calculated Tin fission fragment cross-sections for production in the reaction  $^{238}\text{U}+\text{Be}$ .

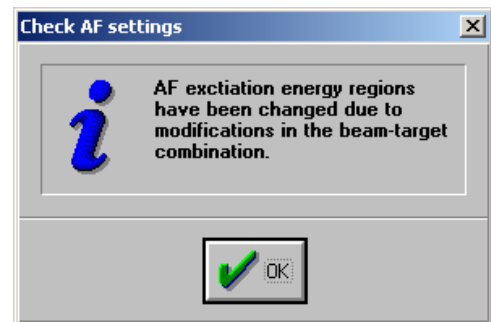


Fig.93.

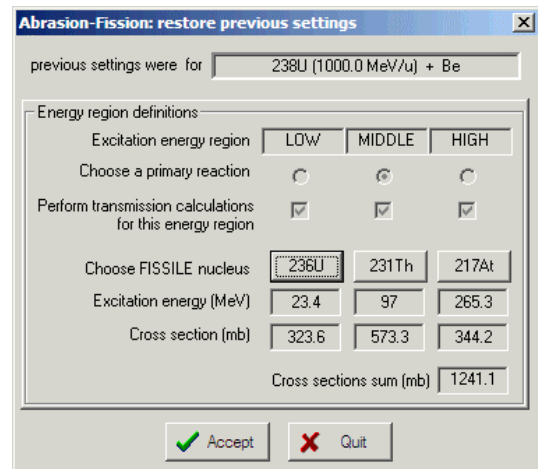


Fig.94. The “Restore previous AF settings” dialog.

### 5.5. Secondary reactions for Abrasion-Fission

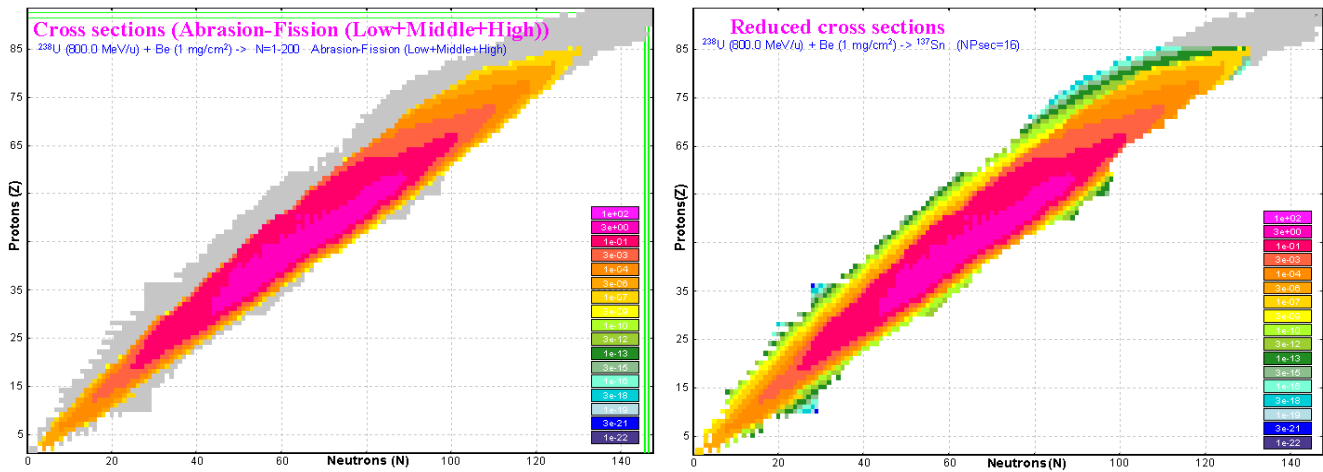
Secondary reactions are a very important component for fragments produced in fission with a low cross-section even in the case of a thin target. As it was already mentioned We recommend using the rectangle filter (bottom rectangle deltas are 30&30, top rectangle 0&0) for SR calculations and not setting the cross-section suppression coefficient very low, as you will see from the figures in this chapter.

Let's suggest that Middle EER is set as the primary reaction in the code. Then the reduced cross-section is calculated using Equation /10/, where  $\sigma_{\text{primary}}^*$  is equal to the production cross-section corresponding to the Middle EER. Total reduced cross-section is defined by the formula:

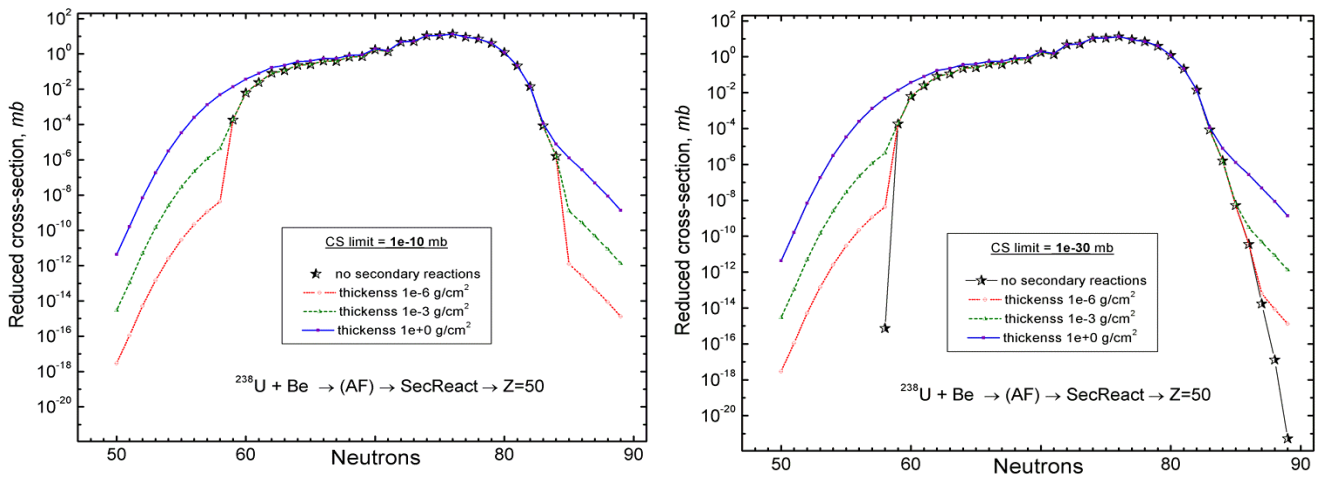
$$\sigma_{\text{total\_reduced}} = \sigma_{\text{Middle}}^* \cdot \tau_{\text{SR}} + \sigma_{\text{Low}} + \sigma_{\text{High}} \quad /12/$$

The reduced cross-section plot utility (4.2.1. Secondary Reactions plots: SR coefficients & reduced cross-sections) shows namely the total reduced cross-section values calculated based on Equation /12/.

Fig.95 shows in the left plot fission production cross-sections (sum of all three EER) in the reaction  $^{238}\text{U}(80\text{MeV/u})+\text{Be}$  calculated for cross-section suppression equal to  $1\text{e-}10$  mb and presents in the right plot total reduced cross-sections for the Be-target thickness equal to  $1\text{ mg/cm}^2$ .



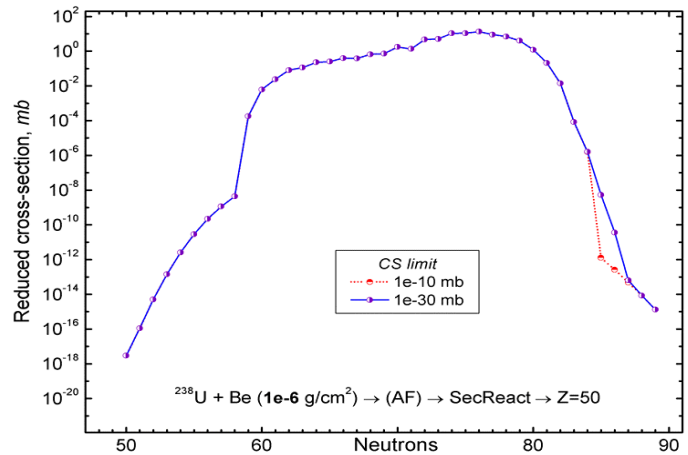
**Fig.95.** Left plot: Fission production cross-sections (sum of all three EER) in the reaction  $^{238}\text{U}(80\text{MeV/u})+\text{Be}$  calculated for cross-section suppression equal to  $1\text{e-}10$  mb. Right plot: the same as the left plot but with SR contribution for the Be-target thickness equal to  $1\text{ mg/cm}^2$ .



**Fig.96.** Total reduced production cross-sections of Tin fission fragments produced in the reaction  $^{238}\text{U}+\text{Be}$  as a function of the target thickness. Left plot corresponds to calculations with the cross-section suppression limit equal to  $1\text{e-}10$  mb, right plot similarly for a value  $1\text{e-}30$  mb.

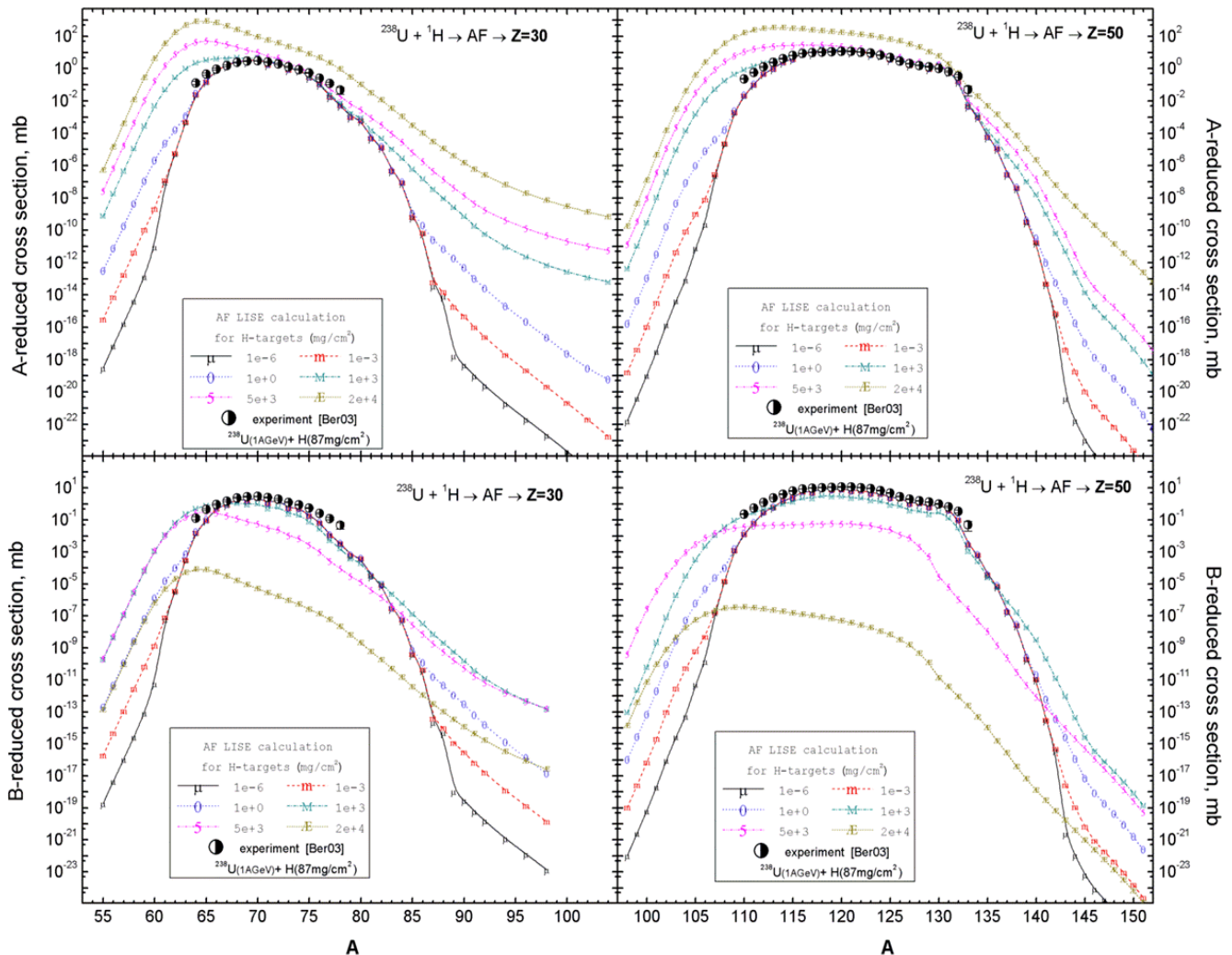
Fig.96 demonstrates how total reduced cross-sections of Tin fission fragments produced in the reaction  $^{238}\text{U}+\text{Be}$  depend on the target thickness.

Fig.97 shows total reduced production cross-sections of Tin fission fragments for two different suppression values in the case of a thin target ( $1\ \mu\text{g}/\text{cm}^2$ ). The small difference is observed just for two neutron-rich isotopes. With increasing target thickness (at least up to  $1\ \text{mg}/\text{cm}^2$ ) this discrepancy disappears.



**Fig.97.** Total reduced production cross-sections of Tin fission fragments produced in the reaction  $^{238}\text{U}+\text{Be}$  ( $1\ \mu\text{g}/\text{cm}^2$ ) as a function of the suppression limit.

Let's assume that we have a primary beam of  $^{238}\text{U}$  with very high energy to exclude "dead" layer of the target from calculations. Is there a limit for target thickness or, taking into account the contribution of secondary reactions, is the fragment production always continuously increasing in value? If this limit exists then where is it located?



**Fig.98.** A(top plots)- & B(bottom plots)- reduced (see text for details) production cross-sections of Zinc (left plots) and Tin (right plots) fission fragments produced in the reaction  $^{238}\text{U}(10\text{AGeV})+p$  as a function of the target thickness.

Fig.98 shows A- & B-reduced production cross-sections of Zinc and Tin fission fragments produced in the reaction  $^{238}\text{U}(10\text{AGeV}) + \text{p}$  as a function of the target thickness. AF EERs settings used for calculations are presented in chapter “5.9.5.  $^{238}\text{U}(1\text{AGeV}) + \text{p}$ ”. The A-reduced cross-section is equivalent to  $\sigma_{\text{total\_reduced}}$  from Equation /12/. The B-reduced cross-section is defined by the formula:

$$\sigma_{\text{reduced}}^B = \frac{R}{N_{\text{target}} \cdot I_{\text{beam}}}, \quad /13/$$

where  $R$  is the yield of fragment of interest after the target [1/s],  $N_{\text{target}}$  in the number of atoms in the target [ $1/\text{cm}^2$ ], and  $I_{\text{beam}}$  is the primary beam intensity [1/s]. The principal difference between “A” & “B” reduced cross-sections is contained in the reaction coefficient of losses, which exists in the B-reduced cross-section:  $\sigma_{\text{reduced}}^B = \sigma_{\text{reduced}}^A \cdot \mathcal{E}_{\text{reaction}}$ .

It is possible to see that the A-reduced cross-section increases with increased target thickness for Zinc isotopes as well as Tin isotopes due to secondary reactions contributions, and the largest gain is achieved for proton rich isotopes.

In the case of B-reduced cross-section it is possible to see that increasing target thickness in four times from  $5 \text{ g/cm}^2$  up to  $20 \text{ g/cm}^2$  decreases reduced cross-sections by 3-4 orders of magnitude. It is possible to conclude that the optimal target thickness to produce the maximum rate of fragments for the reaction  $^{238}\text{U}(10\text{AGeV}) + \text{p}$  is about  $1\text{-}3 \text{ g/cm}^2$ .

## 5.6. Setting up LISE to calculate yield of AF products through the spectrometer

Let’s start to acquaint ourselves with LISE settings for the Abrasion-Fission (AF) mechanism by an example. Assume we need to produce a  $^{81}\text{Zn}$  secondary beam using a primary beam of  $^{238}\text{U}^{86+}$  ions with energy  $80 \text{ MeV/u}$  at the NSCL/MSU.

### 5.6.1. Experiment settings

Let’s assume in the beginning the simple case without charge states, without a wedge, using just one target, without secondary reactions, and with nonzero primary cross-sections. The first two steps are the same as for the case with other reaction mechanisms.

#### 5.6.1.1. Spectrometer choice


Since we plan to use the A1900 fragment separator, we need to first configure LISE++ for this device. This is done as follows:

- a. Start the program LISE++
- b. Select the menu *File* → *Configuration* → *Load*
- c. Choose the file “A1900\_2005A.lcn” in the NSCL directory

#### 5.6.1.2. Primary beam, target, selected fragment

- a. Set the projectile characteristics ( $^{238}\text{U}$ ,  $E=80 \text{ MeV/u}$ ,  $Q=86+$ ) by clicking on the letter “P” of the label “Projectile” or alternatively selecting the menu *Settings* → *Projectile*.
- b. Set the desired fragment ( $^{81}\text{Zn}$ ) too if it hasn’t been done already by clicking on the “F” letter of the label “Fragment” or alternatively selecting the menu *Settings* → *Fragment*.
- c. The target (Be,  $0.1 \text{ mm}$ ) can be entered directly by clicking on the “T” letter of the label “Target” or alternatively selecting the menu *Settings* → *Target*.

### 5.6.2. Abrasion-Fission settings

- Set the reaction mechanism (Abrasion-Fission) by clicking on the  icon or alternatively selecting the menu *Options* → *Production Mechanism*. After that you can see the AF frame where three fissile nuclei and their excitation energies are shown (see Fig.99).
- You need to recalculate the excitation regions parameters according to the beam and target characteristics. In order to make these changes you have to open the “Abrasion-Fission” dialog (see Fig.50) by clicking on the AF frame in the Set-up window (see Fig.100) or alternatively selecting the “Abrasion-Fission settings” button in the “Production mechanism” dialog through the menu *Options* → *Production Mechanism*.
- Make sure, that the break-up and fission de-excitation channels in the “Evaporation settings” are turned on. You can find more detailed information in the chapters about the “Abrasion-Fission” dialog, de-excitation, and fission default parameters. Now just click the multi-purpose button “*Calculate, Use ‘All’ in the code, Apply, Plot*” (see Fig.50) to calculate Abrasion-Fission settings for this beam-target combination to use in the following fragment yield calculations. It is recommended to set “Middle excitation energy region” as a primary reaction (see Fig.51). Click the “Ok” button to leave the dialog. Now you might see several changes in the Set-up window (see Fig.101).

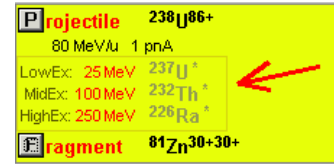


Fig.99. The Abrasion-Fission frame showing excitation regions.

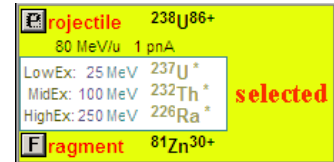
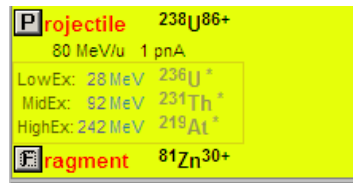




Fig.100. The Abrasion-Fission frame is selected by the mouse.

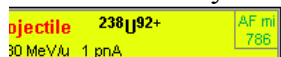
Fig.101. Parts of the Set-up window after AF settings calculations were done. Excitation energy strings color has been changed after modifications of AF settings. The initial color is red (see Fig.99).



### 5.6.3. Spectrometer tuning for the fragment of interest

- Set maximum possible momentum acceptance (5.07%) of the spectrometer using the “I2\_slits” block settings dialog through the Set-up window.
- Set the “Right peak” option in the “Calculate spectrometer settings using....” in the “Preferences” dialog by clicking  or selecting the menu “*Options* → *Preferences*”.

Calculate the fragment separator settings by clicking on  or selecting the menu *Calculations* → *Calculate the spectrometer for setting ion*. The code calculates spectrometer settings based on fragment kinematics of the primary reaction (AF-middle) you set. Therefore the code initially has to calculate AF-middle final fragment and excited fragment production cross-sections, which should be used in kinematics calculations. Kinematics of fission fragment calculations and spectrometer tuning are based on the same procedures as in the case of Coulomb fission. After the code runs, it will set the spectrometer and you can see in the Set-up window the number of AF-middle cross-sections



These cross-sections will be kept in the memory as long as the projectile & target combination, fission properties, and de-excitation properties have been not changed by the user.



### 5.6.4. Yield calculation

Calculate the yield of  $^{81}\text{Zn}$  for these settings by double right clicking on the corresponding nucleus in the table of nuclei. The code calculates consecutively the yields for all of three excitation energy regions (EER). Each EER represents a separate reaction mechanism in the code. This means the code first calculates rates for Middle EER, then changes the primary reaction to Low EER, calculates rates for this region, then High EER and finally comes back to Middle EER. Each EER has its own cross-section matrices, because the code checks cross-section matrices existence before yield calculations. If the matrices are absent for this reaction mechanism or the projectile and target combination or fission and de-excitation properties have been changed then the code calculates fission fragment production cross-sections for these new projectile-target-fission settings. The number of nonzero cross-sections for each EER kept in the memory is shown in the Set-up window (see in Fig.102).

<b>P</b> rojectile	$^{238}\text{U}^{92+}$	AF lo	563
80 MeV/u 1 pnA		AF mi	786
LowEx:	28 MeV $^{236}\text{U}^*$	AF hi	826
MidEx:	92 MeV $^{234}\text{Th}^*$		
HighEx:	242 MeV $^{219}\text{At}^*$		
<b>F</b> ragment	$^{81}\text{Zn}^{30+}$		

Fig.102. The Abrasion-Fission frame showing excitation energy regions (EER) and the number of non-zero cross-sections for each EER.

Fig.103 shows statistics of  $^{81}\text{Zn}$  fragment production. Under the production line in the new version you can see two new lines: reaction mechanism name and sum of reactions. It is visible, that the  $^{81}\text{Zn}$  fragments have been produced in Middle and Low EER reactions. The  $^{81}\text{Zn}$  production cross-section for High EER is equal to zero.

statistics $^{81}\text{Zn}$			
$^{81}\text{Zn}$		Beta- decay (Z=30, N=51)	
Q1 (D1)		30	30
Q2 (D2)		30	30
Q3 (D3)		30	30
Q4 (D4)		30	30
Production Rate	(pps)	9.77e-6	1.71e-4
Reaction		AF_mid	AF_low
Sum of reactions	(pps)	1.8e-4	1.8e-4
CS in the target	(mb)	4.39e-8	8.01e-7
Total transmission	(%)	2.879	2.758
Target	(%)	99.66	99.66

Fig.103. The statistics window of  $^{81}\text{Zn}$  fragment production.

The “Sum of reactions” result value has been included just in the new version and it is equal to the sum of the “Sum of charge states” values. The “Sum of charge states” values are the sum of all charge states produced for one fragment in ONE reaction.

In total we have received a  $^{81}\text{Zn}$  fragment production rate equal to  $1.8\text{e-}4$  pps for 0.1 mm Be-target at the focal plane of the spectrometer.

### 5.6.5. Optimum target

Let’s optimize the target thickness to produce the maximum production rate of  $^{81}\text{Zn}$  fragments by selecting the menu “Calculations → Optimum target”. Results of calculations are shown in Fig.104. The target thickness corresponding to maximum production rate (total:  $9.32\text{e-}4$ , Middle ERR:  $5.2\text{e-}5$ ) is equal to 0.52 mm.

Fig.105 shows the spatial distribution of  $^{81}\text{Zn}$  fission fragments in the dispersive focal plane after the first dipole. You can see the selection of the “Right” peak (corresponding to higher energy) of the fragment momentum distribution by the spectrometer.

**Note:** It is recommended to set such EER as the primary reaction that which contributes most to the fragment production rate. In the case of the reaction  $^{238}\text{U}(80\text{MeV/u}) + \text{Be} \rightarrow (\text{AF}) \rightarrow ^{81}\text{Zn}$  it is the Low EER (see Fig.103). In this case the spectrometer will be set following the kinematics of this reaction mechanism, and the secondary reaction coefficient is applied to the reaction mechanism with most intense production, which gives the most correct estimation of the secondary reactions’ contribution.



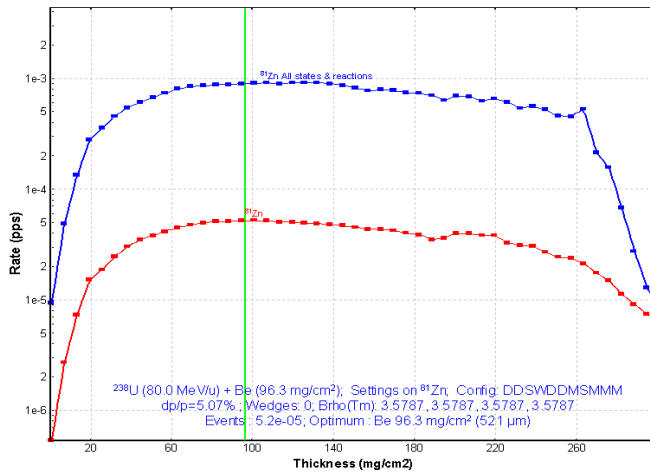


**Fig.104.**  $^{81}\text{Zn}$  fission fragment production rate in the reaction  $^{238}\text{U}(80\text{AMeV})+\text{Be}$  as a function of the target thickness.

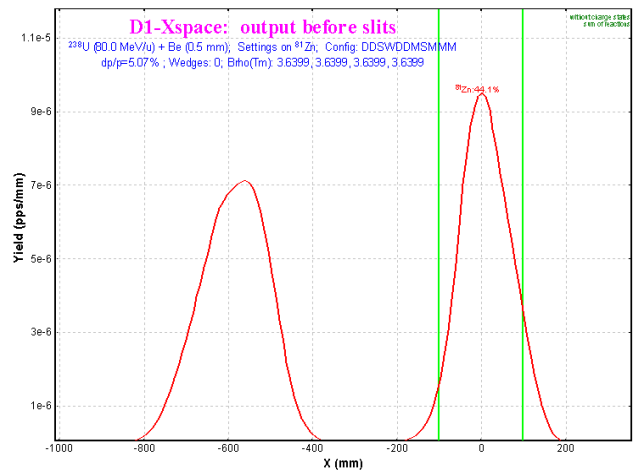


**Fig.105.** Spatial distribution of  $^{81}\text{Zn}$  fission fragments in the dispersive focal plane after the first dipole.

### 5.6.6. Secondary reactions

Let's turn on the secondary reactions contribution in the "SR" dialog by selecting the menu "Options → Secondary reaction in target". Set the Corner rectangle filter for all three procedures in the dialog. Use parameters  $\Delta N=30$  and  $\Delta Z=25$  for the bottom rectangle and 0 & 0 for the top rectangle of the corner filter in the case of fission (see 4.3.1.3. Application of acceleration filters). The SR contribution gives gain about four times even for this not so high energy of the primary beam (Fig.106).

statistics 81Zn			
81Zn		Beta- decay (Z=30, N=51)	
Q1 (D1)		30	30
Q2 (D2)		30	30
Q3 (D3)		30	30
Q4 (D4)		30	30
Production Rate	(pps)	5.36e-5	3.5e-3
Reaction		AF_mid	AF_low
Sum of reactions	(pps)	3.55e-3	3.55e-3
CS in the target	(mb)	4.39e-8	8.01e-7
Total transmission	(%)	3.032	10.87
Target	(%)	98.25	3.78e+2
X space transmission	(%)	100	100
Y space transmission	(%)	100	100
Unreacted in mater.	(%)	98.25	98.25
Unstopped in mater.	(%)	100	100
Secondary Reactions	(coef)	1	3.85

**Fig.106.** The statistics window of  $^{81}\text{Zn}$  fragment production with taking into account the SR contribution.

Fig.107 shows the multi-step production probabilities to produce  $^{81}\text{Zn}$  from the primary reaction  $^{238}\text{U}(80\text{MeV/u})+\text{Be}(96\text{mg/cm}^2) \rightarrow \text{AF}$ . The corner rectangle filter is shown in the figure.

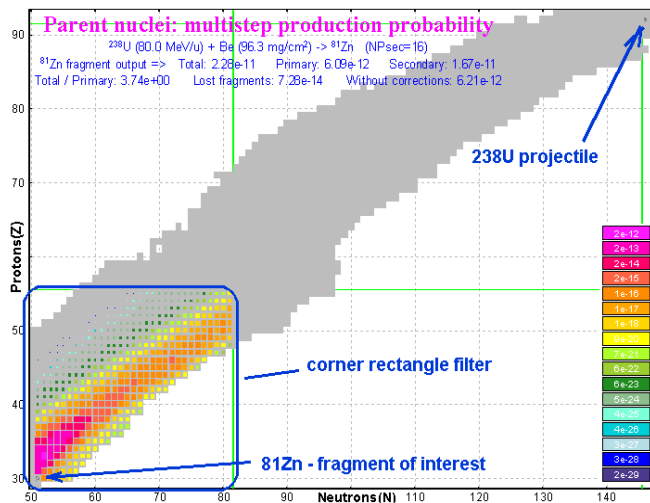


**Fig.107.** Multi-step production probabilities to produce  $^{81}\text{Zn}$  for the primary reaction  $^{238}\text{U}(80\text{MeV/u})+\text{Be}(96\text{mg/cm}^2) \rightarrow \text{AF}$ .

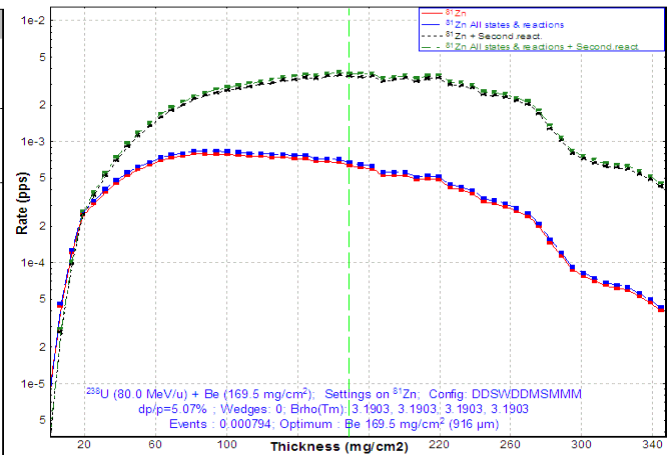


**Fig.108.**  $^{81}\text{Zn}$  fission fragment production rate for the reaction  $^{238}\text{U}(80\text{AMeV})+\text{Be}$  as a function of the target thickness taking into account the SR contribution. The Low EER was set as the primary reaction to calculate  $^{81}\text{Zn}$  fission fragment production.

Fig.108 shows the optimum target thickness plot where the SR contribution was taken into account in the calculations. In the case of using SR contributions the target becomes significantly thicker (0.91 mm).

**Note:** It is necessary to notice that yield calculations become less precise when the amount of stopped fragments in the target exceeds 50 percent due to the analytical LISE fission approach. For example in the reaction  $^{238}\text{U}(80\text{MeV})+\text{Be}$  this happens at thickness  $330\text{ mg/cm}^2$  (1.8 mm).

### 5.6.7. Cleaning

We need to think about purification of the secondary beam from background fragment production, because in a single run there are at once more than 1700 fragments (from different EERs) produced with a total yield of  $3.7\text{e}4$  pps. This is about  $10^7$  times more than the intensity of the  $^{81}\text{Zn}$  secondary beam (see Fig.109).

Let's set a wedge-profile achromatic Be-degrader ( $60\text{ mg/cm}^2$ ) in the intermediate dispersive focal plane I2 (*I2\_wedge*), while decreasing the target thickness down to  $80\text{ mg/cm}^2$  and setting the final slits *FP\_slits* to  $\pm 4\text{ mm}$ . Using the wedge we could decrease the total yield down to 630 pps (see Fig.110).

If we slightly increase the magnetic rigidity, it is possible to decrease background rates further without losing intensity of the fragment of interest, because the main background contribution is coming from low-energy intense isotopes (Fig.111 and Fig.112).

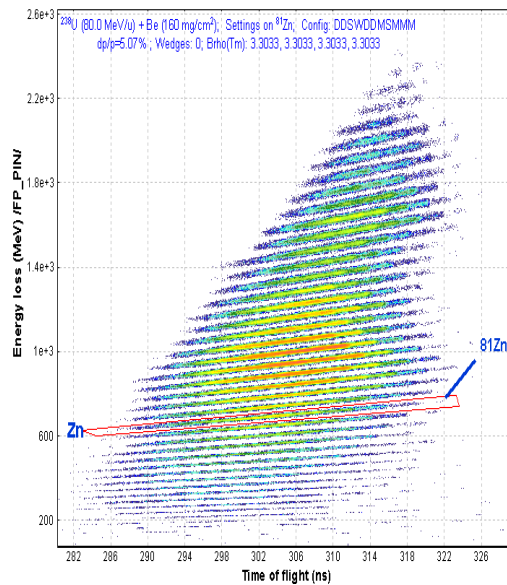


**Fig.109.** Two dimensional identification plot for fission fragments obtained in  $80\text{ MeV/u } ^{238}\text{U} + \text{Be}(160\text{mg/cm}^2)$  at the magnetic rigidity  $3.303\text{ Tm}$ . These statistics correspond to 2 seconds of acquisition. The intensity of the primary beam is equal to 1 pna.

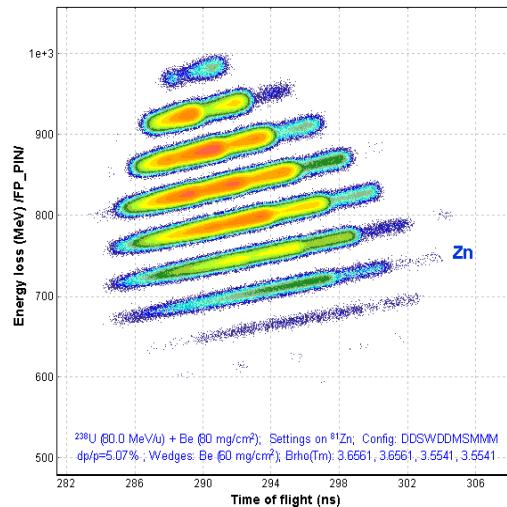


**Fig.110.** Two dimensional identification plot for fission fragments obtained in  $80\text{MeV/u } ^{238}\text{U} + \text{Be}(80\text{mg/cm}^2)$  using an achromatic Be-wedge ( $60\text{mg/cm}^2$ ) in the dispersive intermediate focal plane I2. This statistics corresponds to 4.5 hours of acquisition.

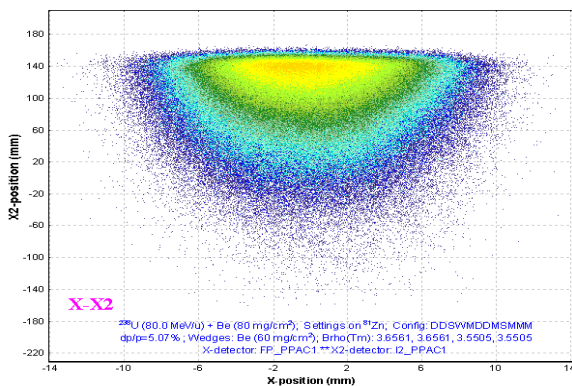


**Fig.111.** 2D-plot of fission fragments. Abscissa axis: horizontal coordinate from PPAC in the final focal plane (*FP\_PPAC1*); ordinate axis: horizontal coordinate from PPAC in the intermediate dispersive focal plane (*I2\_PPAC1*).

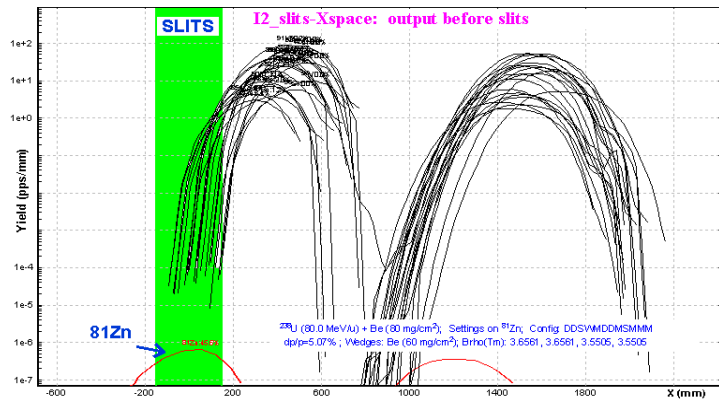


**Fig.112.** Horizontal spatial distribution plot of fission fragments in the reaction  $^{238}\text{U}(80\text{MeV/u})+\text{Be}(80\text{mg/cm}^2)$  using an achromatic Be-wedge ( $60\text{mg/cm}^2$ ) in the intermediate dispersive focal plane (the dispersion is negative).

Let's decrease the momentum acceptance down to 1% and slightly increase the magnetic rigidity by 0.5% to get a 2D-plot with unambiguous identification in Fig.113.

Modifying wedge and target thicknesses as well as slits sizes at Image2 and the focal plane (FP) it is possible to more easily distinguish the secondary beam intensity and the better ratio between the fragment of interest and background.

### 5.6.8. Charge states



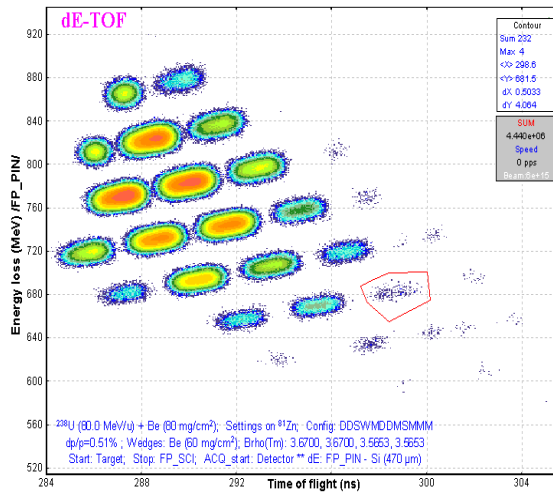
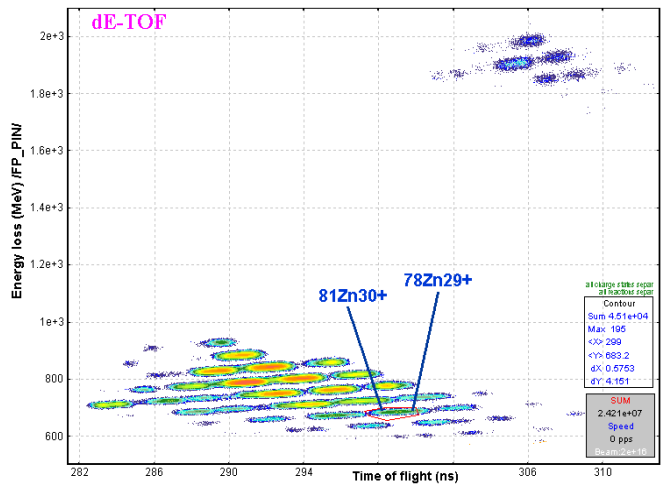
For the previous calculations, we guessed that all the fragments were completely charge stripped. But in reality the problem of charge states is important at this energy (80MeV/u) of a primary beam. In the case of the transmission calculation for charge states, we recommend limiting calculations to only a small region of isotopes using , where the fragments are expected; otherwise, in the case of transmission calculation of all isotopes , the calculation can take more than one hour. Let's turn on the charge state option in the "Preferences" dialog. Let's assume the spectrometer is tuned to fully stripped ions ( $^{81}\text{Zr}^{30+}$ ).

Fig.114 shows a two-dimensional  $dE$ - $ToF$  identification plot for fission fragments obtained in the reaction  $^{238}\text{U}(80\text{MeV/u}) + \text{Be}(80\text{mg/cm}^2)$  using a Be-wedge ( $60\text{mg/cm}^2$ ). Charge states and Secondary reactions options are turned on. If compared with Fig.113 you can see in the upper right corner the new



**Fig.113.** Two dimensional identification plot for fission fragments using an achromatic Be-wedge ( $60\text{mg/cm}^2$ ).  $^{81}\text{Zn}$  is selected by a red contour.



**Fig.114.** Two-dimensional  $dE$ - $ToF$  identification plot for fission fragments obtained in the reaction  $^{238}\text{U}(80\text{MeV/u}) + \text{Be}(80\text{mg/cm}^2)$  using a Be-wedge ( $60\text{mg/cm}^2$ ). Charge states and Secondary reactions options are turned on.

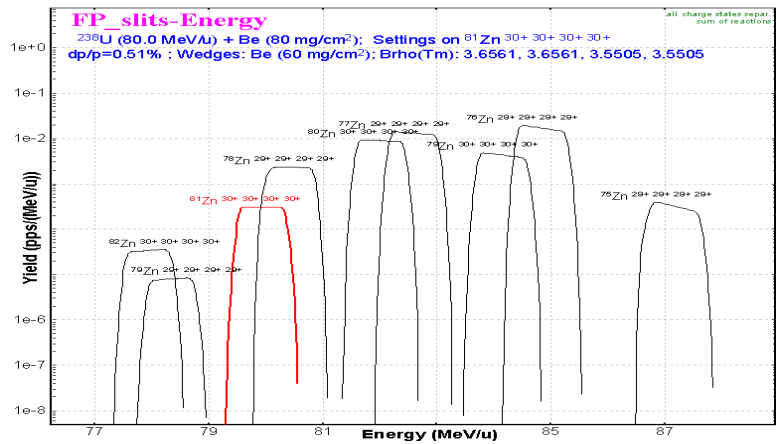


**Fig.115.** Zinc ion energy distributions in the final focal plane of the spectrometer.

group of heavy ions corresponding to elements with  $Z=47-52$ . The charge state of these fragments has been changed by the wedge material from  $Q_{1,2} = Z-2$  to  $Q_{3,4} = Z-3$  or from  $Q_{1,2} = Z-1$  to  $Q_{3,4} = Z-2$ . Using this 2D-plot it is impossible now already to make an unambiguous identification because as you can see the  $^{81}\text{Zr}^{30+}$  and  $^{78}\text{Zr}^{29+}$  ions positions in the plot are overlapping (see also Fig.115). It is possible to make off-line separation

using a third measured value, the total kinetic energy of the fragment (*TKE*).

### 5.6.9. Go to more exotic case of $^{83}\text{Zn}$

Let's set the  $^{83}\text{Zn}^{30+}$  ion as the setting fragment. The peculiarity of this fragment is the fact that the primary fission production cross-section is equal to zero<sup>♥</sup> for the fission fragment cross-section limit set to  $1\text{e-}10\text{ mb}$ .

Fig.116 shows the optimum target thickness plot for  $^{83}\text{Zr}$  where the SR contribution and charge states distribution were taken into account in the calculations. No primary yield for  $^{83}\text{Zn}$  is shown in the plot

Statistics 83Zn		
83Zn Beta- decay (Z=30, N=53)		
Q1 (D1)		30
Q2 (D2)		30
Q3 (D3)		30
Q4 (D4)		30
Zero cross section has been changed due to secondary reactions!		
Production Rate (pps)		1.32e-5
Sum of charge states (pps)		1.32e-5
Reaction		AF_low
Sum of reactions (pps)		1.32e-5
CS in the target (mb)		1.77e-7
Total transmission (%)		0.135

Fig.117. The statistics window of  $^{83}\text{Zn}$  fragment production with the SR contribution.

The  $^{83}\text{Zn}$  production rate for a half-percent momentum acceptance is  $1.3\text{e-}5\text{ pps}$ , suggesting that the reduced production cross-section is equal to  $1.8\text{e-}7\text{ mb}$  (see Fig.117).

Fig.118 demonstrates production and identification of  $^{83}\text{Zn}$  fragment. See inserts in the plot for details.

### 5.6.10. Examples

All the previous examples of calculations are available as LISE files on the LISE-web site using the address: [http://groups.nslc.msu.edu/lise/7\\_5/examples/](http://groups.nslc.msu.edu/lise/7_5/examples/).

Calculation step	Corresponding figure	file
Target 0.1 mm	Fig.103	fission_example
Target 0.52 mm	Fig.104	fission_example_052mm
SR on	Fig.106	fission_example_SR
Calculation of All fragments	Fig.109	fission_example_SR_All
Wedge on	Fig.110	fission_example_wedge
Small acceptance	Fig.113	fission_example_wedge2
Charge states on	Fig.114	fission_example_wedge_charge_81Zn
$^{83}\text{Zn}$ – setting of fragment	Fig.116	fission_example_wedge_charge_83Zn

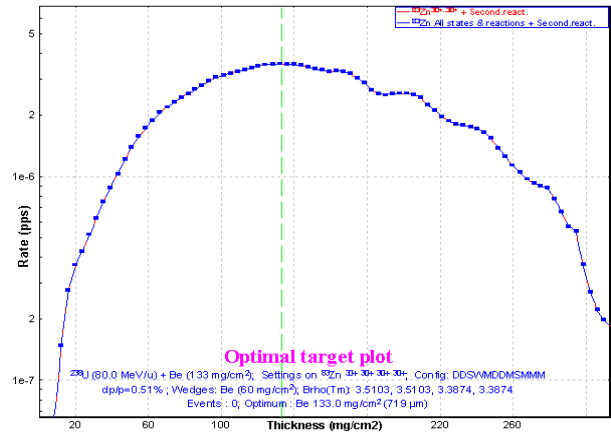


Fig.116.  $^{83}\text{Zn}$  fission fragment production rate as a function of target thickness.  $^{83}\text{Zn}$  primary fission production cross-section is equal to zero.

because the primary fission fragment production cross-section is equal to zero (compare this with the optimum target thickness plot for  $^{81}\text{Zn}$  in Fig.108).

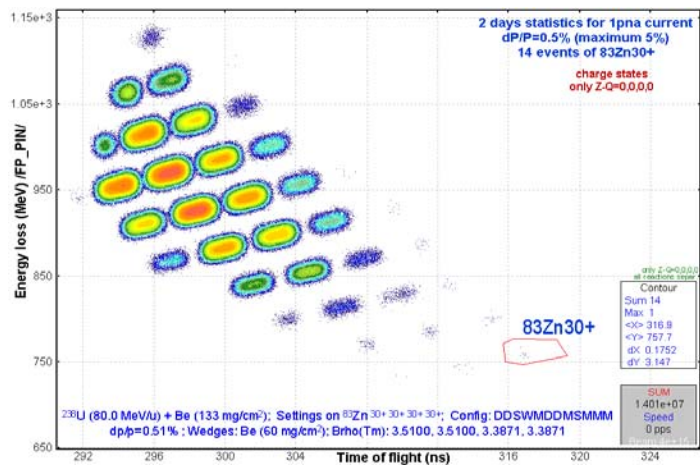


Fig.118. dE-ToF identification plot. See inserts in the plot for details.

<sup>♥</sup> If we decrease the cross-section limit to  $1\text{e-}20\text{ mb}$  we can get a  $^{83}\text{Zn}$  cross-section equal to  $1.31\text{e-}11\text{ mb}$ .



## 5.7. LISE's options modifications connected with the AF mechanism

### 5.7.1. New transmission parameter "Sum of reactions"

Abrasion-Fission is an especial case, because the products of the three excitation energy regions are all at once separated by the spectrometer. Each EER represents an independent reaction. But the user needs to receive a final summary answer. Therefore the new parameter "Sum of reactions" has been incorporated in the list of parameters.

Fig.119 shows statistics for  $^{132}\text{Sn}$  ions transmitted through two-dipoles of the system. As you can see there are 6 charge states for each EER fragment. The "Sum of reactions" parameter represents the sum of all charge states for all reaction mechanisms. The "Sum of charge states" parameter represents the sum of charge states for just ONE reaction mechanism.

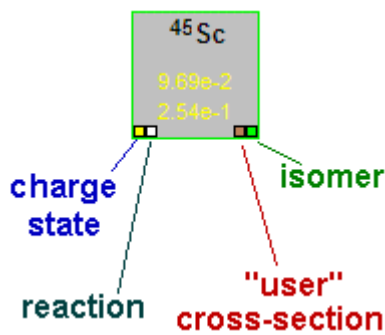


Fig.120. Isotope cell flags.

In the case of transmission calculated for the fragment produced in a reaction which is not set as primary, then the program draws a white small square in the left bottom corner of an isotope cell in the table of nuclides (see Fig.120). Information is given in the figure also by other flags, which can be displayed for certain isotopes.

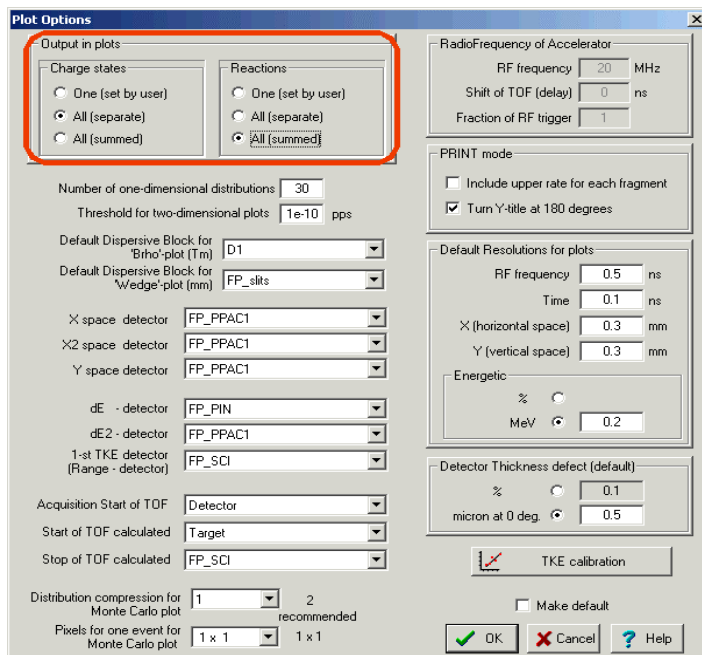


Fig.121. The "Plot options" dialog.

Q1 (D1)	Q2 (D2)	Production Rate (pps)	Sum of charge states (pps)	Reaction (pps)	Sum of reactions (pps)	CS in the target (MB)	Total transmission (%)	Target (%)	X space transmission (%)	Y space transmission (%)	Unreacted in matter (%)	Q (charge) ratio (%)	Unscattered in matter (%)	DA (%)	X angular transmission (%)	Y angular transmission (%)
45	45	2.45e-1	4.35e-1	4.69e-2	2.10e-2	1.047	1.949	9.83	100	100	100	54.35	100	100	100	100
46	46	1.08e-3	1.08e-3	4.69e-2	8.27e+0	1.158	0.872	2.3	100	100	100	54.35	100	100	100	100
47	47	4.63e-3	4.63e-3	4.69e-2	8.27e+0	1.158	0.872	2.3	100	100	100	54.35	100	100	100	100
48	48	2.56e-2	2.56e-2	4.69e-2	8.27e+0	1.158	0.872	2.3	100	100	100	54.35	100	100	100	100
49	49	1.29e-2	1.29e-2	4.69e-2	8.27e+0	1.158	0.872	2.3	100	100	100	54.35	100	100	100	100
50	50	2.48e-3	2.48e-3	4.69e-2	8.27e+0	1.158	0.872	2.3	100	100	100	54.35	100	100	100	100
51	51	5.07e-4	5.07e-4	4.69e-2	8.27e+0	1.158	0.872	2.3	100	100	100	54.35	100	100	100	100
52	52	2.9e-3	2.9e-3	4.69e-2	8.27e+0	1.158	0.872	2.3	100	100	100	54.35	100	100	100	100
53	53	1.42e-3	1.42e-3	4.69e-2	8.27e+0	1.158	0.872	2.3	100	100	100	54.35	100	100	100	100
54	54	5.14e-3	5.14e-3	4.69e-2	8.27e+0	1.158	0.872	2.3	100	100	100	54.35	100	100	100	100
55	55	5.14e-3	5.14e-3	4.69e-2	8.27e+0	1.158	0.872	2.3	100	100	100	54.35	100	100	100	100
56	56	5.14e-3	5.14e-3	4.69e-2	8.27e+0	1.158	0.872	2.3	100	100	100	54.35	100	100	100	100
57	57	5.14e-3	5.14e-3	4.69e-2	8.27e+0	1.158	0.872	2.3	100	100	100	54.35	100	100	100	100
58	58	5.14e-3	5.14e-3	4.69e-2	8.27e+0	1.158	0.872	2.3	100	100	100	54.35	100	100	100	100
59	59	5.14e-3	5.14e-3	4.69e-2	8.27e+0	1.158	0.872	2.3	100	100	100	54.35	100	100	100	100
60	60	5.14e-3	5.14e-3	4.69e-2	8.27e+0	1.158	0.872	2.3	100	100	100	54.35	100	100	100	100
61	61	5.14e-3	5.14e-3	4.69e-2	8.27e+0	1.158	0.872	2.3	100	100	100	54.35	100	100	100	100
62	62	5.14e-3	5.14e-3	4.69e-2	8.27e+0	1.158	0.872	2.3	100	100	100	54.35	100	100	100	100
63	63	5.14e-3	5.14e-3	4.69e-2	8.27e+0	1.158	0.872	2.3	100	100	100	54.35	100	100	100	100
64	64	5.14e-3	5.14e-3	4.69e-2	8.27e+0	1.158	0.872	2.3	100	100	100	54.35	100	100	100	100
65	65	5.14e-3	5.14e-3	4.69e-2	8.27e+0	1.158	0.872	2.3	100	100	100	54.35	100	100	100	100
66	66	5.14e-3	5.14e-3	4.69e-2	8.27e+0	1.158	0.872	2.3	100	100	100	54.35	100	100	100	100
67	67	5.14e-3	5.14e-3	4.69e-2	8.27e+0	1.158	0.872	2.3	100	100	100	54.35	100	100	100	100
68	68	5.14e-3	5.14e-3	4.69e-2	8.27e+0	1.158	0.872	2.3	100	100	100	54.35	100	100	100	100
69	69	5.14e-3	5.14e-3	4.69e-2	8.27e+0	1.158	0.872	2.3	100	100	100	54.35	100	100	100	100
70	70	5.14e-3	5.14e-3	4.69e-2	8.27e+0	1.158	0.872	2.3	100	100	100	54.35	100	100	100	100

Fig.119. Statistics window for  $^{132}\text{Sn}$  ions transmission. File [http://groups.nsl.msu.edu/lise/7\\_5/examples/new\\_parameter.lpp](http://groups.nsl.msu.edu/lise/7_5/examples/new_parameter.lpp)

Sometimes we need to see the dynamics of spatial or energy distributions just for one ion produced by the primary set reaction, but sometimes we are interested just in the sum distribution of all charge states and all reactions at the end of the spectrometer. For this purpose in the “Plot options” dialog, the possibility to define the mode for drawing the charge states and reaction mechanisms has been implemented.

Fig.121 demonstrates the “Plot options” dialog where the red rectangle shows methods for plotting distributions from charge state and reaction settings. There are three modes for charge states as well as for reaction mechanism: One (set by user), All(separate), All(summed). This means there are 9 possible combinations, which are shown in Fig.124. Fig.122 shows energy distributions of  $^{132}\text{Sn}$  ions for the same experimental conditions as Fig.124 in the mode “Charge states: All(Summed) and Reactions: All(separate)”.

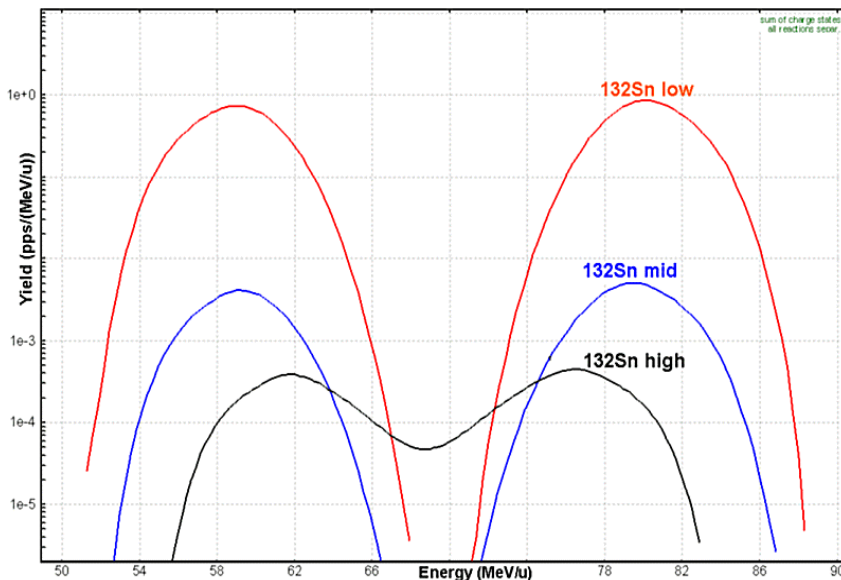


**Fig.122.**  $^{132}\text{Sn}$  fragment energy distribution after the second dipole. Distributions are shown in the mode “Charge states: All(Summed) & Reactions: All(separate)”.

Some modifications connected with incorporation of the new parameter were done also to the “Transmission statistics” dialog (see Fig.123).

**NOTE:** The “All (summed)” mode cannot be applied for Debug distributions, Transmission characteristics plots, and 2D-plots. If distribution’s plot mode is set in the dialog as “All (summed)” then the code will use the “All (separate)” mode plot to draw the distributions.

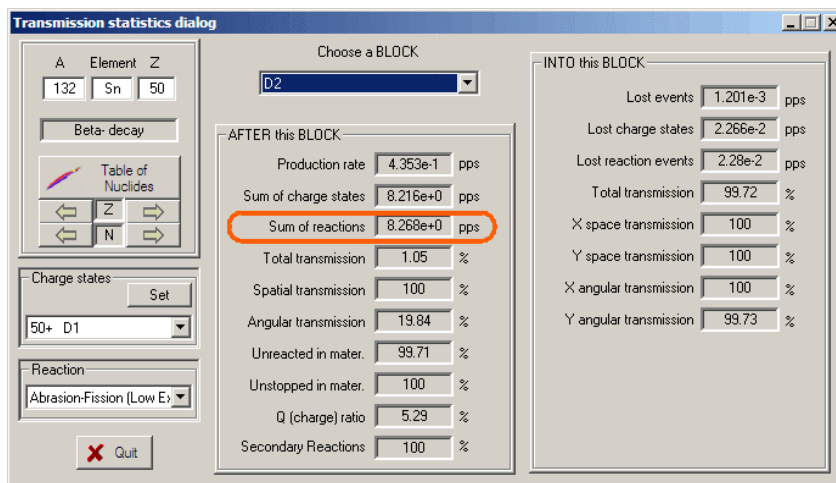


**Fig.123.** The “Transmission statistics” dialog.

**NOTE:** The envelope plot is created only in the “One (set by user)” mode.

**NOTE:** The new version of the code does not support calculations done in the old-version code. The code asks the user for permission to recalculate. Also, the old-version code does not support the new format due to the new parameter “Sum of reactions”. Please pay attention.

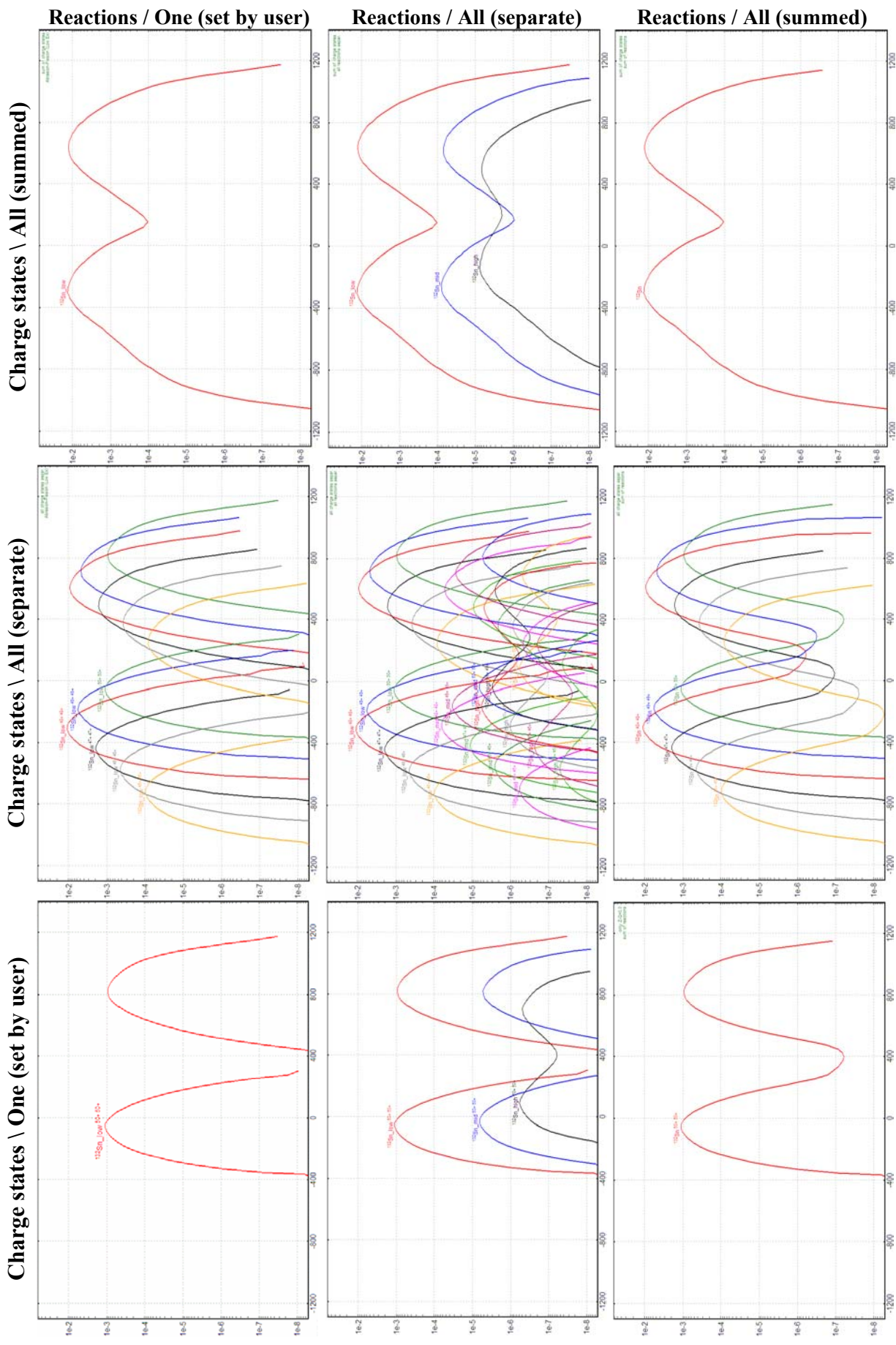


**Fig.124.** Horizontal spatial distributions of  $^{132}\text{Sn}$  ions after the second dipole. File [http://groups.nsl.msu.edu/lise/7\\_5/examples/new\\_parameter.lpp](http://groups.nsl.msu.edu/lise/7_5/examples/new_parameter.lpp)



### 5.7.2. User cross-section file

As for other reactions the LISE++ code can support user cross-sections which can be loaded through the “Cross-section file” dialog (menu “Options”), but **it is necessary to remember** that an experimental cross-section value is the sum of all possible fissile nuclei.

**Important:** This means that you have to turn off two EERs from calculations and leave just one EER! It is better to use the Low EER if you are working in a neutron rich region (see Fig.125), or the High EER in the proton rich case. If you do not turn off the other two EERs as a result you will get the final production cross-section equal to the sum of an user and two EERs cross-section values.

Even when you use the user cross-section file the code calculates cross-sections which should be used for kinematics calculations to find an parent excited fragment. Also calculated cross-sections will be used to calculate the secondary reactions contribution from fragments whose cross-sections are absent in the user cross-section file.

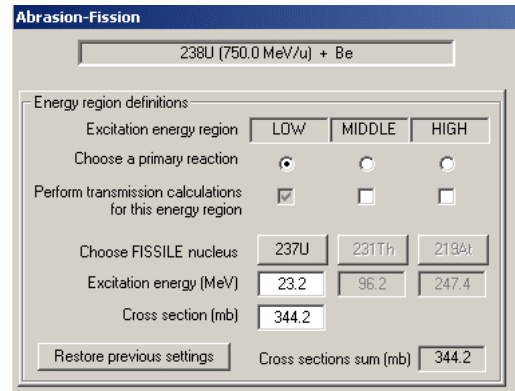


Fig.125. The fragment of the AF dialog in the case of work in the neutron rich region and using cross-section values from the file.

**Note:** Do not forget that the new format of the cross-section file requires the reaction field: information about production reaction is keeping in file (for details see chapter “9.1. User cross-section file”).

### 5.7.3. Transmission result file

Two new columns have been incorporated into the result transmission file due to creation of the Abrasion-Fission reaction mechanism. The first new column shows to what reaction this calculation result belongs (see frames “A” in Fig.126). The second new column shows the secondary reaction coefficient. It is necessary to note that the total transmission coefficient in the result file is different from the statistics window results due to a reduction by the secondary reaction coefficients to avoid values exceeding 100%.

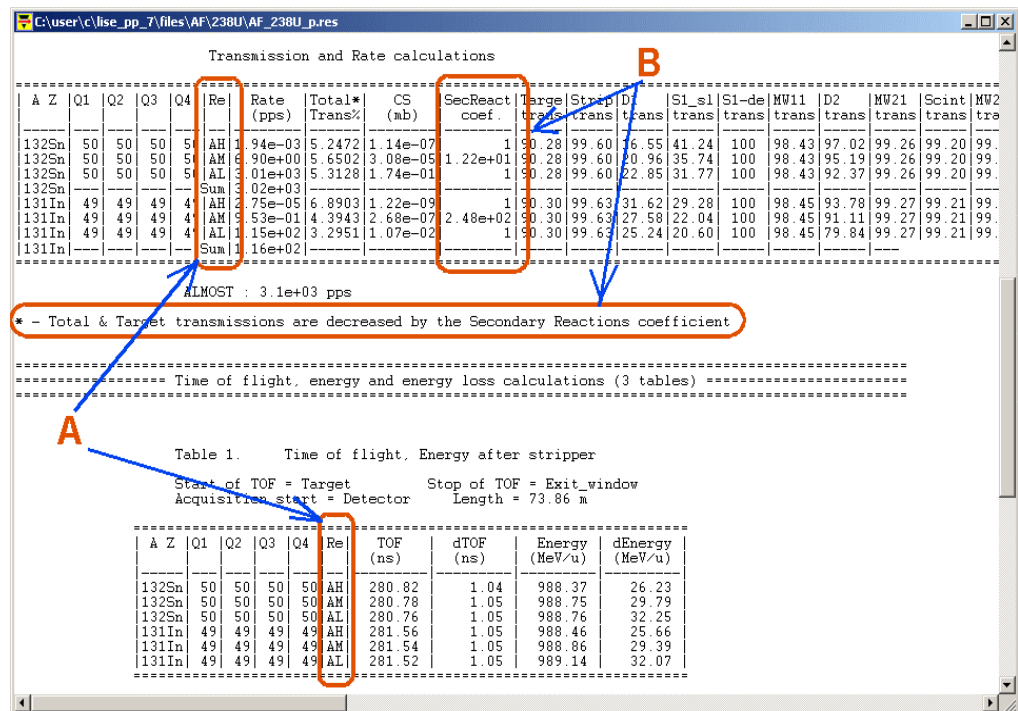


Fig.126. The fragment of the transmission result file listing.

## 5.8. INC fission

The application of the Abrasion-Ablation model to calculate EERs for induced fission of relativistic heavy projectiles by a light target requires an especial analysis. The use of AA is correct in the case of large impact parameters, but in the case when, geometrically speaking, the light target is completely overlapped by the incident projectile (see Fig.127), we assume another reaction mechanism, INC. The excitation energy of a fissile nucleus (or an excited prefragment in the case of evaporation) is higher in the case of INC, compared with Abrasion.

Special corrections were implemented for the geometrical AA model in the code to avoid a sharp fall in cross-sections (see Fig.128) and also to keep the sum of partial abrasion cross-sections equal to the geometrical cross-section:

$$\sigma_{geom} = \sum_{A=1}^{A_{proj}-1} \sigma_{abrasion}^{corrected}(A). \quad /14/$$

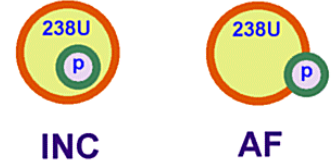


**Fig.127.** Schematic representation of INC and Abrasion from the impact parameter.

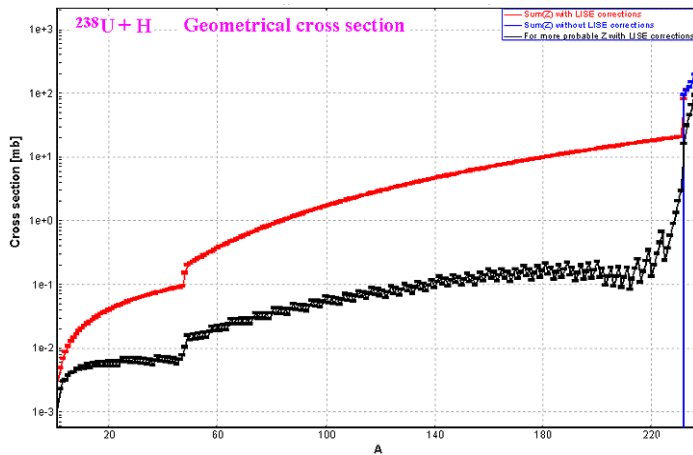


**Fig.128.** Prefragment production cross-sections as the result of abrasion of a  $^{238}\text{U}$  projectile by a proton target as a function of the prefragment mass. The blue(red) line shows LISE calculations without(with) LISE geometrical corrections. The black line shows the production cross-section of the most probable isotope using LISE geometrical corrections.

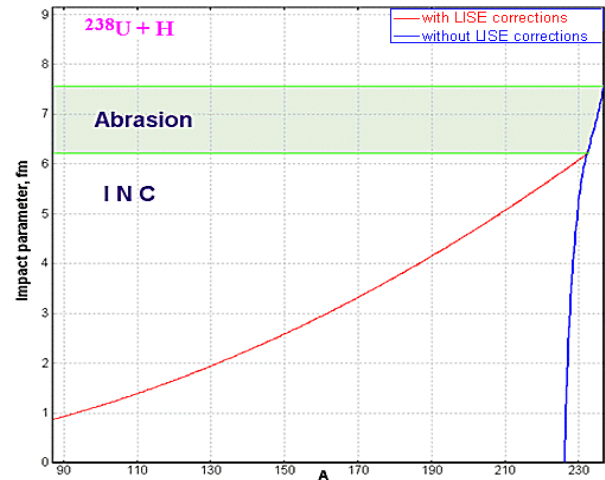


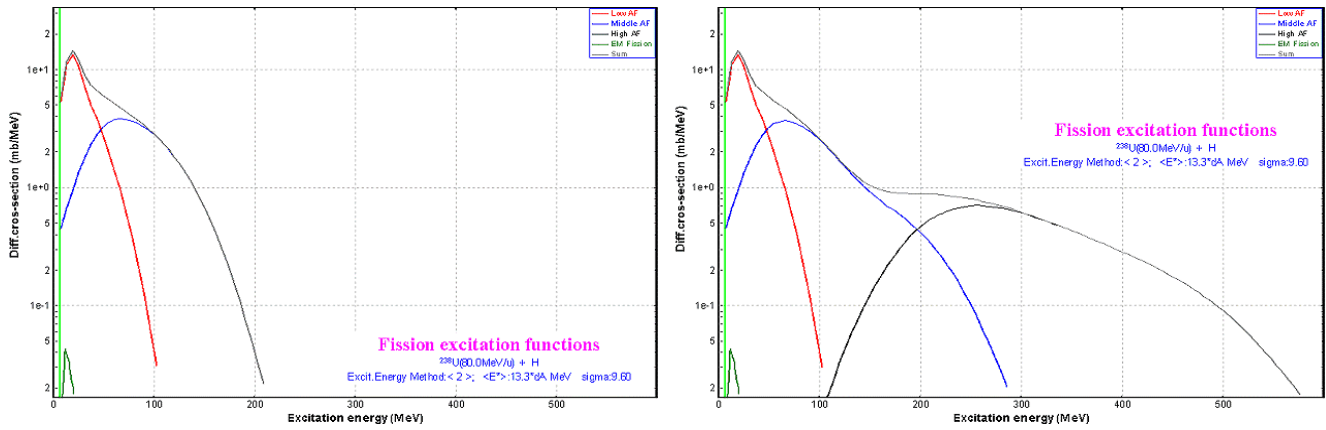
**Fig.129.** Correlation of the prefragment mass and the impact parameter in the reaction  $^{238}\text{U}+p$ . The blue(red) line shows LISE calculations without(with) LISE geometrical cross-sections.

We shall show in this chapter that it is possible to use the Abrasion-Fission model, with slight corrections, for light targets as well, assuming in this case that there is a combination of two processes: Abrasion (non-corrected) and INC (see Fig.129):

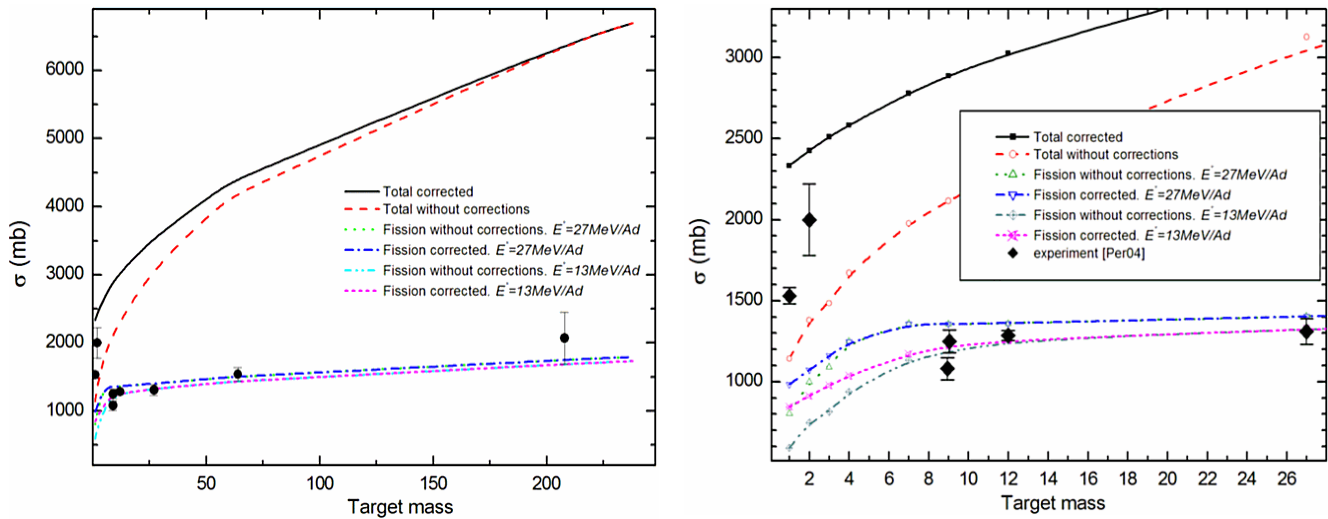
$$\sigma_{geom} = \sum_{A=1}^{A_{proj}-1} \sigma_{abrasion}^{non-corrected}(A) + \sigma_{INC} \quad /15/$$

Fig.130 shows how the LISE geometrical corrections are mirrored in the fission excitation function. The geometrical corrections considerably increase the high energy excitation contribution in fission. However, even these could not predict experimental fission cross-sections with light targets (Fig.131), which is probably explained by the following reasons:

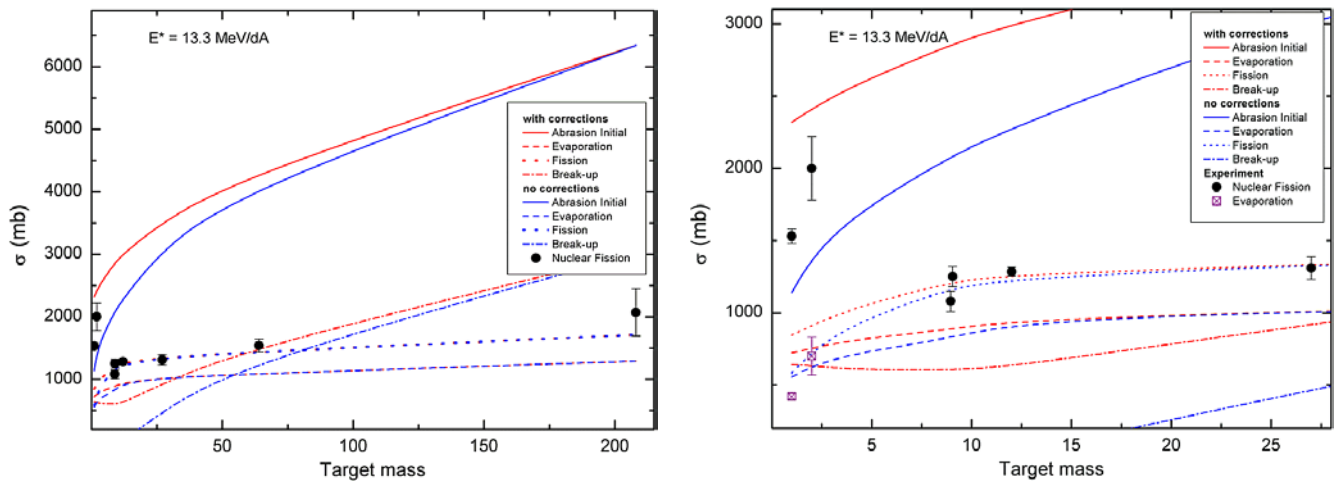
- Prefragments with the same mass are more excited in the INC case compared with Abrasion (corrected);
- AA (corrected) and INC distributions of prefragment production cross-sections have different shapes.



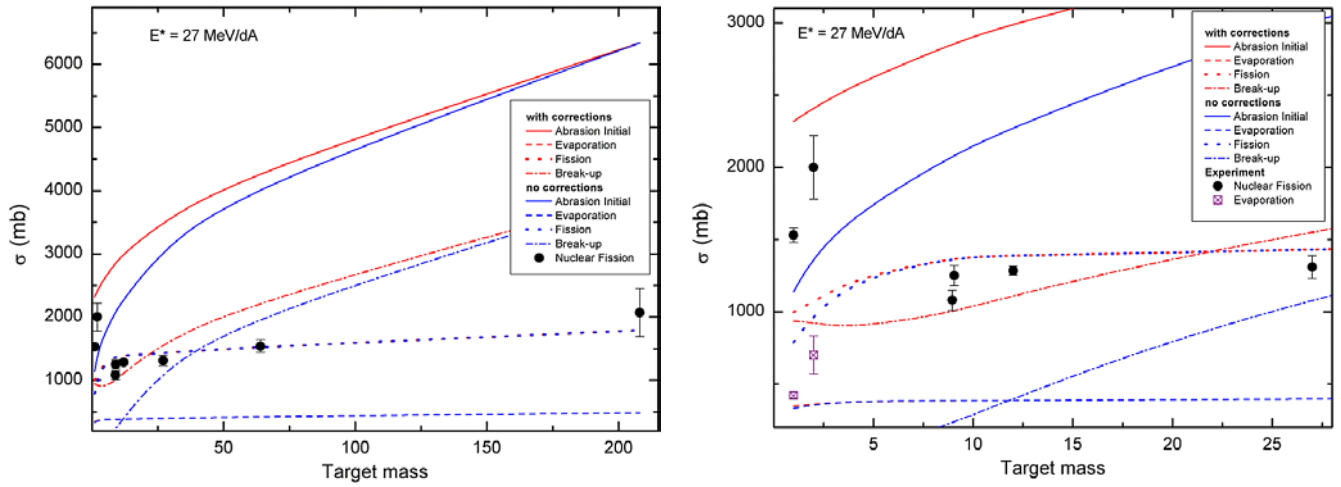
**Fig.130.** Left (Right) plot: fission excitation function calculated for the reaction  $^{238}\text{U}(1\text{A GeV}) + p$  without (with) LISE++ geometrical corrections.



**Fig.131.** Calculated total abrasion and summed abrasion-fission (with and without geometrical corrections for different excitation energies per abraded nucleon) cross-sections and experimental fission cross-sections (without EM component) as a function of the target mass for the projectile  $^{238}\text{U}(1\text{A GeV})$ . The right plot is the same as the left plot but with another abscissa axis scale to detail the light target region. Experimental data are taken from the works [Arm96,Rub96,Per04]. It is possible to see large disagreement between AF calculations and experimental data for proton and deuterium targets on the right plot that can be explained by the involvement of the other reaction mechanism (INC).



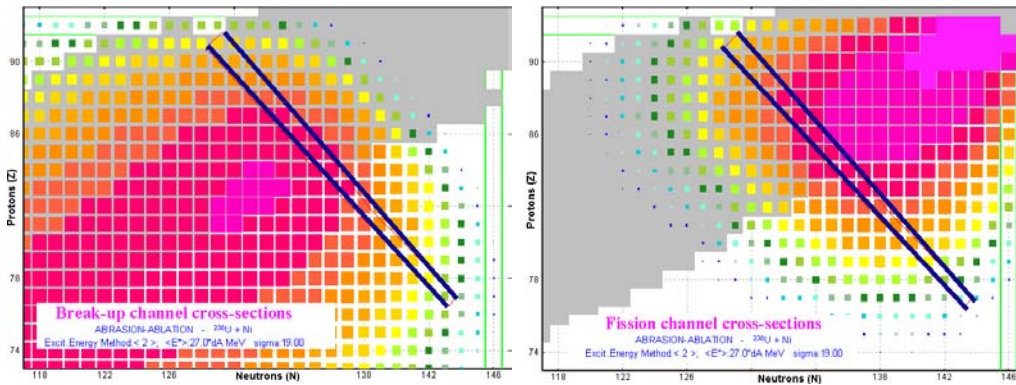
**Fig.132.** Calculated total abrasion and de-excitation channels cross-sections (with and without geometrical corrections for the excitation energy per abraded nucleon equal to 13.3 MeV/dA) and experimental fission (without EM component) and evaporation cross-sections as a function of the target mass for the projectile  $^{238}\text{U}(1\text{A GeV})$ .



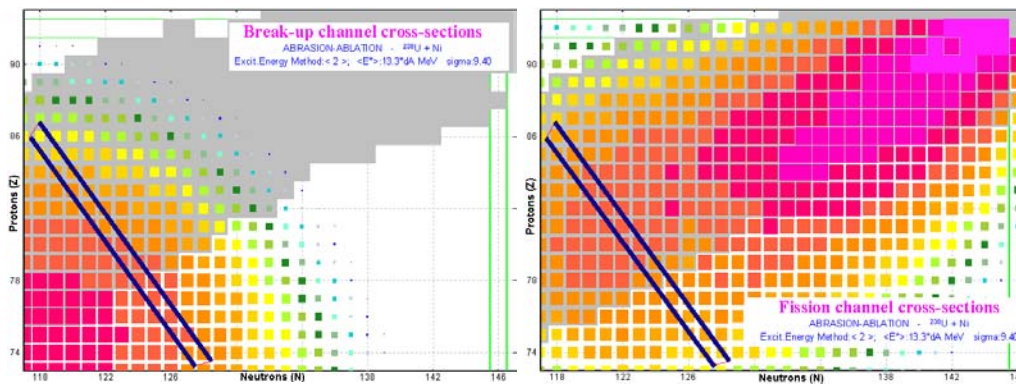
**Fig.133.** Calculated total abrasion and de-excitation channels cross-sections (with and without geometrical corrections for the excitation energy per abraded nucleon equal to 27 MeV/dA) and experimental fission (without EM component) and evaporation cross-sections as a function of the target mass for the projectile  $^{238}\text{U}(1\text{AGeV})$ .

Fig.132 and Fig.133 show experimental fission (without Coulomb fission contribution) and evaporation cross-sections and de-excitation channels after abrasion of  $^{238}\text{U}(1\text{AGeV})$  by the target calculated with and without geometrical corrections. Calculations for Fig.132 and Fig.133 correspond to excitation energies per abraded nucleon of 13.3 and 27 MeV/dA respectively. It is possible to conclude that there is good agreement between fission experimental results and AF calculations with  $E_0^* = 13.3$  MeV/dA for targets heavier than Beryllium, and between evaporation experimental results and calculations with  $E_0^* = 13.3$  MeV/dA.

👉 It is possible to conclude in the case of  $E_0^* = 13.3$  MeV/dA that the INC cross-section is shared between break-up and fission channels in the case of  $p$  and  $d$  targets. There is no contribution into the evaporation channel from the INC mechanism.



**Fig.134.** Break-up (left) and fission (right) channels for abrasion of a  $^{238}\text{U}(1\text{AGeV})$  projectile by a Ni target calculated with  $E_0^* = 27$  MeV/dA. The navy reference lines have the same position on both plots.



**Fig.135.** Break-up (left) and fission (right) channels for abrasion of a  $^{238}\text{U}(1\text{AGeV})$  projectile by a Ni target calculated with  $E_0^* = 13.3$  MeV/dA. The navy reference lines have the same position on both plots.



Using Fig.134 and Fig.135 it is possible to conclude, by depending on excitation energies per abraded nucleon, how many nucleons it is necessary to tear from the  $^{238}\text{U}$  projectile to make the break-up channel dominate over fission.

Fig.136 shows the maximum number of abraded nucleons from a  $^{238}\text{U}$  projectile as a function of the target mass calculated by the LISE++ Abrasion-Ablation model.

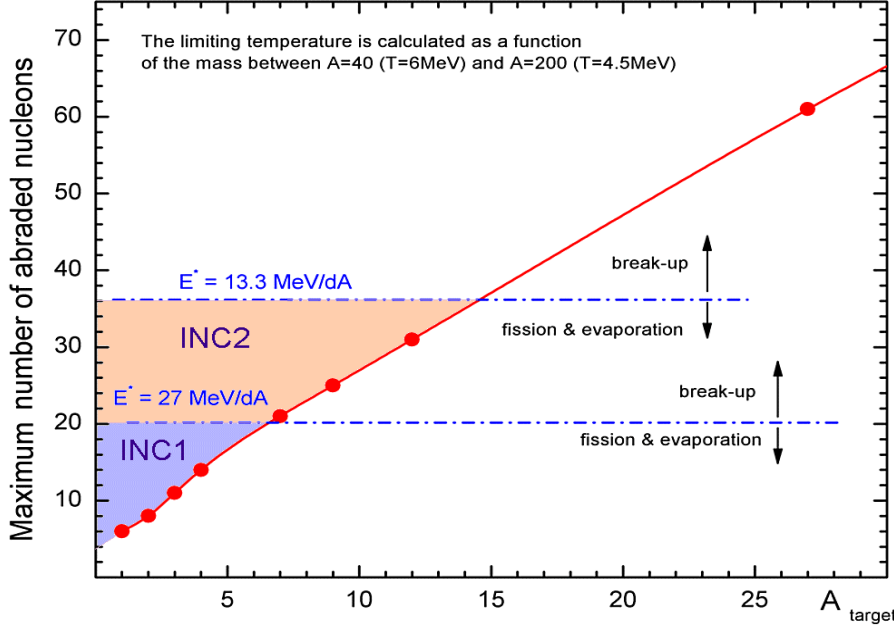


**Fig.136.** Maximum number of abraded nucleons from a  $^{238}\text{U}$  projectile as a function of the target mass calculated with the LISE++ geometrical abrasion-ablation model without LISE geometrical corrections. Two horizontal dash-dot lines corresponding to the two excitation energies (13 & 27 MeV/dA) denote regions where the break-up channel begins to dominate (see Fig.134 and Fig.135).

We suggest that in the INC-region both break-up and fission channels take place, below the blue line, (not including INC-region) fission and evaporation channels, and above the blue line (from definition of this line), just the break-up channel.

The number of abraded nucleons can be calculated by a fast analytical method using the expression for excitation energy  $E^* \cong a \cdot T_{lim}^2$ , where for masses  $A=200-220$  the parameter  $a$  is about  $27 \text{ MeV}^{-1}$ , and the limiting temperature is about 4.4 MeV. Therefore the excitation energy corresponding to the limiting temperature in this mass region is about 530 MeV. The excitation energy of prefragments in the Abrasion-Ablation model is proportional to the number of abraded nucleons and the  $E_0^*$  parameter. Therefore for  $E_0^* = 13.3 \text{ MeV/dA}$  we get  $dA \cong 39$ , and for  $E_0^* = 27 \text{ MeV/dA}$  similarly  $dA \cong 19$ .

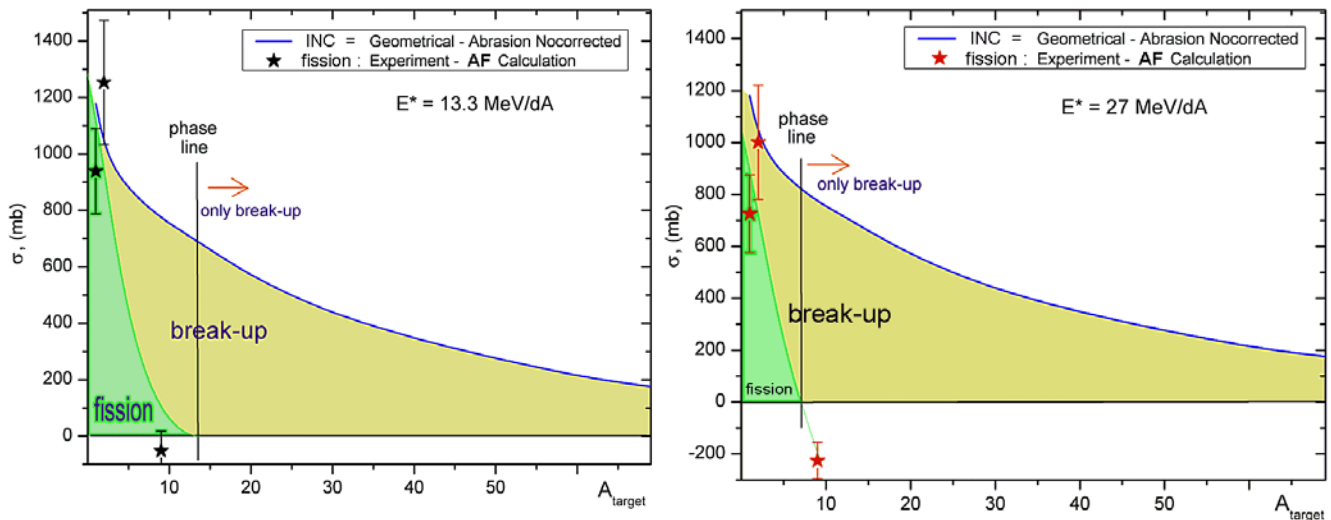


**Fig.137.** INC cross-section as a function of target mass. Experimental fission cross-sections [Per04,Arm96,Rub96] are shown after subtraction of AF calculations without geometrical corrections. The phase line denotes a boundary above which only the break-up takes place (Fig.136). The left plot shows calculations done with  $E_0^* = 13.3 \text{ MeV/dA}$ , and the right plot similarly with  $E_0^* = 27 \text{ MeV/dA}$ .



Fig.137 shows the INC cross-section as a function of target mass. Using experimental points (after subtraction of the AF calculations without geometrical corrections) and phase lines we were trying to determine the fission component in the INC cross-section. It is possible to conclude the following:

- For  $E_0^*=13.3$  MeV/dA (left plot in Fig.137), it is possible to connect the reduced experimental points and the phase line. For  $p$  and  $d$  targets, de-excitation in the INC reaction mechanism goes through the fission channel; whereas in the case of Be-target and heavier it goes through the break-up de-excitation channel.
- For  $E_0^*=27$  MeV/dA (right plot in Fig.137) the reduced experimental value for a Be-target is not consistent with systematic error and can not be explained by the INC reaction mechanism.
- Experimental fission cross-sections for **He** and **Li targets** could considerably help with the further development of the model.
- A target of light mass, to which corresponds the lowest experimental fission cross-section, can serve as a test to estimate an excitation energy of the prefragment after abrasion (see Fig.136).

### 5.8.1. Recommended EER parameters for light targets in the LISE++ Abrasion-Fission model

Based on conclusions of the previous chapter we recommend using excitation energy of the prefragment after abrasion of  $E_0^*=13.3$  MeV/dA. Keeping values for Low and Middle EERs calculated by AA without LISE geometrical corrections, we are taking High EER from AA with these cross-sections. The next step is modification of the High EER cross-section assuming contributions from the INC process.

The code does not calculate AA+INC parameters. You can load already existing files, or enter EER parameters manually based on principles described below.

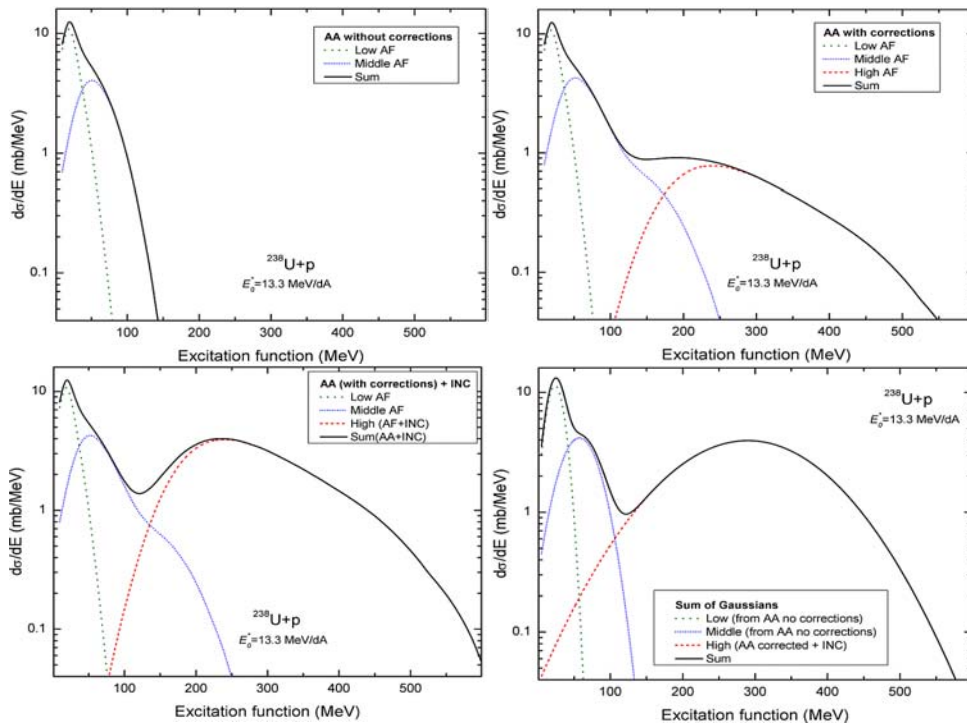
#### 5.8.1.1. Hydrogen target

Fig.138 shows fission excitation functions and their EER components calculated by different methods for the reaction  $^{238}\text{U}(1\text{AGeV})+p$ . The EER parameters are given in Table 14. For the final summed fission cross-section of the AA+INC method we used the experimental value of 1530 mb [Ber03]. The Coulomb fission cross-section of a Hydrogen target for  $^{238}\text{U}(1000\text{AGeV})$  is less 1mb.

There is not a sharp boundary between low and middle excitation energy regions. In Bernas' experiment [Ber03] the asymmetrical fission cross-section was measured to be equal to  $105\pm 10\text{mb}$ . To reproduce this value in the code we have to set the low-energy boundary to 20 MeV, and the Low EER has the following parameters:  $^{237}_{92}\text{U}_{145}$ ,  $E^*=18.2\text{MeV}$ ,  $\sigma=157$  mb.

**Table 14.** EERs for the reaction  $^{238}\text{U}(1\text{AGeV})+p$  calculated by different methods. Region boundaries were set to 40 & 180 MeV.

Method	$\Sigma\sigma$ , mb	Low			Middle			High		
		A, Z, N	$E^*$	$\sigma$ , mb	A, Z, N	$E^*$	$\sigma$ , mb	A, Z, N	$E^*$	$\sigma$ , mb
AA without corrections	591.3	$^{236}_{92}\text{U}_{144}$	23.8	331.5	$^{234}_{91}\text{Pa}_{143}$	57.4	259.7			
AA with corrections	845.1	$^{236}_{92}\text{U}_{144}$	23.5	323.8	$^{232}_{90}\text{Th}_{142}$	75.7	352.1	$^{215}_{84}\text{Po}_{131}$	289.9	169.2
<b>AA + INC</b>	1530.5	$^{236}_{92}\text{U}_{144}$	23.8	331.5	$^{234}_{91}\text{Pa}_{143}$	57.4	259.7		289.9	<b>939.3</b>



**Fig.138.** Fission excitation functions and their components calculated for the reaction  $^{238}\text{U}(1\text{AGeV}) + p$ .

Left top plot: without LISE++ geometrical corrections.

Right top: with corrections.

Left bottom: AA+INC. See Table 14 for details.

Right bottom: Sum of three normal distributions with EER parameters from AA+INC. The standard deviations of the distributions are taken from LISE calculations and are equal to 11.59, 24.85, and 94.7 MeV.

Fig.139 shows fission excitation functions calculated by different methods for the reaction  $^{238}\text{U}(1\text{AGeV}) + p$ . Compare the AA+INC excitation function with Fig.140. Fig.140 was modified to show qualitatively where break-up and evaporation de-excitation channels are located based on expected shapes and experimental cross-section values. Fission and total cross-sections were measured correspondingly  $1530 \pm 150$  and  $1990 \pm 170$  mb [Ber03], whereas in the reaction  $\bar{p}(1.2\text{ GeV}) + ^{238}\text{U}$ , reaction cross-section was measured to be  $2200 \pm 130$  mb [Gol96]. The geometrical cross-section is about 2.3 barn. The file “examples/afission/AF\_238U\_p.lpp” with AA+INC settings is provided by the LISE installation package.

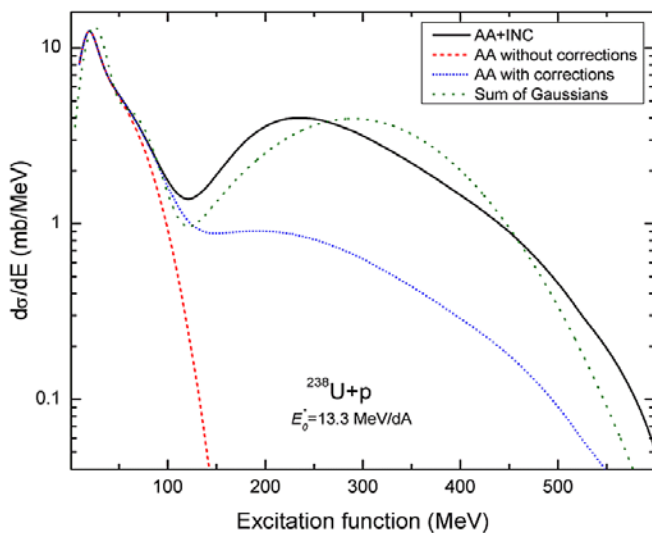


**Fig.139.** Fission excitation functions calculated by different methods for the reaction  $^{238}\text{U}(1\text{AGeV}) + p$ . Compare the AA+INC excitation function with the dashed line in Fig.140.

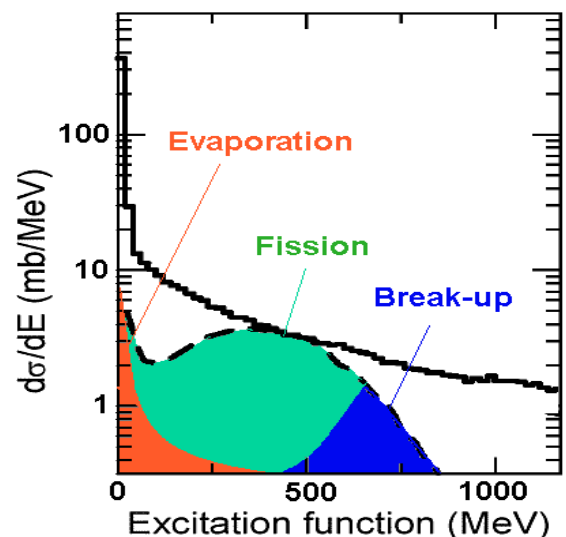


**Fig.140.** Total reaction cross-section as a function of the excitation energy induced right after the collision, before an eventual pre-equilibrium or break-up process and the consecutive sequential decay<sup>▲</sup>

<sup>▲</sup> The dashed line corresponds to the reaction  $\bar{p}(1.2\text{ GeV}) + ^{238}\text{U}$  ( $\sigma_{\text{react}} = 2200 \pm 130$  mb) measured in the work [Gol96]. The figure was imported from [Jur04] and then was updated.

### 5.8.1.2. Deuterium target

Table 15 shows fission EER parameters calculated by different methods for the reaction  $^{238}\text{U}(1\text{A GeV})+d$ . For the final summed fission cross-section of the AA+INC method we took 1700 mb in order not to exceed the geometrical cross-section when adding the evaporation cross-section:

Experiment	$\sigma, mb$	$s(\sigma), mb$	Ref
Fission	2000	220	[Per04]
Evaporation	700	130	[Cas01]
Total	2700	350	[Per04]
Geom (calc)	2427		

**Table 15.** EERs for the reaction  $^{238}\text{U}(1\text{A GeV})+d$  calculated by different methods. Region boundaries were set to 40 & 180 MeV.

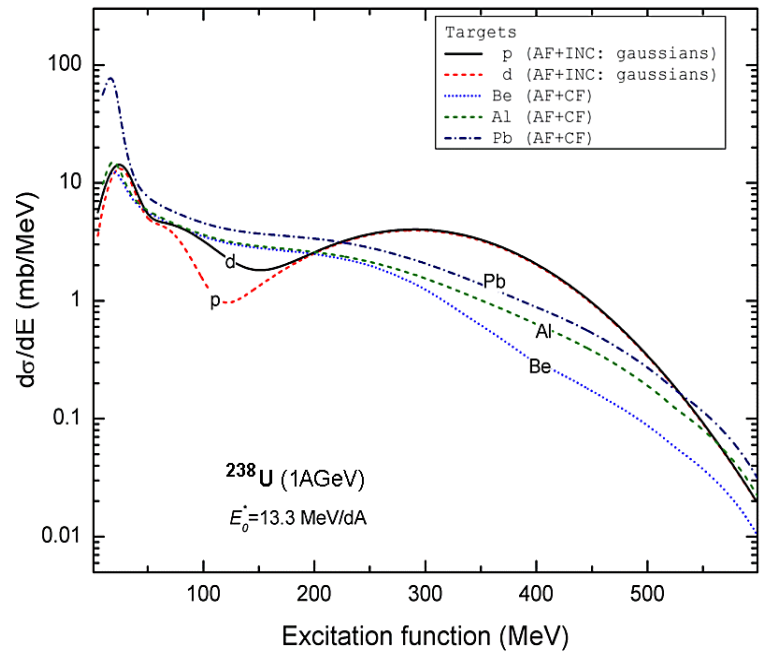


**Fig.141.** Fission excitation functions in the reaction of  $^{238}\text{U}(1\text{A GeV})$  with different targets.

Method	$\Sigma\sigma, mb$	Low			Middle			High		
			$E^*$	$\sigma, mb$	$A, Z, N$	$E^*$	$\sigma, mb$		$E^*$	$\sigma, mb$
AA without corrections	745.3	$^{236}_{92}\text{U}_{144}$	23.5	319.9	$^{232}_{90}\text{Th}_{142}$	74.6	425.4			
AA with corrections	912.5	$^{236}_{92}\text{U}_{144}$	23.5	319.3	$^{231}_{90}\text{Th}_{141}$	79.0	427.0	$^{215}_{84}\text{Po}_{131}$	290.2	166.2
<b>AA + INC</b>	<b>1700</b>	$^{236}_{92}\text{U}_{144}$	23.5	319.9	$^{232}_{90}\text{Th}_{142}$	74.6	425.4	$^{215}_{84}\text{Po}_{131}$	290.2	<b>954.7</b>

The file “examples/afission/AF\_238U\_d.lpp” with AA+INC settings is provided by the LISE installation package.

### 5.8.1.3. Targets with $Z \geq 2$

We recommend EER settings for light targets with  $Z \geq 2$  based on systematics in the right plot of Fig.132 and the left plot of Fig.137.

- He and Li targets: fission cross-sections should be about 1300 mb, and the INC fission contribution will be about 50% of the total INC cross-section.
- For targets with  $Z \geq 4$  it is not necessary to apply the INC fission contribution because, as it is possible to see in Fig.132, there is a good agreement between experimental values and calculations done with geometrical corrections for the excitation energy of the prefragment after abrasion  $E_0^* = 13.3 \text{ MeV/dA}$ .

Fig.141 shows fission excitation functions in the reaction  $^{238}\text{U}(1\text{A GeV})$  on different targets.

## 5.9. Comparison with experimental data

Default AF settings (evaporation, fission, and excitation energy of prefragment) were used for comparisons with experimental data summed in Table 16.

**Table 16.** Experimental works used for comparisons with LISE AF calculations.

Ref.	Reaction	Energy, AMeV	$\sigma_{EM}$	$\sigma_{fis}$ total	$\sigma_{fis}$ partial	$\sigma_{reaction}$ and others	TKE
Ber94	Pb( $^{238}\text{U}$ ,fis)	750			yes		
Aum95	Al,Cu,Pb( $^{238}\text{U}$ ,xn)	600,950			yes	yes	
Arm96	Pb,Be( $^{238}\text{U}$ ,fis)	750	yes	yes	yes	yes	
Hes96	Pb,Cu,Al( $^{238}\text{U}$ ,fis)	750		yes		yes	
Rub96	Be,C,Al,Cu,In,Au,U ( $^{238}\text{U}$ ,fis)	600, 1000	yes	yes			
Ber97	B,Pb( $^{238}\text{U}$ ,fis)	750	yes	yes			
End01	$^1\text{H}$ ( $^{208}\text{Pb}$ ,fis)	1000		yes	yes	yes	yes
End02	$^2\text{H}$ ( $^{208}\text{Pb}$ ,fis)	1000		yes	yes	yes	yes
Ben01	$^1\text{H}$ ( $^{197}\text{Au}$ ,fis)	800		yes	yes		yes
Ben02	$^1\text{H}$ ( $^{197}\text{Au}$ ,fis)	800		yes			
Ber03	$^1\text{H}$ ( $^{238}\text{U}$ ,fis)	1000		yes	yes	yes	yes
Tai03	$^1\text{H}$ ( $^{238}\text{U}$ ,evapor)	1000			yes	yes	
Arm04	p( $^{238}\text{U}$ ,spallation)	1000					

Analysis of experimental data (total nuclear fission cross-sections) on induced fission in reactions of relativistic  $^{238}\text{U}$  projectiles with light targets has already been done in chapter “5.8. INC fission”.

### 5.9.1. Total fission cross-sections of $^{238}\text{U}$ at relativistic energies

Fig.142 shows the extracted experimental [Rub96 and references therein] total fission cross-sections as a function of the atomic number of the target at 0.6 and 1 GeV per nucleon. LISE calculations were done for two prefragment excitation energy values, 13.3 and 27 MeV/dA. The observed strong increase with  $Z_{target}$  is due to the electromagnetic contribution.

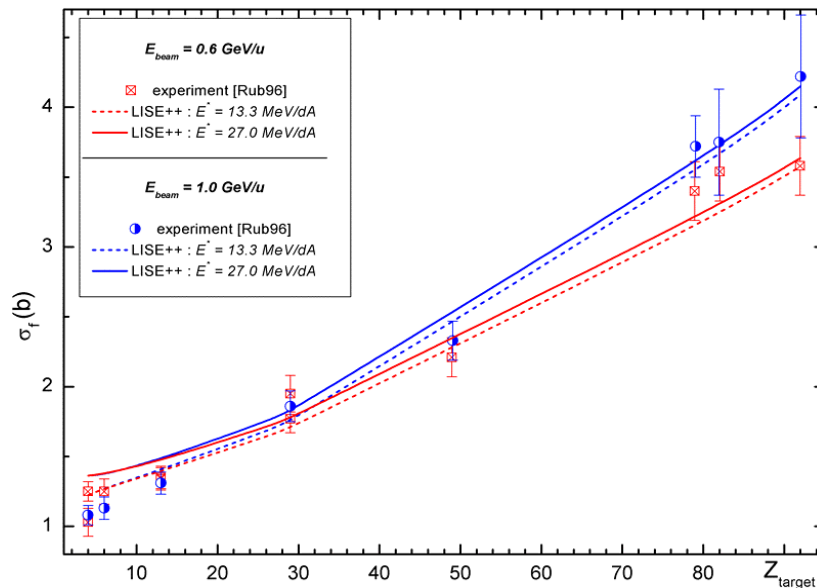


**Fig.142.** Total fission cross-sections of  $^{238}\text{U}$  at energies between 0.6 and 1 GeV per nucleon. See inset in the figure for details. LISE calculations were done for two prefragment excitation energy values. 13.3 and 27 MeV/dA.

### 5.9.2. $^{208}\text{Pb}(1\text{AGeV}) + p, d$

The aim in the present analysis is to find parameters of the LISE AF model to describe experimental fission fragment production cross-sections in the reactions  $^{208}\text{Pb}(1\text{AGeV}) + p, d$  [Enq01,Enq02], and thus to show that the program can be used for calculation of fission fragment yields in similar reactions. Table 17 shows parameters characterizing the fission process of the  $^{208}\text{Pb}(1\text{AGeV})+p$  [Enq01] and  $^{208}\text{Pb}(1\text{AGeV})+d$  [Enq02].

**Table 17.** Parameters characterizing the fission process of the  $^{208}\text{Pb}(1\text{AGeV})+p$  [Enq01] and  $^{208}\text{Pb}(1\text{AGeV})+d$  [Enq02] systems.

Reaction	$\sigma_{\text{fiss}}$ (mb)	$\bar{A}$	$\bar{Z}$	$\sigma_A$	$\sigma_Z$	$\bar{E}_{\text{kin}}$ (MeV)	$\sigma_{\text{frag}}$ (b)
$^{208}\text{Pb} + d$	$157 \pm 26^a$	$90.7 \pm 1.0$	$39.6 \pm 0.5$	$16.1 \pm 0.8$	$6.6 \pm 0.3$	$64 \pm 4$	$1.91 \pm 0.24^b$
$^{208}\text{Pb} + p$	$169 \pm 31^a$	$89.6 \pm 1.1$	$39.0 \pm 0.7$	$17.4 \pm 1.0$	$7.3 \pm 0.5$	$58 \pm 5$	$1.68 \pm 0.22^c$

<sup>a</sup> For elements from titanium (Z=22) to tellurium (Z=52).

<sup>b</sup> For elements from cesium (Z=52) to lead

<sup>c</sup> For elements from promethium (Z=61) to lead

The Abrasion-Ablation model cannot help us to get hints for the EER parameters; as it was developed for Abrasion-Fission in the case of uranium beams:

- The high fission barrier ( $\geq 20$  MeV) of nuclei with  $Z < 82$  makes it possible to exclude low excitation energy fission from calculations. Break-up energy in the region  $Z \leq 82$  is about 500 MeV from Fig. 8.
- The maximum numbers of abraded nucleons from the geometrical AA model are equal to 7 for a proton target and 9 for a deuterium target. Without geometrical corrections, the AA model predicts very small fission cross-sections, 4.5 mb for a  $^2\text{H}$ -target (see Table 18) and 0.2 mb for a  $^1\text{H}$ -target (see Table 19).
- The AA model with geometrical correction shows that we can use just **ONE excitation energy region** with excitation energy about 300 MeV.

It is possible to conclude that the Abrasion-Fission cross-section is negligible in these reactions and that all fission events are due to the INC process.

**Table 18.** Calculated and recommended EERs for the reaction  $^{208}\text{Pb}(1\text{AGeV}) + d$ . The region boundaries were set to 40 & 180 MeV.

Method	$\Sigma\sigma$ , mb	Middle			High		
		A, Z, N	$E^*$	$\sigma$ , mb	A, Z, N	$E^*$	$\sigma$ , mb
AA without corrections	4.5	$^{198}_{80}\text{Hg}_{118}$	127.3	4.5			
AA with corrections	56.3	$^{197}_{80}\text{Hg}_{117}$	147.6	6.6	$^{184}_{75}\text{Re}_{109}$	305.3	49.7
<b>Recommended: experiment</b>	<b>200</b>	$^{197}_{79}\text{Au}_{120}$	<b>350</b>	<b>200</b>			

**Table 19.** Calculated and recommended EERs for the reaction  $^{208}\text{Pb}(1\text{AGeV}) + p$ . The region boundaries were set to 40 & 180 MeV.

Method	$\Sigma\sigma$ , mb	Middle			High		
		A, Z, N	$E^*$	$\sigma$ , mb	A, Z, N	$E^*$	$\sigma$ , mb
AA without corrections	0.2	$^{198}_{80}\text{Hg}_{118}$	96	0.2			
AA with corrections	50.5	$^{197}_{80}\text{Hg}_{117}$	154.7	4.8	$^{184}_{75}\text{Re}_{109}$	304.4	50.5
<b>Recommended: experiment</b>	<b>175</b>	$^{198}_{80}\text{Hg}_{116}$	<b>300</b>	<b>175</b>			



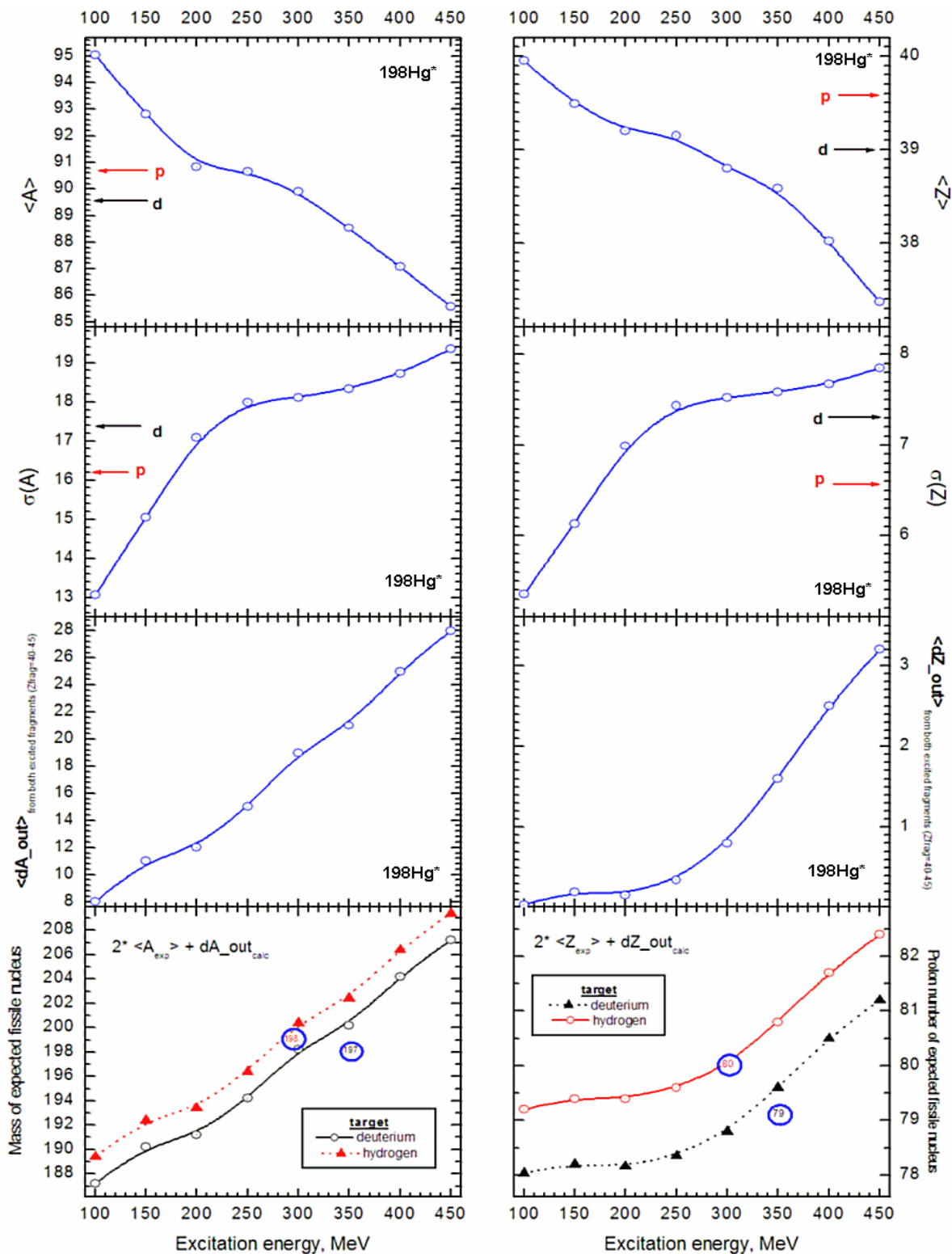


**Fig.143.** Calculated  $^{198}\text{Hg}$  fission parameters as a function of excitation energy. The mean value of the mass and elemental distributions,  $\langle A \rangle$  and  $\langle Z \rangle$ , and their standard deviations,  $\sigma_A$  and  $\sigma_Z$ , are given in the two top rows. Arrows show experimental results on p- & d-targets [Enq01,Enq02].

$\langle dA_{\text{out}} \rangle$  and  $\langle dZ_{\text{out}} \rangle$  plots show the mean values of emitted nucleons and protons respectively from both excited fragments before reaching their final states.

Bottom row: calculated mass and charge of the fissile nucleus using experimental values of  $\langle A \rangle$  and  $\langle Z \rangle$  [Enq01,Enq02] and the calculated number of emitted nucleons and protons. Blue circles show values which give the best agreement with experimental results.

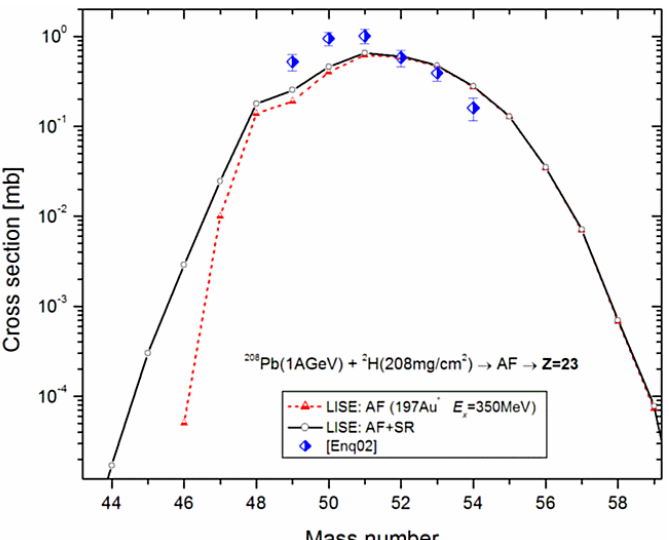
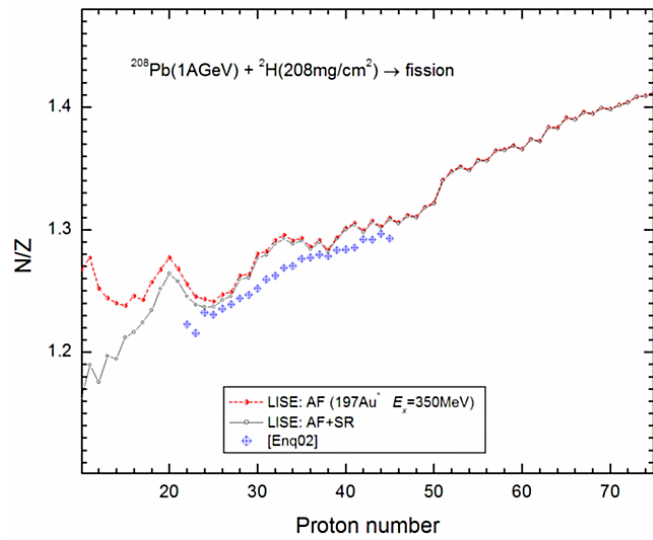
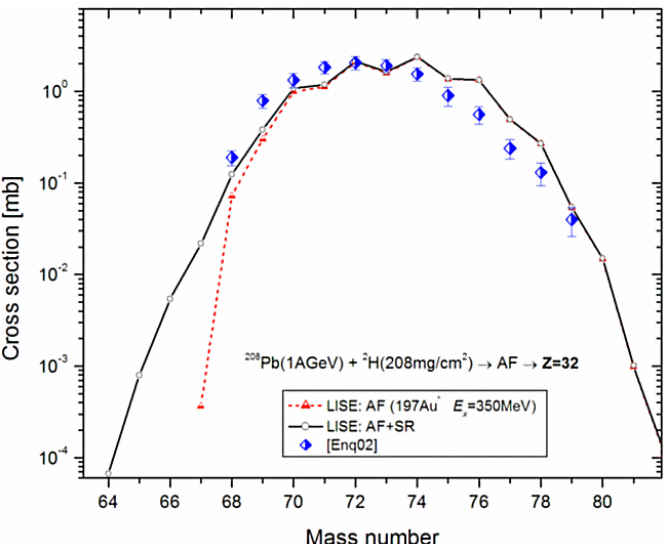
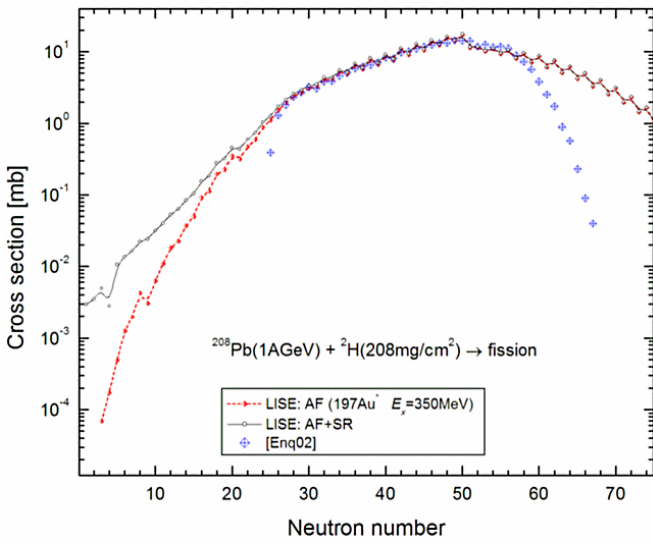
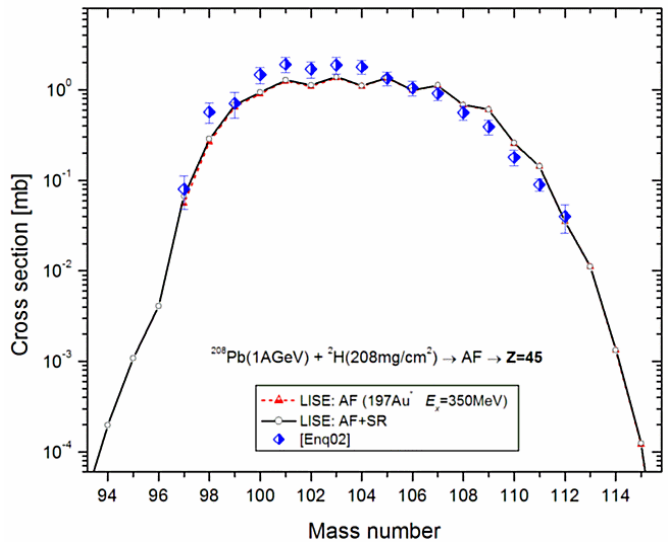
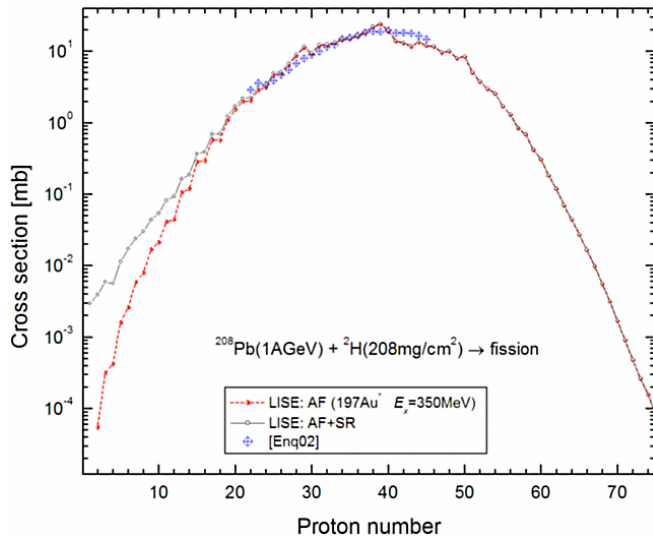


**Fig.144.** Experimental [Enq02] integrated distributions from spallation-fission reactions in  $^{208}\text{Pb}(1\text{AGeV})+d$  and calculated by LISE AF, assuming the fissile nucleus  $^{197}\text{Au}$  with  $E_x=350\text{ MeV}$ . Middle plot: no corrections were done for absent experimental results (compare with Fig.159).

**Fig.145.** Isotopic production cross-sections for spallation-fission products ( $Z=23,32,45$ ) from the reaction  $^{208}\text{Pb}(1\text{AGeV})+d$  obtained in work [Enq02] and calculated by LISE AF, assuming the fissile nucleus  $^{197}\text{Au}$  with  $E_x=350\text{ MeV}$ .

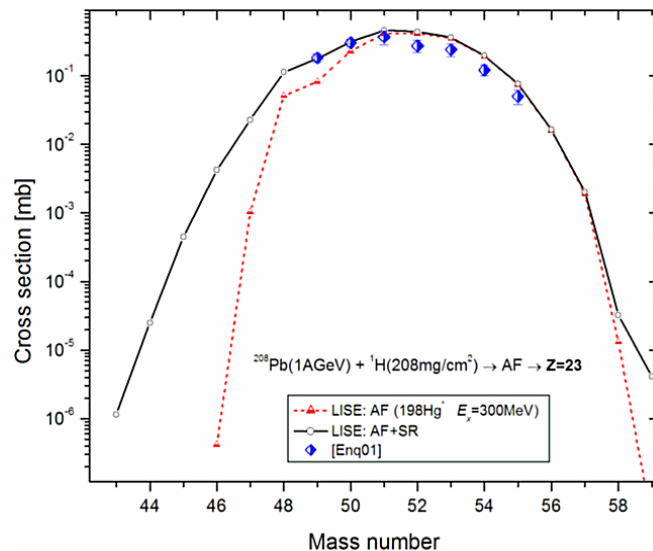
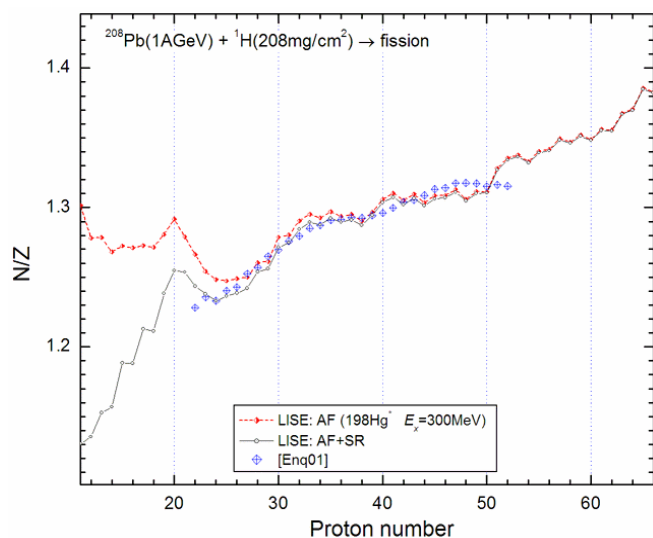
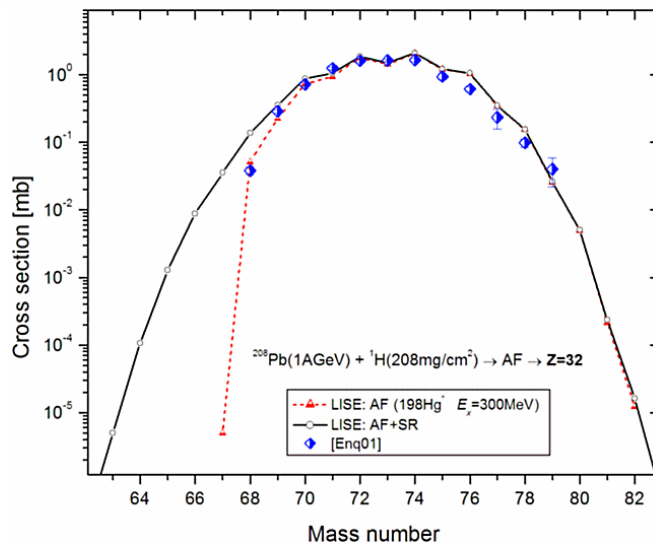
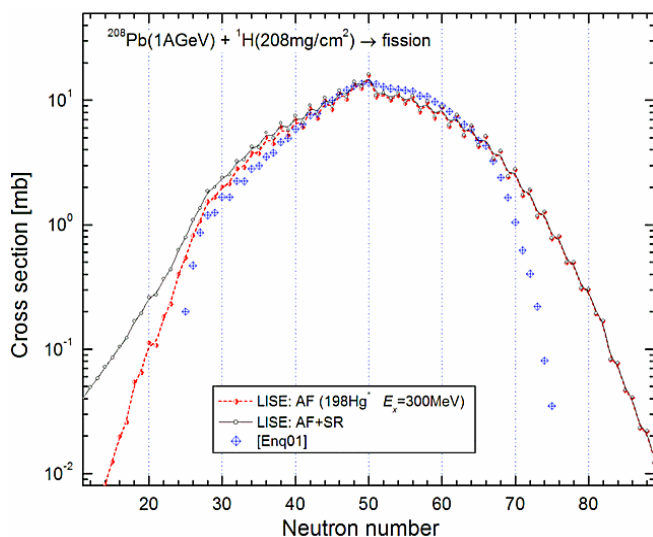
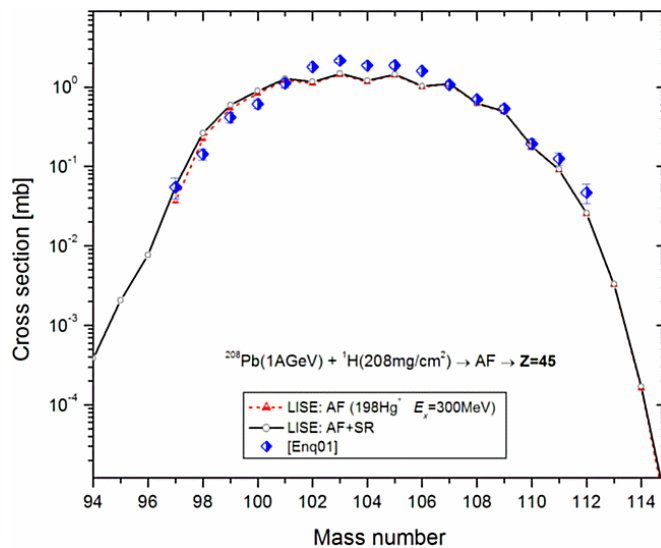
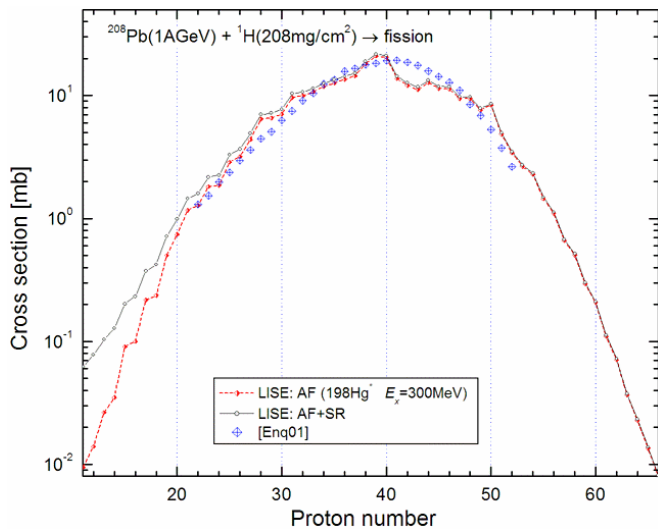


**Fig.146.** Experimental [Enq01] integrated distributions from spallation-fission reactions in  $^{208}\text{Pb}(1\text{AGeV})+p$  and calculated by LISE AF, assuming the fissile nucleus  $^{198}\text{Hg}$  with  $E_x=300\text{MeV}$ . Middle plot: no corrections were done for absent experimental results (compare with Fig.159).

**Fig.147.** Isotopic production cross-sections for spallation-fission products ( $Z=23,32,45$ ) from the reaction  $^{208}\text{Pb}(1\text{AGeV})+p$  obtained in work [Enq01] and calculated by LISE AF, assuming the fissile nucleus  $^{198}\text{Hg}$  with  $E_x=300\text{MeV}$ .

Fig.143 shows calculated  $^{198}\text{Hg}$  fission parameters as a function of excitation energy. Using the experimental fission characteristics from Table 17 and taking into account that an expected fissile nucleus has an excitation energy about 300-400 MeV.

Based on the fact that  $\sigma_A$  and  $\sigma_Z$  are larger in the case of a deuterium target and using calculations from Fig.143 it is possible to suggest that the excitation energy in the case of a deuterium target is about 50-100 MeV higher than in the case of a hydrogen target. Using the bottom pictures in Fig.143 it is possible to assume that fissile nuclei are found in the region  $A=196-200$  and  $Z=79-80$ . The comparison with experimental data has shown, that the best agreement is reached for  $^{198}\text{Hg}$  with  $E_x=300$  MeV in the case of a hydrogen target and for  $^{197}\text{Au}$  with  $E_x=350$  MeV in the case of a deuterium target.

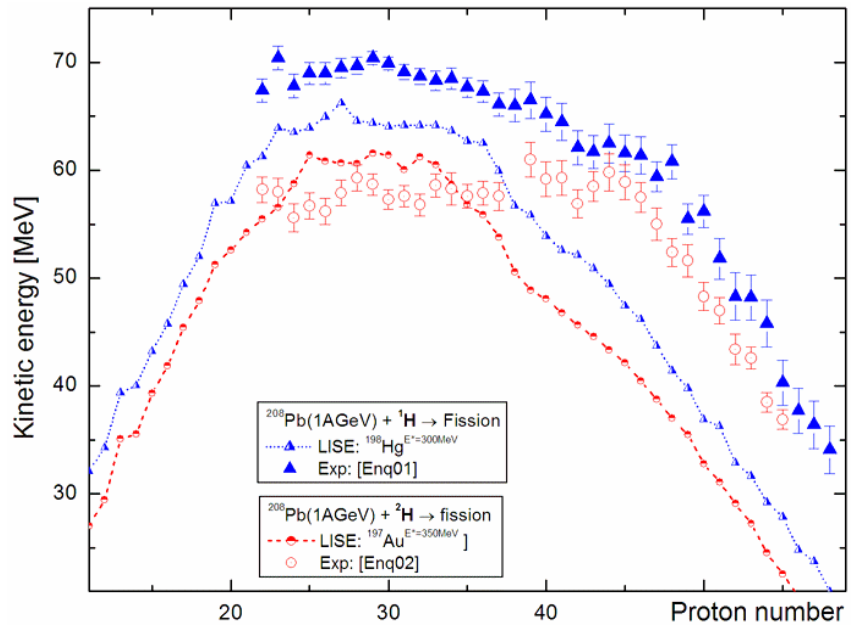


**Fig.148.** Measured and calculated by LISE fission-fragment mean kinetic energies as a function of their proton number for the data of [Enq01, Enq02] ( $^{208}\text{Pb}(1\text{AGeV})+p,d$ ).

Fig.144 and Fig.146 show experimental integrated distributions from spallation-fission reactions in  $^{208}\text{Pb}(1\text{AGeV}) + ^2\text{H}, ^1\text{H}$  and calculated by LISE AF. Fig.145 and Fig.147 show isotopic production cross-sections of spallation-fission products ( $Z=23,32,45$ ) from the reaction  $^{208}\text{Pb}(1\text{AGeV}) + ^2\text{H}, ^1\text{H}$  obtained in work and calculated by LISE AF.

Fig.148 shows measured and calculated by LISE fission-fragment mean kinetic energies as a function of their proton number for the data of  $^{208}\text{Pb}(1\text{AGeV}) + p,d$ .

LISE++ files “AF\_208Pb\_p.lpp” and “AF\_208Pb\_d.lpp” contain experimental cross-section data for the reactions  $^{208}\text{Pb}(1\text{AGeV}) + p,d$  [Enq01,Enq02] and can be loaded from the site [http://groups.nsl.msu.edu/lise/7\\_5/examples/](http://groups.nsl.msu.edu/lise/7_5/examples/) or from the “\files\examples\afission\” directory.

**Note.** All this analysis of experimental fission fragment production cross-sections in the reactions  $^{208}\text{Pb}(1\text{AGeV}) + p,d$  was done using the previous version of the code without the first item in Equation /11/. We recommend repeating Fig.143 procedures to get new excitation energy regions. The new results probably will be slightly different from those given here.

Experimental data with the  $^{238}\text{U}$  beam were analyzed using with the “full” version of Equation /11/.

### 5.9.3. $^{238}\text{U}(1\text{A GeV}) + \text{Pb}$

To compare LISE calculations with experimental data for the reaction  $^{238}\text{U}+\text{Pb}$  we used the work [Enq99]. The experiment was performed at the GSI fragment separator. The primary beam of  $^{238}\text{U}$  with an energy of 1A GeV impinged on a 50.5 mg/cm<sup>2</sup> lead target. A secondary reaction contribution for this thin target (1.45e+20 atoms/cm<sup>2</sup>) is negligible. Reactions of U-projectiles on a lead target at this energy are characterized by a large contribution from Coulomb fission.

**Table 20.** EERs calculated by LISE and actually used for fission fragment yield calculations in the reaction  $^{238}\text{U}(1\text{A GeV})+\text{Pb}$ . Excitation energy of the prefragment after abrasion was set to  $E_0^* = 13.3 \text{ MeV/dA}$ .

Method	$\Sigma\sigma$ , mb	Low			Middle			High		
		A, Z, N	$E^*$	$\sigma$ , mb	A, Z, N	$E^*$	$\sigma$ , mb	A, Z, N	$E^*$	$\sigma$ , mb
Abrasion-Ablation	3587.7	$^{238}_{92}\text{U}_{146}$	17.3	2279.9	$^{231}_{90}\text{Th}_{141}$	97.5	746.8	$^{215}_{84}\text{Po}_{131}$	286.1	561.1
Actually used for AF calculations	4080.0	$^{238}_{92}\text{U}_{146}$	17.3	2280	$^{230}_{90}\text{Th}_{140}$	100	500	$^{214}_{84}\text{Po}_{130}$	300	1300

Calculated EER parameters for the reaction  $^{238}\text{U}(1\text{A GeV})+\text{Pb}$  are shown in Table 20. The file “AF\_238U\_Pb.lpp” containing experimental cross-section data [Enq99] can be loaded from the site [http://groups.nsl.msu.edu/lise/7\\_5/examples/](http://groups.nsl.msu.edu/lise/7_5/examples/).

Neutron shells for the semi-empirical fission model [Ben98] were changed in LISE for this analysis according to [Sch00]:  $N_1=83$ ,  $dU_1=-2.65$ ,  $C_1=0.7$ , and  $N_2=90$ ,  $dU_2=-3.8$ ,  $C_2=0.15$  (see Fig.149).

Comparison results between LISE calculation and experimental data [Enq99] are shown in Fig.150 (neutron fission cross-section), Fig.151 (N/Z ratio as a function of fragment proton number).

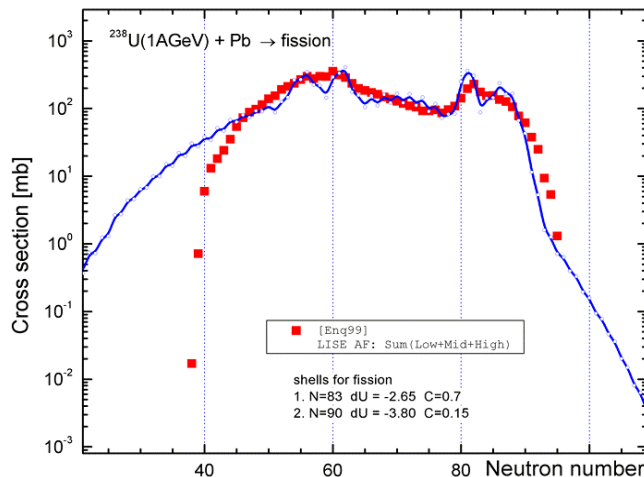


**Fig.150.** Measured [Enq99] and calculated by LISE neutron fission cross-sections for the reaction  $^{238}\text{U}(1\text{A GeV})+\text{Pb}$ .

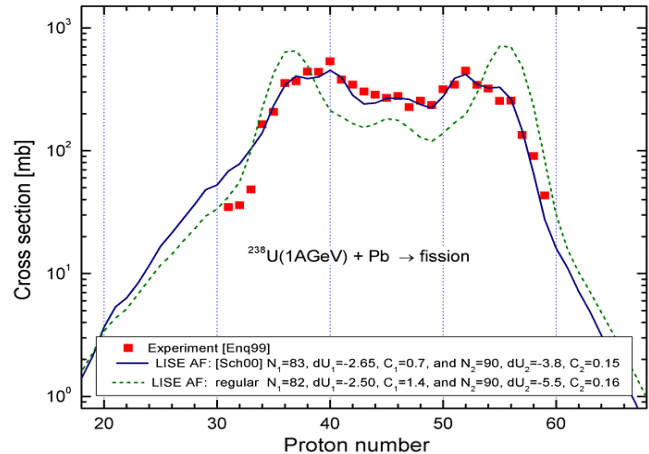


**Fig.149.** Experimental [Enq99] and calculated by LISE elemental fission cross-sections for the reaction  $^{238}\text{U}(1\text{A GeV})+\text{Pb}$ . LISE calculations were done with different parameters of the neutron shells of the fission model [Ben98].

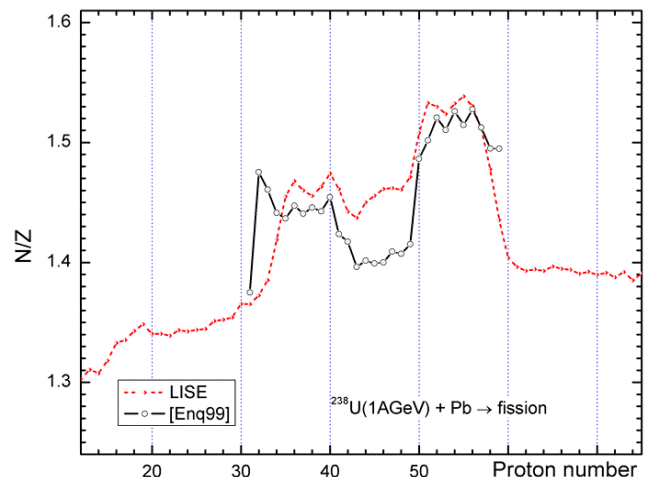


**Fig.151.** Experimental [Enq99] and calculated by LISE N/Z ratios as a function of their proton number for the reaction  $^{238}\text{U}(1\text{A GeV})+\text{Pb}$ .



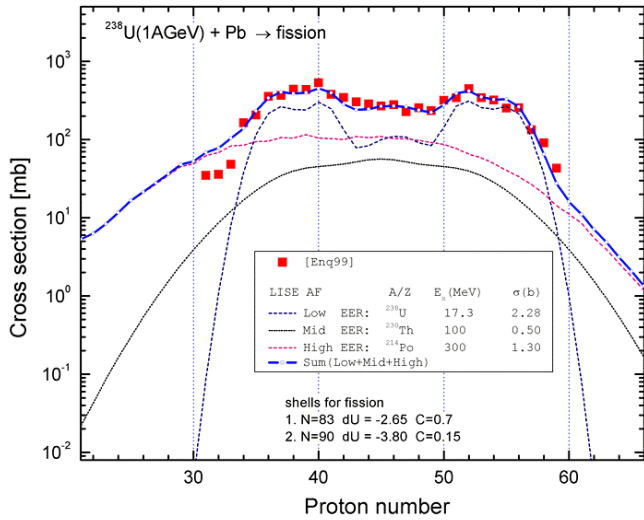


**Fig.152.** Measured [Enq99] and calculated by LISE elemental fission cross-sections for the reaction  $^{238}\text{U}(1\text{AGeV})+\text{Pb}$ . Contributions from different EERs are shown in the plot also.

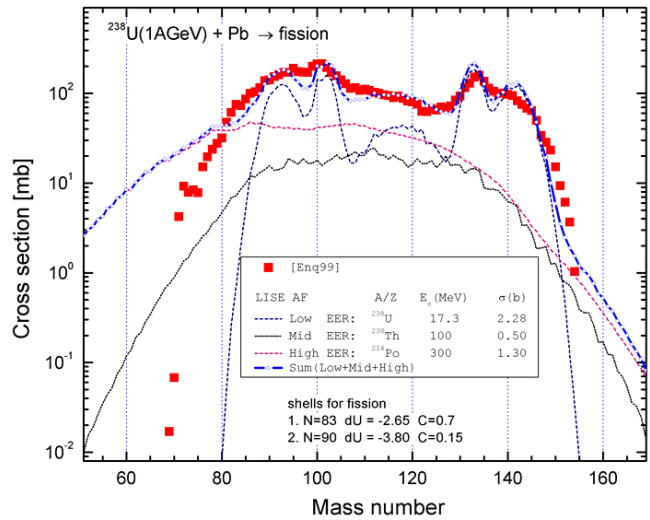


**Fig.153.** Experimental [Enq99] and calculated by LISE mass fission fragment cross-sections for the reaction  $^{238}\text{U}(1\text{AGeV})+\text{Pb}$ .

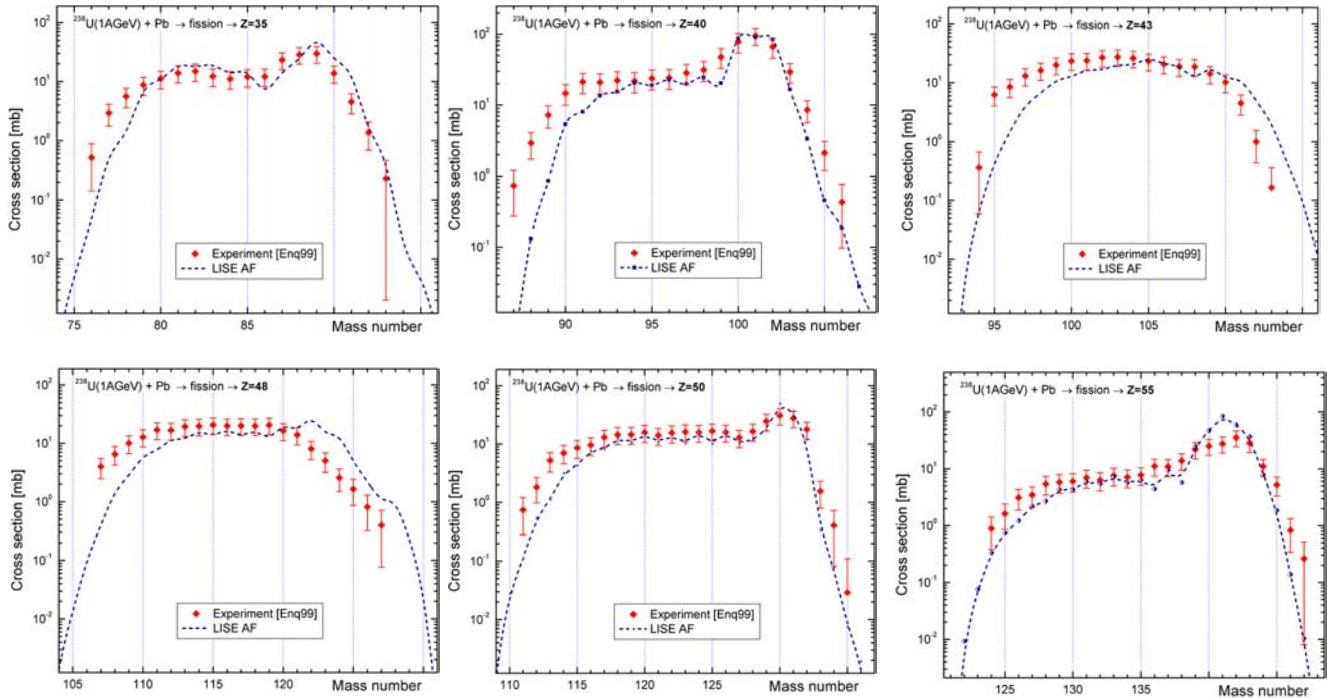


**Fig.154.** Isotopic production cross-sections for fission products ( $Z=35,40,43,48,50,55$ ) from the reaction  $^{238}\text{U}(1\text{AGeV})+\text{Pb}$  obtained in work [Enq99] and calculated by the LISE AF model for the excitation energy of the prefragment after abrasion  $E_0^* = 13.3 \text{ MeV}/dA$ . Load the “AF\_238U\_Pb.lpp” file for details.

Fig.152 (Fig.153) shows experimental and calculated by LISE elemental (mass) fission cross-sections for the reaction  $^{238}\text{U}(1\text{AGeV})+\text{Pb}$ . Contributions from different EERs are shown in the plots also.

Fig.154 shows isotopic production cross-sections for fission products ( $Z = 35, 40, 43, 48, 50, 55$ ) from the reaction  $^{238}\text{U}(1\text{AGeV})+\text{Pb}$  obtained in work [Enq99] and calculated by the LISE AF model.

### 5.9.4. $^{238}\text{U}(750\text{AMeV}) + \text{Be}$

To compare LISE calculations with experimental data for the reaction  $^{238}\text{U}+\text{Be}$  we used the work [Ber97]. The experiment was performed at the GSI fragment separator. The primary beam of  $^{238}\text{U}$  with an energy of 750AMeV impinged on a  $1\text{ g/cm}^2$  beryllium target. A secondary reaction contribution in calculated cross-sections was not included for comparison with experimental data.

**Table 21.** EERs calculated by LISE and actually used for fission fragment yield calculations for the reaction  $^{238}\text{U}(750\text{ AMeV})+\text{Be}$ . The region boundaries were set to 40 & 180 MeV.  $E_0^* = 13.3\text{ MeV/dA}$ .

Method	$\Sigma\sigma$ , mb	Low			Middle			High		
		A, Z, N	$E^*$	$\sigma$ , mb	A, Z, N	$E^*$	$\sigma$ , mb	A, Z, N	$E^*$	$\sigma$ , mb
Abrasion-Ablation calculations	1207.5	$^{236}_{92}\text{U}_{144}$	23.4	323.2	$^{231}_{90}\text{Th}_{141}$	97.0	573.4	$^{218}_{85}\text{At}_{133}$	249	310.9
Actually used for AF calculations	1050.0	$^{236}_{92}\text{U}_{144}$	23.5	200	$^{226}_{90}\text{Th}_{136}$	100	500	$^{220}_{88}\text{Ra}_{132}$	250	350

EER parameters (AA calculated and actually used in fission production calculations) for the reaction  $^{238}\text{U}(750\text{AMeV})+\text{Be}$  are shown in Table 21. The LISE file “AF\_238U\_Be.lpp” with corresponding settings, which contains experimental cross-section data [Ber97], can be loaded from the site

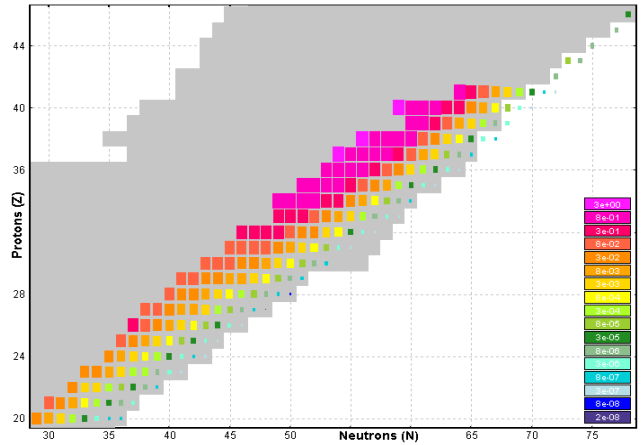


**Fig.155.** LISE two-dimensional plot of the experimental isotopic cross-sections for fission-fragments obtained in 750AMeV  $^{238}\text{U}+\text{Be}$  (Ber97).

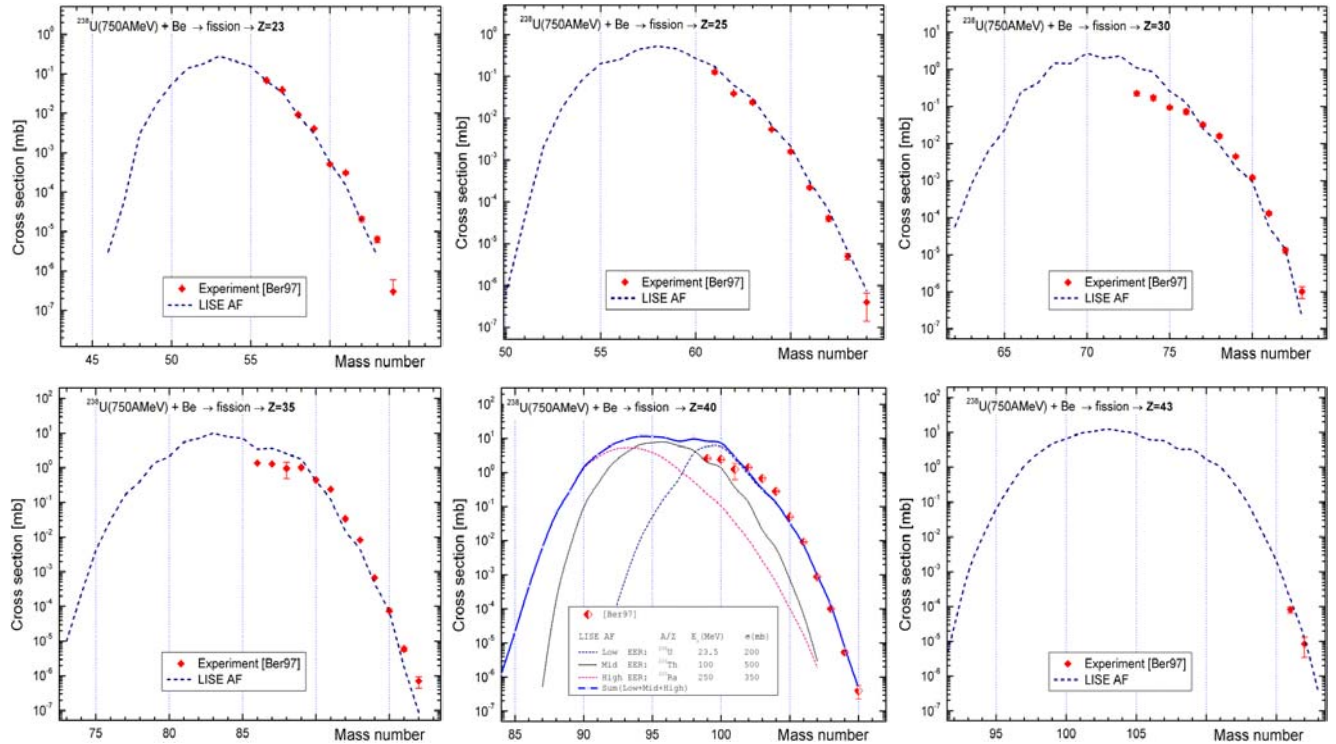


**Fig.156.** Isotopic production cross-sections for fission products ( $Z=23,25,30,35,40,43$ ) from the reaction  $^{238}\text{U}(750\text{AMeV})+\text{Be}$  obtained in work [Ber97] and calculated by the LISE AF model for the excitation energy of the prefragment after abrasion  $E_0^* = 13.3\text{ MeV/dA}$ . Load the “AF\_238U\_Be.lpp” file for details.

[http://groups.nsl.msu.edu/lise/7\\_5/examples/](http://groups.nsl.msu.edu/lise/7_5/examples/). As in the previous chapter, neutron shells for the semi-empirical fission model were set in LISE for this analysis according to [Sch00]:  $N_1=83$ ,  $dU_1=-2.65$ ,  $C_1=0.7$ , and  $N_2=90$ ,  $dU_2=-3.8$ ,  $C_2=0.15$ .

The experiment [Ber97] was devoted to the study of the neutron-rich side of the table of nuclides (see Fig.155). More than a hundred new nuclear species were identified including  $^{78}\text{Ni}$ , for which a cross-section of 300 pb was measured. Values of  $120\pm 40$  mb were found for the cross-section of  $^{238}\text{U}$  low excitation fission on Be. The total fission was measured cross-section to be 1.03 barn for the U/Be system [Hes96].

Fig.156 shows isotopic production cross-sections for fission products ( $Z=23,25,30,35,40,43$ ) from the reaction  $^{238}\text{U}(750\text{AMeV})+\text{Be}$  obtained in work [Ber97] and calculated by the LISE AF model.

### 5.9.5. $^{238}\text{U}(1\text{AGeV}) + p$

To compare LISE calculations with experimental data for the reaction  $^{238}\text{U}+p$  we used the work [Ber03]. The experiment was performed at the GSI fragment separator. The primary beam of  $^{238}\text{U}$  with an energy of 1AGeV impinged on a  $87.2\text{ mg/cm}^2$  liquid hydrogen target. The secondary reaction contribution in calculated cross-sections is shown for comparison with experimental data.

**Table 22.** EERs calculated by LISE and actually used for fission fragment yield calculations for the reaction  $^{238}\text{U}(1\text{ AGeV})+p$ . The region boundaries were set to 40 & 180 MeV.  $E_0^*=13.3\text{ MeV/dA}$ .

Method	$\Sigma\sigma$ , mb	Low			Middle			High		
		$A, Z, N$	$E^*$	$\sigma$ , mb	$A, Z, N$	$E^*$	$\sigma$ , mb	$A, Z, N$	$E^*$	$\sigma$ , mb
Abrasion-Ablation calculations	891.4	$^{237}_{92}\text{U}_{145}$	23.5	343.6	$^{232}_{90}\text{Th}_{142}$	75.3	373.9	$^{215}_{84}\text{Po}_{131}$	290	173.2
AF + INC fission (5.8.1.1. Hydrogen target)	1530.5	$^{236}_{92}\text{U}_{144}$	23.8	331.5	$^{234}_{91}\text{Pa}_{143}$	57.4	259.7	$^{215}_{84}\text{Po}_{131}$	289.9	939.3
Actually used for AF calculations	<b>1550.0</b>	$^{236}_{92}\text{U}_{144}$	<b>23</b>	<b>150</b>	$^{226}_{90}\text{Th}_{136}$	<b>75</b>	<b>550</b>	$^{220}_{89}\text{Ac}_{131}$	<b>180</b>	<b>850</b>

EER parameters (AA calculated and actually used in fission production calculations) for the reaction  $^{238}\text{U}(1\text{AGeV}) + p$  are shown in Table 22. The LISE file “AF\_238U\_p.lpp” with corresponding settings, which contains experimental cross-section data [Ber03], can be loaded from the site [http://groups.nsl.msu.edu/lise/7\\_5/examples/](http://groups.nsl.msu.edu/lise/7_5/examples/). As in the previous chapter (except dU1 parameter), neutron shells for the semi-empirical fission model were set in LISE:  $N_1=83$ ,  $dU_1=-2.0$ ,  $C_1=0.7$ , and  $N_2=90$ ,  $dU_2=-3.8$ ,  $C_2=0.15$ .

To get better agreement with experimental results we have made two global changes in EERs of “AF+INC” method: transfer  $\Delta\sigma=200$  mb from the Low EER to the Middle EER and change to more proton rich Middle and High fissile nuclei, from  $^{234}\text{Pa}$  ( $N/Z=1.57$ ) to  $^{226}\text{Th}$  ( $N/Z=1.51$ ) and from  $^{215}\text{Po}$  ( $N/Z=1.56$ ) to  $^{220}\text{Ac}$  ( $N/Z=1.48$ ) accordingly. It is probably that these changes can be explained by increasing the excitation energy per abraded nucleon as well as increasing dissipation influence through beta parameter (see Fig.13).

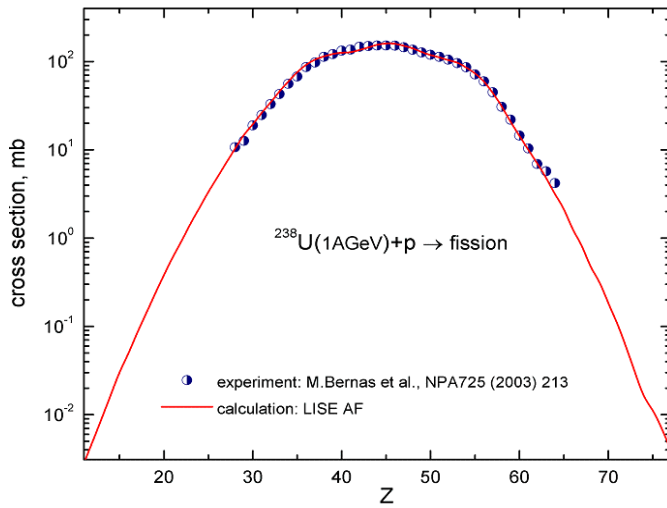


**Fig.157.** Measured [Ber03] and LISE calculated elemental fission cross-sections for the reaction  $^{238}\text{U}(1\text{AGeV})+p$ .

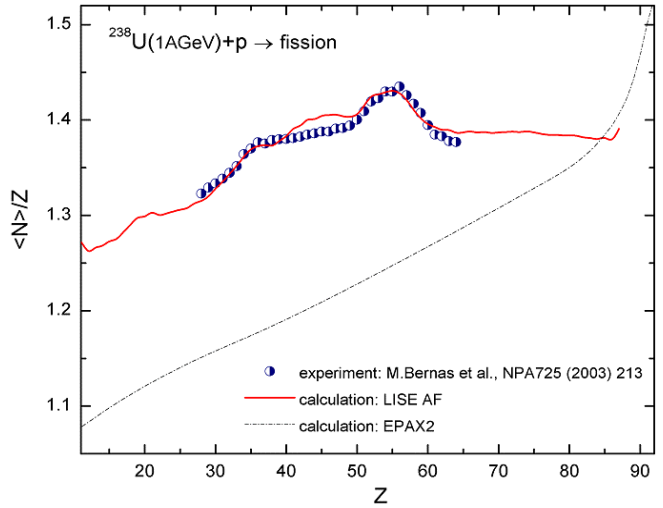


**Fig.158.** Experimental [Ber03] and LISE calculated  $N/Z$  ratios as a function of their proton number for the reaction  $^{238}\text{U}(1\text{AGeV})+p$ .

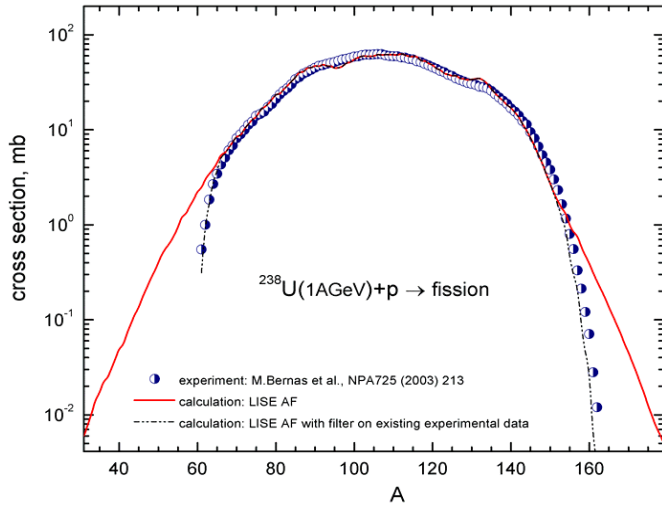


**Fig.159.** Measured [Ber03] and LISE calculated mass fission cross-sections for the reaction  $^{238}\text{U}(1\text{AGeV})+p$ . The dash-dot line represents calculated data filtered to existing experimental data ( $Z=28-64$ ).

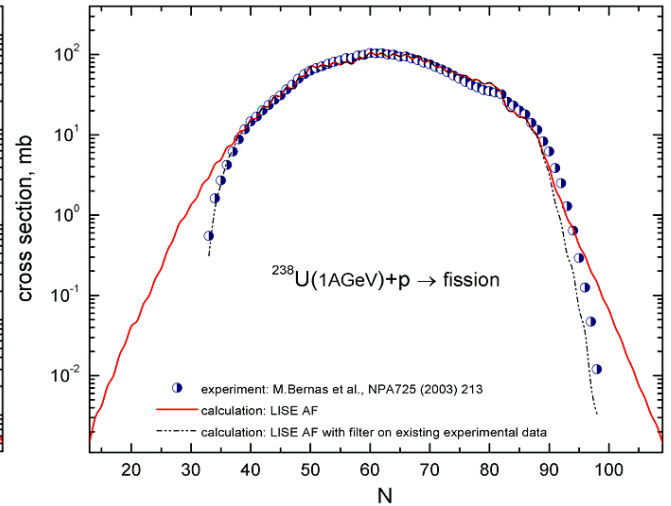


**Fig.160.** Experimental [Ber03] and LISE calculated neutron fission fragment cross-sections for the reaction  $^{238}\text{U}(1\text{AGeV})+p$ . The dash-dot line represents calculated data filtered to existing experimental data ( $Z=28-64$ ).

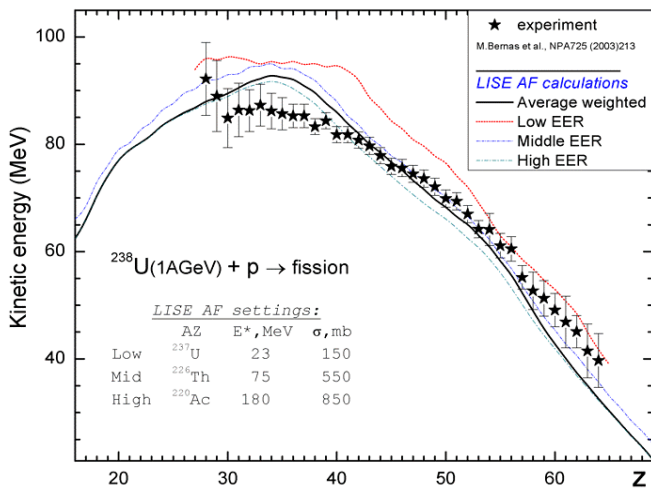


**Fig.161.** Measured and LISE calculated fission-fragment mean kinetic energies as a function of their proton number for the data [Ber03] ( $^{238}\text{U}(1\text{AGeV})+p$ ).

Comparisons of results from LISE calculation and experimental data [Ber03] are shown in Fig.157 (elemental fission cross-section), Fig.158 ( $N/Z$  ratio as a function of fragment proton number), Fig.159 (mass fission cross-section), Fig.160 (neutron fission cross-section), and Fig.161 (fragment kinetic energy).

Fig.162 shows isotopic production cross-sections for fission products ( $Z = 30, 35, 40, 43, 47, 50, 54, 59, 64$ ) from the reaction  $^{238}\text{U}(1\text{AGeV})+p$  obtained in work [Ber03] and calculated by the LISE AF model.



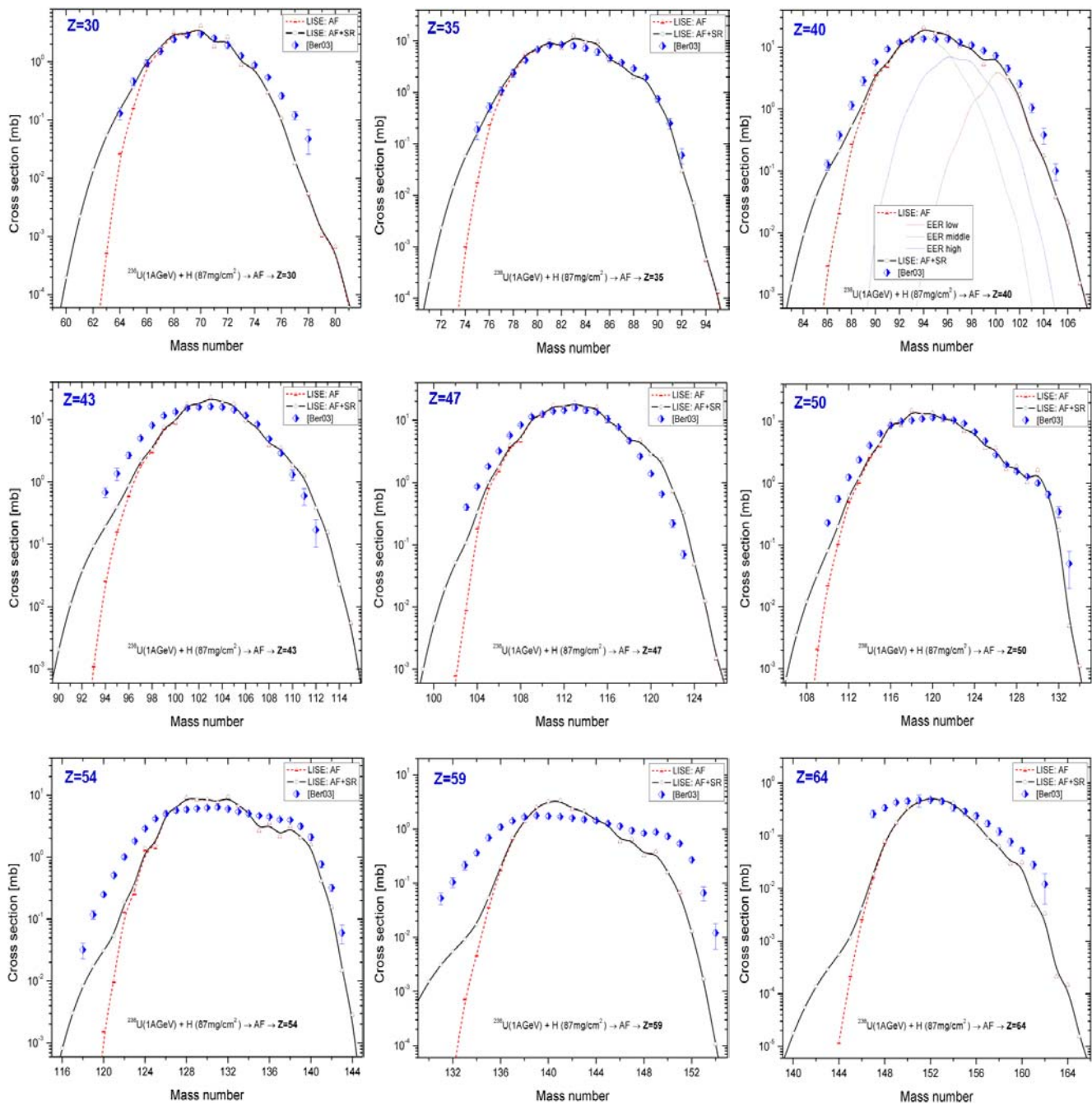


**Fig.162.** Isotopic production cross-sections for fission products ( $Z=30,35,40,43,47,50,54,59,64$ ) from the reaction  $^{238}\text{U}(1\text{AGeV})+p$  obtained in work [Ber03] and calculated by the LISE AF model. Load the “AF\_238U\_p.lpp” file for details.

Six example files devoted to Abrasion-Fission are included in the LISE installation package:

- |                |                |
|----------------|----------------|
| AF_208Pb_d.lpp | AF_208Pb_p.lpp |
| AF_238U_p.lpp  | AF_238U_d.lpp  |
| AF_238U_Be.lpp | AF_238U_Pb.lpp |

The user can load them from the “files\examples\afission\” directory.



## 6. New utilities

### 6.1. User cross-section analysis using Abrasion-Ablation model

The purpose of the new utility is to find parameters for the prefragment excitation energy distribution (mean value and deviation) which best correspond to experimental data. The “user cross-section analysis” can be loaded from the “Utilities” menu (see Fig.163).

The analysis might be run if the following four conditions are satisfied:

1. The “Projectile fragmentation” reaction mode is selected;
2. Abrasion-ablation is the selected production cross-section method;
3. There are more than two user cross-sections in memory;
4. The “File” cross-section option is set to “on” in the “Options” dialog.

If one of these conditions is not fulfilled then an error message will appear in the bottom of the dialog instead of the line “Press Escape to interrupt analysis” (see Fig.163).

Before running the analysis the user has to define the following parameters:

1. “Local line to analyze” - click the corresponding button to define the set of data important for you (for example the neutron removal line). It may be  $Z$ ,  $N$ ,  $A$ , or  $N-Z$  lines. The code compares experimental data and calculated values separately for the global set of data and for the local line defined by the user (see for details chapter “3.2. User CS in plots” [http://groups.nsl.msu.edu/lise/6\\_4/lise++\\_6\\_4.pdf](http://groups.nsl.msu.edu/lise/6_4/lise++_6_4.pdf)).
2. “Calculate down to  $Z$ ” - initially is set to 1, but if you want to make the analysis faster and you do not need light elements’ cross-sections then it may be increased. Obviously it is better to set this parameter greater than or equal to the lowest charge value of experimental data.
3. Minimal and maximal values of excitation energy and its deviation as well as the number of calculated points ( $N_{\langle E^* \rangle}$  and  $N_{\text{sigma}}$ ) for both cases.
4. “Weights of analysis value” – determines contribution of each of the four calculated values in the final result:

$$Final = w_1 \cdot Lo\chi^2_{\text{local}} + w_2 \cdot LoD_{\text{local}} + w_3 \cdot Lo\chi^2_{\text{total}} + w_4 \cdot LoD_{\text{total}} \quad /16/$$

where  $Lo\chi^2 = \ln(\chi^2)$  and  $LoD = \sum_{i=1}^N |\log_{10}(y_{\text{exp}}) - \log_{10}(y_{\text{calc}})| / N$ .

If the “Correct for the number of data points used” checkbox is set to “on” then the code calculates the  $Lo\chi^2$  value in the following way:  $Lo\chi^2 = \ln(\chi^2/N)$ , where  $N$  is the number of points used for the analysis.

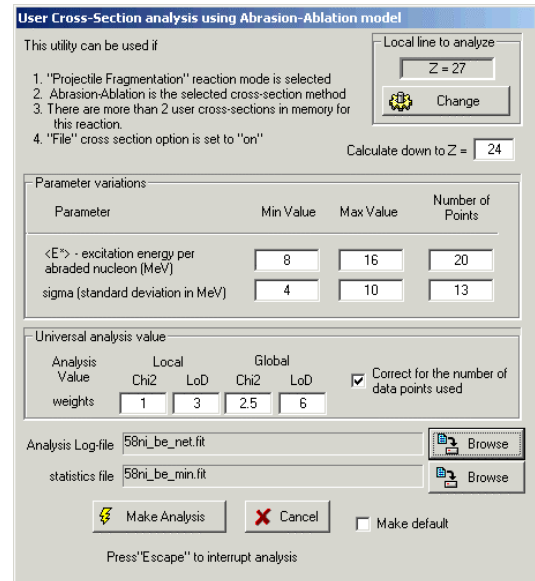


Fig.163. The “User cross-sections analysis” dialog.

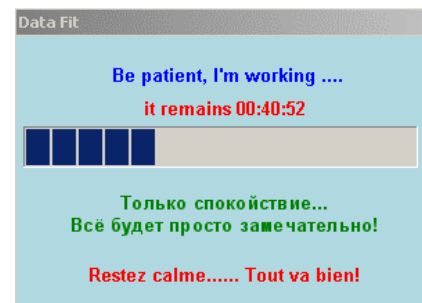
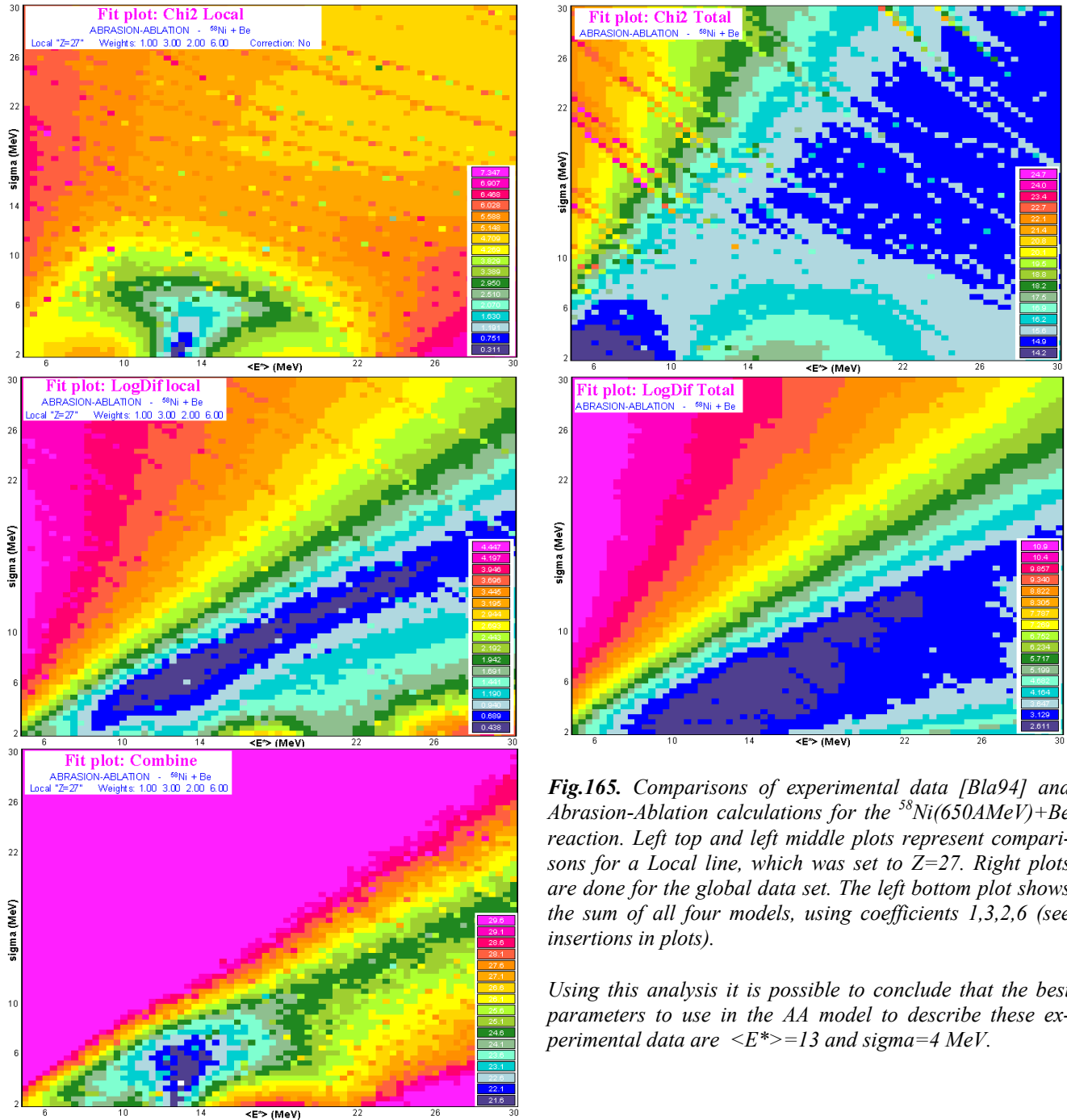


Fig.164.

The program will run the Abrasion-Ablation model  $N_{\langle E^* \rangle} \times N_{\text{sigma}}$  times after the user clicks the “Make analysis” button. During the calculation process the information window shows approximately how much time is remaining (see Fig.164).



**Fig.165.** Comparisons of experimental data [Bla94] and Abrasion-Ablation calculations for the  $^{58}\text{Ni}(650\text{AMeV})+\text{Be}$  reaction. Left top and left middle plots represent comparisons for a Local line, which was set to  $Z=27$ . Right plots are done for the global data set. The left bottom plot shows the sum of all four models, using coefficients 1,3,2,6 (see insertions in plots).

Using this analysis it is possible to conclude that the best parameters to use in the AA model to describe these experimental data are  $\langle E^* \rangle = 13$  and  $\text{sigma} = 4$  MeV.

After calculations are completed the program creates five two-dimensional plots (see Fig.165), four of them correspond to  $Lo\chi^2_{\text{local}}$ ,  $LoD_{\text{local}}$ ,  $Lo\chi^2_{\text{total}}$ ,  $LoD_{\text{total}}$  values and one represents the final result based on Equation /16/. The code also creates two text files, a statistics file and a log file, for each calculation. An analysis log-file shows calculated values for each combination “Energy-Sigma”; hereafter this file can be used by other programs (for example Excel or Origin) to determine optimum weights of models. The statistics file gives minimum values and their coordinates (energy, sigma) for each of the five models:

model	minimum	Energy	Sigma	maximum
Chi2 L	3.111e-01	12.61	2.00	7.787e+00
LD L	4.384e-01	12.25	6.06	4.698e+00
Chi2 T	1.425e+01	5.72	2.81	2.535e+01
LD T	2.611e+00	12.25	3.22	1.141e+01
comb T	2.153e+01	12.97	3.62	4.741e+01

**Note:** The code automatically uses a linear scale for two-dimensional plots using the minimum and maximum calculated values. It is recommended to decrease the step in the “Linear scale” dialog manually to get a more detailed picture as was shown in Fig.165.

### 6.1.1. AA parameters corresponding to EPAX

There was a question: what parameters should be set in the AA model in order for its calculation results to corresponded to EPAX calculations for different combinations of primary beam and production target?

In order to conduct this analysis using the new utility it is necessary to do the following steps:

- ❑ Set a very thin target thickness;
- ❑ Set the EPAX2.15 parameterization as the model for fragmentation production cross-sections in the “Production mechanism” dialog;
- ❑ Calculate reduced cross-sections and save them in a user CS file (extension \*.cs2) using the “Secondary reactions” dialog;
- ❑ Load the obtained file into the operating memory through the “User CS file” dialog;
- ❑ Open the “User cross-sections analysis using Abrasion-Ablation model” (see Fig.163) dialog and begin the analysis.

**Table 23.** AA parameters obtained to match EPAX results for different projectile & beam combinations.

Beam	Target	$E_x \pm d(E_x)$	$\sigma_{Ex} \pm d(\sigma_{Ex})$	Minimum prefragment mass	Local line and limit for calculations	Minimum mass corresponding to local line	Special case
<sup>124</sup> Sn	Be	25.9 <sup>2.6</sup>	13.5 <sup>3.4</sup>	101	Z = Zb-4 = 46	91	✓
<sup>112</sup> Sn	Be	12.3 <sup>1.6</sup>	7.4 <sup>1.4</sup>	90	Z = Zb-4 = 46	91	
<sup>112</sup> Sn	Ta	11.8 <sup>1.0</sup>	7.4 <sup>0.9</sup>	4	Z = Zb-4 = 46	91	
<sup>86</sup> Kr	Be	19.7 <sup>0.7</sup>	10.0 <sup>1.8</sup>	66	Z = Zb-6 = 30	55	✓
<sup>86</sup> Kr	Be	17.9 <sup>0.6</sup>	13.0 <sup>0.6</sup>	66	Z = Zb-2 = 34	64	
<sup>86</sup> Kr	Ta	20.6 <sup>3.1</sup>	10.8 <sup>2.9</sup>	1	Z = Zb-6 = 30	55	
<sup>78</sup> Kr	Be	14.2 <sup>0.7</sup>	9.8 <sup>1.2</sup>	58	Z = Zb-6 = 30	55	
<sup>78</sup> Kr	Ta	12.4 <sup>1.3</sup>	8.6 <sup>1.2</sup>	1	Z = Zb-6 = 30	55	
<sup>64</sup> Ni	Be	11.6 <sup>1.2</sup>	7.0 <sup>1.3</sup>	45	Z = Zb-6 = 22	39	
<sup>58</sup> Ni	Be	11.7 <sup>1.2</sup>	6.0 <sup>1.3</sup>	39	Z = Zb-6 = 22	39	
<sup>48</sup> Ca	Be	13.2 <sup>1.4</sup>	9.3 <sup>1.0</sup>	30	Z = Zb-6 = 14	22	✓
<sup>48</sup> Ca	Be	10.2 <sup>1.5</sup>	10.3 <sup>1.3</sup>	30	Z = Zb-2 = 18	31	
<sup>40</sup> Ca	Be	9.7 <sup>1.1</sup>	4.4 <sup>1.7</sup>	23	Z = Zb-6 = 14	22	
<sup>40</sup> Ar	Be	6.1 <sup>1.5</sup>	3.3 <sup>1.9</sup>	23	Z = Zb-6 = 12	20	
<sup>36</sup> Ar	Be	8.9 <sup>0.7</sup>	4.8 <sup>1.7</sup>	19	Z = Zb-6 = 12	20	

AA parameters obtained to match EPAX results for <sup>36,40</sup>Ar, <sup>40,48</sup>Ca, <sup>58,64</sup>Ni, <sup>78,86</sup>Kr, <sup>112,124</sup>Sn projectiles on Be and Ta targets are shown in Table 23.

The following options and parameters of the AA model were kept in the analysis:

Dimension of evaporation:	32	Geom. corrections:	No
Decay Modes:	1n,2n,1p,2p, $\alpha$	BarFac:	1
State density:	C	Masses:	Database0 + LDM2
Take into account unbound nuclei:	Yes	Excitation energy:	Method "C" without LISE geometrical corrections

The parameters of User CS matching by the AA model were used:

Excitation energy ( $E_x$ ):	5-35 MeV, 70 points	Weights:	1,2,3,6
Sigma of $E_x$ distribution:	2-25 MeV, 70 points	Corrections for the number of data points:	Yes
Local line to analyze:	Z=Zb-6 (*)	Calculate down to Z:	Zb-6 (*)

\* where Zb is the atomic number of the projectile. There are several combinations where Z=Zb-4 and Zb-2 were used for the analysis (Table 23).

Fig.166 and Fig.167 show calculated cross-sections of Silicon isotopes and isotones N=24 produced in  $^{48}\text{Ca}$  fragmentation on a Be target. Parameters  $E_x=13.2$  and  $\sigma=9.3$ , according to Table 23, were used for AA calculations. Fig.168 shows four combined plots resultant from matching AA and EPAX calculations for reactions  $^{64}\text{Ni}+\text{Be}$ ,  $^{124}\text{Sn}+\text{Be}$ ,  $^{112}\text{Sn}+\text{Be}$ , Ta. Fit by double gaussian function was used to define  $E_x$  and  $\sigma$  positions as well as to obtain their standard deviations.

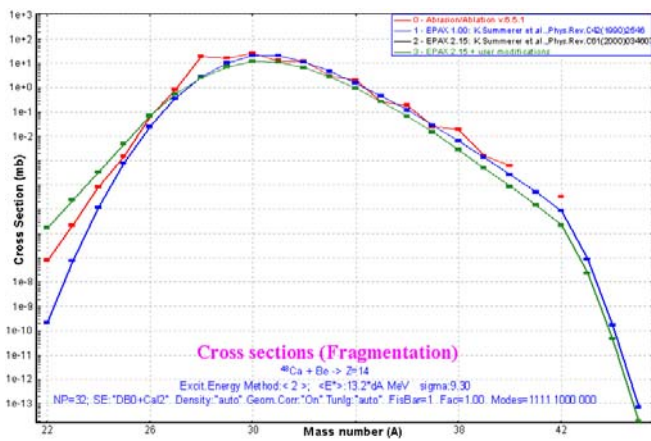


**Fig.166.** Calculated cross-sections of Silicon isotopes produced in  $^{48}\text{Ca}$  fragmentation on a Be target. Parameters  $E_x=13.2$  and  $\sigma=9.3$ , according to Table 23, were used for AA calculations.

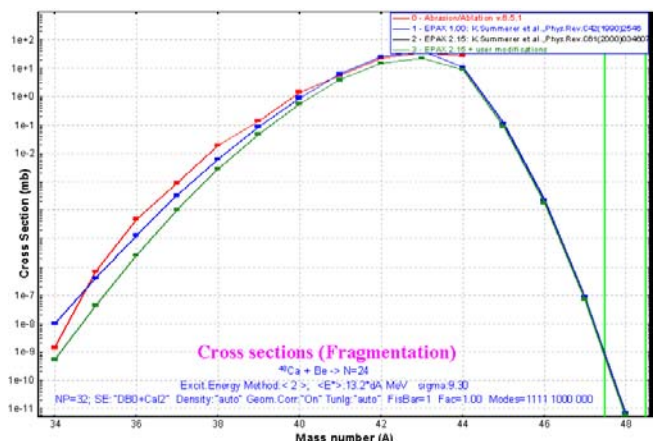


**Fig.167.** Calculated cross-sections of isotones N=24 produced in  $^{48}\text{Ca}$  fragmentation on a Be target. Parameters  $E_x=13.2$  and  $\sigma=9.3$ , according to Table 23, were used for AA calculations.

The “Minimum prefragment mass” column represents the minimum mass of excited prefragment which can be obtained from the projectile due to abrasion by the target nucleus.

The special case mark shows cases when the minimum of prefragment mass number is more than 7 units greater than the minimum mass number corresponding to the local line. These cases correspond to light (Be) target and neutron-rich beams ( $^{48}\text{Ca}$ ,  $^{86}\text{Kr}$ ,  $^{124}\text{Sn}$ ). For these cases the AA model (peripheral process) is not valid, because it is impossible to reproduce light masses without additional LISE geometrical corrections or a significant increase of the excitation energy to reproduce EPAX calculations. For example the INC (central collisions) model should be used to describe these data.

Data shown in Table 23 are plotted in Fig.169 as excitation energy versus width of excitation energy distribution and in Fig.170 as excitation energy as a function of projectile element number. From these figures it is possible to select out two data sets, “Regular” and “Neutron-rich”.

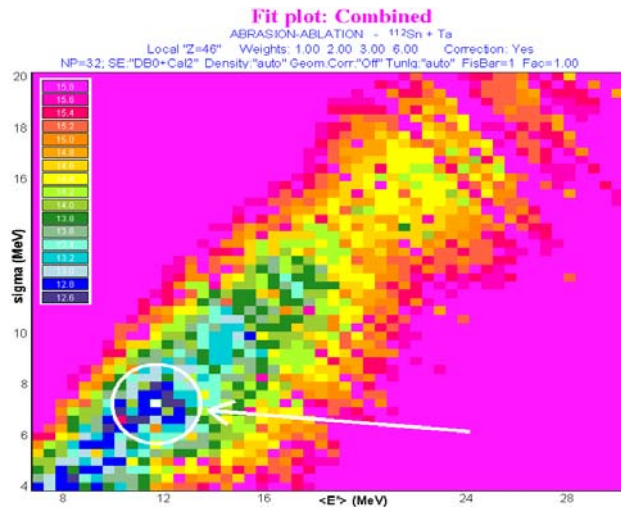
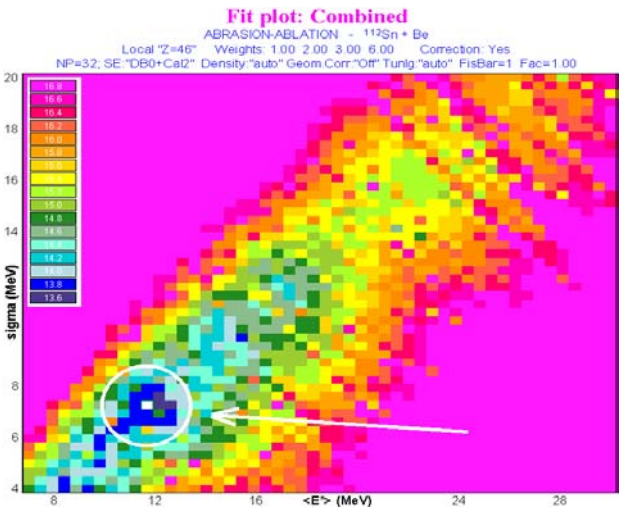
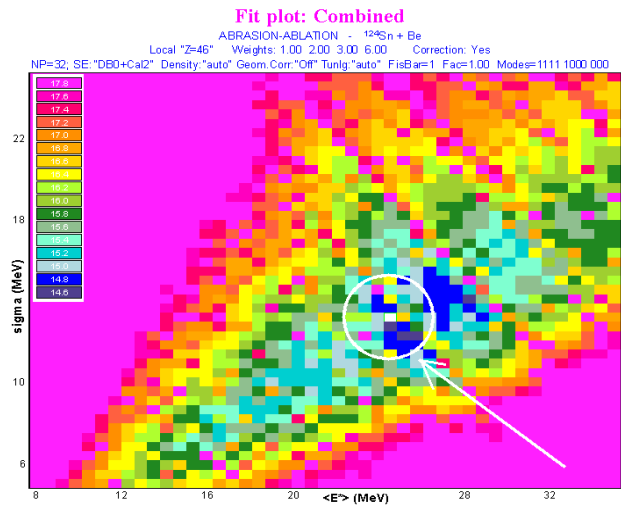
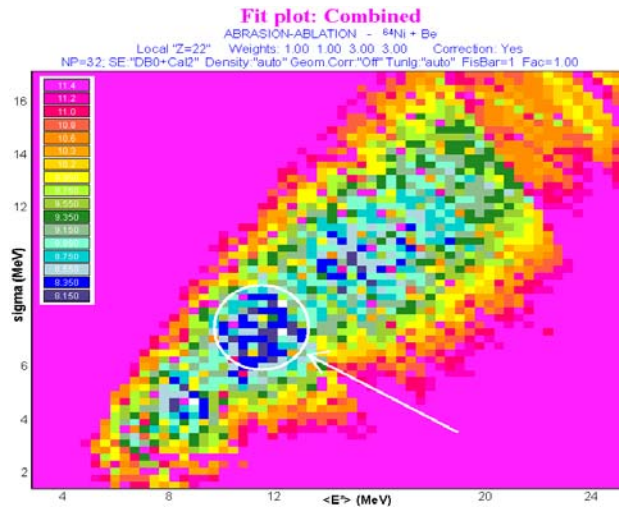


**Fig.168.** The Combined plots resultant from matching AA and EPAX calculations for reactions  $^{64}\text{Ni}+\text{Be}$  (left top plot),  $^{124}\text{Sn}+\text{Be}$  (right top plot),  $^{112}\text{Sn}+\text{Be}$  (left bottom plot), and  $^{112}\text{Sn}+\text{Ta}$  (right bottom plot). White circles show approximately the data regions which were fitted by the double gaussian function.

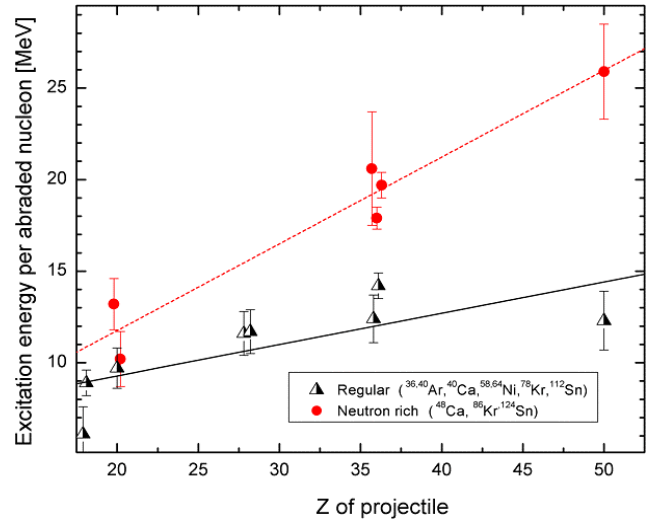
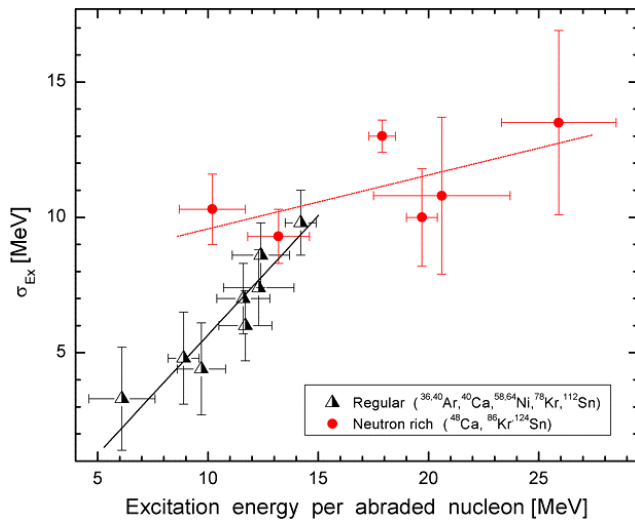


**Fig.169.** Widths versus mean values of excitation energy distributions from Table 23 obtained by matching EPAX values with the AA model.

**Fig.170.** Excitation energies per abraded nucleon from Table 23 versus projectile element number obtained by matching EPAX values with the AA model.

Black solid and dashed red lines are linear fits of “regular” and “neutron rich” datasets respectively. Fit parameters are shown in Table 24.



**Table 24.** Results of the linear fit ( $Y = A*X + B$ ) of data sets in Fig.169 and Fig.170.

Plot	Data set	A Slope value	dA standard error	B Intercept value	dB standard error	R Correlation coefficient	SD Standard deviation of the fit
Fig.169	Neutron rich	0.474	0.059	2.289	2.050	0.97	1.52
Fig.169	Regular	0.171	0.061	5.861	1.903	0.75	1.80
Fig.170	Neutron rich	0.199	0.116	7.585	2.157	0.65	1.45
Fig.170	Regular	0.817	0.126	-2.458	1.404	0.94	0.84

## 6.2. Optimum charge state combination

To which charge state combination is it necessary to set the spectrometer to produce the maximum fragment rate at the end of the spectrometer? In order to find a solution the user must determine the average ion charge state of the fragment after each “material & dispersive block” combination (for example blocks “Target” and “Dipole D1”). Try to find a combination for the example file “charge\_state\_optimum.lpp” (the file can be found in [http://groups.nslc.msu.edu/lise/7\\_5/examples/](http://groups.nslc.msu.edu/lise/7_5/examples/)). This example was made especially so that before each of four dipoles the setting fragment passes through materials with different atomic number.

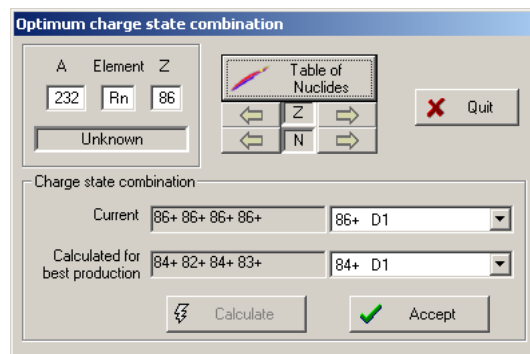


**Fig.171.** The “Optimum charge state combination” dialog (from the “Calculations” menu). Calculations were done for the example file “charge\_state\_optimum.lpp”.

The new utility “Optimum charge state combination” (see Fig.171), which can help to the user to solve this problem, has been incorporated into the code and is available in the “Calculations” menu. This utility is especially relevant for calculation of optimum target thickness, because the charge state combination is a function of target thickness. In the next chapters we will demonstrate the capabilities of the new utility for other utilities.

After loading the dialog it is necessary to choose the isotope of interest and click the “Calculate” button. How does the code look for the best combination?

1. It saves all settings of optical blocks;
2. The charge state option is turned on (if initially it was turned off);
3. The code sorts out all possible charge state combinations. The spectrometer is tuned for each combination;
4. The program finds a charge state combination giving maximum output and displays the result in the dialog (see Fig.171).

If the user clicks the “Cancel” button then all previous settings are restored. To set the new settings based on these calculations it is necessary to click the “Accept” button. If the user has decided to accept these values, and the charge state option was initially turned off in the program, the program remains in the “charge state on” mode, and the user receives a message on it (see Fig.172).



**Fig.172.**

### 6.3. Charge state combination calculation for the optimal target thickness utility

The utility to determine the optimum charge state combination (see the previous chapter) has been incorporated into the subroutine for optimal target thickness calculations. In order to use this option the user has to select the corresponding checkbox in the “Choose fragment” dialog of the optimal target thickness utility (see Fig.173).

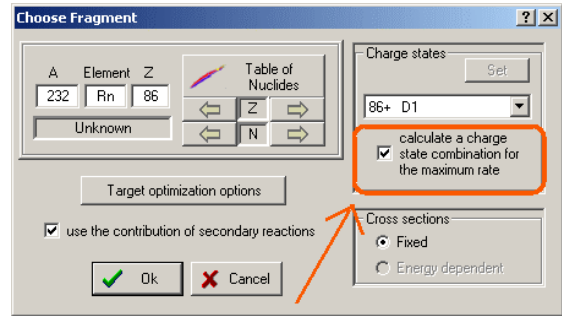


Fig.173. The “Choose fragment” dialog for the optimal target thickness utility.

We will demonstrate this new possibility using the example “optimum\_target\_and\_charge\_states.lpp” (the file can be found in [http://groups.nscl.msu.edu/lise/7\\_5/examples/](http://groups.nscl.msu.edu/lise/7_5/examples/)).

Why do we need this utility? Suppose that we do not know what is the best charge state combination to get the maximum rate, and we take the fully stripped fragment because the target is “light” (Lithium) and the primary beam energy is high enough (400MeV/u). Running the optimal target thickness utility in the regular mode we get that the optimum thickness is about to 600 mg/cm<sup>2</sup> (see Fig.174). We expect only about 20 events per second of the setting fragment for the given charge state combination.

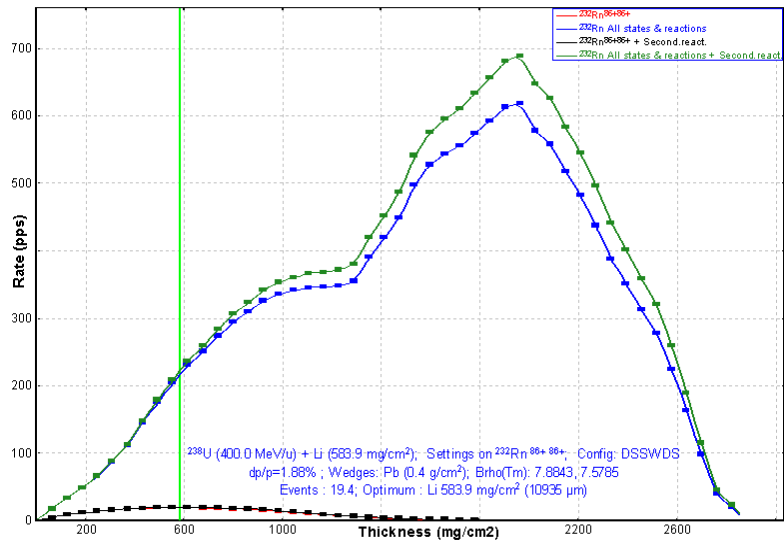


Fig.174. Rate of <sup>232</sup>Rn ions as a function of the target thickness. The spectrometer was tuned on the <sup>232</sup>Rn<sup>86+86+</sup> ion.

Determination of the optimal target thickness with searching the charge state combinations consists of three steps.

**First step:** Calculation of target thickness without charge states (see Fig.175). Usually the code uses the dependence of fragment rate on target thickness to define the optimum thickness; in this case the fragment rate is decreased by the standard deviation ( $\sigma_{\text{charge}}$ ) of the charge state distribution, which is calculated for various average fragment energies after the target (stripper). If  $\sigma_{\text{charge}}$  is less 0.5 then the value 0.5 is used instead  $\sigma_{\text{charge}}$ .

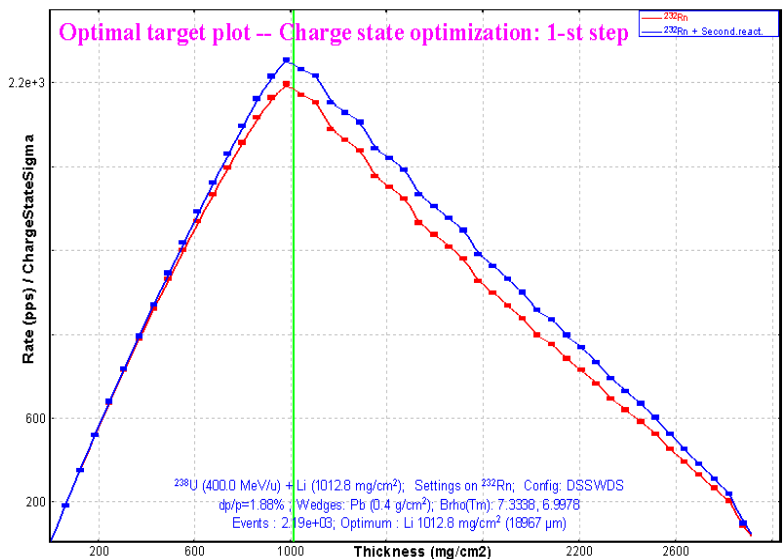
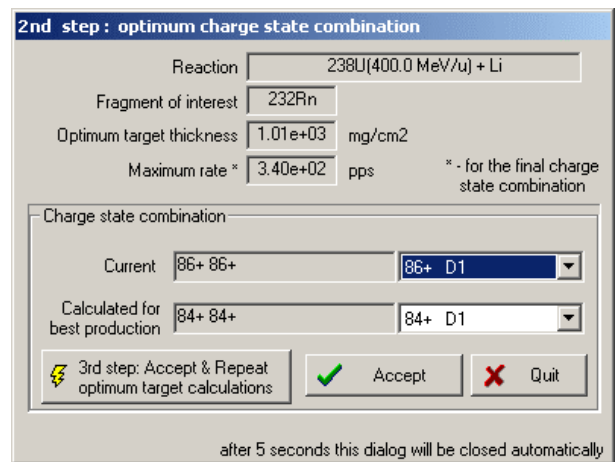


Fig.175. Optimal target thickness & Charge state optimization. Step 1: calculation of reduced fragment yield without charge states.

**Second step:** The program calculates an optimum charge state combination for the target thickness (1.01 g/cm<sup>2</sup>) obtained on the first step. Using the “2nd step optimization” dialog (see Fig.176) the user can click one of the following buttons:

- ❑ Cancel: leave the dialog and restore previous settings;
- ❑ Accept: accept the charge state combination (afterwards, leave the dialog or continue calculations);
- ❑ 3<sup>rd</sup> step: Accept the charge state combination and repeat optimum target calculations.

If no option is selected within 5 seconds, then the program automatically starts the third step of calculations.



**Fig.176.** Optimal target thickness & Charge state optimization.

Step 2: calculation of optimum charge state combination for the target thickness obtained on the first step.

**Third step:** The program calculates an optimum target thickness for the charge state combination (84+ 84+) obtained on the second step. The final thickness is equal to 1.285 g/cm<sup>2</sup>, which corresponds to 342 events per second of the <sup>232</sup>Rn<sup>84+84+</sup> ions without secondary reactions contribution (see Fig.177).

Actually the yield difference for thicknesses 1.01 and 1.28 g/cm<sup>2</sup> obtained respectively on the first and third steps is insignificant (see Fig.177), and moreover if we take the sum of all charge states then the value 1.1g/cm<sup>2</sup> is preferable. Due to this fact the user can skip the third step, using only the first two steps as was done for the “Rate & transmission calculation batch mode” utility (see the next chapter).

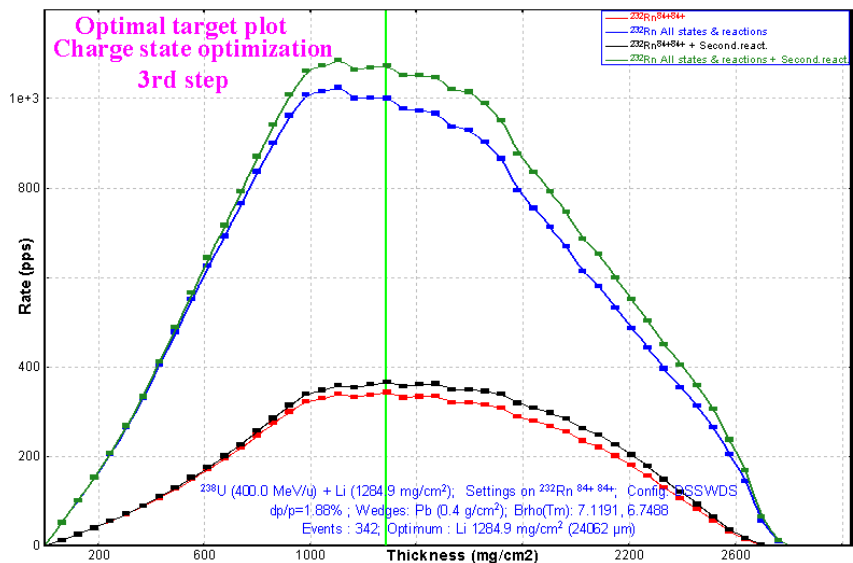


**Fig.177.** Optimal target thickness & Charge state optimization.

Step 3: calculation of fragment yield with charge states combination obtained on the second step.

### 6.3.1. Target optimization options

Several items connected with target optimization were moved from the “Preferences” dialog (the “Options” menu) into the new “Target optimization options” dialog (see Fig.178). This dialog is available in a few different places:

- ❑ The “Preferences” dialog (menu “Options”);
- ❑ The “Choose nucleus for Target optimization” dialog (see Fig.173) (menu “Calculations”);

- The “Rate & transmission calculation: batch mode” dialog (see Fig.180) (menu “Utilities”).

The new parameter “Method to search optimal target” has been incorporated into the code and can be changed in the “Target optimization options” dialog. The next chapter is devoted to this new parameter.

### 6.3.2. Optimal target searching methods

The plot of calculated yields as a function of target thickness is the result of the target optimization process. This plot contains four curves when taking into account secondary reactions’ contributions in yield calculations. The new version allows the user to choose what curve will be used to define the optimal target. Fig.179 shows calculated target yields as a function of target thickness. Vertical lines show maximum values of distributions. Depending on the choice of searching mode in the “Target optimization options” dialog (see Fig.178) the final answer can be any one of these four maxima.

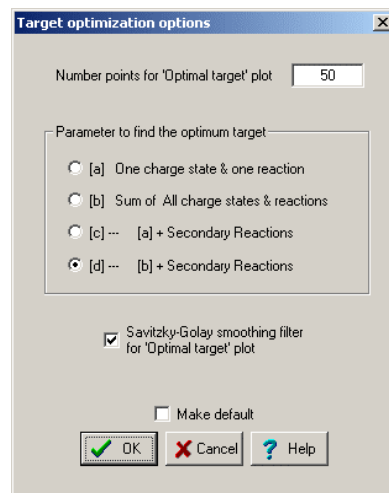


**Fig.178.** The “Target optimization options” dialog.

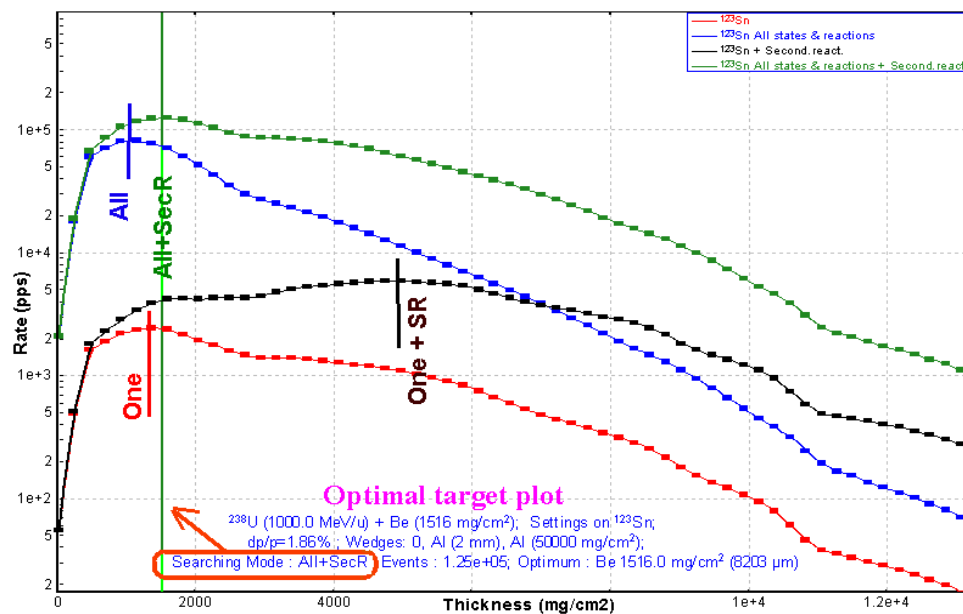


**Fig.179.** Calculated target yields as a function of target thickness for the production of  $^{123}\text{Sn}$  from fission of a  $^{238}\text{U}$  beam on a Be target. Short vertical lines show the maximum of each of the curves.

### 6.4. Rate & transmission calculation batch mode

The new utility “Rate & transmission batch mode” available via the “Utilities” menu has been incorporated into the code to run a long-term calculation task with different options. Using this utility, the user can obtain a text file with calculated parameters (optimum target thickness, best charge state combination, yield, transmission and secondary reactions contribution coefficients) for each fragment of a nuclide rectangle set in the “Rate & transmission batch mode” dialog (see Fig.180).

Before running the LISE++ code in the batch-mode it is necessary to:

1. set a nuclide rectangle choosing two opposite corners (see the “Calculation rectangle” frame in Fig.180);
2. choose options which will be applied in the calculation process for each fragment of the nuclide rectangle;
3. set the name of the file where information will be saved.

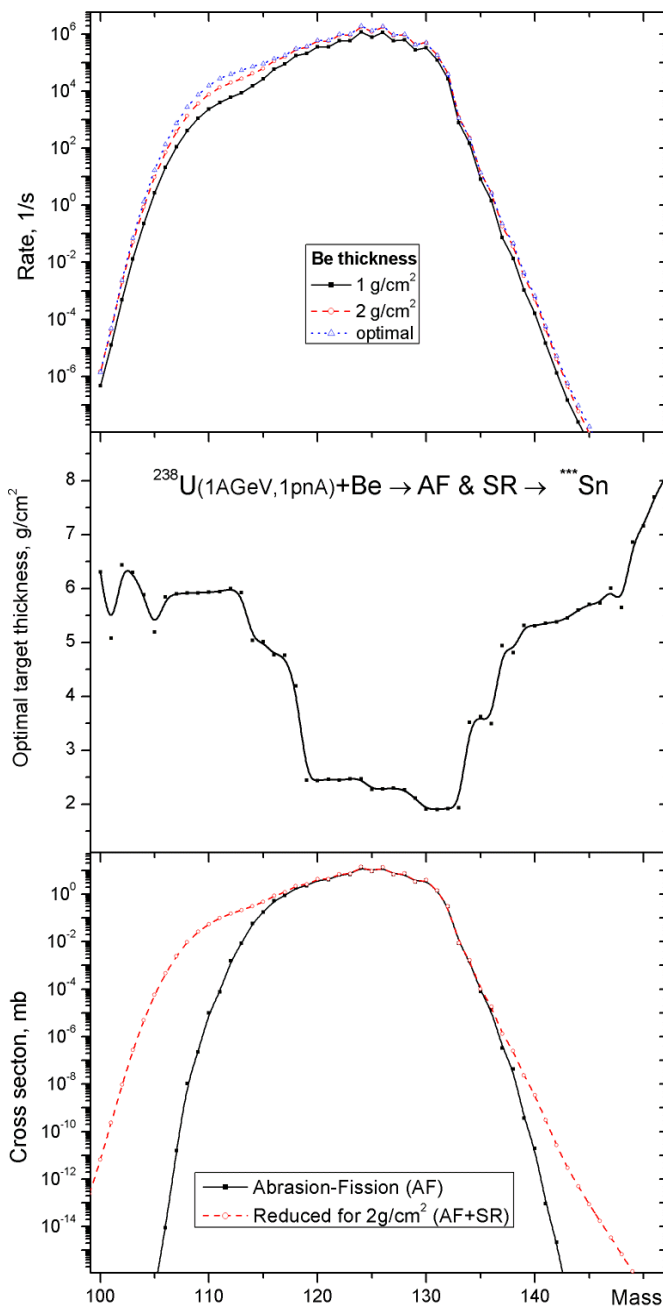


**Fig.181.** Top plot: Calculated rates of Tin isotopes produced in the fission of  $^{238}\text{U}(1\text{AGeV}, 1\text{pnA})$  on a Be-target taking into account secondary reactions' contributions. Calculations were done for target thickness equal to  $1\text{ g/cm}^2$ ,  $2\text{ g/cm}^2$ , and for optimal thickness calculated to obtain the maximum yield of given isotope (see the middle plot).

Bottom plot: Calculated AF and reduced cross-sections (assuming the thickness  $2\text{ g/cm}^2$ ) of Tin isotopes produced in the fission of  $^{238}\text{U}(1\text{AGeV}, 1\text{pnA})$  on a Be-target.

whereas increasing target thickness in the case of masses 119-133 leads to decreasing transmission. The example file [“AF 238U Be batch mode for Tin isotopes.lpp”](#) was used to prepare the plots in Fig.181.

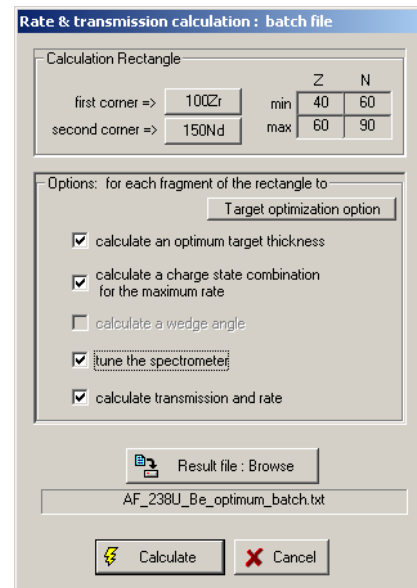


**Fig.180.** The “Rate & transmission calculation: batch mode” dialog.

This new utility allows one to calculate the optimal target thicknesses for a large region of nuclides, which would be tiresome if done manually using the “Optimal target” utility from the “Calculations” menu. Thus using the batch mode utility, the top and middle plots in Fig.181 have been created. An unexpected result was obtained for optimal target thicknesses to produce Tin isotopes in the fission of  $^{238}\text{U}(1\text{AGeV})$  on a Be-target (see the middle plot in Fig.181). For Tin isotopes with masses 119-133 the optimal target thickness is about  $2\text{ g/cm}^2$ , whereas for lighter and heavier isotopes the optimal target becomes considerably thicker. It is possible to explain this by looking at the bottom plot in Fig.181, which shows calculated AF and reduced cross-sections (assuming a thickness  $2\text{ g/cm}^2$ ) of Tin isotopes produced in the fission of  $^{238}\text{U}(1\text{AGeV})$  on a Be-target. The secondary reactions contribution dominates for the proton-rich side from mass about 117, and for the neutron-rich side from the mass about 135. If production of isotopes happens mostly from secondary reactions' contributions, then certainly we need to increase the target



## 6.5. Target and wedge optimization

The utility to determinate the optimum target and wedge combination has been incorporated into the new version. The user defines himself what is more important to him in the final result: intensity or purity through the use of weights. The utility is available in the “Calculations” menu.

Firstly, the user has to choose a fragment of interest as well as turning on/off the “charge state optimization” and “Secondary reactions contribution” options using the dialog shown in Fig.173.

The second step is setting the optimization process parameters in the “Target & wedge optimization” dialog (see Fig.182).

The “**Keep value**” combobox is initially set to “no keep value”. This means that settings of all optical blocks can be recalculated to provide the maximum transmission of the setting fragment. The user can choose to keep an optical dispersive block value for the transmission calculations. In this case other optical blocks settings will be recalculated for the setting fragment based on this kept value.

*Note:* If the “calculate the charge state combination” option has been turned on in the first step, then the “Keep value” combobox won’t be available.

The “**Wedge block**” combobox allows the user to select a wedge block whose thickness will be modified in the optimization process. The combobox is initially assigned to the enabled wedge block, which is the first one in the spectrometer line. If there are no enabled wedge blocks then this combobox is not available and neither are wedge thickness cells.

Target and wedge thickness ranges as well as number of thickness sets can be defined in the “**Material thickness**” block. The product of target and wedge set numbers defines how many times the code will change the spectrometer settings: target and wedge settings, and subsequent spectrometer tuning for the setting fragment. These changes can be seen in the “Setup” window during the optimization process.

When the user loads the “Target & Wedge optimization” dialog, the code calculates minimum and maximum thickness values automatically in the following way: the code calculates setting fragment and projectile ranges in the target in both cases suggesting an energy of the primary beam when taking into account the stripper thickness. The maximum range value ( $R_{max}$ ) is used to define minimum (5% of  $R_{max}$ ) and maximum (80% of  $R_{max}$ ) thickness for the optimization process. The wedge material is used instead of the target material to define the maximum range by the same way as was done for the target, but minimum and maximum values are defined in this case as (1% of  $R_{max}$ ) and (70% of  $R_{max}$ ) respectively. If you want to recalculate material range values manually at the next dialog loading then press the “**Calculate Max & Min values**” button.

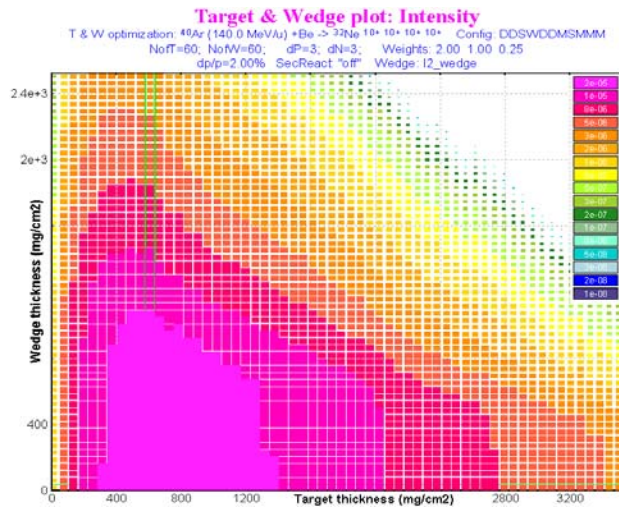
The “Isotope Rectangle for calculations” allows one to define how many nuclei  $N_{isotopes} = (2 \cdot dP + 1) \cdot (2 \cdot dN + 1)$  surrounding the fragment of interest will be included in transmission calculations. We define the **purity** value as equal to the ratio of the intensity of the setting fragment to the sum of all calculated isotope yields:

Fig.182. The “Target & Wedge optimization” dialog.

$$Purity(Z, N) = \frac{Rate(Z, N)}{Rate(Z_{beam}, N_{beam}) + \sum_{i=Z-dP}^{Z+dP} \sum_{k=N-dN}^{N+dN} Rate(i, k)} \quad /17/$$

A large area for the “Isotope rectangle” leads to more precise calculation of the purity value, but obviously takes more time. It is also recommended to calculate the primary beam transmission. This option is turned on by default.

After the user has defined the optimization parameters, the optimization process is started by clicking the “Make analysis” button. The optimization process can be canceled by pressing “Escape”. The information window shows approximately how much time is remaining (similar to Fig.164).



**Fig.183.** The “Target & Wedge **Intensity**” plot for  $^{32}\text{Ne}$  isotopes produced in  $^{40}\text{Ar}(140\text{AMeV})+\text{Be}$  and selected by the A1900 spectrometer with 2% momentum acceptance.

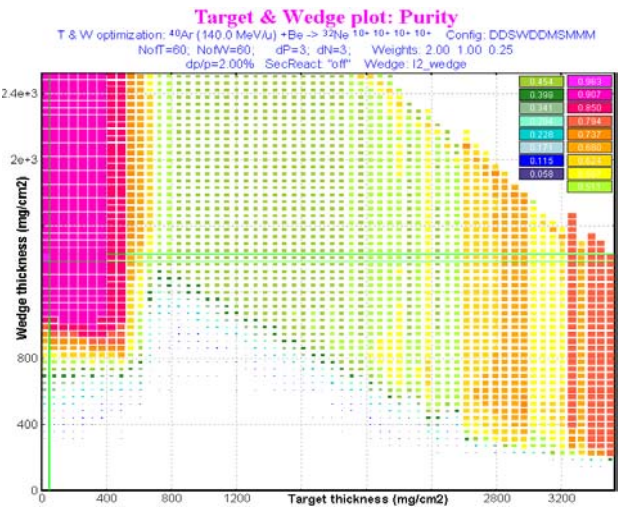


**Fig.184.** The “Target & Wedge **Purity**” plot for  $^{32}\text{Ne}$  isotopes produced in  $^{40}\text{Ar}(140\text{AMeV})+\text{Be}$ . The “Isotope rectangle” values were set to  $dP=3$  and  $dN=3$ .

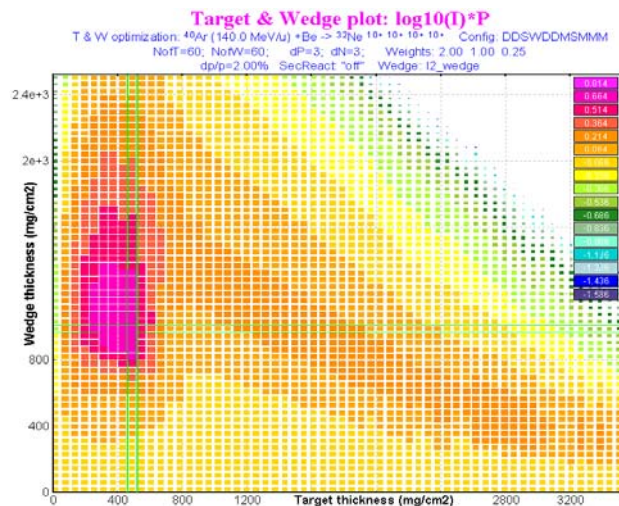


**Fig.185.** The “Target & Wedge **IP**” plot for the same optimization process as in Fig.183 and Fig.184.

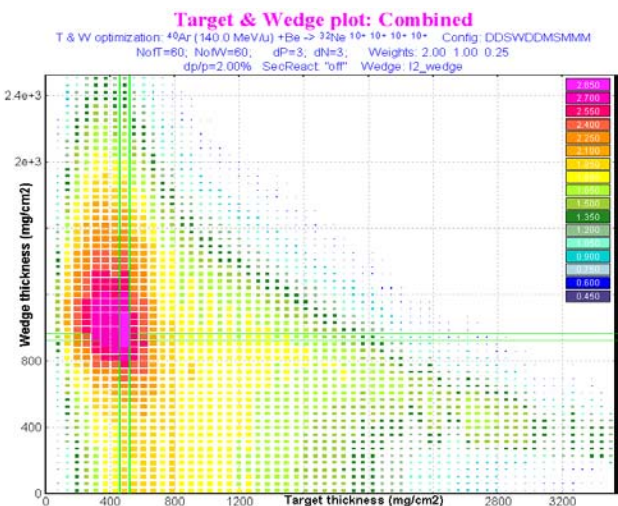


**Fig.186.** The “Target & Wedge **Combined**” plot. Weights are equal to 2, 1.5, 0.25 for Ir, P, and IP values.

Four plots (Intensity, Purity, IP, Combined) and one text file (the filename can be changed by the user using the “Browse” button) will be created and displayed for the user as a result of the optimization. The 1<sup>st</sup> plot “**Intensity**” shows the calculated  $Rate(Z,N)$  value from target and wedge thicknesses (Fig.183). The 2<sup>nd</sup> plot “**Purity**” (Fig.184) show calculated  $Purity(Z,N)$  values according to Eq./17/.

The program calculates 4 reduced values (*Ir*, *P*, *IP*, *Combined*) based on these two plots.

***Ir*** : intensity normalized reduced value. First we calculate the array of reduced values  $I_{it,iw} = \log_{10} [Rate(t_{ib}, w_{iw})]$ , where *t* is the target thickness value, *w* is the wedge thickness,  $it=1,2..N_{target}$ ,  $iw=1,2..N_{wedge}$ . The next step is normalization  $Ir_{it,iw} = I_{it,iw} / \max(I)$ .

***P*** : purity normalized value  $P_{it,iw} = \text{purity}_{it,iw} / \max(\text{purity})$ .

***IP***: product of *Ir* and *P* values. As the product of two normalized values, any *IP* array element cannot be more than 1. The *IP* value plot is the third optimization result plot (see Fig.185).

***Combined*** : sum of products *Ir*, *P* and *IP* values with their weights (*WI*, *WP*, *WIP*):

$$Combined = Ir \cdot WI + P \cdot WP + IP \cdot WIP, \quad /18/$$

where weight values should be defined by the user in the “Target & wedge optimization” dialog (see Fig.182) before optimization. The ***Combined*** value plot is the fourth optimization result plot (see Fig.186). Combined values cannot be more than the sum of weights (*WI*, *WP*, *WIP*).

The green horizontal and vertical lines on plots show the maximum value included in this plot.

The text file contains information about calculated intensity, purity and all reduced values for each target & wedge combination used in the optimization process (see Fig.187). Information about a maximum value for each plot and their location (target and wedge thicknesses) are shown at the bottom of this file (see Table 25 and Table 26). This output statistics file can be used by other programs (for example Excel or Origin) for subsequent analysis.

**Fig.187.** LISE window showing the output statistics file containing the optimization process protocol and statistics information.

**Table 25.** Maximum values for each plot (Fig.183, Fig.184, Fig.185, Fig.186) and their location (target and wedge thicknesses). All this information is kept at the bottom of the output statistics file (see Fig.187).

Plot	Maximum value	Target (mg/cm <sup>2</sup> )	Wedge (mg/cm <sup>2</sup> )
Intensity	2.726e-05	6.098e+02	2.000e+01
Purity	9.633e-01	2.000e+01	1.407e+03
IP	7.974e-01	4.919e+02	9.868e+02
Combined	2.896e+00	4.919e+02	9.447e+02

**Table 26.** Intensity, Purity, and IP values corresponding to target and wedge thickness values when the Combined value reaches the maximum.

Model	Combined
Intensity	2.260e-05
Purity	8.295e-01
IP	7.911e-01

**Recommendations:**

Before the optimization process it is recommended to set wedge angle close to the value which corresponds to the optimal wedge thickness value (or use curved profile degrader – the best choice!)

Set “wedge selection” slits (I4 for A1900 for example) to a value corresponding to 95% of the wedge selection transmission for the optimal target and wedge combination.

If you do not know at least approximately these values then run the optimization process twice:

- run the first time with small  $N_{target}$  and  $N_{wedge}$ ,



- then set wedge angle and slits using calculated target and wedge combination using the combined plot,
- increase  $N_{target}$  and  $N_{wedge}$ ,
- narrow the target and wedge thickness regions around the expected location of the optimum combination,
- run the optimization process again.

### 6.5.1. Secondary Reactions contribution option

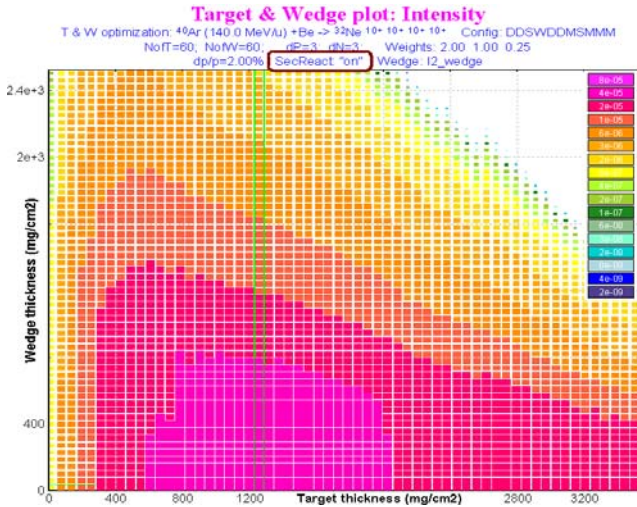


**Fig.188.** The “Target & Wedge Intensity” plot the same as Fig.183 but with SR contributions.

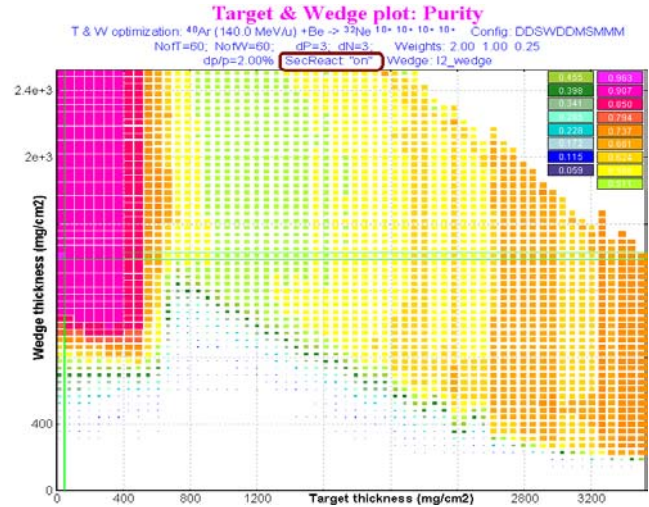


**Fig.189.** The “Target & Wedge Purity” plot the same as Fig.184 but with SR contributions.

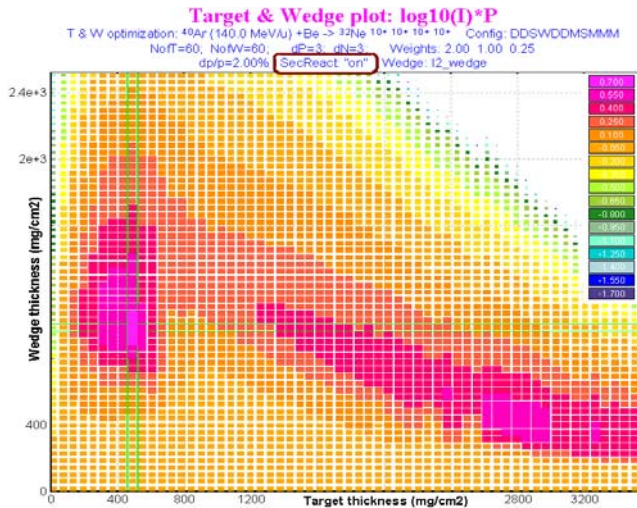


**Fig.190.** The “Target & Wedge IP” the same as Fig.185 but with SR contributions.

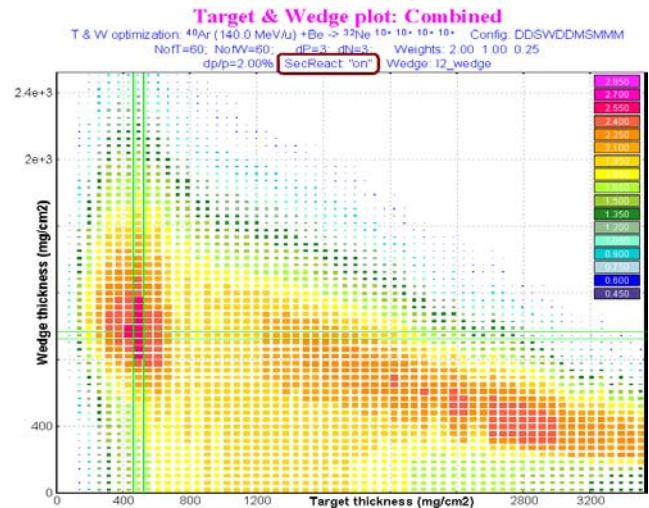


**Fig.191.** The “Target & Wedge Combined” plot the same as Fig.186 but with SR contributions.

Fig.188-191 show result plots for the same settings which were used in the previous chapter for the  $^{32}\text{Ne}$  optimization process but in this case including the secondary reactions contribution. Compare these plots with Fig.183-186. Statistics information for the optimization process with SR contribution is shown in Table 27 and Table 28. Compare this information with data in Table 25 and Table 26.

**Table 27.** Maximum values for each plot (Fig.188-191) and their location (target and wedge thicknesses).

Plot	Maximum value	Target (mg/cm <sup>2</sup> )	Wedge (mg/cm <sup>2</sup> )
Intensity	4.895e-05	1.259e+03	2.000e+01
Purity	9.633e-01	2.000e+01	1.407e+03
IP	7.171e-01	4.919e+02	9.868e+02
Combined	2.686e+00	4.919e+02	9.447e+02

**Table 28.** Values corresponding to the maximum Combined value.

Model	Combined
Intensity	3.202e-05
Purity	8.433e-01
IP	7.142e-01

### 6.5.2. “Keep value” parameter

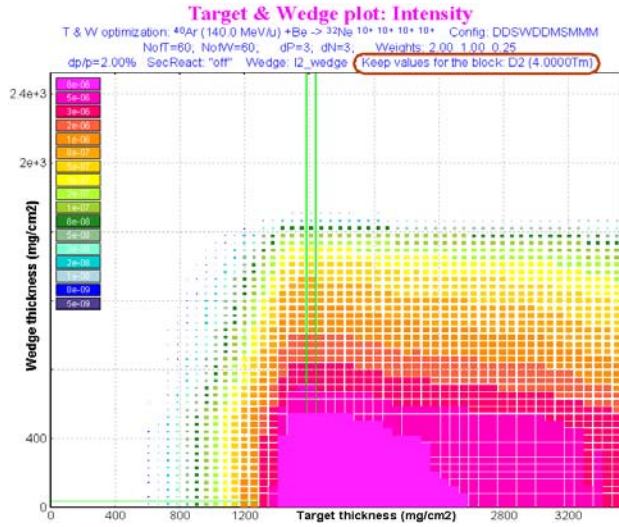


Fig.192. The “Target & Wedge Intensity” plot the same as Fig.183 but the second dipole value was kept equal to 4.0 Tm.

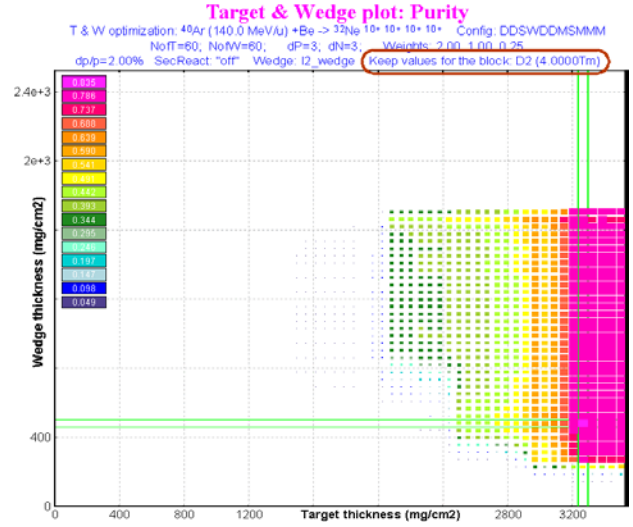


Fig.193. The “Target & Wedge Purity” plot the same as Fig.184 but the second dipole value was kept equal to 4.0 Tm.

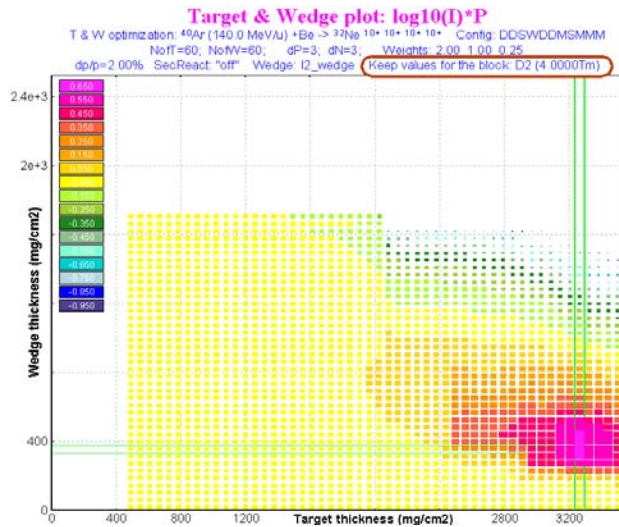


Fig.194. The “Target & Wedge IP” the same as Fig.185 but the second dipole value was kept equal to 4.0 Tm.

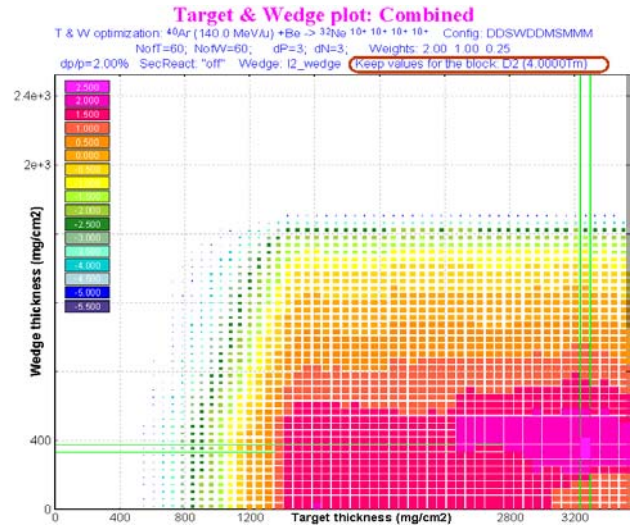


Fig.195. The “Target & Wedge Combined” plot the same as Fig.186 but the second dipole value was kept equal to 4.0 Tm.

Fig.192-195 show result plots for the same settings which were used for Fig.183-186 but in this case the second dipole value was kept equal to 4.0 Tm. Compare these plots with Fig.183-186. Statistics information for the optimization process with SR contribution is shown in Table 29 and Table 30. Compare this information with data in Table 25 and Table 26.

Table 29. Maximum values for each plot (Fig.192-195) and their location (target and wedge thicknesses).

Plot	Maximum value	Target (mg/cm <sup>2</sup> )	Wedge (mg/cm <sup>2</sup> )
Intensity	1.166e-05	1.613e+03	2.000e+01
Purity	8.353e-01	3.264e+03	4.824e+02
IP	6.669e-01	3.264e+03	3.563e+02
Combined	2.507e+00	3.264e+03	3.563e+02

Table 30. Values corresponding to the maximum Combined value.

Model	Combined
Intensity	5.567e-06
Purity	8.205e-01
IP	6.669e-01

Note: The “Charge state optimization” and the “keep value” options cannot be used simultaneously in the target & wedge optimization process.



### 6.5.3. Target and wedge optimization for charge states

In this chapter we shall calculate the target-wedge combination for the  $^{208}\text{Pb}$  (100 MeV/u) + Au  $\rightarrow$   $^{196}\text{Os}$  reaction considering three different situation:

- without charge states;
- the separator is tuned to only one charge state combination (fully stripped);
- with spectrometer tuned to the charge state combination giving maximum yield of the setting fragment.

Now we shall analyze all three cases. The A1900 fragment separator ( $\Delta p/p=2\%$ ) and the achromatic curved profile Be-degrader will be used to determine the optimum target-wedge combination.

#### 6.5.3.1. No charge states

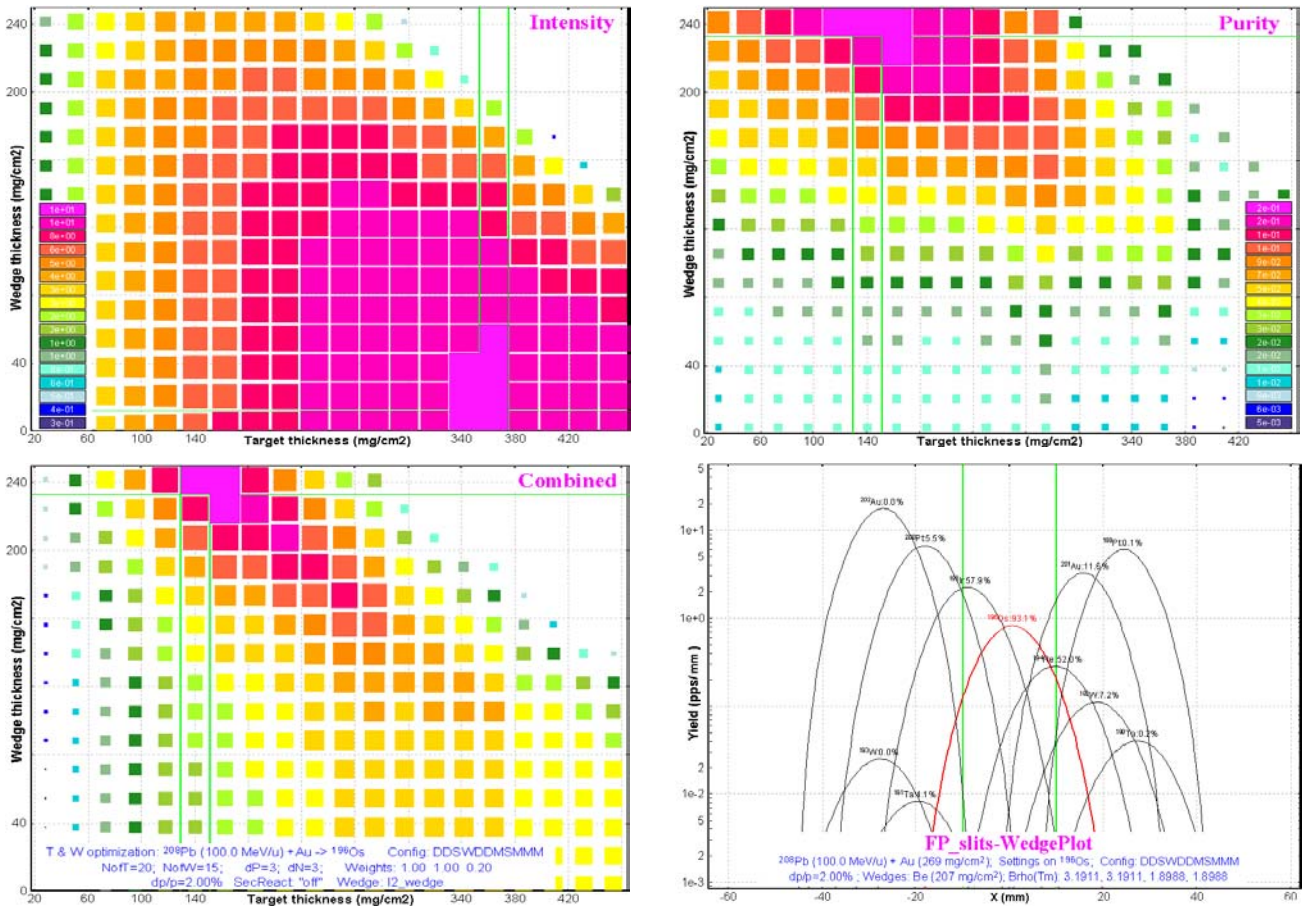


**Fig.196.** The Intensity (left top), Purity (right top), and Combined (left bottom) target-wedge optimization plots for the  $^{208}\text{Pb}(100\text{ MeV/u}) + \text{Au} \rightarrow ^{196}\text{Os}$  reaction assuming no charge states are included. The wedge selection plot (right bottom) shows spatial distributions of separated fragments at the end of the spectrometer. Calculations were done for target and wedge thicknesses equal to 269 and 207 mg/cm<sup>2</sup> respectively. Plot statistics are given in Table 31 and Table 32.

**Table 31.** Maximum values for the target-wedge optimization plots on Fig.196 and their location (target and wedge thicknesses).

Plot	Maximum value	Target (mg/cm <sup>2</sup> )	Wedge (mg/cm <sup>2</sup> )
Intensity	1.308e+01	3.644e+02	3.440e+00
Purity	2.697e-01	1.403e+02	2.410e+02
IP	5.579e-01	1.627e+02	2.240e+02
Combined	1.649e+00	1.403e+02	2.410e+02

**Table 32.** Values corresponding to the maximum Combined value.

Model	Combined
Intensity	4.542e+00
Purity	2.697e-01
IP	5.407e-01

### 6.5.3.2. Spectrometer tuned to only one charge state combination

The target-wedge optimization plots in the case of the spectrometer tuned to fully stripped ions are shown in Fig.197. On the Intensity plot (Fig.197) it is possible to see the second island of maximum values in the region: target thickness is about 140-240 mg/cm<sup>2</sup> and 120-160 mg/cm<sup>2</sup> for wedge thickness. This island corresponds to transmission of ions with charge state 75+75+74+74+ even though the spectrometer is tuned to fully stripped ions. Transmission of fully stripped ions in this thickness region is equal to zero.

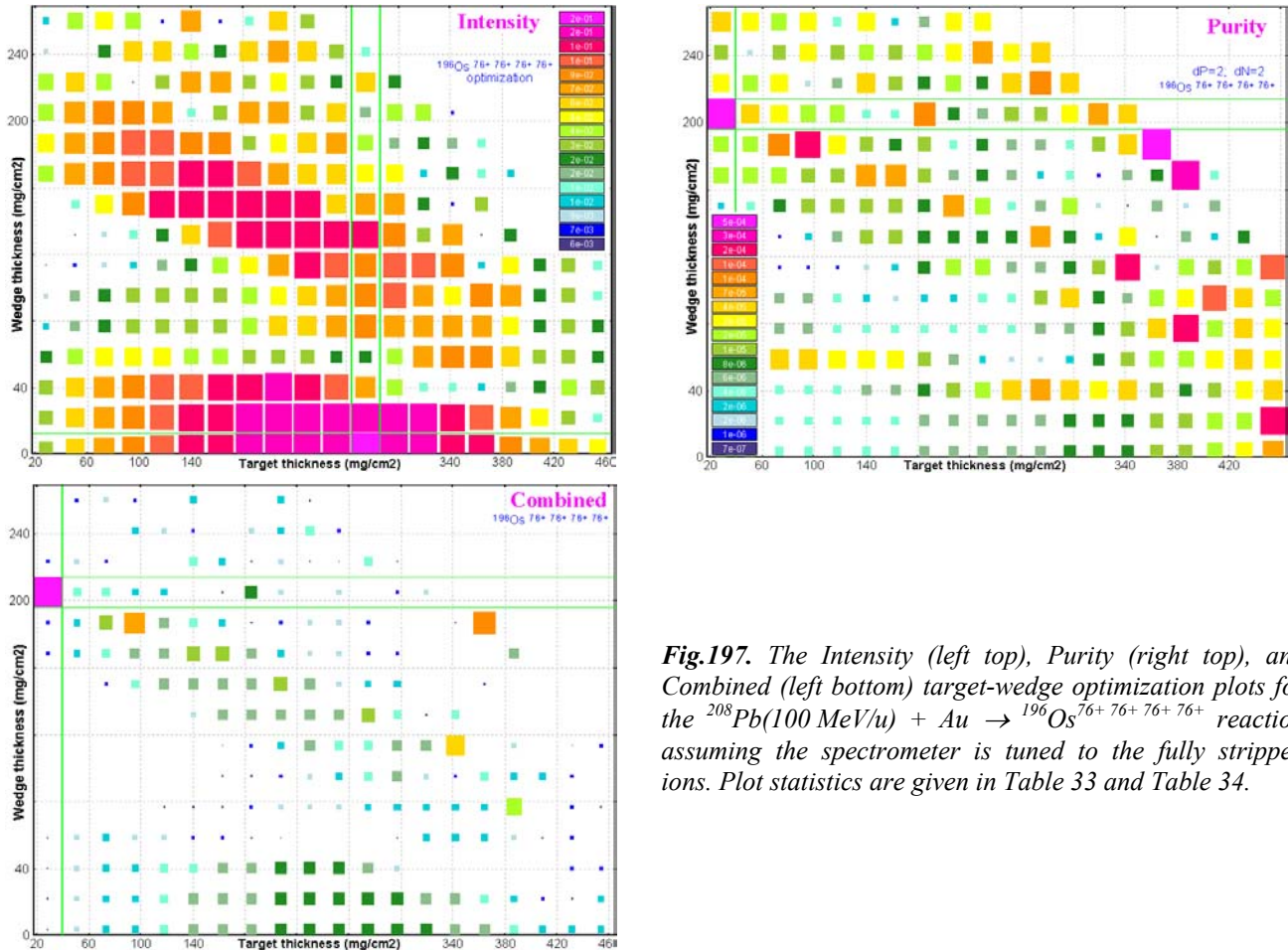


**Fig.197.** The Intensity (left top), Purity (right top), and Combined (left bottom) target-wedge optimization plots for the  $^{208}\text{Pb}(100\text{ MeV}/u) + \text{Au} \rightarrow ^{196}\text{Os}^{76+76+76+76+}$  reaction assuming the spectrometer is tuned to the fully stripped ions. Plot statistics are given in Table 33 and Table 34.

Such sharp peaks on the Purity plot (Fig.197) are explained by the very small yield of the isotope of interest (0.001-0.01%) in contrast to background and also by the small area ( $dN=2$ ,  $dP=2$ ) taken for the background calculation. As soon as yield of more intense neighbor background isotope decreases due to momentum or “wedge” selections, the setting fragment purity increases sharply. The picture will be smoothed by increasing the isotope rectangle size (for example  $dN=4$ ,  $dP=4$ ). Such a small size of the isotope rectangle is made desirable by the time spent on the optimization. So for your general information, the calculations take about 7-11 hours for this reaction with the charge state option turned on, the rectangle size equal to ( $dN=2$ ,  $dP=2$ ) and target and wedge thickness steps both equal to 20.

**Table 33.** Maximum values for each plot on Fig.197 and their location (target and wedge thicknesses).

Plot	Maximum value	Target (mg/cm <sup>2</sup> )	Wedge (mg/cm <sup>2</sup> )
Intensity	2.313e-01	2.748e+02	3.440e+00
Purity	6.046e-04	2.830e+01	2.050e+02
IP	3.182e-01	9.552e+01	1.867e+02
Combined	3.549e+00	2.830e+01	2.050e+02

**Table 34.** Values corresponding to the maximum Combined value.

Model	Combined
Intensity	4.350e-02
Purity	6.046e-04
IP	2.744e-01



### 6.5.3.3. Optimization of the charge state combination

The target-wedge optimization plots in the case of tuning the spectrometer on the best charge state combination to produce a maximum yield of the fragment of interest are shown in Fig.198. The best charge state combinations for different target and wedge thicknesses are shown in the Combined plot (Fig.198).

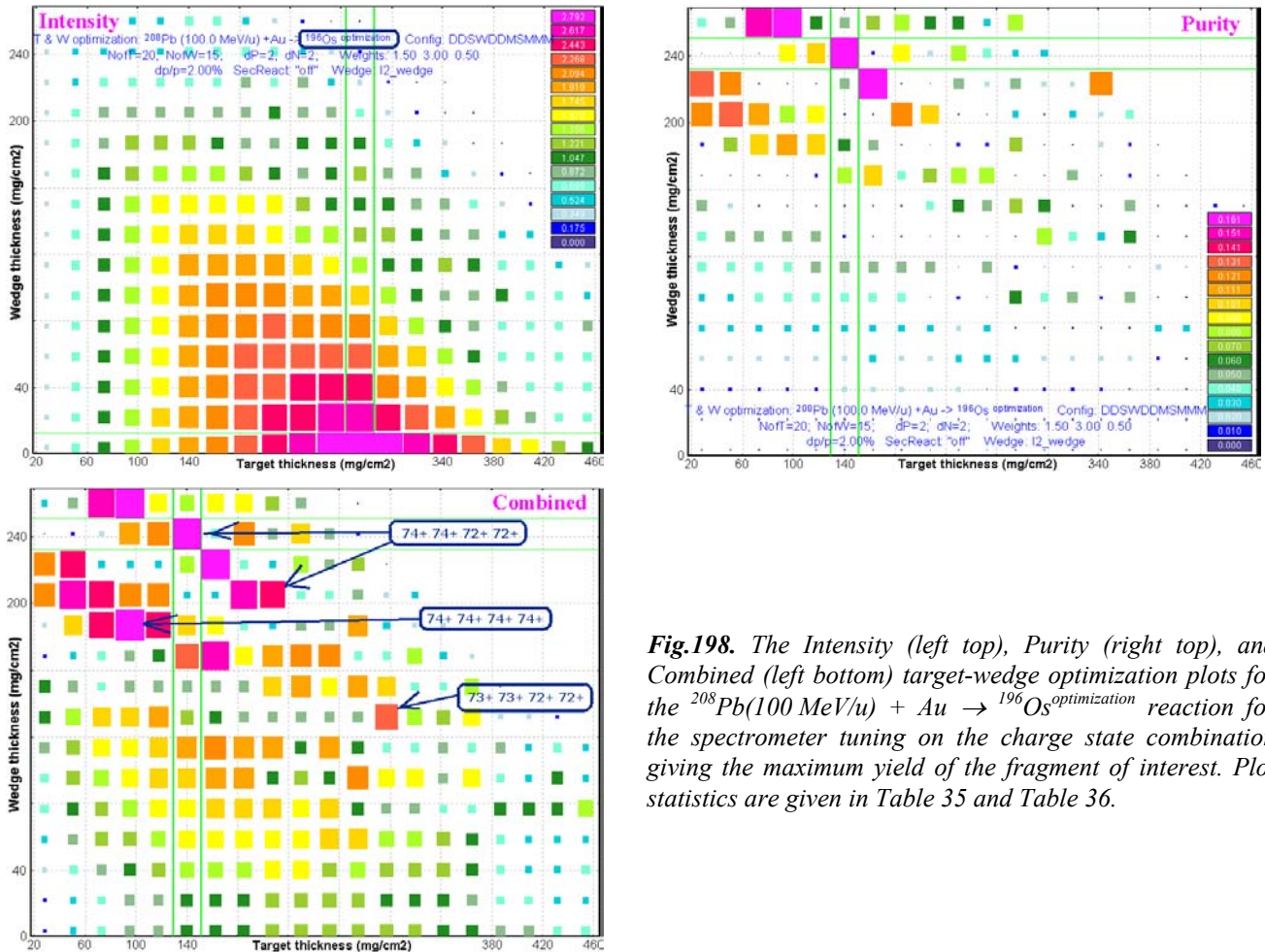


**Fig.198.** The Intensity (left top), Purity (right top), and Combined (left bottom) target-wedge optimization plots for the  $^{208}\text{Pb}(100\text{ MeV}/u) + \text{Au} \rightarrow ^{196}\text{Os}$  optimization reaction for the spectrometer tuning on the charge state combination giving the maximum yield of the fragment of interest. Plot statistics are given in Table 35 and Table 36.

Sharp peaks in the Purity plot have the same nature (very small purity and small isotope rectangle size) as in the previous section devoted to the spectrometer tuned to just one charge state.

**Table 35.** Plot maximum values on Fig.198 and their location (target and wedge thicknesses).

Plot	Maximum value	Target (mg/cm <sup>2</sup> )	Wedge (mg/cm <sup>2</sup> )
Intensity	2.966e+00	2.748e+02	3.440e+00
Purity	1.709e-01	1.403e+02	2.417e+02
IP	4.416e-01	1.627e+02	2.233e+02
Combined	3.857e+00	1.403e+02	2.417e+02

**Table 36.** Values corresponding to the maximum Combined value.

Model	Combined
Intensity	7.959e-01
Purity	1.709e-01
IP	4.286e-01

### 6.5.3.4. Results

It should be noted that the target and wedge thickness values calculated for the combined plot in the case charge state optimization are exactly the same as those produced for the case without charge states (see Table 37). These cells are selected by yellow background color.

**Table 37.** Combined plot statistics from Tables 31-36 and Fig.199.

Method	No charge states	One charge state	Charge state optimization	Charge state optimization*	Charge state optimization** (Fig.199)
Isotope rectangle ( $\pm dN, \pm dP$ )	3, 3	2, 2	<b>2, 2</b>	<b>4, 4</b>	<b>5, 5</b>
Target (mg/cm <sup>2</sup> )	<b>140.3</b>	28.3	<b>140.3</b>	112.9	158.3
Wedge (mg/cm <sup>2</sup> )	<b>241.0</b>	205.0	<b>241.7</b>	248.9	220.5
Intensity	4.542e+00	4.350e-02	7.959e-01	5.054e-1	6.79e-1
Purity	0.270	6.046e-04	0.171	0.0468	0.02605
IP	5.41e-01	2.74e-01	4.29e-01	5.04e-01	8.62e-01

\* Target range: 70-220 mg/cm<sup>2</sup>, *NofT*=15; Wedge range: 160-260 mg/cm<sup>2</sup>, *NofW*=10; Weights: 1, 1, 0.2.

\*\* Target range: 100-200 mg/cm<sup>2</sup>, *NofT*=25; Wedge range: 210-260 mg/cm<sup>2</sup>, *NofW*=20; Weights: 2, 1, 0.2. See results in Fig.199.

**Recommendation:**

By analogy with the one-dimensional case (see chapter 6.3. Charge state combination calculation for the optimal target thickness utility) in order to decrease target-wedge optimization time for the case of optimum charge state combination calculations it is recommended to do the following:

- Find the best target-wedge combination without charge states;
- Turn on the charge state option (The “Preference” dialog);
- Check on the “Charge state optimization” checkbox (see Fig.173);
- Set the target and wedge search area with the center obtained in the step without charge states;
- Reduce the target and wedge search area. For example if the previous thickness range was 100 – 3000 mg/cm<sup>2</sup> at 30 steps (*NofT* or *NofW*), and the thickness value from the optimization without charge states was 1700 mg/cm<sup>2</sup>, then set the range 1500 – 1900 mg/cm<sup>2</sup> at 9 steps;
- Make *dN* and *dP* large enough to avoid the “sharp peak” effect in the case of low purity of the fragment of interest;
- Increase the “Intensity” weight in the case of “sharp” peaks to decrease their influence on the combined plot.

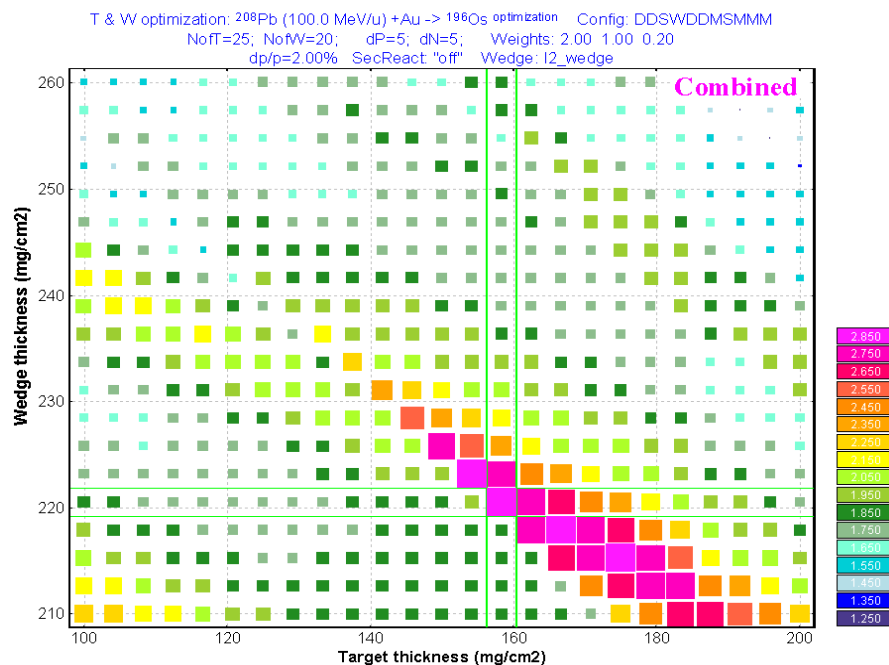


**Fig.199.** The Combined target-wedge optimization plot for the <sup>208</sup>Pb(100 MeV/u) + Au → <sup>196</sup>Os optimization reaction for the spectrometer tuned to the charge state combination giving the maximum yield of the fragment of interest. Plot statistics are given in Table 37.

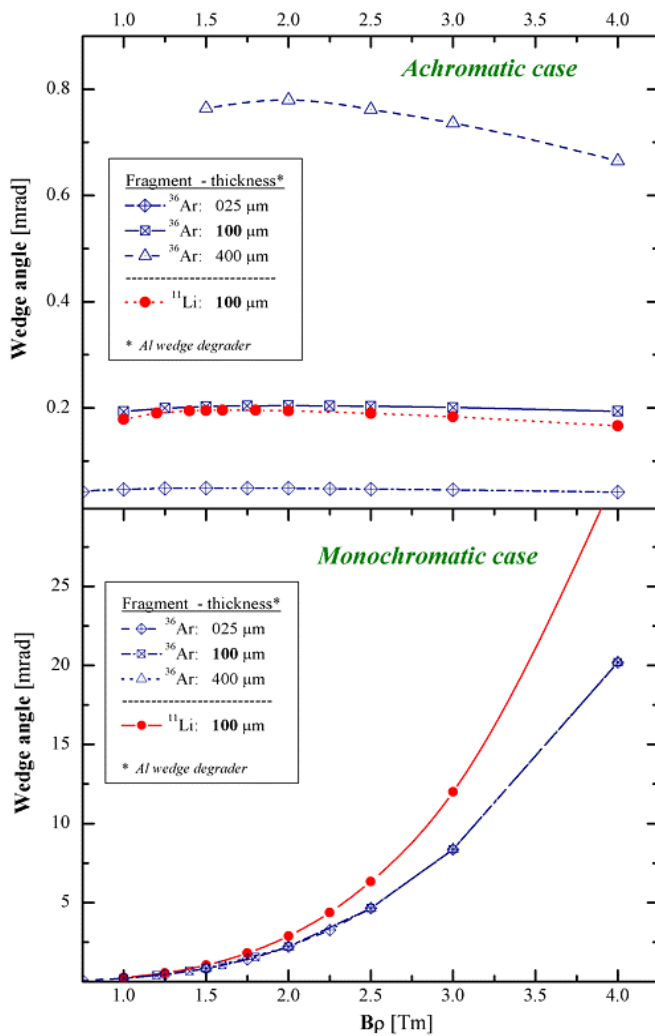
The following parameters were used for calculations:  
 Target range: 100-200 mg/cm<sup>2</sup>, *NofT*=25;  
 Wedge range: 210-260 mg/cm<sup>2</sup>, *NofW*=20;  
 Weights: 2, 1, 0.2

### 6.5.4. Wedge-shape and curved profile degraders properties

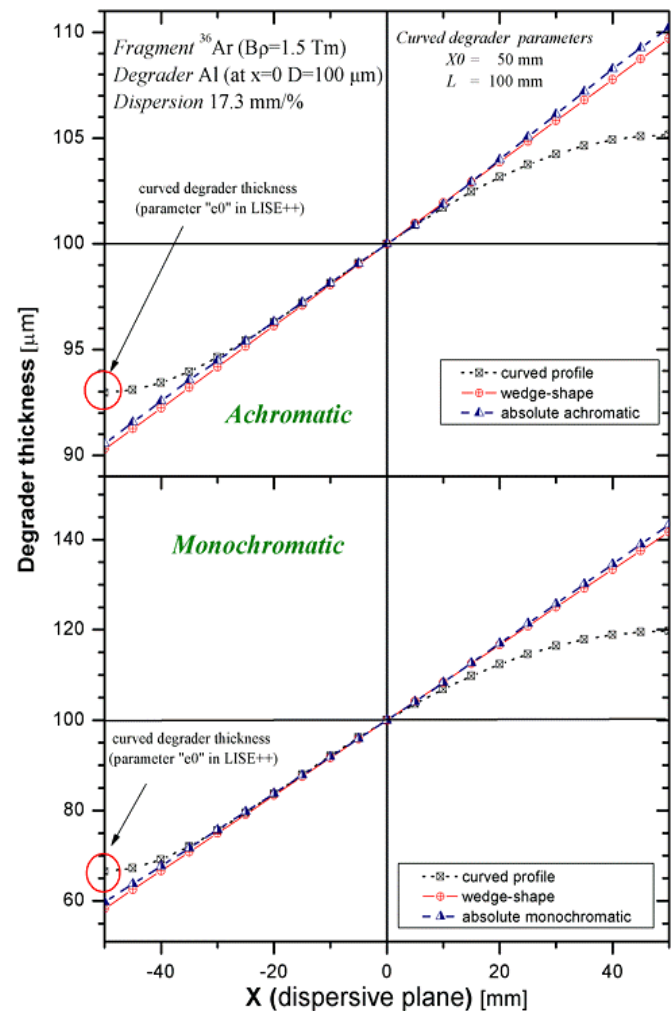
We need an analysis of wedge-shape and curved profile degraders properties to know what kind of degrader can be used in the dispersive focal plane for the “Optimum target” and the “Optimum target and wedge” utilities because, for example, the user may wish to have an achromatic focus at the end of spectrometer independently from the target or wedge thickness. Must we recalculate a wedge angle on each calculation step? Or will achromatic properties be retained if we change the target thickness?

Fig.200 shows the angle of several wedge-shape Al-degraders as a function of magnetic rigidity for isotopes of  $^{36}\text{Ar}$  and  $^{11}\text{Li}$  in the achromatic and monochromatic modes. From this figure **it is possible to conclude** the following for the **achromatic mode**:

- The angle of achromatic wedge is mostly a function of a degrader thickness and a momentum dispersion;
- The angle of wedge-shape degrader **does not change** much for a fixed degrader thickness for different energies and different isotopes;
- This means that **it is possible to keep one angle value** (calculated just once to be achromatic at one point) for all calculation steps in the “Optimal target” utility in the achromatic mode thus saving all achromatic properties.



**Fig.200.** The angle of several wedge-shape Al-degraders as a function of magnetic rigidity for isotopes of  $^{36}\text{Ar}$  and  $^{11}\text{Li}$  in the achromatic mode on the top plot and the monochromatic mode accordingly on the bottom one. The momentum dispersion in the wedge position is equal to 17.3 mm/%.



**Fig.201.** The effective thickness of degraders in the dispersive focal plane as a function of a horizontal coordinate in the achromatic mode on the top plot and the monochromatic mode accordingly on the bottom one. Calculations were done for the  $^{36}\text{Ar}$  fragment at  $B\rho = 1.5 \text{ Tm}$ .

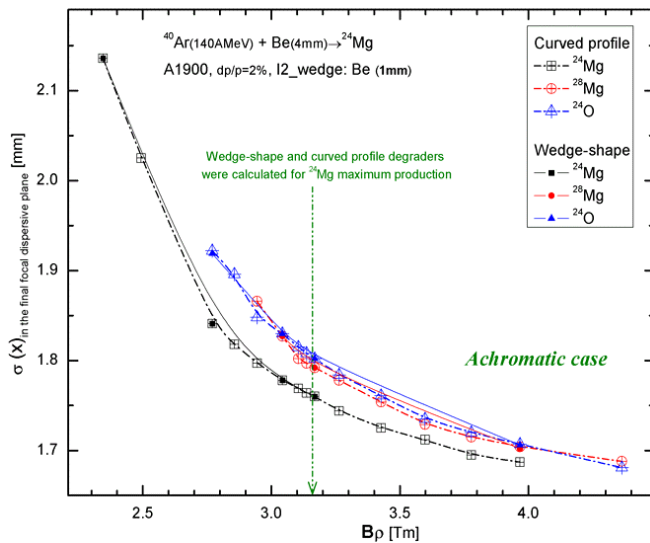


It is possible to conclude the following from Fig.200 for the **monochromatic mode**:

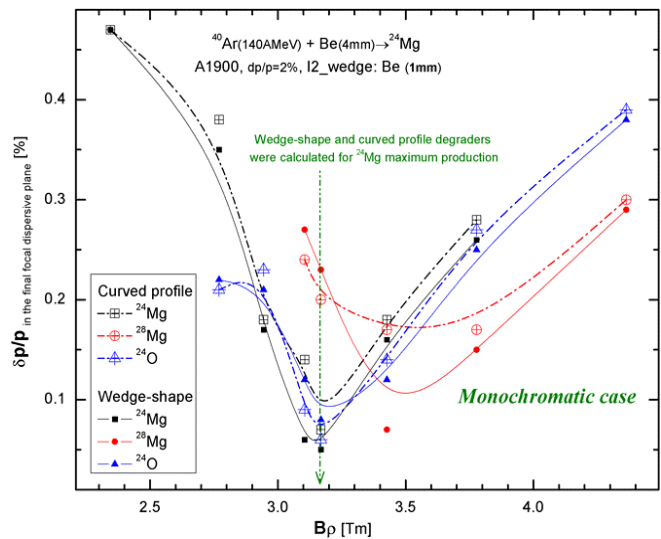
- The angle of wedge-shape degrader **does not change** much for other degrader thicknesses;
- The angle of monochromatic wedge mostly is a **function of a fragment and its energy**;
- This means that it is **not possible to keep one angle value** for all calculation steps in the **“Optimal target” utility in the monochromatic mode** while keeping all monochromatic properties.

Fig.201 shows the effective thickness of degraders in the dispersive focal plane as a function of a horizontal coordinate in the achromatic and monochromatic modes. From plots on this figure it is possible to make two statements:

- The wedge-shape degrader is more close to absolute achromatic (monochromatic) degrader than the curved profile degrader. This is an evident advantage of wedge-shape degraders over the curved profile degrader.
- **Edge aberrations in Curved Profile Degraders:** To avoid large deviations from the ideal achromatic (monochromatic) degrader on the wings of the curved profile degrader (CPD) it is necessary to build the CPD on a long base. For example if momentum slit size is  $\pm 20$  mm, than the CPD base (parameter  $L$ ) should be 2-3 times longer and equal to 80-120 mm.



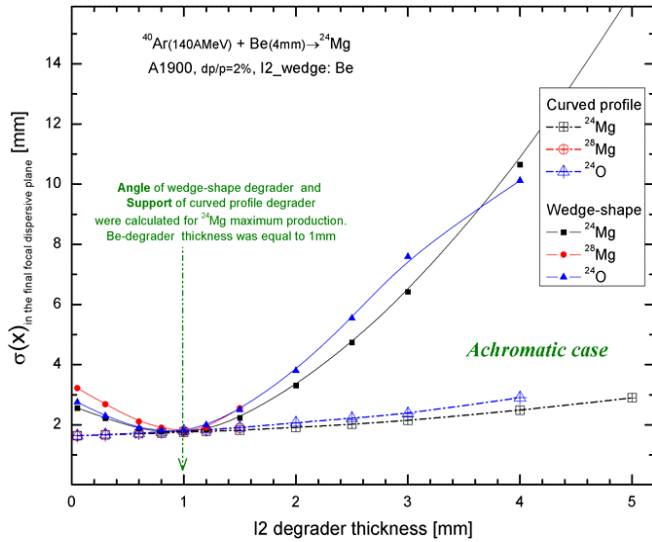
**Fig.202.** The  $^{24,28}\text{Mg}$ , and  $^{24}\text{O}$  fragment spot sizes in the final focal plane of the A1900 spectrometer for the wedge-shape and curved profile Be-degraders (1mm) as a function of magnetic rigidity. The wedge-shape angle and curved profile support were calculated for the **achromatic** mode at the  $B\rho$ -value corresponding to  $^{24}\text{Mg}$  maximum production.



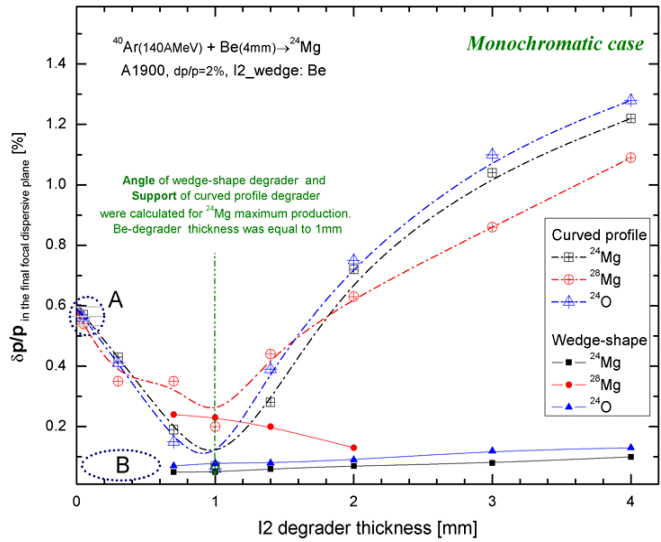
**Fig.203.** The  $^{24,28}\text{Mg}$ , and  $^{24}\text{O}$  fragment momentum widths in the final focal plane of the A1900 spectrometer for the wedge-shape and curved profile Be-degraders (1mm) as a function of magnetic rigidity. The wedge-shape angle and curved profile support were calculated for the **monochromatic** mode at the  $B\rho$ -value corresponding to  $^{24}\text{Mg}$  maximum production.

Fig.202 and Fig.203 show the  $^{24,28}\text{Mg}$ , and  $^{24}\text{O}$  fragment spot sizes (achromatic mode) and momentum widths (monochromatic mode) respectively in the final focal plane of the A1900 spectrometer for the wedge-shape and curved profile Be-degraders (1mm) as a function of magnetic rigidity. It is visible from Fig.202 that calculation results for both types of degrader are identical at magnetic rigidity values of 2.5-5 Tm. At the same time from Fig.203 it is visible, that the monochromatic effect is lost with changes of the magnetic rigidity value. Therefore, as for wedge-shape degrader, we can conclude the following for CPD:

- it is **possible to keep one curved profile support** (calculated just once to be achromatic in one point) for all calculation steps in the **“Optimal target” utility** in the **achromatic mode**, thus saving all achromatic properties;
- It is **not possible to keep one curved profile support** for all calculation steps in the **“Optimal target” utility** in the **monochromatic mode**.
- It is necessary to note that the **momentum width** in the case of using **wedge-shape degrader** in the monochromatic mode is **better** than in the case of the CPD (see Fig.203); this is explained by CPD edge aberrations.



**Fig.204.** The  $^{24,28}\text{Mg}$ , and  $^{24}\text{O}$  fragment spot sizes in the final focal plane of the A1900 spectrometer for the wedge-shape and curved profile Be-degraders (1mm) as a function of degrader thickness. The wedge-shape angle and curved profile support were calculated **ONCE** for the **achromatic** mode at the  $B\rho$ -value corresponding to  $^{24}\text{Mg}$  maximum production and were used for all degrader thickness points.



**Fig.205.** The  $^{24,28}\text{Mg}$ , and  $^{24}\text{O}$  fragment momentum widths in the final focal plane of the A1900 spectrometer for the wedge-shape and curved profile Be-degraders (1mm) as a function of degrader thickness. The wedge-shape angle and curved profile support were calculated **ONCE** for the **monochromatic** mode at the  $B\rho$ -value corresponding to  $^{24}\text{Mg}$  maximum production and were used for all degrader thickness points.

Fig.204 and Fig.205 show  $^{24,28}\text{Mg}$ , and  $^{24}\text{O}$  fragment spot sizes (achromatic mode) and momentum resolutions (monochromatic mode) respectively in the final focal plane of the A1900 spectrometer for the wedge-shape and curved profile Be-degraders as a function of degrader thickness. Wedge-shape angles and curved profile supports for both figures were calculated **ONCE** at the  $B\rho$ -value corresponding to  $^{24}\text{Mg}$  maximum production and were used for all degrader thickness points. It is visible from Fig.204 that the CPD keeps its achromatic properties at change of degrader thickness for one curved profile support, whereas the wedge-shape degrader on the contrary does not keep them if changing degrader thickness and keeping the wedge angle. For the monochromatic case the situation is changed: the wedge-shape degrader saves monochromatic properties at change of degrader thickness, and the CPT does not. Therefore it is possible to conclude based on that said above:

- It is **not possible to keep one angle value**<sup>▼</sup> (calculated just once to be achromatic in one point) and it is **possible to keep one curved profile support** for all calculation steps in the **“Optimal target & wedge” utility** in the **achromatic mode** thus saving all achromatic properties.
- It is **not possible to keep one angle value**<sup>♦</sup> and **one curved profile support** for all calculation steps in the **“Optimal target & wedge” utility** in the **monochromatic mode**.

**Recommendation:** use the curved profile degrader for the “Optimal Target and Wedge” utility!

<sup>▼</sup> For details see the analysis for wedge-shape degrader in chapter 6.5.5.1. Acceptance.

<sup>♦</sup> But it is possible to use a wedge-shape degrader for the monochromatic mode if the “keep value” parameter is on, or by other words the fragment energy before the wedge is constant for all calculation steps.

### 6.5.5. Setting discussions

In this chapter we shall analyze an influence of momentum acceptance, “wedge selection” slits, type of degrader (CPD and wedge-shape), and fragment nature (using as examples isobars A=32) on the optimum target and wedge combination for the  $^{40}\text{Ar}(140\text{MeV/u})+\text{Be}$  reaction using the A1900 fragment separator. The following parameter designations are used in figures in this chapter:

*Table 38. Parameter designations for figures in this chapter.*

1D-plot	Designation for 1D-plots	Origin 2D plot	Description of parameter
<b>Y-axis</b>	<b>Parameter</b>		
Intensity	I_max	Intensity	Maximum intensity value
	CB_intensity	Combined	Intensity corresponding to the largest Combined value
	P_intensity	Purity	Intensity corresponding to P_max
Purity	P_max	Purity	Maximum purity value
	CB_purity	Combined	Purity corresponding to the largest Combined value
	I_purity	Intensity	Purity corresponding to I_max
Thickness	I_target	Intensity	Target thickness corresponding to I_max
	I_wedge	Intensity	Wedge thickness corresponding to I_max
	P_target	Purity	Target thickness corresponding to P_max
	P_wedge	Purity	Wedge thickness corresponding to P_max
	CB_target	Combined	Target thickness corresponding to the largest Combined value
	CB_wedge	Combined	Wedge thickness corresponding to the largest Combined value

#### 6.5.5.1. Acceptance

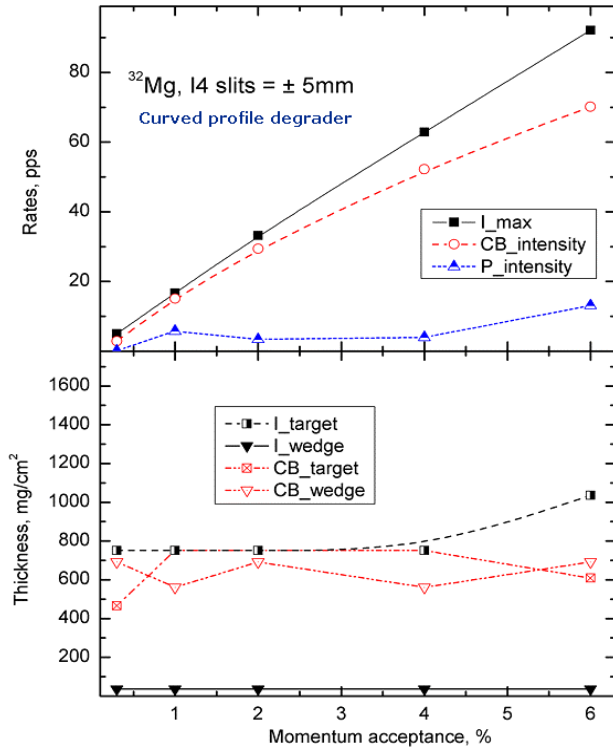


**Fig.206.** Top plot: The  $^{32}\text{Mg}$  fragment maximum possible production rate ( $I_{\text{max}}$ ) and the rate corresponding to the largest Combined value ( $CB_{\text{intensity}}$ ) versus the A1900 momentum acceptance. Bottom plot: Target and wedge thicknesses corresponding to rate curves in the top plot.

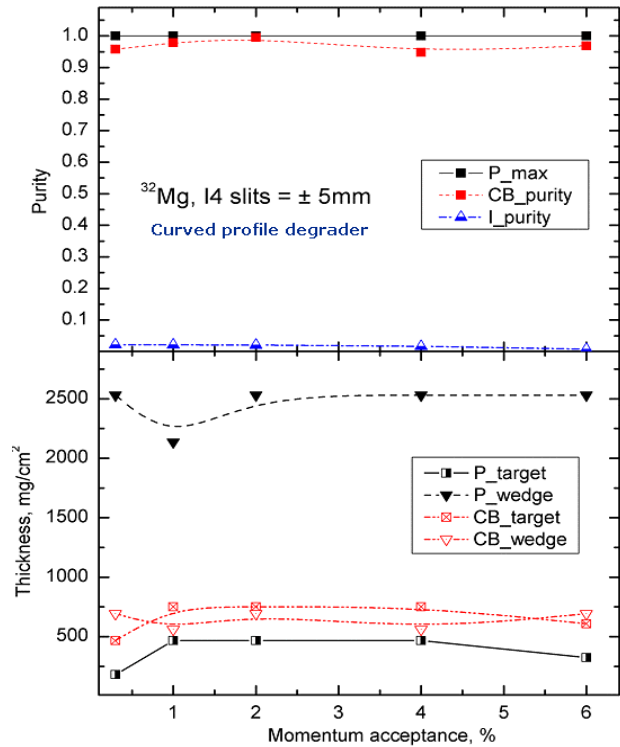


**Fig.207.** Top plot: The  $^{32}\text{Mg}$  fragment maximum possible purity and the purity corresponding to the largest Combined value versus the A1900 momentum acceptance. Bottom plot: Target and wedge thicknesses corresponding to rate curves in the top plot. Calculations were done with the curved profile degrader.

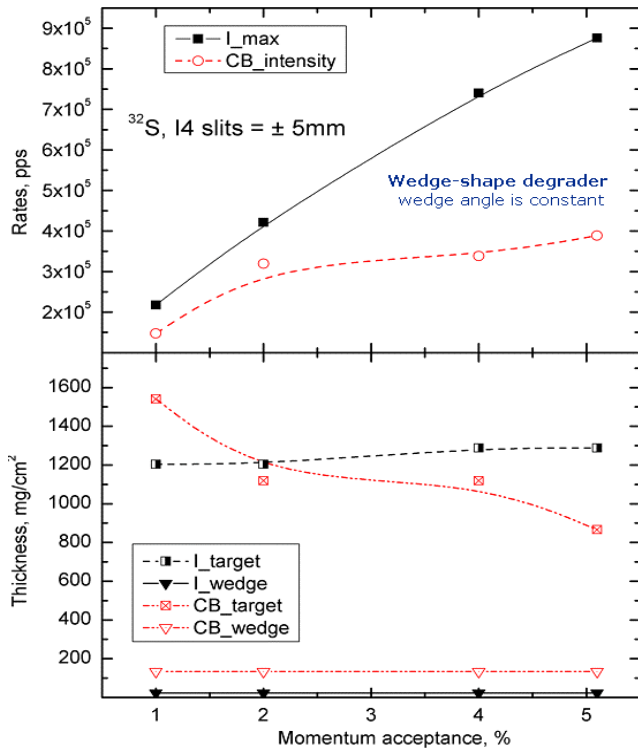


**Fig.208.** Top plot: The  $^{32}\text{S}$  fragment maximum possible production rate ( $I_{max}$ ) and the rate corresponding to the largest Combined value ( $CB_{intensity}$ ) versus the A1900 momentum acceptance. Calculations were done with the *wedge-shape degrader*.

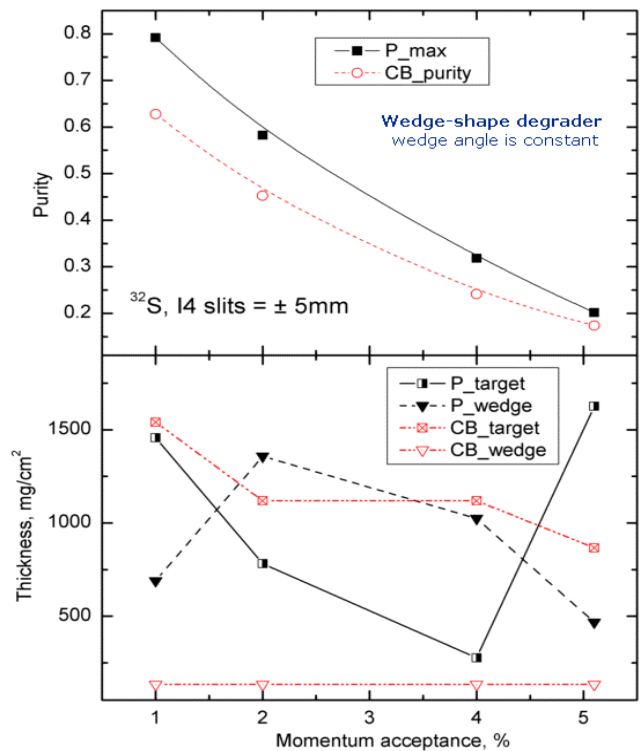


**Fig.209.** Top plot: The  $^{32}\text{S}$  fragment maximum possible purity and the purity corresponding to the largest Combined value versus the A1900 momentum acceptance. Calculations were done with the *wedge-shape degrader*.

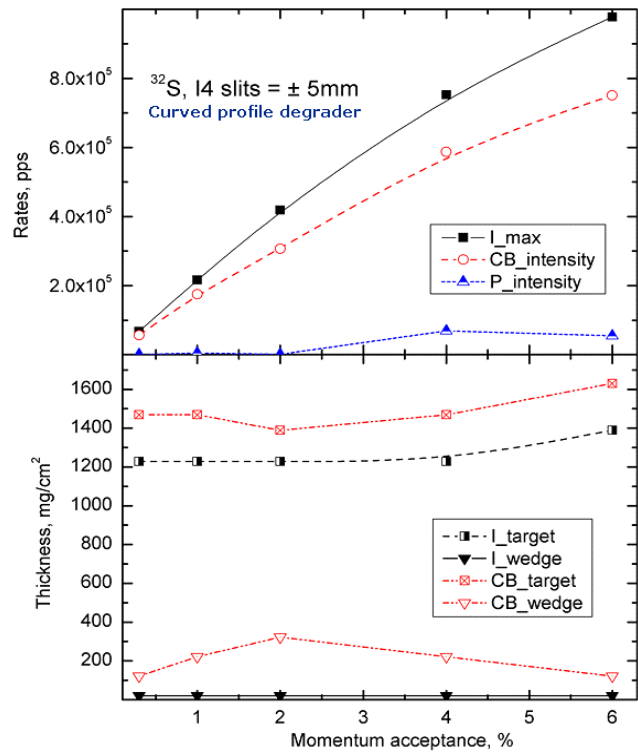


**Fig.210.** Top plot: The  $^{32}\text{S}$  fragment maximum possible production rate ( $I_{max}$ ) and the rate corresponding to the largest Combined value ( $CB_{intensity}$ ) versus the A1900 momentum acceptance. Calculations were done with the *curved profile degrader*.

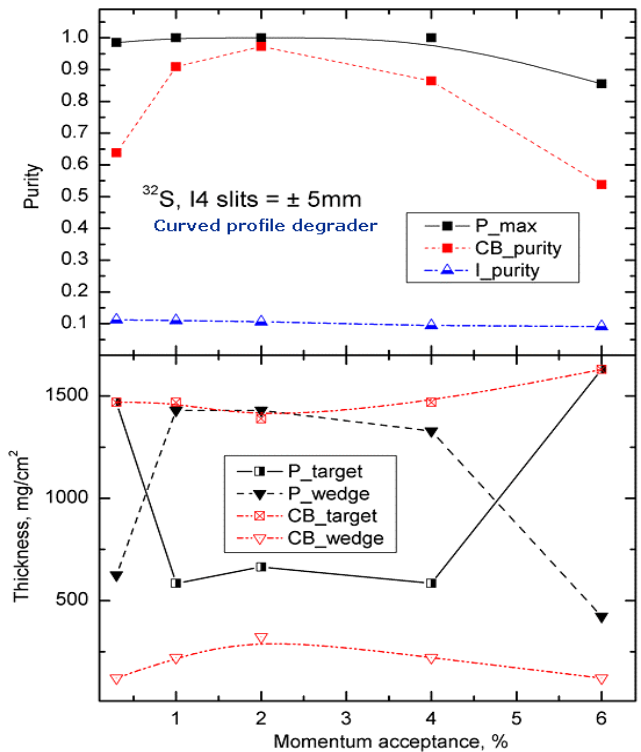


**Fig.211.** Top plot: The  $^{32}\text{S}$  fragment maximum possible purity and the purity corresponding to the largest Combined value versus the A1900 momentum acceptance. Calculations were done with the *curved profile degrader*.

### 6.5.5.2. Wedge selection slits

Fig.212 and Fig.213 show maximum and optimum production rate of the  $^{32}\text{Mg}$  and  $^{32}\text{S}$  fragments as well as corresponding target and wedge thickness values. We do not comment on these results, but leave this process for the reader.

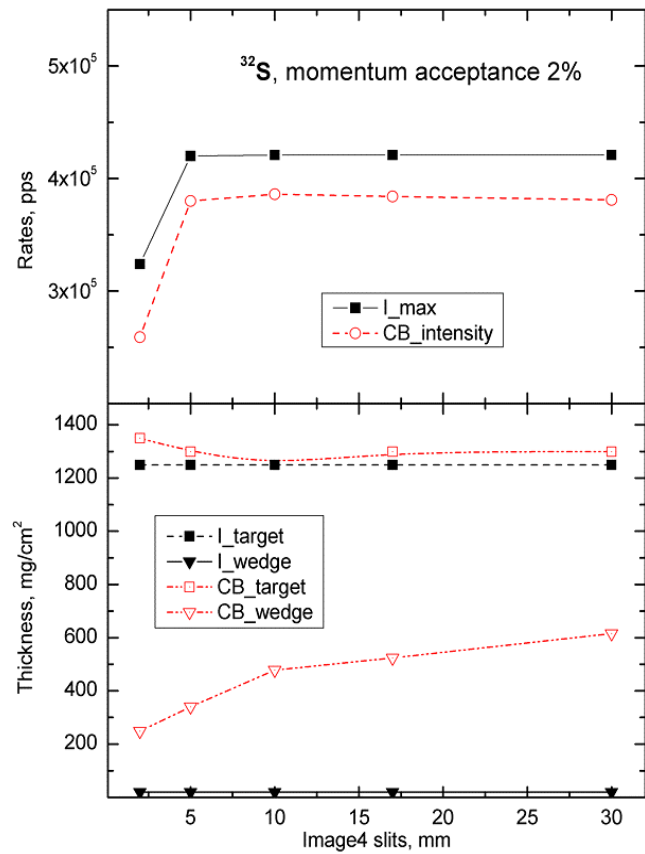
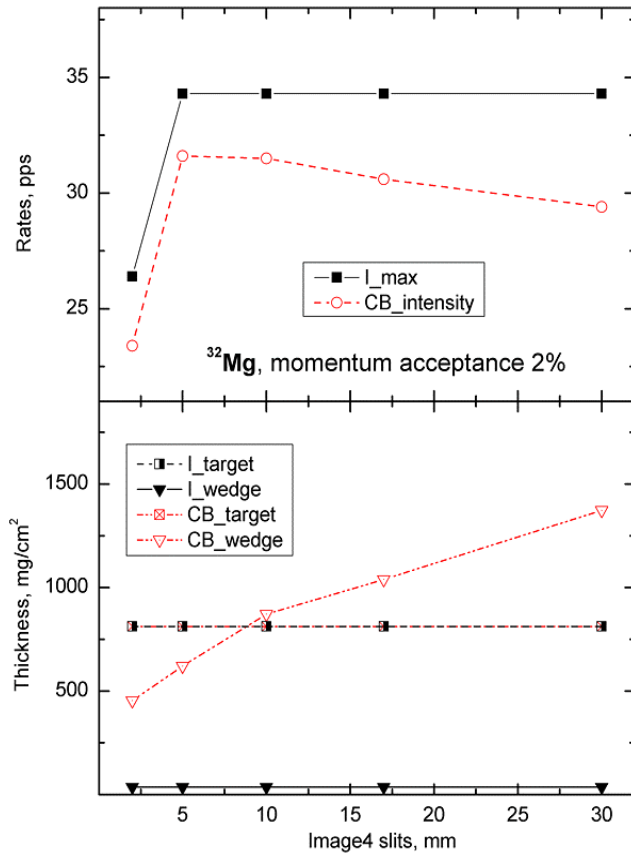


**Fig.212.** Top plot: The  $^{32}\text{Mg}$  fragment maximum possible production rate ( $I_{max}$ ) and rate corresponding to the largest Combined value (intensity) versus size of the Image4 slit.

Bottom plot: Target and wedge thicknesses corresponding to production rate curves in the top plot.

Calculations were done with the **curved profile degrader**.

**Fig.213.** Top plot: The  $^{32}\text{S}$  fragment maximum possible production rate ( $I_{max}$ ) and rate corresponding to the largest Combined value (intensity) versus size of the Image4 slit.

Bottom plot: Target and wedge thicknesses corresponding to production rate curves in the top plot.

Calculations were done with the **curved profile degrader**.

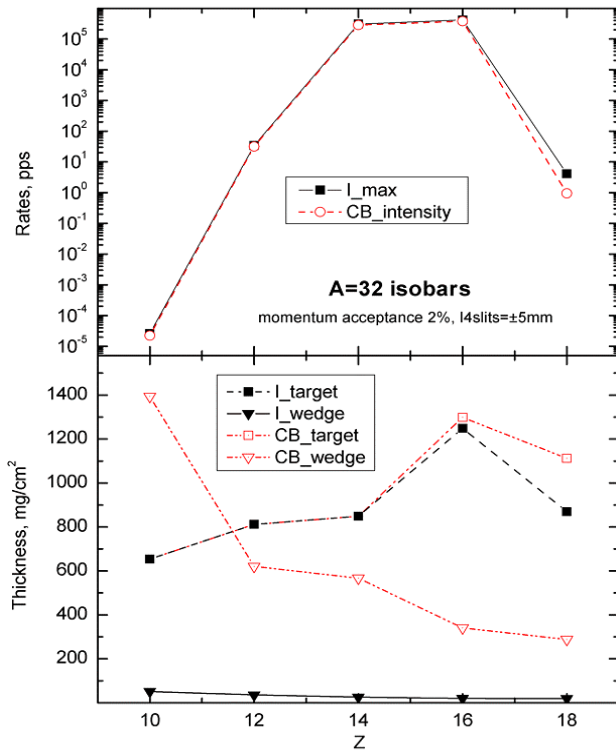
### 6.5.5.3. Isobars $A=32$

Fig.214 and Fig.215 show maximum and optimum production rate and purity of isobars  $A=32$  as well as corresponding target and wedge thickness values.

Fig.216 shows the Combined target-wedge optimization plots for isobars  $A=32$ .

These calculations were done for the  $^{40}\text{Ar}(140\text{MeV/u})+\text{Be}$  reaction using the A1900 fragment separator with the momentum acceptance being equal to 2% and on Image4 slits size of  $\pm 5\text{mm}$ . The curved profile degrader was used in calculations in the intermediate dispersive focal plane.





**Fig.214.** Top plot: The fragment maximum possible production rate ( $I_{max}$ ) and rate corresponding to the largest Combined value (intensity) for isobars  $A=32$ .

Bottom plot: Target and wedge thicknesses corresponding to production rate curves in the top plot.

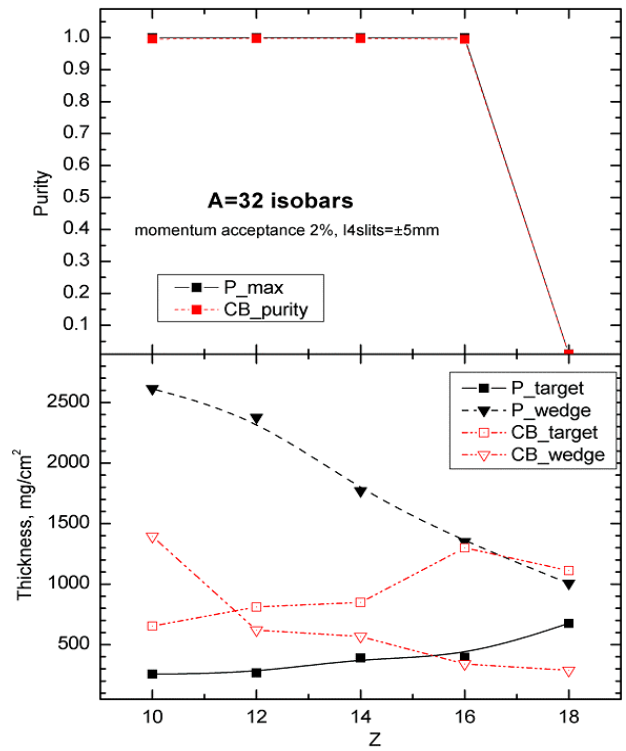


**Fig.215.** Top plot: The fragment maximum possible purity and purity corresponding to the largest Combined value for isobars  $A=32$ .

Bottom plot: Target and wedge thicknesses corresponding to production rate curves in the top plot.

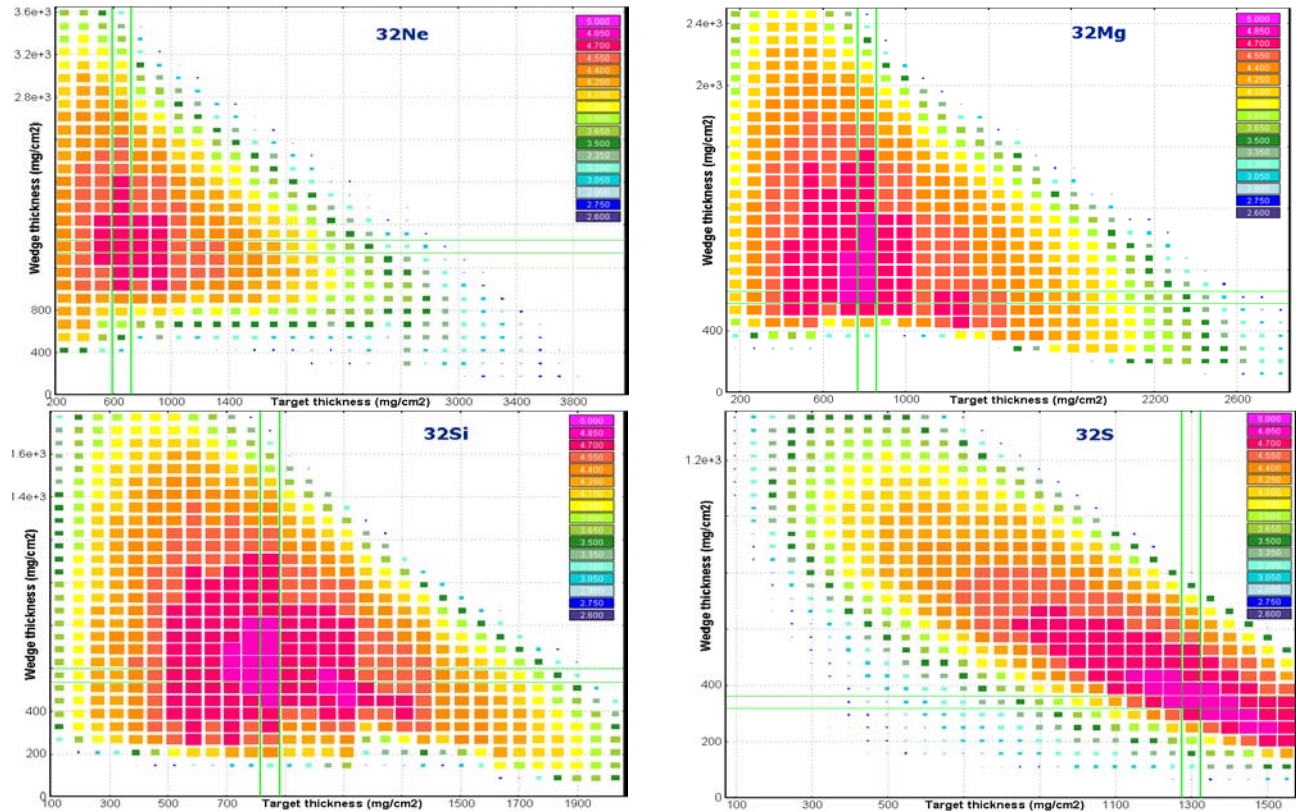


**Fig.216.** The Combined target-wedge optimization plots for isobars  $A=32$ .

## 7. Masses. AME2003

The new evaluation of atomic masses AME2003 [AME03] has been incorporated into the LISE++ code (version 7.2) replacing the previous nuclide mass database [Aud95]. Errors of nuclide characteristics also have been added in the database and might be edited or plotted (see Fig.217 and Fig.218).

Accurate predictions of the production cross-sections of rare isotopes are important in the study of astrophysical processes and in the location of the drip-lines. Reaction models involved in the LISE++ code as *Abrasion - Ablation*, *LisFus* (fusion – evaporation models), and *Coulomb fission* rely on parameterization of the nuclear masses. This may lead to large inaccuracies in the case of discrepancies between mass parameterization and the experimental masses.

Representation of nuclei as liquid drops has been very successful in predicting their properties and masses, especially those along the valley of stability.

However, a large discrepancy is observed between the classical LD mass formula and experimental values due to the shell structure. LISE++ uses a new mass formula with shell crossing (see [http://groups.nsl.msu.edu/lise/6\\_1/lise++\\_6.htm#\\_Toc26162476](http://groups.nsl.msu.edu/lise/6_1/lise++_6.htm#_Toc26162476)). A new LDM fit with shell crossing corrections has been performed using the new evaluation of atomic masses.

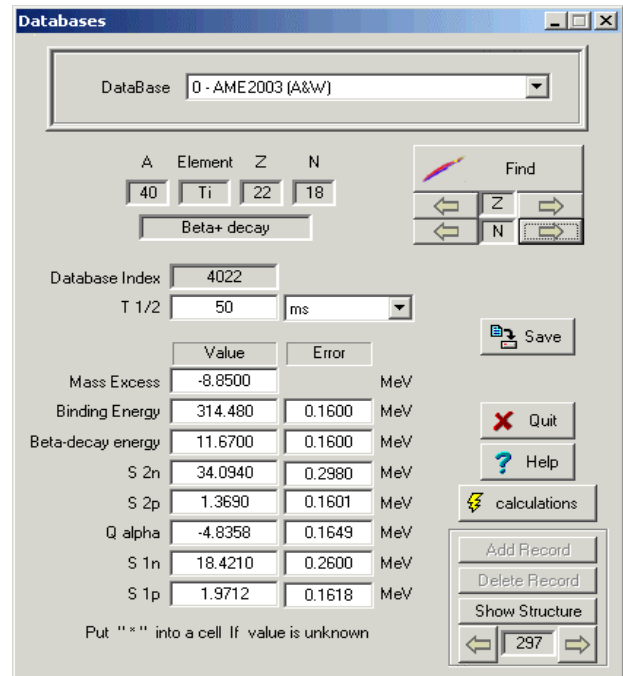


**Fig.217.** The “Databases” dialog. The new version allows to work (edit, plot) with isotope value errors.

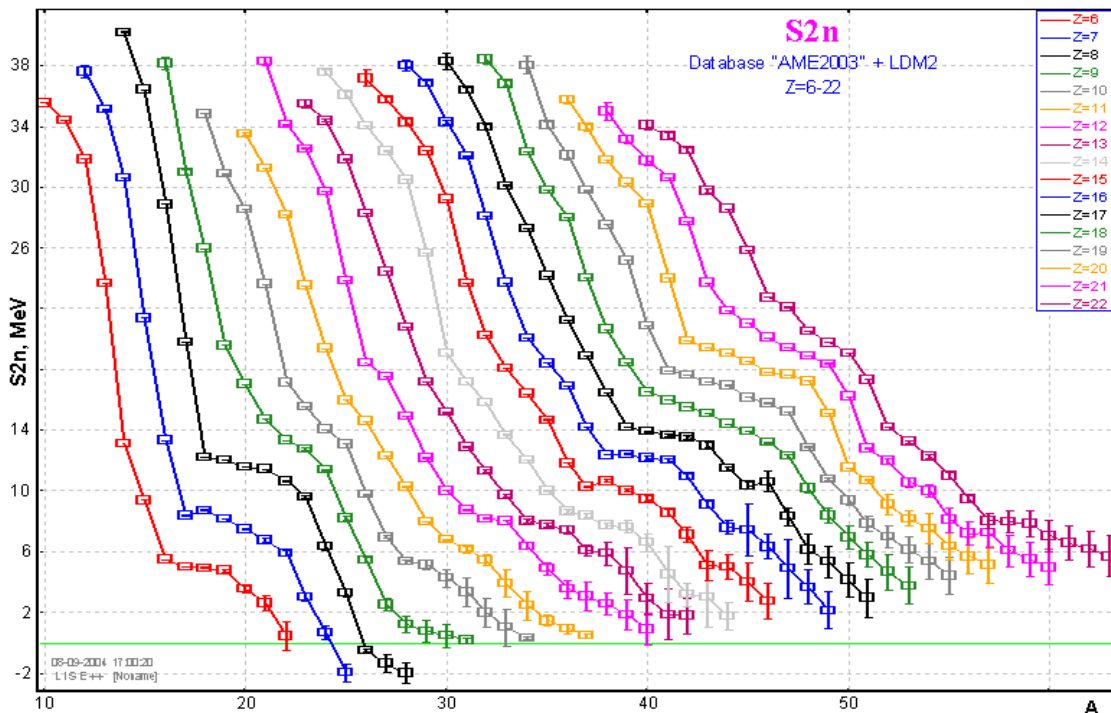


**Fig.218.** Two neutron separation energy of elements with atomic numbers 6-22 plotted by the LISE++ code.

## 7.1. New mass excess files in the LISE package

The new mass excess files “user\_mass\_excess\_TUYY.lme” (Z=1-112), “HFB8.lme” (Z=8-120), and “HFB9.lme” (Z=8-110) are provided in the LISE installation package.

The “user\_mass\_excess\_TUYY.lme” file is created based on the empirical mass formula with proton-neutron interaction by Takahiro Tachibana, Masahiro Uno, Masami Yamada, and So Yamada [Hau88]. The data were extracted from the page <http://www.phys.nthu.edu.tw/~nap/toimass.html>.

The mass excess files “HFB8.lme” and “HFB9.lme” [HFB9] are based on the Hartree-Fock-Bogoliubov + PLN method and were obtained from <http://www-astro.ulb.ac.be/Nucdata/Masses/hfb8-plain> and <http://www-astro.ulb.ac.be/Nucdata/Masses/hfb9-plain> accordingly.

*Note:* It is recommended to use AME2003 + LISE LDM#2 values for regular calculations with LISE++. The TUYY mass excess file can be used as an alternative file for comparison and to show predicted masses very far from the stability line (so called “unknown” isotopes. See the next chapter for details) where the shell crossing corrections for LDM#2 do not act.

## 7.2. “Unknown” - new type of isotope designation for the table of nuclides

“There is no clear definition of the dripline...”

M.Thoennessen [Tho04]

There are several different definitions of drip-line in the “Reaching the limits of nuclear stability” review [Tho04]. We are not going to discuss them, but we need to introduce some definitions to characterize the new type of isotope designation for the table of nuclides in the LISE++ code.

But for a start we answer on the question:

### Why do we need new type of designation?

1. Show to LISE’s users nuclei which are possibly particle bound based on theoretical predictions (see Fig.219);
2. Use this type of isotopes in transmission calculations (see Fig.220);
3. Use this type of isotopes for Database plots, because the code is looking for extremities to plot isotope characteristics (see Fig.226);
4. Calculate and keep in the memory AA and AF cross-sections and secondary reactions contribution for this type of isotopes.

### 7.2.1. Particle bound, quasi bound and unbound nuclei

The new type of isotope designation “Unknown” means that the isotope was initially set as “doesn’t exist” (black color), but if the user run a mass model which predicts this isotope be **particle**

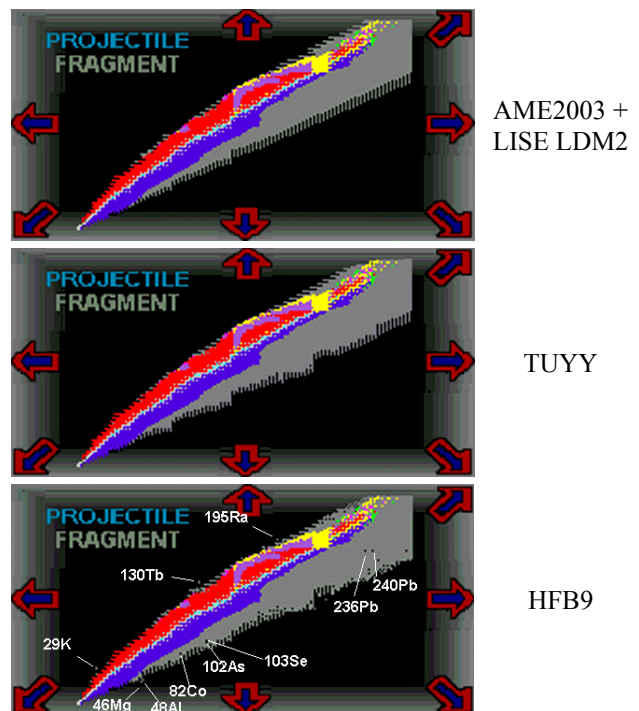


**Fig.219.** The LISE’s navigation scheme with different sets of “unknown” isotopes calculated by different models.

**bound**, then the code changed the state of this nuclide from “Doesn’t exist” to “Unknown”. Unknown isotopes are marked by gray color in the table of nuclides (see Fig.220) and the navigation scheme (see Fig.219).

We use the following definitions in the code:

“**particle bound**” if all four separation energies ( $S_{1n}$ ,  $S_{2n}$ ,  $S_{1p}$ ,  $S_{2p}$ ) are positive\*.

“**particle quasi bound**” if all statements are valid:

$$S_{1n} > 0, \quad S_{1p} + V_{B0\_p} > 0,$$

$$S_{2n} > 0, \quad S_{2p} + V_{B0\_2p} > 0,$$

$$Q_\alpha - V_{B0\_alpha} < 0,$$

but at least one from  $S_{1p}$  or  $S_{2p}$  separation energies is negative ( $S_{1p} < 0$  or  $S_{2p} < 0$ ).

“**particle unbound**” if one of these five statements is valid:

$$S_{1n} < 0, \quad S_{1p} + V_{B0\_p} < 0,$$

$$S_{2n} < 0, \quad S_{2p} + V_{B0\_2p} < 0,$$

$$Q_\alpha - V_{B0\_alpha} > 0;$$

Fig.221 visually demonstrates the arrangement of these conditions. With increasing angular momentum these levels will move up. The “Absolute zero” value shows a level below which an isotope is always particle unbound at any angular momentum. The “Particle quasi bound” expression has appeared because for small but negative values of separation energies an isotope can be found to be particle bound (in other words can be identified in an experimental way) due to the Coulomb barrier, for example B.Blank and collaborators work [Bla00] where  $^{48}\text{Ni}$  isotopes were unambiguously identified:

Decay mode	Separation energy		$V_{B0}$
	AME2003	TUYY	
1p	-0.4050 ( $\pm 0.711$ )	-0.1610	5.73
2p	-3.0650 ( $\pm 0.615$ )	-2.8321	10.55

Particle bound properties (or decay modes) calculated from database or mass formula it is possible to see in the “Isotopes” dialog (see fragment “C” in Fig.223). Depending on isotope properties, the “Particle absolutely unbound” state can be marked as “2p+CB unbound”, “1p+CB unbound”, “alpha+CB unbound”, “1n unbound”, or “2n unbound”, and the “Particle quasi bound” state can be seen as “1p unbound” or “2p unbound”. Recall that just **particle bound isotopes** can be moved from the “doesn’t exist” state to the “unknown” state as a result of searching by the code.

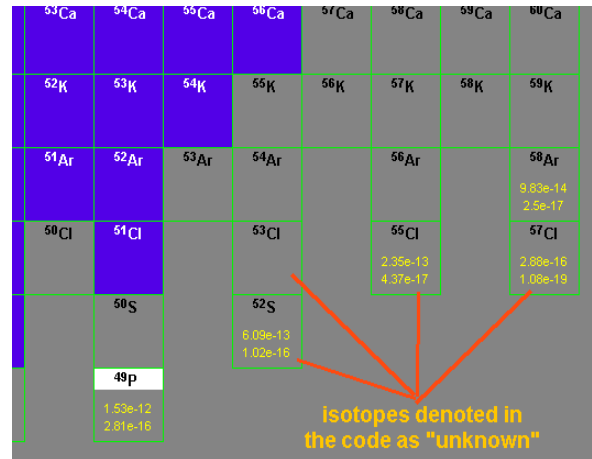


Fig.220. Fragment of the LISE nuclide table where transmission calculation results are shown for unknown isotopes.

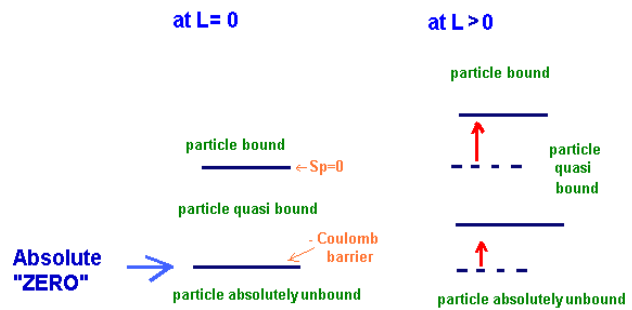


Fig.221. Scheme for particle bound, quasi bound and unbound definitions.

\* it has been decided to assign the “particle bound” property for nuclei with  $Q_\alpha - V_{B0\_alpha} < 0$  and  $Q_\alpha > 0$  when the code searches “unknown” isotopes.



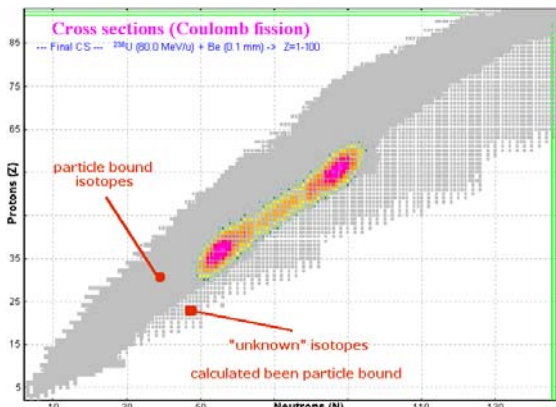


Fig.222. Designation of particle bound and "unknown" nuclides on 2D plots.

"hfb9.lme" file as the user mass excess file (marked "A" in Fig.224) and set the "1 User's ME" item as mass method (marked "B").

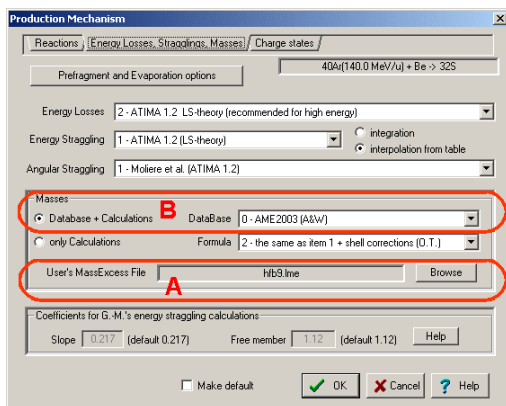


Fig.224. The "Masses" panel of the "Production mechanism" dialog.

The new version allows one to plot all calculations by different methods in one plot with different options. See Fig.225 and Fig.226 for modification details.

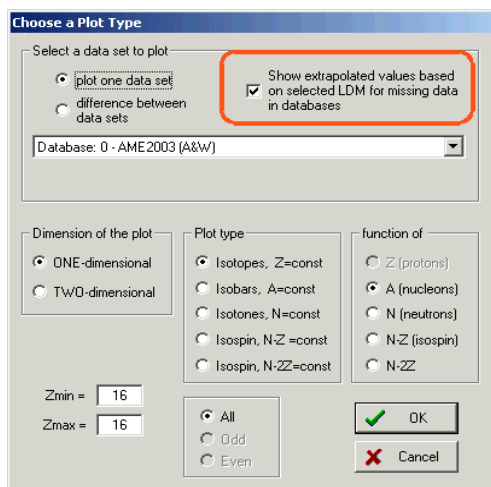


Fig.225. The "Database Plot options" dialog.

### 7.2.2. How to load information from the user mass excess file in the navigation scheme

In order to reload information in the navigation scheme (Fig.219) it is necessary to load the "Production mechanism" dialog from the "Options" menu. For example to use the HFB9 model, it is necessary to choose the

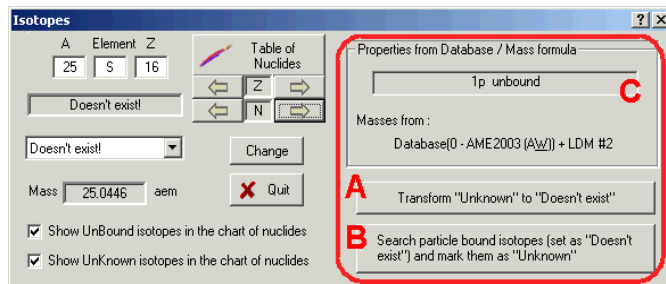


Fig.223. The "Isotopes" dialog.

Load the "Isotopes" dialog (see Fig.223) from the "Options" menu. Click the button "Transform 'Unknown' to 'Doesn't exist'" (marked "A" in Fig.223) to clean the navigation table from previous calculations. Click the "Search particles.." button (marked "B" in Fig.223) to find particle bound isotopes and move some of them which marked as "doesn't exist" into "unknown" state (see result of this operation in Fig.219).

The LISE installation package contains the "table.iso" file with information for the table of nuclides where "unknown" isotopes have already been set based on the TUYU model.

### 7.2.3. Modifications in the database plot

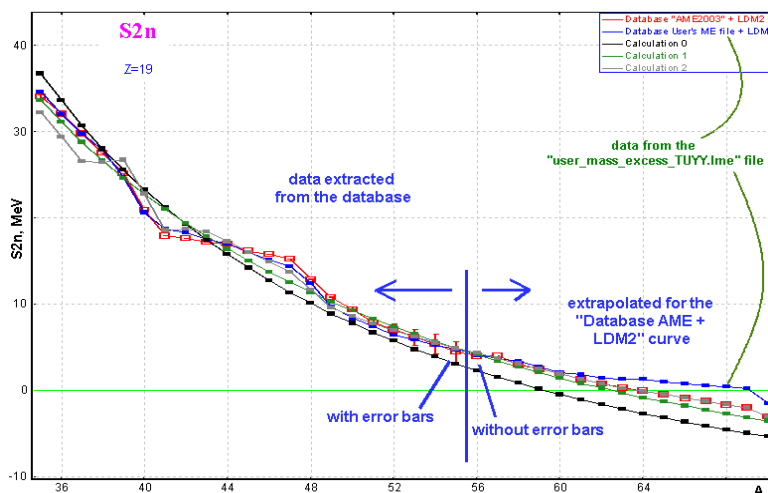


Fig.226. Two neutrons separation energy of Potassium isotopes.



## 8. LISE++ block structure development

### 8.1. New material block: FaradayCup

The new material block “FaradayCup” was incorporated in the program (see Fig.227). Primary goal of the FaradayCup block (by analogy with reality) to stop transmission calculation in it. Initially the program guesses the FaradayCup block is made from W-material of  $10^7$  millimeters. If we put a regular material block with the same thickness, and any optical block will be somewhere behind this



Fig.227. A portion of the “Set-up” dialog showing the “Faraday cup” block button.

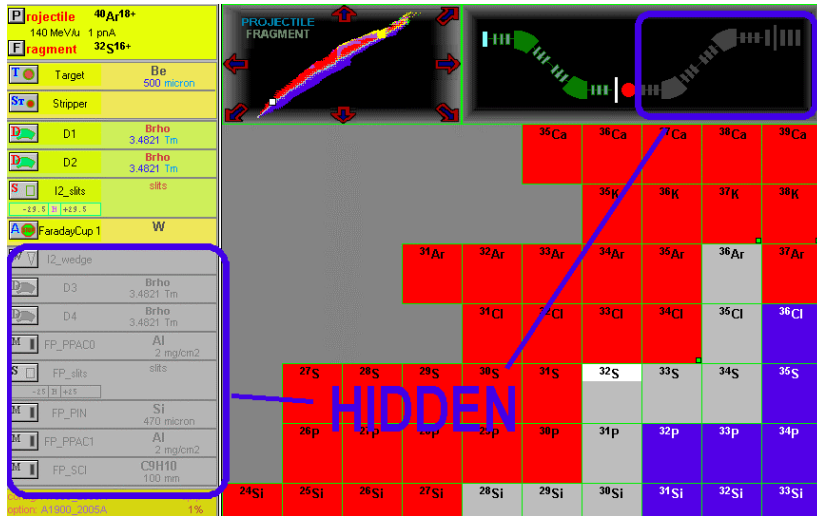


Fig.228. A portion of the LISE window demonstrating the “FaradayCup” block action.

block then the code will show transmission 0%. The code assumes no more blocks (see Fig.228) behind the FaradayCup block and shows transmission from the target up to the FaradayCup block (see Fig.229). In addition, no materials are shown in the Physical calculator behind the Faraday cup.

If identification detectors were set behind the FaradayCup block in the Plot options” dialog then calculations will be done just up to the FaradayCup block, and the FaradayCup block will be used instead of these identification detectors.

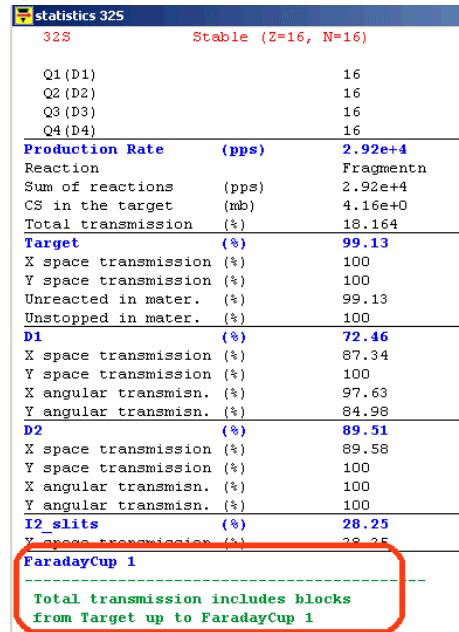


Fig.229. Transmission statistics window. Calculation were done up to the FaradayCup block. It is possible to see in the bottom of figure the message about blocks involved in calculations.

### 8.2. Append blocks in the current open configuration from other LISE files

The new version allows the create of new configurations by appending blocks from an existing file (\*.lpp or \*.lcn) into the current open document through the “File” menu (Fig.230). The user has to specify a location where new blocks will be inserted (see Fig.231).

Fig.232 shows a spectrometer built by the “Append blocks” command.



Fig.232. The spectrometer consisting of two A1900 fragment-separators built with the help of the “Append blocks from file” command.

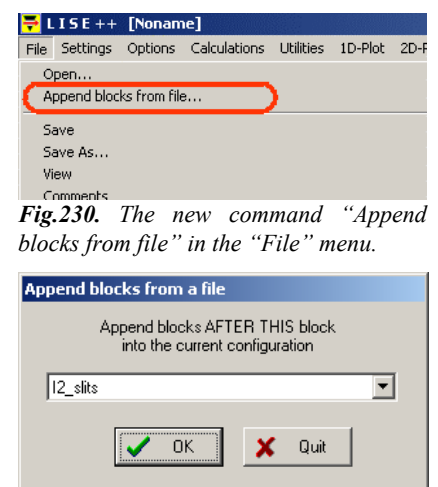


Fig.230. The new command “Append blocks from file” in the “File” menu.

Fig.231.

## 9. Different

### 9.1. User cross-section file

The extension of user cross-section file accepted by the LISE++ code, depends on in what application the file was created:

Extension	Application	Type of cross-sections
*.cs	LISE++: the cross-section file dialog	All calculated by LISE++ reaction mechanism models: Abrasion-ablation, Fusion-residues, Abrasion-Fission, Coulomb fission
*.cs2	LISE++: the secondary reactions dialog	<b>Reduced</b> (sum of all process involved in fragment production including secondary reactions contribution)
*.cs4	PACE4	Fusion-residues

#### 9.1.1. User cross-section file: reaction property

The format of user cross-section file has been changed in the new version. The new data field “Reaction” was added in the user cross-section record in the code to keep in the operating memory as well as in the cross-section file.

The fifth column in the user CS file (see the “Cross-section file format” frame in Fig.233) shows a reaction label to assign this cross-section record to determine reaction. The new version allows one to keep user cross-sections in the memory for different reaction mechanisms. The reaction field should begin with the letter “R”, and the next number shows the reaction type.

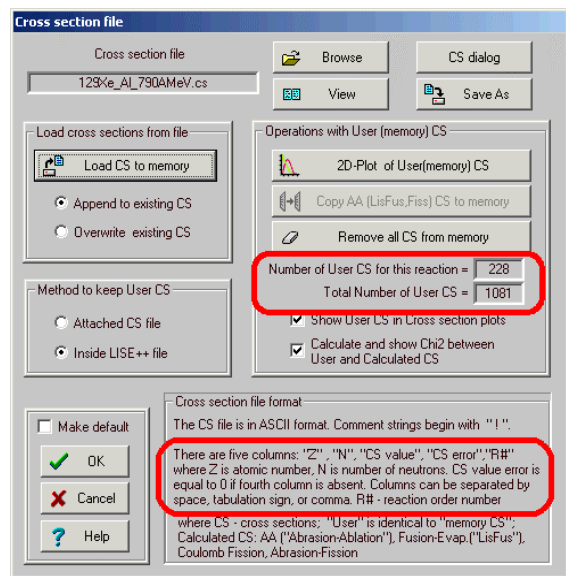


Fig.233. The “User cross-section file” dialog.

Index	Reaction	Index	Reaction
R0	Fragmentation	R4	Abrasion-Fission (Low Ex)
R1	Fusion -> Residual	R5	Abrasion-Fission (Mid Ex)
R2	Fusion -> Fission	R6	Abrasion-Fission (High Ex)
R3	Coulomb fission	R8	ISOL method

If the reaction field is omitted in a CS file, then the CS records will be assigned to the current reaction set in the code. When the user saves a CS file, the reaction field is always written in a user cross-section file (if the “Method to keep User CS” is set as “Attached CS file”) or in the LISE document currently opened (option “Inside LISE++ file”).

Using the “Cross-sections” dialog (see Fig.234) it is possible to list and edit user cross-sections for any reaction independently from the current reaction mechanism set in the code.

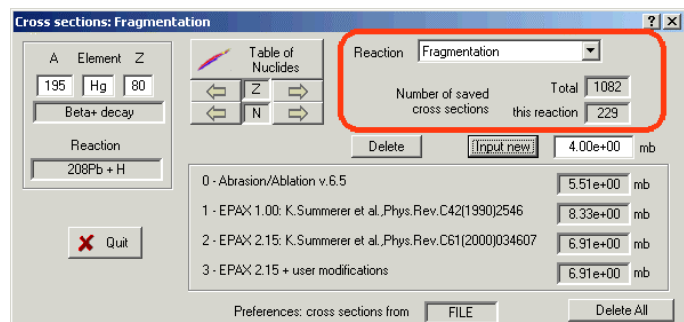
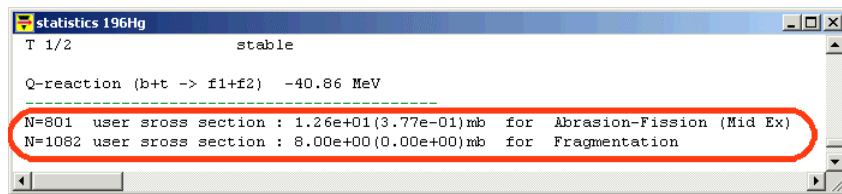


Fig.234. The “Cross-sections” dialog.

Presence of a user cross-section for an isotope can be also seen in the table of nuclides (see red and blue squares in Fig.235) as well as in the statistics window (see Fig.236).



**Fig.235.** The  $^{196}\text{Hg}$  isotope square of the table of nuclides. The red square in left bottom corner shows that there is a user cross-section in the memory and this cross-section value is applied for current calculations. The blue square shows the existence of a user cross-section value for a reaction mechanism, which is not currently being used.



**Fig.236.** Portion of the transmission statistics window showing not only the presence of user cross-sections in the memory for this isotope, but their details as well.

### 9.1.2. User file of reduced cross-sections

There is a very simple method to make your work with the code faster:

do not repeat AF and secondary reactions calculations using a file with reduced CS. The User file of Reduced CS consists of three columns (no CS error and reaction columns).

- ❑ First it is necessary to calculate all AF cross-sections, then all secondary reactions contribution coefficients.
- ❑ Afterwards you have to save the calculated reduced cross-section values using the Secondary reactions dialog. Reduced cross-section is the sum of cross-sections of all EERs including the secondary reactions contribution.
- ❑ Turn off secondary reactions and leave just one working EER in the Abrasion-Fission dialog.
- ❑ Load the user file with reduced CS as a regular user CS file in the “Cross-section file” dialog.

**NOTE:** If you are saving calculated cross-sections in AF mode then remember that cross-sections will be saved JUST for ONE current excitation energy region.

**NOTE:** If you load an experimental AF cross-section file then you have to leave one EER and turn off the two other one because the experimental cross-section is the sum of cross-sections from all fissile nuclei.

### 9.1.3. CS files in LISE++ package

The new version installation package contains new user CS files for reactions of  $^{238}\text{U}$  and  $^{208}\text{Pb}$  beams with different targets.

**Table 39.** The “LISE\CrossSections\PublishedData” directory listing of files with published experimental cross-section values.

Subdirectory	File name	Reference
	129Xe_Al_790AMeV	[Rei98]
	136Xe_Al_760AMeV	[Zei92]
	40Ar_Be_1AGeV	[Oza00]
	40Ar_C_240AMeV	[Sym79]
	48Ca-Ta_90AMeV	[Not02]
	58Ni_Be_650AMeV	[Bla94]
208Pb\	208Pb_1H_1AGeV_evap	[Enq01]
	208Pb_1H_1AGeV_fission	[Enq01]
	208Pb_2H_1AGeV_evap	[Enq02]
	208Pb_2H_1AGeV_fission	[Enq02]
238U\	238U_Be_750AMeV_fission	[Ber97]
	238U_Pb_1AGeV_fission	[Enq99]
	238U_Pb_1AGeV_fragmentation	[Enq99]
	238U_p_1AGeV_fission	[Ber03]
	238U_p_1AGeV_spallation	[Tai03]

We recommend erasing the “LISE\CrossSections\PublishedData” directory before installation of the version 7.5 because locations of several CS files from previous versions were changed.

## 9.2. Curved profile degrader modifications

The new version is able to keep all properties of the curved profile inside the LISE++ file (\*.lpp). In the previous version the user could only attach a curved profile file to a LISE++ file.

The new version supports curved profile files created by the previous versions.

The “Current profile” is a separate class in the code which belongs to the Wedge class. Initially, when the code loads, “Current profile” does not exist. To create the “Current profile” the user has to load the Wedge dialog and run the Curved profile utility (see Fig.237).

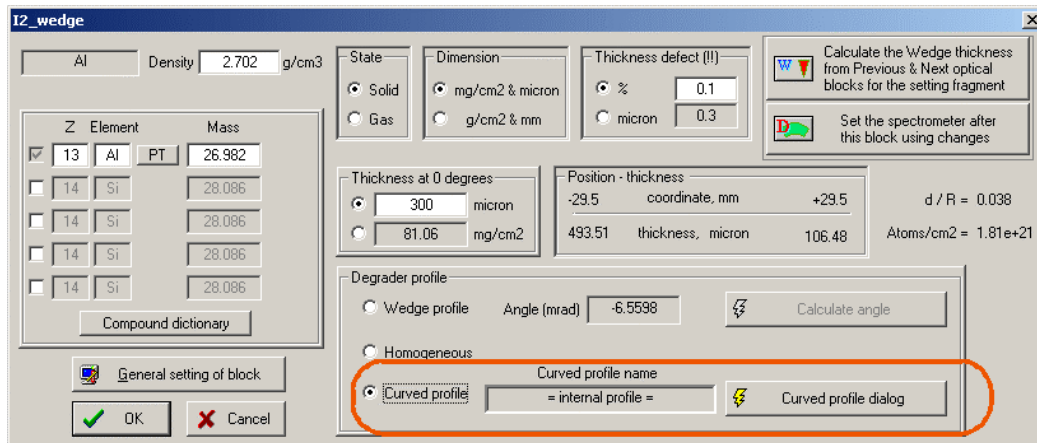


Fig.237. The Wedge dialog.

There are three possible variations in the “Curved profile name” message window (see Fig.237):

1. no current profile!
2. = internal profile =
3. the name of an attached curved degrader file (as in previous versions)

To create a new “current profile” the user has to complete the following steps (see Fig.238):

- a. Choose the block: to calculate the angle for the setting mode after it (for example “D4”);
- b. Choose the mode (Acromatic, Monochromatic, User-Deifned);
- c. Define X0 & L;
- d. Click the “Calculate” button;
- e. Choose the method to keep “current profile” (Inside LISE++ or the attached file);
- f. Click the “Make it current” button if calculations complete without any warnings;

You can make some comments, which will be saved together with the profile in LISE++ file as well as in the attached file in the corresponding mode. Do not correct curved degrader files (or LISE++ files) manually by text editors. The code checks a special structure of file and you can get an error message if, for example, you modified the comment line number 4 where the code keeps the settings of the “current profile” such as distribution dimension size.

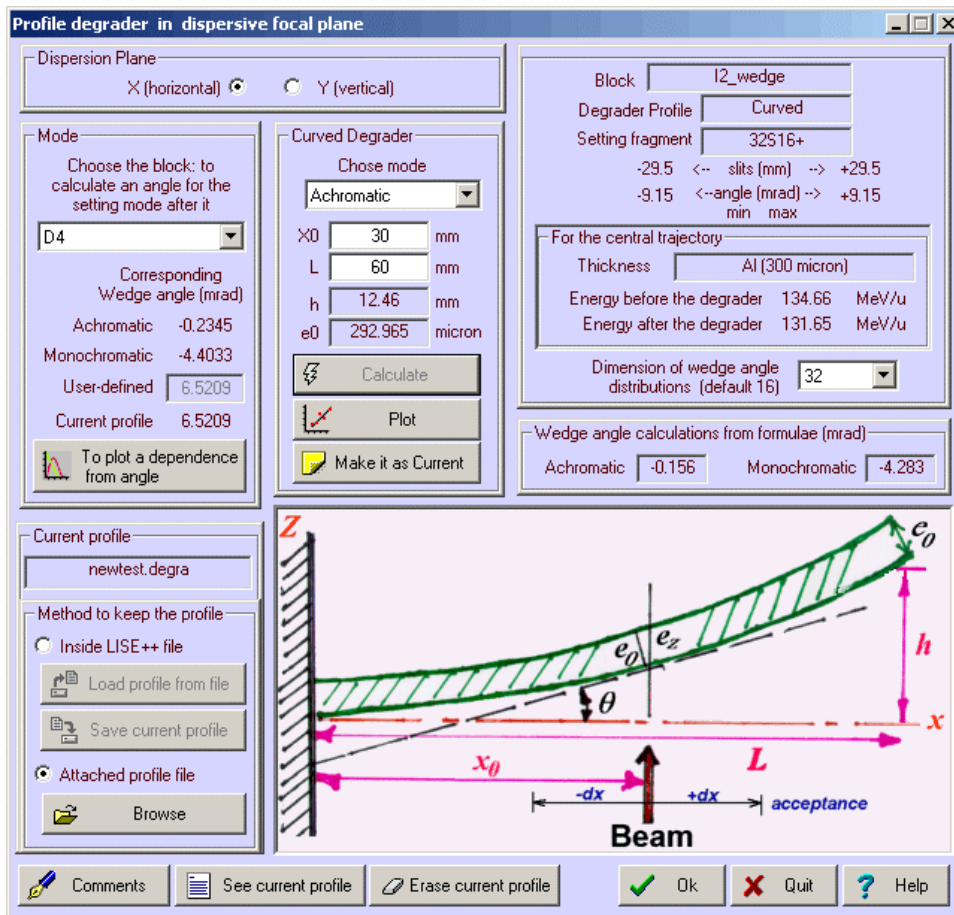


*Fig.238. The Curved profile degrader dialog.*

**Load profile from file** – load a profile from an external file “\*.degra” to be the current profile. This works only if the “method to keep profile” is set to “Inside LISE++ file”

**Save current profile** – save the current profile to an external file “\*.degra”. This works only if the “method to keep profile” is set to “Inside LISE++ file”

**Browse** – load a profile from an external file and accept it as the current profile (only for mode “Attached profile file”). When you open a LISE++ file where the wedge block has a reference to an attached curved profile file, the code automatically loads the curved profile into the current profile.

“LISE/degrader” is the default directory for curved profile files.

Use the **Erase current profile** button if you want to use the Wedge profile mode and do not want to keep curved profile settings in a LISE file.

If the user quits the Wedge dialog pressing “Cancel” then all wedge settings, including curved profile, settings will be restored.

Even if the user chooses the “Wedge profile” for degrader profile mode, the existing current curved profile **will be kept** in the code and saved in LISE++. To avoid this you have to erase the “current profile” in the “Curved profile degrader” dialog.




### 9.3. Logotypes and references

In the version 7.5 by clicking on a logotype in the left bottom corner of the code the user can load a web site connected with this logotype. Logotypes of laboratories and scientific organizations, which have made or are making contributions to the development of the program, each appear 6 seconds.

Logotype	Organization	WEB address
	FLNR Dubna Russia	<a href="http://flerovlab.jinr.ru/flnr/">http://flerovlab.jinr.ru/flnr/</a>
	JINR Dubna Russia	<a href="http://www.jinr.ru/">http://www.jinr.ru/</a>
	GANIL Caen France	<a href="http://www.ganil.fr/">http://www.ganil.fr/</a>
	IPN Orsay France	<a href="http://ipnweb.in2p3.fr/">http://ipnweb.in2p3.fr/</a>
	CEA France	<a href="http://www.cea.fr/">http://www.cea.fr/</a>
	IN2P3 France	<a href="http://www.in2p3.fr/">http://www.in2p3.fr/</a>
	NSCL East Lansing USA	<a href="http://www.nscl.msu.edu/">http://www.nscl.msu.edu/</a>
	MSU East Lansing USA	<a href="http://www.msu.edu/">http://www.msu.edu/</a>
	National Science Foundation USA	<a href="http://www.nsf.gov/div/index.jsp?org=PHY">http://www.nsf.gov/div/index.jsp?org=PHY</a>
	Department of Energy USA	<a href="http://www.sc.doe.gov/np/">http://www.sc.doe.gov/np/</a>
	GSI Darmstadt Germany	<a href="http://www.gsi.de/">http://www.gsi.de/</a>

## 9.4. 2D-plots: contours & projections

### 9.4.1. Contour dialog

In the new version during work with Monte Carlo or cross-section 2D-plots it is possible to take advantage of some new utilities: contours and projections. Using the icon  in the 2D-plot toolbar the user can load the Contour dialog (see Fig.239) to begin creation of a new contour, to save a contour from the operating memory in a file or to load a contour from a file. Only one contour can be in memory. The extension of contour files is “\*.contour”, and by default the contour files are found in the “LISE\Spectra” directory.

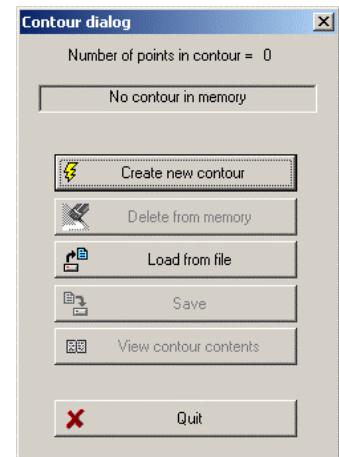


Fig.239. The Contour dialog. No contours in memory.

Fig.240 and Fig.241 show contour examples for 2D cross-section and Monte Carlo plots respectively.

In the case of a 2D cross-section plot (Fig.240) the rectangle with coordinates  $X \pm dX$ ,  $Y \pm dY$  will be inside of the contour (or for window projections in the slice created by user zoom) if the central point (X,Y) is found inside the contour if even the contour line crosses this rectangle.

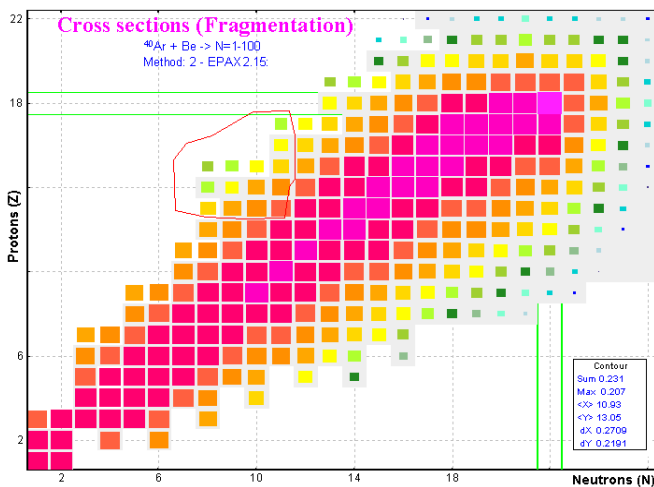


Fig.240. The contour example for a 2D cross-section plot.

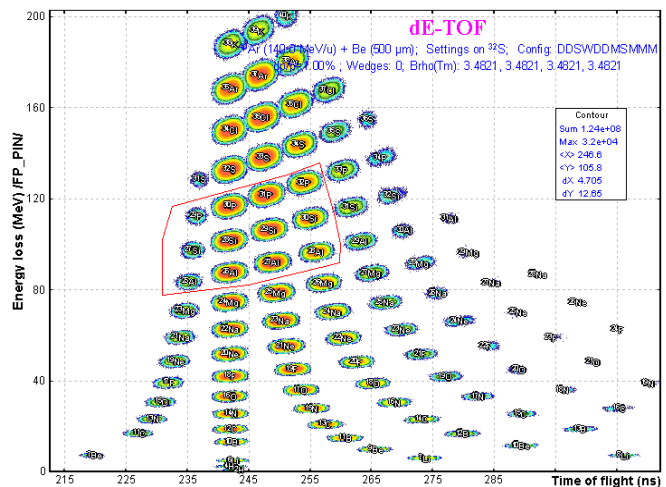


Fig.241. The contour example for a Monte Carlo plot.

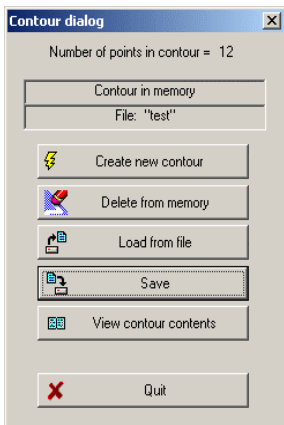



Fig.242. The Contour dialog. The “Test” contour in the memory.

If the contour already exists in memory the Contour dialog looks as shown in Fig.242. The user can manipulate a contour in memory: save, view, erase. The contour content is shown in Fig.243.

#### 9.4.1.1. Window and contour projections on an axis for 2D Cross-section plot

Contour contents		
02-08-2005 16:04:55 Version 7.4.166		
Plot name : Cross sections (Fragmentation)		
X-axis: Neutrons (N)		
Y-axis: Protons (Z)		
Number of points: 12		
1:	6.578	15.346
2:	6.6353	12.908
3:	7.8938	12.601
4:	9.5242	12.506
5:	11.126	12.553
6:	11.326	14.045
7:	11.555	14.4
8:	11.526	16.459
9:	11.326	17.642
10:	9.8102	17.595
11:	8.1226	16.459
12:	7.1215	16.104

Fig.243. Contents of the contour file.

Clicking the  icon in the 2D-plot toolbar the user loads the “Projections” dialog (Fig.244) to select the type of projection: on what axis (horizontal or vertical) as well as what data (for the contour or for the whole window). Fig.245 shows the projection of the contour in Fig.241 on the horizontal axis.

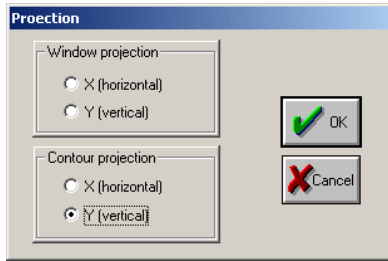


Fig.244. The Projection dialog.

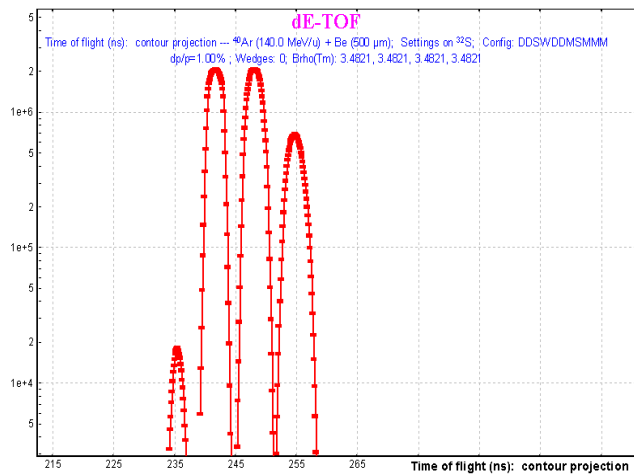


Fig.245. The horizontal projection of the contour in Fig.241.

### 9.5. Fission channel for the fusion-evaporation excitation function plot

Initially the Fusion-Residue reaction mechanism was incorporated into the code disregarding the fission deexcitation channel of the excited compound nucleus. In the new version the fission channel was included in the list of possible deexcitation channels, and in connection with this, the fission channel was also added in the fusion-residue excitation function plot. The user can turn on/off the fission channel in the “Fusion cross-section plot” dialog (Fig.246).

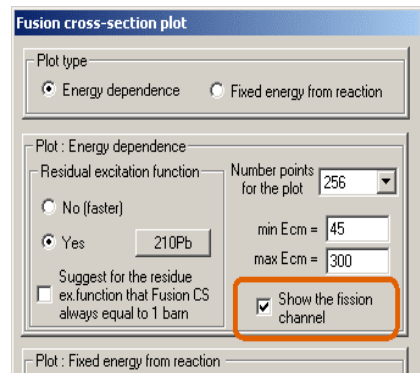


Fig.247 shows the  $^{210}\text{Pb}$  excitation function in the reaction  $^{12}\text{C} + ^{208}\text{Pb}$ .

Fig.246. Portion of the “Fusion cross-section plot” dialog.

**Note:** The fission channel calculation may increase the time to calculate fusion-residues excitation function, because in the previous version if the fusion-residues cross-section became very small with increasing excitation energy then the evaporation cascade automatically was stopped, even if the last point (“max Ecm” in Fig.246) was not yet reached. In the case of fission the calculation always goes to the last point.

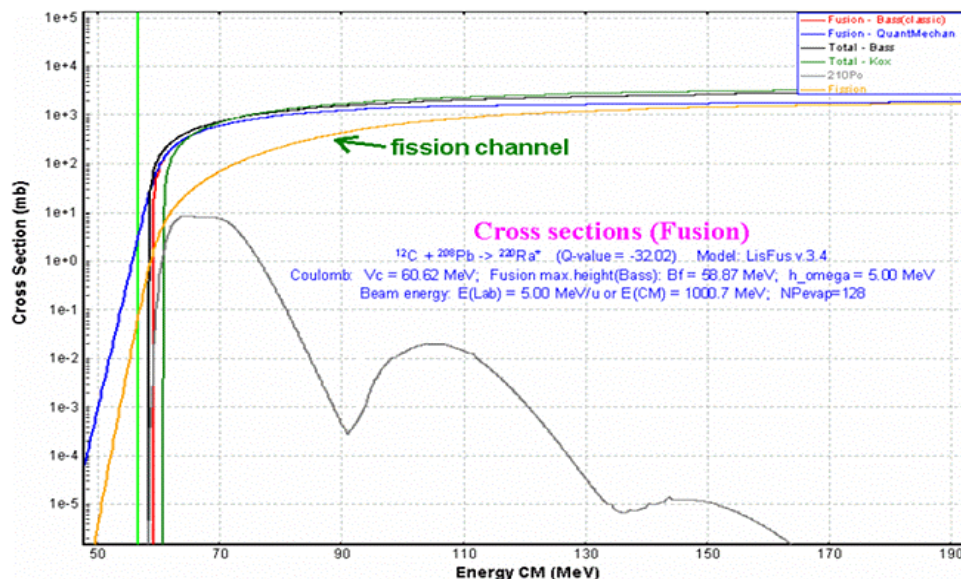


Fig.247.  $^{210}\text{Pb}$  excitation function in the reaction  $^{12}\text{C} + ^{208}\text{Pb}$ .

## 9.6. Abrasion-Ablation: fast mode for heavy projectiles

In the new version it is possible to speed up the cross-section calculation process when using the Abrasion-Ablation model for heavy projectiles, taking into account secondary reactions contributions. The principal difference between the fast mode of AA and the regular is the dimension of the evaporation distributions, which is equal to 8 for the fast mode of AA. It is impossible to manually set such a small value in the “Evaporation options” dialog.

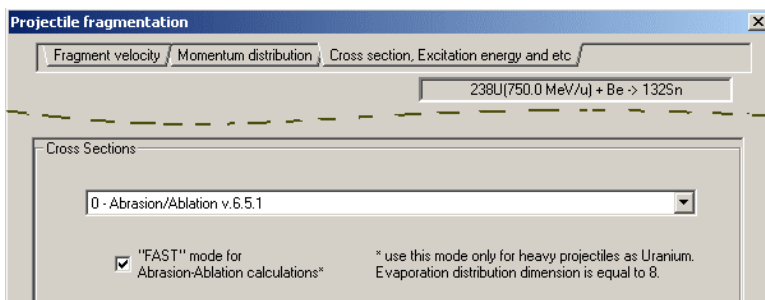


Fig.248. Fragment of the “Projectile fragmentation” dialog.

To select the AA fast mode it is necessary to choose the AA model and set the flag in the “fast mode” checkbox in the “Projectile fragmentation” dialog (Fig.248).



Fig.249. Fragment of the “Set-up” window.

The following messages, when fragmentation is set as the reaction mechanism in the code, will be shown in the left bottom corner of the code, depending on the model to being used to calculate the production cross-section (see Fig.249):

Cross-section model	Message
EPAX	Fragmentation
Abrasion-Ablation	Fragmentation-AA
Fast mode of Abrasion-Ablation	Fragmentation-AA fast

## 9.7. The “About” dialog modifications

The “About” dialog contains the information on the LISE and LISE++ codes official publication, which can be used for citation. Clicking on one of the selected papers (Fig.250) will load it in your default browser.

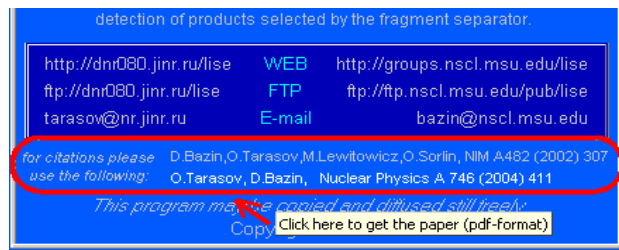


Fig.250. Portion of the “About LISE++” dialog.

## 9.8. PACE4: User's limits for Angular and Energy distributions of residues

The PACE4 code after ending calculation displayed energy and angular distribution tables just for the 15 most intense fusion residual nuclei. This restriction was caused by the limited operating memory and output file size, and decreased the time necessary for calculation and sorting. However, some remarks from the users have arrived encouraging the inclusion of low intensity products as well. We have decided not to increase the number of tables to solve this problem, but to give to the user the possibility to choose products to be displayed based on their intensity. The user determines the intensity window in the first dialog (right bottom corner of this dialog) of the program (see Fig.251).

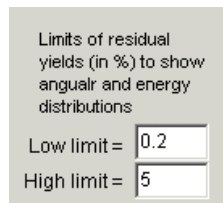


Fig.251.

### 9.9. Gas density dialog

Be very careful with the gas density calculation using the “Gas density” dialog! The calculations will be correct only for a molecular formula (see Fig.252). This dialog cannot be used for a gas mixture!

In the case of a gas mixture, to correctly calculate energy loss in material or interaction cross-sections it is better to enter a percentage ratio, but the gas density should be input **manually**. Let's consider a case of the ionization chamber filled by gas mixture of Argon (90%) and butylene (10%). The “Gas density” dialog will

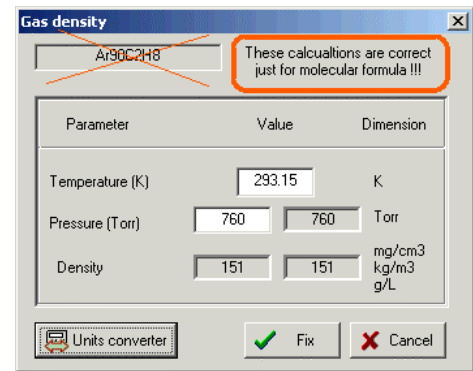


Fig.252. The “Gas density” dialog.

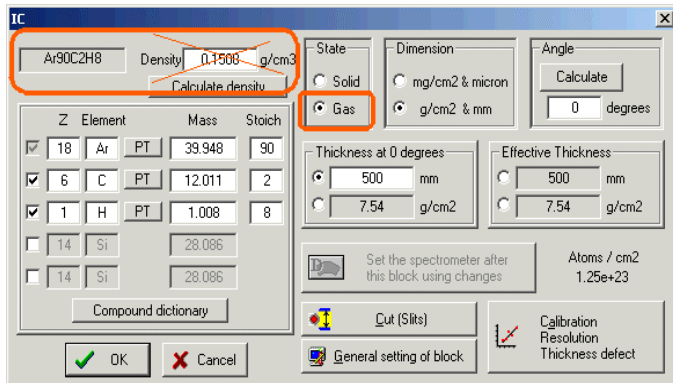


Fig.253. The “Material Thickness” dialog.

automatically calculate for you the density value of 0.1508 g/cm<sup>3</sup> (see Fig.253). However, the density of this mixture should actually be near to argon density (0.0016608 g/cm<sup>3</sup> at P=760 Torr). Therefore, it is recommended in the case of gas mixture at the beginning to input the mixture components and percentages, and then manually to input a density value, because if the percentage or components were changed then the program automatically calculates the density.

### 9.10. Block labels for the transport envelope

Block labels were incorporated for the envelope transport plots (Fig.254).

### 9.11. Drift block

It is possible to have drift block parameters shown in the Set-up window (Fig.255).

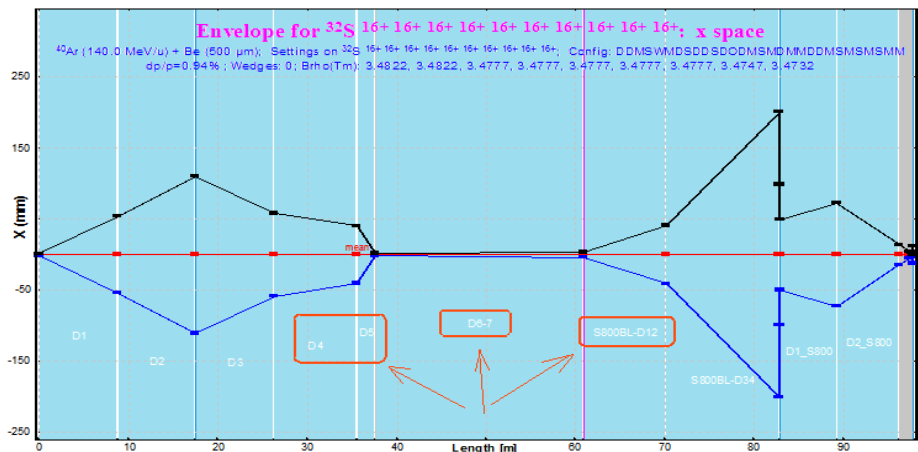


Fig.254. The <sup>32</sup>S transport envelope.

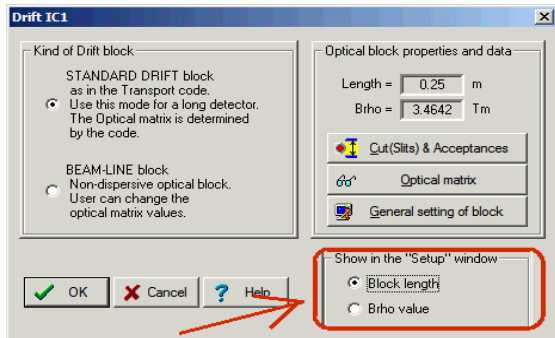


Fig.255. The “Drift block” dialog and drift block parameters in the “Set-up” window.





### 9.12. Compound targets for AA calculations, fusion-residues and fission reactions

The new version allows one to use a compound target for AA calculations, fusion-evaporation and fission reactions. The user can select what target component will be used for cross-section calculations (see Fig.256). Just one material component can be used for this purpose.

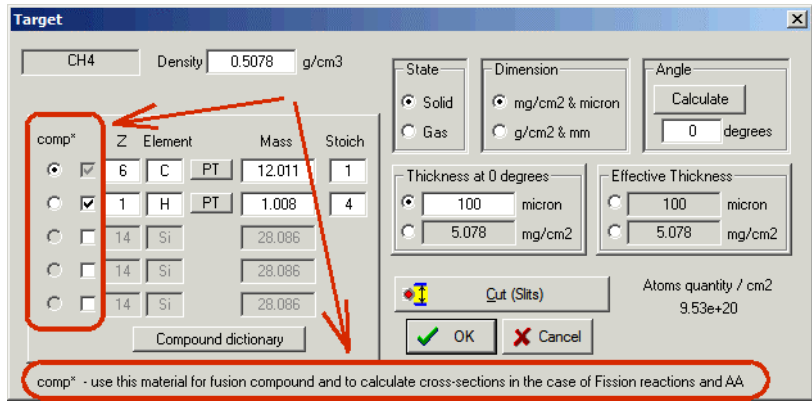


Fig.256. The “Target” dialog for compound material for fission reactions.

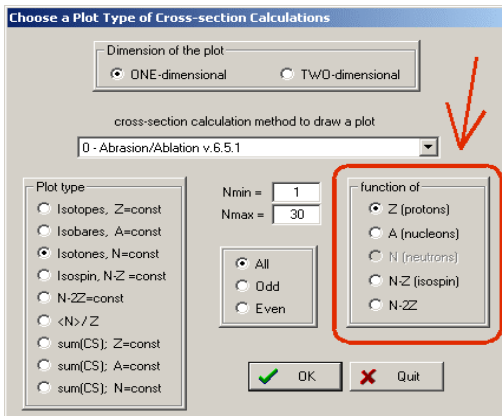


Fig.257. The “Cross-section plot” dialog.

### 9.13. Choice of horizontal axis for 2D-plots

All dialogs connected to 2D-plots (cross-sections, isotope database values, transmission values etc) were modified to give an opportunity to choose a horizontal axis from the list of axes possible for this plot type (Fig.257).

This novelty was incorporated into the program just before the completion of this documentation. For this reason almost all plot dialogs in the documentation were shown in the old style.

### 9.14. Version numbers

Version 7.2 devoted to implementation of the AME2003 database was the latest announced version. However we used the version number 7.3.\* just for the NSCL internal purpose to keep the program without global modifications, only for bug corrections. Version number 7.4.\* was used temporarily for global development of the code.

If a previous version (below 7.5) saved file contains calculation results, then the code (v.7.5) recalculates them due to changes in the list of transmission coefficients and implementation of the total reaction yield value.

### 9.15. LISE user statistics

Fig.259 shows in which countries there is interest in LISE++. The statistics correspond to the past two years, and are based on identified visits of the LISE sites\* (Fig.258).

Fig.260 shows statistics among US universities and laboratories.

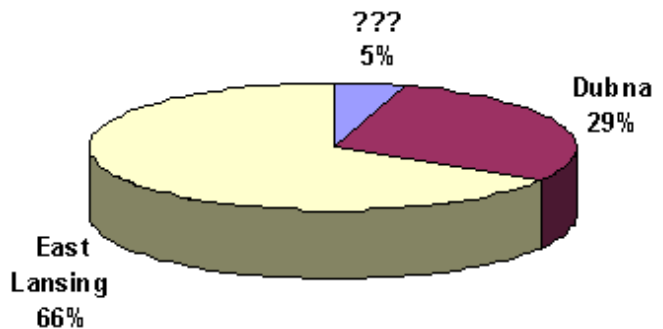
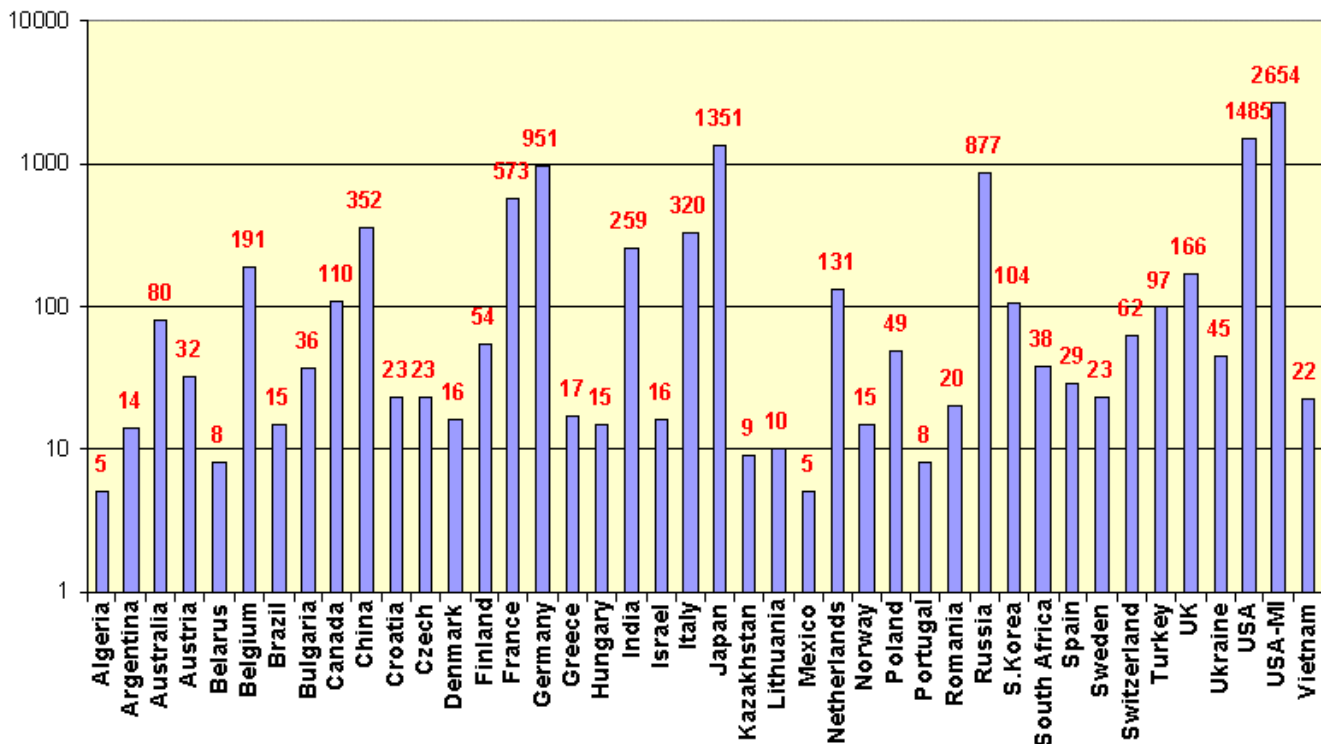
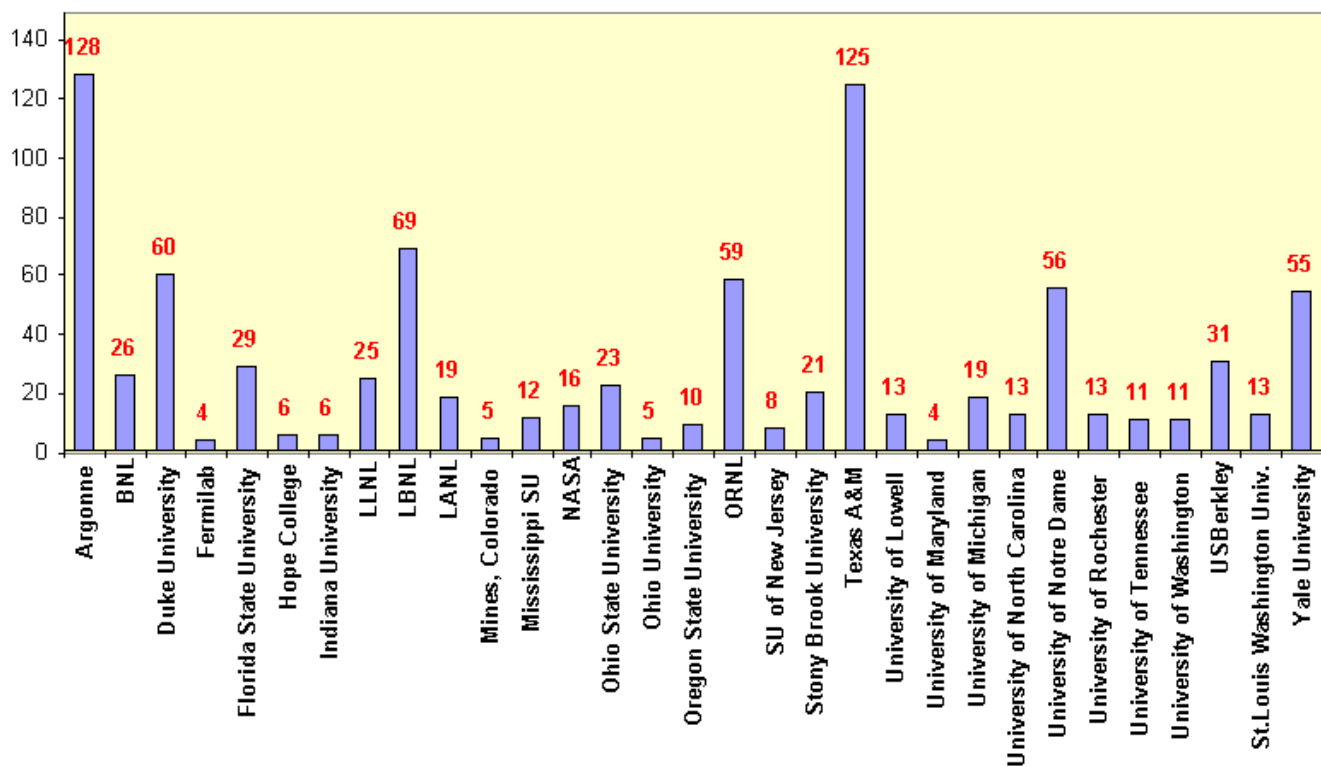


Fig.258. Statistics between LISE sites.

\* Due to temporary problems with the work of dnr080 server (at Dubna) about 30-40 percent of all hits were lost.



**Fig.259.** User statistics for the LISE web sites. The “USA” label refers to number of hits excluding MSU & NSCL contributions. The “USA-MI” label includes just hits from MSU or NSCL. Statistics are shown whenever the number of hits was more than 4.



**Fig.260.** User statistics of the LISE web sites for US universities and laboratories (without MSU and NSCL). Statistics are shown if the number of hits was more than 3.

## 10. User requests and bugs report

There are several corrections and user requests what we want to note.

### 10.1. Corrections

<ul style="list-style-type: none"> <li>▪ <i>Optical matrix: validation procedure of input value;</i></li> <li>▪ <i>Fusion-residue transmission: cross-section calculation procedure.</i></li> </ul> <p style="text-align: right;">D.Morrissey (NSCL)</p>	<i>Fixed</i>
<ul style="list-style-type: none"> <li>▪ <i>The Range plot subroutine.</i></li> <li>▪ <i>The “Block material” dialog.</i></li> <li>▪ <i>Universal parameterization (low limit for separation energy)</i></li> <li>▪ <i>Wedge angle calculation</i></li> </ul> <p style="text-align: right;">M.Haussman (NSCL)</p>	<i>Fixed</i>
<ul style="list-style-type: none"> <li>▪ <i>Calculation of charge state distribution after the target &amp; stripper in the non-equilibrium mode.</i></li> <li>▪ <i>Surviving probability: weight error.</i></li> </ul> <p style="text-align: right;">H.Weik (GSI)</p>	<i>Fixed</i>
<ul style="list-style-type: none"> <li>▪ <i>Charge states for Monte Carlo plots.</i></li> <li>▪ <i>The Envelope plot.</i></li> <li>▪ <i>Reactions in target (surviving coefficient) for light target.</i></li> <li>▪ <i>Correction in the Set-up window refresh procedure</i></li> </ul> <p style="text-align: right;">OT</p>	<i>Fixed</i>
<p><i>Kantele’s Spectrometric calculator: subroutines ICCK and ICCTot.</i></p> <p style="text-align: right;">A.Andreev (TRIUMF)</p>	<i>Fixed</i>
<p><i>Gas density calculator</i></p> <p style="text-align: right;">OT, S.Lukyanov (Dubna&amp;NSCL)</p>	<i>See chapter 9.9.</i>
<p><i>2D-ellipse plot</i></p> <p style="text-align: right;">S.Lukyanov(Dubna&amp;NSCL), OT</p>	The same problem with the "Goodies" dialog and result files. <i>Fixed.</i>
<p><i>Angular straggling (plane – space)</i></p> <p style="text-align: right;">Sam Austin (NSCL)</p>	<i>Fixed</i>
<p><i>Set-up window redraw process for target inclination</i></p> <p style="text-align: right;">L.Perrot, F.de Oliviera, C.Stodel (GANIL)</p>	Very old and confused bug ☹ <i>Fixed</i>
<p><i>Memory leaks</i></p> <p style="text-align: right;">OT M.Haussman (NSCL)</p>	Serious bugs which can result in code crash in the batch mode. <i>99% Fixed</i>
<p><i>Joint fusion residue and primary beam transmission</i></p> <p><a href="http://groups.nsl.msu.edu/lise/7_5/examples/fusion_and_primary_beam.lpp">http://groups.nsl.msu.edu/lise/7_5/examples/fusion_and_primary_beam.lpp</a></p> <p style="text-align: right;">Z.Podolyak (Surrey)</p>	<i>Fixed. See Fig.261.</i>

statistics $^{136}\text{Xe}$								
$^{136}\text{Xe}$ Stable (Z=54, N=82)								
Q1 (stripper)	51	50	49	48	48	47	47	46
Production Rate (pps)	1.51e-4	1.99e+0	2.02e+3	5.16e-14	3.14e+5	9.74e-12	1.17e+7	4.63e-10
Sum of charge states (pps)	6.25e+9	6.25e+9	6.25e+9	6.48e-7	6.25e+9	6.48e-7	6.25e+9	6.48e-7
Reaction	BEAM	BEAM	BEAM	FusRes	BEAM	FusRes	BEAM	FusRes
Sum of reactions (pps)	0.25e+9	0.25e+9	0.25e+9	0.25e+9	0.25e+9	0.25e+9	0.25e+9	0.25e+9
CS in the target (mb)	beam	beam	beam	2.52e-9	beam	2.52e-9	beam	2.52e-9
Total transmission (%)	2.42e-12	3.18e-8	3.23e-5	7.96e-6	0.005	0.002	0.187	0.072

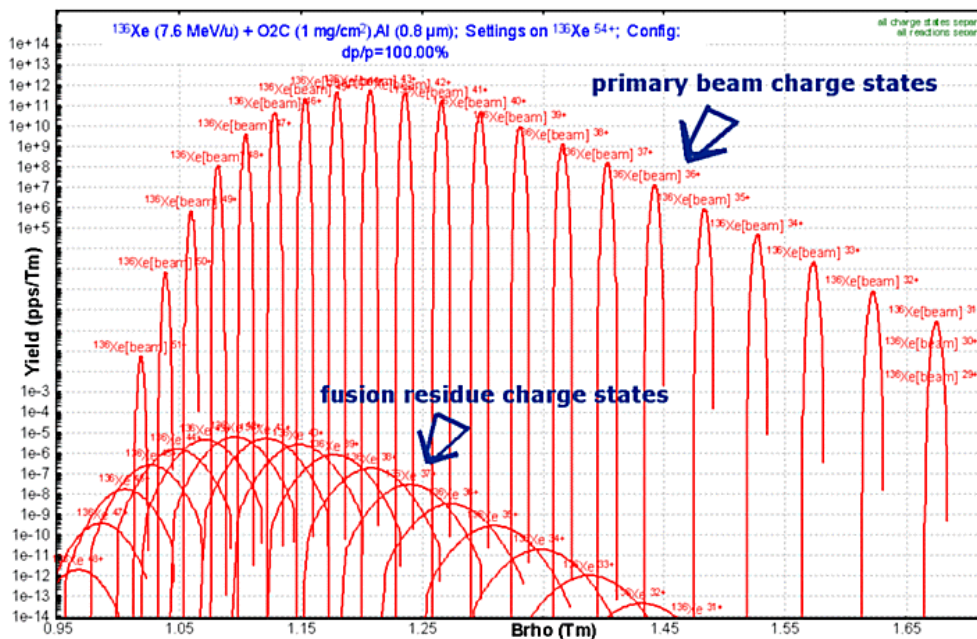


Fig.261. A portion of the statistics window (top plot) and  $B\rho$  distribution plot (bottom plot) of the  $^{136}\text{Xe}$  ions produced in  $^{136}\text{Xe}(7.6\text{MeV/u}) + \text{CO}_2(1\text{mg/cm}^2) + \text{Al}(0.8\mu\text{m})$ .

## 10.2. User requests

Keeping the curved profile degrader in the LISE++ file. The A1900 group (NSCL)	Modified. See chapter 9.2.
PACE4: User's limits for Angular and Energy distributions of residues. L.Penescu (GANIL), Andrey Blazhev (University of Sofia)	Implemented. See chapter 9.8.
Transport envelope: block labels. D.Morrissey (NSCL)	Implemented. See chapter 9.10.
Drift block: $B\rho$ -value in the Set-up window. D.Morrissey (NSCL)	Implemented. See chapter 9.11.
Compound target for the fusion-residues reaction. A.Semchenkov (GSI)	Modified. See chapter 9.12.
Choice of horizontal axis for 2D-plot. M.Thoennessen (NSCL)	Modified. See chapter 9.13.
New FRS configurations: "FRS - TA-Cave C.lcn", "FRS - TA-ESR.lcn", "Super-FRS.lcn", "FRS- TA-S4 new standard.lcn". H.Weick (GSI)	Implemented in the LISE installation package.

## 11. Next steps development

### 11.1. First priority

#### *Long-term*

- Secondary reactions in wedge; secondary target block
- Monte Carlo transmission

#### *Short-term*

- Compilation of LISE documentation based on all LISE version announcements.
- New reaction mechanism: Binary reactions (just kinematics)
- New block: RF kicker (deflector system for proton-rich fragments).
- New block: Solenoid (selection due to angular distribution).
- Create more help-files.

### 11.2. Second priority task

- LISE++ paper
- Abrasion-Fission paper
- Fusion-Fission reaction mechanism
- Possibility to use the angular momentum in fusion-fission & residues calculations.

### 11.3. Third priority task

- Alternative models to calculate fission fragment distributions
- Three-body kinematics calculator
- Charge state distribution model for low energies.
- Wedge (including curved profile wedge) inclination.
- "Water" wedge procedure (wedge with one moving plane and filled by liquid).
- Development of the spallation mechanism in the code.
- Development of a database of experimental data from various fission and fragmentaton experiments.
- Create the possibility to insert a material before the target. (to take into account energy loss, straggling, charge states)
- Develop a subroutine to calculate a reduced dispersion for large values of  $dp/p$ .
- Abrasion-Ablation as a function of the primary beam energy (as done for momentum distribution of products of projectile fragmentation)



## Acknowledgements

The authors thank Mr. Matthew Amthor for carefully proofreading this manual.

We are grateful to Prof. Brad Sherrill for continuous support and guidance. Fruitful discussions with Prof. Michael Thoennessen and Prof. Dave Morrissey are gratefully acknowledged.

The LISE++ authors thank Dr. Jorge Pereira Conca for help in developing the Abrasion-Fission model.

We are very appreciative of Dr. Marc Hausmann, Dr. Helmut Weik, and the A1900 staff for so intensely using the code and bugs searching.

Thanks to everyone who sent wishes and remarks allowing the modification of the LISE++ code for the best possible performance.

## References:

- [AME03] G.Audi, A.H.Wapstra and C.Thibault, Nucl. Phys. **A 729** (2003) 337.
- [Arm96] P.Armbruster et al., Z.Phys.**A355** (1996) 191-201.
- [Arm04] P.Armbruster et al.,Phys. Rev. Lett. **93** (2004) 212701.
- [Aud95] G.Audi and A.H.Wapstra, Atom. Data and Nucl.Data Tables (1995) 1.
- [Aum95] T.Aumann et al., Z.Phys. **A352** (1995) 163-169.
- [Baz02] D.Bazin, O.B.Tarasov, M.Lewitowicz, O.Sorlin, [NIM A482 \(2002\) 307-327](#).
- [Ben98] J.Benlliure et al., Nuclear Physics **A628** (1998) 458-478.
- [Ben01] J.Benlliure et al., Nuclear Physics **A683** (2001) 513-539.
- [Ben02] J.Benlliure et al., Nuclear Physics **A700** (2002) 469-491.
- [Ber03] M.Bernas et al, Nucl.Phys. **A725** (2003) 213-253.
- [Ber97] M.Bernas et al., Nucl.Phys. **A616** (1997) 352-362,  
M.Bernas et al., Phys.Lett. **B415** (1997) 111.
- [Bha86] K.H.Bhattm, P.Grange and B.Hiller, Phys.Rev.C **33** (1986) 33.
- [Bla94] B.Blank et all., Phys.Rev.C**50** (1994) 2398.
- [Bla00] B.Blank et all., Phys.Rev.Lett. **84** (2000) 1116.
- [Boh40] N.Bohr and J.A.Wheeler, Phys.Rev. **56** (1939) 426.
- [Coh74] S.Cohen, F.Plasil, W.J.Swiatecki, Ann.Phys. **82** (1974) 557.
- [De96] J.N.De et al., Phys.Rev.C**53** (1996)
- [Enq99] T.Enqvist et al., Nucl.Phys. **A658** (1999) 47-66.
- [Enq01] T.Enqvist et al., Nucl.Phys. **A686** (2001) 481-524.
- [Enq02] T.Enqvist et al., Nucl.Phys. **A703** (2002) 435-465.
- [Hau88] Atomic. Data Nucl. Data Tables **39**, 185 (1988); edited by P.E. Haustein.
- [HBF9] M.Samyn, S.Goriely, P.-H.Heenen, J.M.Pearson, F.Tondeur, Nucl.Phys. **A700** (2001) 142;  
S.Goriely, M.Samyn, P.-H.Heenen, J.M.Pearson, F.Tondeur, Phys. Rev. **C66** (2002) 024326;

- M.Samyn, S.Goriely, J.M.Pearson, Nucl. Phys. **A725** (2003) 69;  
 S.Goriely, M.Samyn, M.Bender, J.M.Pearson, Phys.Rev. **C68** (2003) 054325;  
 M.Samyn, S.Goriely, M.Bender, J.M.Pearson, Phys.Rev. **C70** (2004) 044309;  
 S.Goriely, M.Samyn, J.M.Pearson, M.Onsi, Nucl.Phys. **A750** (2005) 425.
- [Hes96] M.Hesse et al., Z. Phys. **A355** (1996) 69–75.  
 [Gol96] F.Goldenbaum et al., Phys.Rev.Lett. 77 (1996) 1230-1233.  
 [Ign95] A.V.Ignatyuk et al., Nucl.Phys.**A593** (1995) 519-534.  
 [Jur02] B.Jurado, Ph.D. thesis, University Santiago de Compostela, 2002.  
 [Jur03] B.Jurado, K.-H.Schmidt, J.Benlliure, Phys.Lett. **B553** (2003) 186-190.  
 [Jur04] B.Jurado et al., arXiv nucl-ex / 0403006, submitted to Nucl.Phys.A.  
 [Kra40] H.A.Kramers, Physika VII 4 (1940) 284.  
 [Lan80] W.Lang et al., Nucl.Phys. **A345** (1980) 34.  
 [LISE71] [http://groups.nsl.msu.edu/lise/7\\_1/lise++\\_7\\_1.pdf](http://groups.nsl.msu.edu/lise/7_1/lise++_7_1.pdf)  
 [Mam98] A.Mamdouh, J.M.Pearson, M.Rayet and F.Tondeur, Nucl. Phys. **A644** (1998) 389.  
 [Mam01] A.Mamdouh, J.M.Pearson, M.Rayet and F.Tondeur, Nucl. Phys. **A679** (2001) 337.  
 [Mye66] W.D.Myers, W.J.Swiatecki, Nucl.Phys. **81** (1966) 1.  
 [Per04] Jorge Pereira Conca, PhD thesis, Universidad de Santiago de Compostela (USC), 2004.  
 [Rub03] V.A.Rubchenya and J.Äystö, EURISOL research report, Jyväskylä 2003.  
 [Rub96] Th.Rubehn et al., Phys.Rev. **C53** (1996) 3143-3146.  
 [Sch00] K.-H.Schmidt, J.Benlliure, P.Armbruster, private communications.  
 [Sch01] K.-H.Schmidt et al., Nucl.Phys. **A685** (2001) 60-71.  
 [Sch02] K.-H.Schmidt et al., Nucl.Phys. **A710** (2002) 157-179.  
 [Sie86] A.Sierk, Phys. Rev. **C33** (1986) 2039.  
 [Smi93] G.N.Smirenkin (1993) IAEA-Report INDC(CCP)-359.  
 [Tar03] O.Tarasov and D.Bazin, NIM **B204** (2003) 174-178.  
 [Tai03] J.Taieb et al., Nucl.Phys. **A724** (2003) 413-430.  
 [Tho04] M.Thoennessen, Rep. Prog. Phys. **67** (2004) 1187-1232.